

A Thesis Submitted for the Degree of PhD at the University of Warwick

Permanent WRAP URL:

<http://wrap.warwick.ac.uk/81993>

Copyright and reuse:

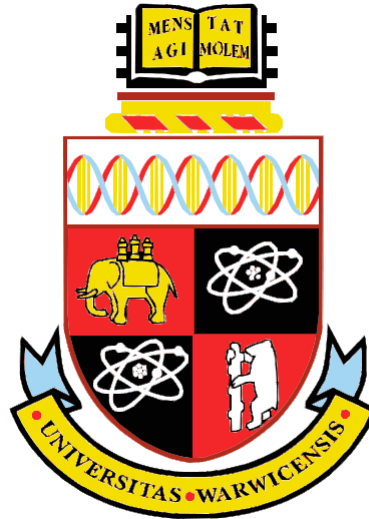
This thesis is made available online and is protected by original copyright.

Please scroll down to view the document itself.

Please refer to the repository record for this item for information to help you to cite it.

Our policy information is available from the repository home page.

For more information, please contact the WRAP Team at: wrap@warwick.ac.uk



Study of Cutting Speed on Ultrasonic Assisted Drilling of Carbon Fibre Reinforced Plastics

by

Aniruddha Gupta

A dissertation submitted in partial fulfilment of the requirements for the degree of
Doctor of Philosophy

at

WMG

University of Warwick

Declaration

This thesis is the original work of the author submitted to the University of Warwick in support of the application for the degree of Doctor of Philosophy. The research was performed at WMG department in the University of Warwick. Practical machining work associated with the ultrasonic assisted drilling using new tools described in Section 6.1 was performed with the assistance of Mr. Iain McEwen (an undergraduate student at School of Engineering) as part of the undergraduate student's project co-supervision. All of the data analysis was carried out exclusively by the author. The X-ray CT scanning of samples for the drilling trials described in Section 6.1 was performed in collaboration with Miss Nadia Kourra (an EngD. candidate at WMG) and Professor Mark Williams (Product Evaluation Technologies Group Leader at WMG). All of the X-ray CT scanning and image processing explained in Section 5.3 was performed by Ms. Nadia Kourra and the variation of specific parameters (Exit delamination area in Section 5.4.1 and maximum radius in Section 5.4.2) with respect to drilling depth was provided to the author for analysis. The first set of practical machining work associated with HSS drills detailed in Section 6.2 was carried out with the assistance of Mr. Brandon Souter (an undergraduate student at School of Engineering) as part of the undergraduate student's project co-supervision. The rest of the practical machining work in Section 6.2 and all of the analysis of data were performed out exclusively by the author. The rest of the experimental work in this thesis and the analysis of associated data were performed by the author. This thesis has not been submitted in whole or in part as consideration for other degree qualification at this or any other university. Where the work of other researchers has been used/cited, it has been suitably acknowledged.

Aniruddha Gupta

WMG

University of Warwick

July, 2016

Acknowledgements

I would like to express my deepest gratitude towards my supervisor Dr Stuart Barnes for accepting me as his student. I would like to thank him for providing me his great support, technical guidance and pushing me to extend my boundaries of knowledge throughout the thesis work. His patience and confidence in my abilities, valuable discussions, continuous inspiration and inquisitive questions have always given me a reason to put in extra effort into my research. Special thanks to Dr. Helen Ascroft for her unofficial continuous support and guidance on the methodologies and experimental work conducted in this research.

I would like to thank Mr. Darren Grant (WMG Technician) for his help, support and guidance on the practical machining work carried out in this thesis. I would also like to thank other WMG technicians Mr. Martyn Wilkins, Mr. Zachary Parkinson and Mr. Stefan Kousoulas for their support on the experimental work performed.

I would like to extend my appreciation to Dr. Mike Keeble, Dr. Evans Mogire (Technical Development Manager, Buehler UK, Ltd.) and Mr. Lewis Curry (WMG Technician) for their help and support with the optical microscopy, precision cutting, mounting and polishing work using Buehler equipment.

I would like to thank The WMG Centre for High Value Manufacturing Catapult for providing the machining centre, SGS Carbide Tool (UK) Ltd. for supplying the drilling tools, and BAE Systems for supplying the workpiece material.

I would like to thank Mr. Alexander Garrido for his kind help and guidance on thesis structuring. I would like to thank my colleagues at IARC 2nd floor for cheering me up and making a great working atmosphere during the time of my research. I would also like to thank all of my friends for keeping me motivated during the hard times in my research.

Finally, and most importantly, I would like to thank my parents for their eternal and unconditional love, care and support on everything since the beginning.

Without all the support, this research would not have been possible.

List of publications and presentations

- **Gupta A**, Barnes S, McEwen I, Kourra N, Williams MA. Study of cutting speed variation in the ultrasonic assisted drilling of carbon fibre composites. ASME 2014 International Mechanical Engineering Congress and Exposition; Montreal, Canada: ASME; 2014. p. V02BTA038 [Conference Proceedings (Peer Reviewed)]
- Kourra N, Warnett J, Attridge A, Kiraci E, **Gupta A**, Barnes S, Metrological study of CFRP drilled holes with x-ray computed tomography. *Int J Adv Manuf Technol.* 2015:1-11
- ‘Analysis of drilled holes on carbon fibre material with X-ray computed tomography’ by Kourra, Nadia, Williams, M. A. (Mark A.), Attridge, Alex, Warnett, Jason, Barnes, Stuart and **Gupta, Aniruddha**, 2014 IEEE International Workshop on Metrology for Aerospace (MetroAeroSpace), Benevento, Italy, 29–30 May 2014, (Number CFP1432W)
- ‘Advances in Cryogenic and Ultrasonic assisted Machining’ Stuart BARNES, Helen ASCROFT, Pipat BHUDWANNACHAI, Aishah Najiah DAHNEL, **Aniruddha GUPTA** at 16th International Conference on Machine Design and Production, June 30-July 03 2014, İzmir, Turkey
- ‘Effect of Pilot Hole in the Conventional and Ultrasonic Assisted Drilling of Carbon Fibre Composites’ by **Aniruddha Gupta** (a Technical presentation) at WMG Doctoral Research and Innovation Conference – 2015 at International manufacturing centre, University of Warwick, 30th June and 1st July-2015
- ‘Effect of chisel edge in ultrasonic assisted drilling of carbon fibre reinforced plastics (CFRP)’ by **Aniruddha Gupta**, Helen Ascroft, Stuart Barnes at *7th HPC 2016 – CIRP Conference on High Performance Cutting*, 31 May - 02 June 2016, Chemnitz, Germany (DOI: 10.1016/j.procir.2016.04.026)
- ‘Ultrasonic assisted Machining’ Helen ASCROFT, Stuart BARNES, Aishah Najiah DAHNEL, **Aniruddha GUPTA**, Nor Farah Huda A.H, David RAY at 17th International Conference on Machine Design and Production, 12-15 July 2016, Bursa, Turkey

Abstract

Workpiece damage generated during conventional drilling (CD) of carbon fibre reinforced plastics (CFRP) (such as delamination, matrix cracking, fibre pull out etc.) results in reduced fatigue strength, poor assembly tolerance and compromised structural integrity of the component. Avoidance of such damage during drilling of CFRP is a challenge for the aircraft and aerospace industries. At present, it requires a lot of resources and huge cost in order to generate damage free holes in CFRP in the industries. Therefore, the industries (such as BAE Systems) are looking for alternative hole producing processes for damage free drilling. It has been reported that thrust force during drilling should be reduced in order to reduce exit delamination. Ultrasonic assisted drilling (UAD) has been found to reduce the cutting and thrust forces during drilling of metals when compared to CD. Although limited attempts employing UAD indicate a reduction in thrust and cutting forces and damage when machining CFRP, this process has not been examined in detail with respect to optimising machining parameters in relation to machining theory. In addition, there has been limited research regarding the effect of the UAD process on overall workpiece damage as a result of drilling of CFRP. The focus of this research was the identification of the mechanism responsible for thrust force reduction in UAD in comparison to CD during drilling of CFRP which would help in selecting the machining parameters resulting in minimum workpiece damage. Consequently, the cutting speeds resulting in reduced forces and damage were investigated.

As a fundamental concept in machining theory, higher rake angles result in lower cutting forces and improved surface roughness. Calculations of effective normal rake angle at the cutting edge of a twist drill in UAD revealed a maximum of 62° and 49° effective rake angle at 10 and 100 m/min (40160 Hz, 7.3 μm peak-to-peak amplitude) respectively for a new tool. Employing knowledge of the effective rake angle, experiments were performed at specific cutting speeds in order to examine the effects of UAD on forces and damage during drilling of CFRP and compared to CD. Further work employed a pilot hole to remove the contribution of chisel edges so that influence of effective rake angles at the cutting edges could be examined. Through-hole drilling tests, comparing UAD and CD, employing a constant feed rate of 0.05 mm/rev and two cutting speeds (10 and 100 m/min) were carried out. At 10 m/min, there was a reduction in thrust force and torque of 55 % and 45 %, respectively when utilising UAD with a new tool. 40 % reduction in thrust force and 46 % in torque with 52 μm of tool wear corresponded to 36 % reduction in entrance delamination and 22 % reduction in exit delamination at 10 m/min. At 100 m/min, 20 % reduction in thrust force and 30 % in torque was obtained respectively; however, this did not yield a significant reduction in entrance or exit delamination. Analysis of internal damage did, however, reveal a 55 % reduction in internal damage (i.e. fibre pull-out and fibre disorientation) at 100 m/min. Thus, the key contribution of this research is that low cutting speed is required in UAD in order to achieve the greatest reduction in machining forces (and hence, delamination) at entrance and exit of a hole in comparison to CD. The reason for this was discovered to be higher effective rake angle at low cutting speed in UAD causing the reduction in thrust force and torque. Furthermore, reduction of internal damage in a hole required higher cutting speed in UAD. The results imply that the cutting speed should be varied during drilling a hole in CFRP. In UAD, the cutting speed should be lower at entrance and exit of a hole and higher for drilling the intermediate part. Whereas in CD, the cutting speed should be higher at entrance and exit and lower during drilling of intermediate part keeping the feed rate constant in order to achieve the minimum workpiece damage during drilling of CFRP. The proposed variation of cutting speed during drilling of a hole is possible in the machine used in the present research.

ABSTRACT	IV
1 INTRODUCTION	1
1.1 BACKGROUND.....	1
1.2 AIMS AND OBJECTIVES	5
2 INTRODUCTION TO CFRP	6
2.1 OVERVIEW OF COMPOSITE MATERIALS	6
2.1.1 Reinforcement	6
2.1.2 Matrix.....	8
2.2 POLYMER MATRIX COMPOSITES (PMC)	10
2.2.1 Fibre Reinforcement for PMC	10
2.2.2 Matrix for PMC.....	13
2.3 CARBON FIBRE REINFORCED PLASTICS (CFRP)	16
2.4 PROPERTIES AND APPLICATIONS OF CFRP.....	17
3 LITERATURE REVIEW OF THE DRILLING OF CFRP	20
3.1 MECHANISM OF CHIP FORMATION AND DAMAGE DURING MACHINING OF CFRP IN SEVERAL RELATIVE ORIENTATIONS	20
3.2 DAMAGE DURING CONVENTIONAL DRILLING	26
3.2.1 Entrance and exit delamination	26
3.2.2 Damage on the machined surface	27
3.3 CONCEPT OF CRITICAL THRUST FORCE AND DELAMINATION.....	27
3.4 METHODOLOGIES TO ASSESS AND QUANTIFY THE DAMAGE AROUND A DRILLED HOLE.....	28
3.4.1 Entrance and exit delamination	29
3.4.2 Quantification of entrance and exit delamination	38
3.4.3 Assessment and quantification of internal damage in a drilled hole	43
3.5 ATTEMPTS TO MINIMISE THE DAMAGE THROUGH CONVENTIONAL DRILLING OF CFRP	48
3.5.1 Machining parameters	48
3.5.2 Pilot holes.....	49
3.5.3 Tool geometry	54
3.5.4 Tool wear and material	61
3.6 ATTEMPTS TO MINIMISE THE DAMAGE DURING DRILLING OF CFRP THROUGH NON – CONVENTIONAL MANUFACTURING PROCESSES.....	64
3.6.1 Laser Processing	64
3.6.2 Water jet and Abrasive water jet machining (WJM and AWJM).....	65
3.6.3 Ultrasonic machining.....	66
3.6.4 Rotary ultrasonic machining	66
3.6.5 Vibration assisted machining	67
3.6.6 Vibration assisted drilling (VAD) of CFRP	71
3.6.7 Ultrasonic assisted drilling (UAD) of CFRP.....	76
3.7 CONCLUSIONS FROM THE REVIEW	82
4 EFFECTIVE RAKE AND CLEARANCE ANGLES IN CD AND UAD FOR A TWIST DRILL GEOMETRY	85
4.1 CONVENTIONAL MACHINING	85
4.2 ORTHOGONAL AND OBLIQUE CUTTING	87
4.3 CUTTING TOOL GEOMETRY.....	87
4.3.1 Various rake and clearance angles in a cutting tool geometry	88
4.3.2 Importance of work reference system	91
4.4 GEOMETRY OF TWO FLUTE TWIST DRILL IN WORK REFERENCE SYSTEM.....	92
4.5 ULTRASONIC ASSISTANCE ON A TWIST DRILL DURING DRILLING	94
4.6 EFFECTIVE RAKE AND CLEARANCE ANGLES IN CD AND UAD FOR A TWIST DRILL GEOMETRY IN WORK REFERENCE SYSTEM	98
5 EXPERIMENTAL METHODOLOGY	112

5.1	EQUIPMENT	112
5.1.1	Machining centre	112
5.1.2	Force measurement	113
5.1.3	Ultrasonic amplitude measurement	115
5.2	WORKPIECE MATERIAL.....	119
5.3	SAMPLE PREPARATION AND INSPECTION METHODOLOGIES	124
5.3.1	Sectioning, mounting and polishing of the samples	124
5.3.2	Optical microscopy and scanning electron micrography (SEM).....	126
5.4	DAMAGE ANALYSIS THROUGH X-RAY CT SCANNING	128
5.4.1	Exit delamination	132
5.4.2	Internal damage	134
5.5	DAMAGE ANALYSIS THROUGH SECTIONING, MOUNTING AND POLISHING	136
5.5.1	Crack propagation depth.....	137
5.5.2	Fibre pull out and disorientation.....	137
5.5.3	Maximum delamination depth at entrance and exit	139
5.6	TOOL WEAR MEASUREMENT	143
5.6.1	Setup for tool wear measurement.....	143
5.6.2	Tool wear quantification	144
5.7	EXPERIMENTAL TOOLING AND PROCEDURE	146
5.7.1	Phase 1: Preliminary experiment to investigate theoretical effective normal rake angles in CD and UAD and its effect on damage	147
5.7.2	Phase 2: Effect of cutting edge using pilot holes	152
5.7.3	Phase 3: Effect of cutting and chisel edges when drilling with Tungsten carbide drills.....	157
6	RESULTS AND DISCUSSION	163
6.1	PHASE 1: PRELIMINARY EXPERIMENT TO INVESTIGATE THEORETICAL EFFECTIVE NORMAL RAKE IN CD AND UAD AND ITS EFFECT ON DAMAGE.....	163
6.1.1	Effective normal rake angle and clearance angle calculation for current drill geometry	163
6.1.2	Results of thrust force and tool wear.....	167
6.1.3	Results of damage analysis	175
6.1.4	Machined surface.....	186
6.1.5	Cutting temperature variation	193
6.1.6	Chip analysis.....	196
6.1.7	Discussion.....	198
6.1.8	Conclusions from Phase-1	204
6.2	PHASE 2 – EFFECT OF CUTTING EDGE USING PILOT HOLES	206
6.2.1	Effective normal rake angle and clearance angle calculation for the current drill geometry	207
6.2.2	Results of thrust force, torque and tool wear.....	209
6.2.3	Results of damage analysis	222
6.2.4	Discussion.....	236
6.2.5	Conclusions from Phase-2	240
6.3	PHASE 3 - EFFECT OF CUTTING AND CHISEL EDGES WHEN DRILLING WITH TUNGSTEN CARBIDE DRILLS.....	241
6.3.1	Effective normal rake angle at 10 and 100 m/min cutting speeds at current drill geometries	242
6.3.2	Results of thrust force, torque and tool wear.....	245
6.3.3	Results of damage quantification and analysis	263
6.3.4	Machined surface.....	278
6.3.5	Analysis of chip fragments	279
6.3.6	Discussion.....	280
6.3.7	Conclusions from Phase-3	286
6.4	CONFIRMATION OF EFFECT OF LARGER ‘EFFECTIVE’ NORMAL RAKE ANGLES AT SAME INTERMITTENT CUTTING ACTION	288
6.4.1	Conclusion	294
7	CONCLUSIONS	295

7.1	THE MECHANISM ASSOCIATED WITH CUTTING EDGES IN A TWIST DRILL CAUSING THE REDUCTION IN MACHINING FORCES IN UAD OF CFRP AND ITS RELATIONSHIP WITH CUTTING SPEED.....	295
7.2	THE UNDERLYING RELATIONSHIP IN-BETWEEN MACHINING FORCES, OVERALL WORKPIECE DAMAGE (ENTRANCE/EXIT DELAMINATION AND INTERNAL DAMAGE) AND CUTTING SPEED IN CD AND UAD OF CFRP.....	296
7.2.1	Forces and delamination at entrance and exit.....	296
7.2.2	Internal damage.....	297
7.3	INFLUENCE OF TOOL WEAR ON THE EFFECTIVENESS OF UAD WITH RESPECT TO CUTTING SPEED.....	298
8	SUGGESTIONS FOR FUTURE WORK.....	300
	REFERENCES.....	303
	APPENDICES.....	315

List of Tables

Page

Table 2-1: Mechanical properties of typical composite materials in the fibre-axis direction in various matrix systems, Note: ^a Data from [60], ^b Data from [63], ^c Data from [64], ^d Data from [65]	9
Table 2-2: Applications of PMCs in various industrial areas [49]	10
Table 2-3: Comparison of density, Young's Modulus, tensile strength, specific Modulus and specific strength of CFRP to metals, Note: ^a data from [67], ^b data from [65]	16
Table 2-4: Comparison of thermal properties of CFRP to metals [55]	18
Table 5-1: Technical data of type 9257 B dynamometer	114
Table 5-2: Technical data of type 9271 A dynamometer	114
Table 5-3: Properties of the HTM 552 material provided by BAE Systems	119
Table 5-4: Orientation of the carbon fibres in every layer of workpiece material	123
Table 5-5: Grinding and polishing steps followed for polishing the carbon fibre composite samples [189] (Comp. = complementary)	126
Table 5-6: Data table for maximum damage depth at entrance/exit and internal damage at two perpendicular planes in a hole	142
Table 5-7: Data table for three-flute twist drill used in the current experimental study	147
Table 5-8: Machining parameters used in current experimental study	150
Table 5-9: Details of pilot-hole drill used in the present experiment [192]	153
Table 5-10: Details of the main drill used in the present experiment [193]	153
Table 5-11: Ultrasonic parameters used in the current experiment for UAD with and without pilot hole	157
Table 5-12: Data of 2-flute twist drills used for main-hole drilling in the present study	157
Table 5-13: Details of pilot-hole drills used in the current experimental study	159
Table 5-14: Summary of the drilling tests performed in Phase-3	160
Table 5-15: Ultrasonic experimental parameters (frequencies and peak-to-peak amplitude) for Phase-3	161
Table 6-1: Thrust force data for drilling with fresh tool	172
Table 6-2: Thrust force (N) data for CD with worn tool	173
Table 6-3: Thrust force (N) data for UAD with worn tool	173
Table 6-4: Reduction in thrust force due to UAD in comparison to that in CD with worn tool	174
Table 6-5: Area delamination factor values obtained from CT scanning	176
Table 6-6: Average maximum radius values obtained from CT scanning	177
Table 6-7: Maximum damage depth data at entrance in CD for three times repetitions with worn tool	179
Table 6-8: Maximum damage depth data at entrance in UAD for three times repetitions with worn tool	179
Table 6-9: Data table for average crack propagation and fibre-pull out data in the holes drilled by fresh tools	180
Table 6-10: Data table for internal damage in CD from the holes drilled with a worn tool	182
Table 6-11: Data table for internal damage in UAD from the holes drilled with a worn tool	182
Table 6-12: Data table for maximum damage at exit in the holes drilled by a new tool	183
Table 6-13: Maximum damage depth at exit data obtained from the holes drilled by worn tool in CD	184

Table 6-14: Maximum damage depth at exit data obtained from the holes drilled by worn tool in UAD	184
Table 6-15: Thrust force data for CD	214
Table 6-16: Thrust force data for UAD.....	214
Table 6-17: Torque data for CD	216
Table 6-18: Torque data for UAD.....	216
Table 6-19: Flank wear data for CD.....	218
Table 6-20: Flank wear data for UAD.....	218
Table 6-21: Data table for wear area in chisel edge in CD and UAD without pilot hole tests	220
Table 6-22: Data table for maximum damage at entrance in the cases of with and without pilot-holes in CD	224
Table 6-23: Data table for maximum damage at entrance in the cases of with and without pilot-holes in UAD	224
Table 6-24: Data table for maximum damage at exit in the cases of conventional without and with pilot holes drilling	225
Table 6-25: Data table for maximum damage at exit in the cases of ultrasonic assisted without and with pilot holes drilling	225
Table 6-26: Data table for average internal damage in the cases of CD with and without pilot-holes.....	229
Table 6-27: Data table for average internal damage in the cases of UAD with and without pilot-holes.....	229
Table 6-28: Data for average thrust force at 10 m/min cutting speed and 0.05 mm/rev feed rate in all the drilling sets of CD, UAD, with and without pilot holes.....	247
Table 6-29: Data for average thrust force at 100 m/min cutting speed and 0.05 mm/rev feed rate in all the drilling sets of CD, UAD, with and without pilot holes.....	248
Table 6-30: Data for average torque values in CD and UAD at 10 m/min cutting speed and 0.05 mm/rev feed rate.....	252
Table 6-31: Data table for average torque values in CD and UAD at 100 m/min cutting speed and 0.05 mm/rev feed rate	253
Table 6-32: Tool wear data at 10 m/min cutting speed and 0.05 mm/rev feed rate for all the cases	255
Table 6-33: Tool wear data at 100 m/min cutting speed and 0.05 mm/rev feed rate for all the cases.....	256
Table 6-34: Data of radius of curvature in the case of UAD with and without pilot hole drilling.....	260
Table 6-35: Negative axial rake angles of twist drills at the outermost corner of cutting edge.....	262
Table 6-36: Effective normal rake angle in UAD for hole 1 and hole 60 in the case of UAD with pilot.....	262
Table 6-37: Data for maximum delamination damage depth at entrance at 10 m/min cutting speed	264
Table 6-38: Data for maximum delamination damage depth at entrance at 100 m/min cutting speed	264
Table 6-39: Data for maximum damage depth at exit at 10 m/min cutting speed and 0.05 mm/rev feed rate	270
Table 6-40: Data for maximum damage depth at exit at 100 m/min cutting speed and 0.05 mm/rev feed rate	271

Table 6-41: Average internal damage data for selected holes at 10 m/min and 0.05 mm/rev feed rate in CD and UAD	276
Table 6-42: Average internal damage data for selected holes at 100 m/min and 0.05 mm/rev feed rate in CD and UAD	276
Table 6-43: Comparison of feed rate and maximum velocity due to ultrasonic assistance at 10 and 100 m/min	282
Table 6-44: Data table for average thrust forces at 10 m/min cutting speed and 26.5 mm/min feed rate in the cases of CD, UAD with and without pilot hole drilling.....	291
Table 6-45: Data table for average thrust forces at 100 m/min cutting speed and 26.5 mm/min feed rate in the cases of CD, UAD with and without pilot hole drilling.....	291

List of Figures

Page

Figure 2-1: Property variation in composite materials with respect to size and shape of reinforcement [49]	7
Figure 2-2: Strong covalent bonds in the basal planes and weak van der Waals bonds amongst the basal planes in the graphite structure [59]	12
Figure 2-3: Alignment of basal planes in carbon fibres [69].....	13
Figure 2-4: Curing process of thermoset and thermoplastic resins [48].....	15
Figure 2-5: Comparison of specific strength and Specific Modulus of polymer composites and aerospace metal alloys, L- Longitudinal direction; AS4 and T300 are different varieties of carbon fibres [67];.....	17
Figure 3-1: (a) Relative fibre orientations during one rotation of twist drill and (b) representation of twist drill with unidirectional CFRP material shown by Eneyew and Ramulu [75]	20
Figure 3-2: Machining notations in the study of Wang and Zhang [82]	21
Figure 3-3: Machining of 0° relative fibre orientation with (a) positive rake angle (b) negative rake angle [74]	22
Figure 3-4: Orthogonal machining of 45° relative orientation by (a) positive rake angle and (b) negative rake angle tool [74]	23
Figure 3-5: Deformation and bending of the fibres in the cutting direction of tool found in the orthogonal machining of 90° relative orientation of carbon fibres [74]	23
Figure 3-6: SEM image displaying smearing of matrix in the orthogonal machining of 90° relative orientation fibres covering fibres from the top view of machined surface in the work of Wang Zhang [83]	24
Figure 3-7: Bending of the fibres and irregular surface formation during orthogonal machining of 135° relative orientation of carbon fibres demonstrated by Wang et al. [74]	25
Figure 3-8: SEM image of fibre pull-out and sub-surface damage on the machined surface during orthogonal machining of 150° relative fibre orientation reported by Wang and Zhang [83].....	25
Figure 3-9: Entrance or Peel-up delamination during conventional drilling [86]	26
Figure 3-10: Push-out or exit delamination during conventional drilling [86]	27
Figure 3-11: Image processing using ImageJ software technique to identify the delaminated diameter and area around a 5 mm diameter hole after capturing the digital image through the Mitutoyo microscope developed by Davim et al. [93].....	30
Figure 3-12: Measurement of the maximum diameter of exit delamination through visual inspection in Mitutoyo TM 500 toolmakers' microscope used by Davim and Reis [96]	30
Figure 3-13: Side view of a drilled hole in a CT scanned image displaying maximum delamination in the plies near to the exit but not exactly at the exit ply around a 6 mm diameter hole in CFRP, reported by Kourra et al. [101].	31
Figure 3-14: (a) X-ray radiograph of exit delamination and (b) processed image for damage quantification for a 6 mm diameter hole in the work of Duraó et al. [104].....	34
Figure 3-15: X-ray CT scanning setup used by Kourra et al. [101].....	35
Figure 3-16: 3D reconstruction of specimen using back projection algorithms in X-ray CT scanning technique [101].....	35

Figure 3-17: Detection of delaminated region through (a) ultrasonic C-scan and (b) X-ray CT scanning for a 10 mm diameter hole in the work of Tsao and Hocheng [112]	36
Figure 3-18: Identification of maximum diameter of delamination in drilled hole in the work of Karnik et al. [16].....	38
Figure 3-19: Delamination height and width considered as damage criteria in the work of Faraz et al. [119].....	40
Figure 3-20: Area delamination measurement around 4 mm diameter hole in the work of Faraz et al. [95]	41
Figure 3-21: Two extreme cases of (a) Fine cracks (b) uniform delamination considered in the work of Davim et al. [93].....	41
Figure 3-22: Diameter delamination factor (F_d) and adjusted delamination factor (F_{da}) calculated around 5 mm diameter hole in the work of Davim et al. [93].	42
Figure 3-23: Increase in the average surface roughness of carbon fibre composite with increase in feed rate in the work of Zitoune at al. [125].....	44
Figure 3-24: (a) Angular positions of surface roughness measurement in the work of Eneyew and Ramulu [75].....	45
Figure 3-25: (a) Average and (b) maximum peak-to-valley surface roughness variation at various angular locations in the work of Eneyew and Ramulu. [75]	46
Figure 3-26: Comparison between the fibre pull-out information obtained from confocal laser microscope and surface profilometer in the work of Wang et al. [8]. In addition, Increase in surface roughness with increase in (a) cutting speed (b) feed rate (R_a = average surface roughness and R_y = peak-to-valley height).....	47
Figure 3-27: Sources of thrust force in a drill during drilling process and maximum thrust force coming from centre of chisel edge due to indentation [131]	49
Figure 3-28: Lower thrust force obtained in the case of with-pilot hole than that in the case of without-pilot hole drilling in the work of Won and Dharan [20]	51
Figure 3-29: Effect of feed rate on thrust force when using pilot holes in the work of Won and Dharan [20]	51
Figure 3-30: Thrust force in the cases of with and without pilot holes with 10 mm diameter drill at various feed rates and 1000 rpm spindle speed in the work of Tsao and Hocheng [21] (ξ = chisel edge length to diameter ratio)	52
Figure 3-31: Effect of pilot hole drilling at (a) Thrust force, (b) entrance delamination and (c) exit delamination in the work of Faraz and Biermann [99].....	53
Figure 3-32: Thrust force generated in the cases of twist, brad, dagger and step drills used in the work of Durao et al.[129]	56
Figure 3-33: Comparison of exit delamination from the twist, brad, dagger and step drills used in the work of Durao et al. [129].....	56
Figure 3-34: A bullet shaped drill geometry proposed by piquet et al. [79]	56
Figure 3-35: Comparison between the cutting mechanism of 2-flute twist drill and the proposed geometry of bullet shaped drill in Figure 3-34 by Piquet et al.[79] (F_2 = conventional 2-flute twist drill, OP_1 = proposed geometry of 3-flute drill).	57
Figure 3-36: (a) Twist drill, (b) Candle stick drill and (c) saw drill having 10 mm diameter used in the work of Hocheng and Tsao [13, 17].....	59
Figure 3-37: Thrust force data for various drills in the work of Hocheng and Tsao [13]	59
Figure 3-38: (a) core twist drill, (b) core saw drill, (c) core candle stick drill (d) step core twist drill, (e) step core saw drill and (f) step candle stick drill having 10 mm outer drill diameter experimented in the work of Tsao and Chiu [108]	60

Figure 3-39: Thrust force variation with respect to feed rate with and without a backup plate in the work of Tsao Hocheng [133], Although experimental thrust force with backup plate increased but it was lower than the theoretical critical thrust force required for delamination.....	61
Figure 3-40: SEM Image of cutting edge rounding due to at the cutting edge of uncoated tungsten carbide tool in the work of Lliescu et al. [138].....	62
Figure 3-41: Schematic of ultrasonic machining [31].....	66
Figure 3-42: Edge chipping at the exit of the hole during RUM in the work of Feng et al. [156]. The distance between ‘a’ and ‘b’ was found to be 600 μm defined as chipping size in their work. The maximum thickness of the edge chipping was 207.9 μm in their work.	67
Figure 3-43: Intermittent cutting action of cutting tool explained by Brehl and Dow [161]	69
Figure 3-44: Thrust force variation in VAD at various cutting, feed speeds and ASR at 30 Hz frequency in the work of Sadek et al. [30]	72
Figure 3-45: Thrust force variation in the hybrid variation drilling [39]	74
Figure 3-46: Thrust force reduction due to VAD of CFRP in the work of Wang et al. [38]	75
Figure 3-47: Experimental setup of Makhdum et al. for UAD of CFRP [163]	77
Figure 3-48: Longer spiral chip formation in UAD in the work of Makhdum et al. [164]	77
Figure 3-49: Thrust force from (a) CD and UAD of CFRP by Makhdum et al. [40] and (b) CD and UAD of cortical bone by Alam et al. [23]	79
Figure 4-1: Machining action of a cutting tool in a shaping process (borrowed from [168])	86
Figure 4-2: Demonstration of (a) orthogonal and (b) oblique cutting [171]	87
Figure 4-3: Schematic to visualize axial, orthogonal and normal rake angles in a single point turning tool.....	90
Figure 4-4: Visualization of rake and clearance angles in work reference system in threading operation (borrowed from [168]).....	91
Figure 4-5: Salient features of a two flute twist drill in (a) axial projection and (b) side view [171]	92
Figure 4-6: Schematic displaying the variation in velocity along the cutting edge in axial projection view	93
Figure 4-7: Rotational, vibrational and feed motions of the drill during vibration assisted drilling	94
Figure 4-8: Schematic for the projection of the cutting edges of a twist drill on the plane of paper displaying the rotational and vibrational motions applied on the cutting edge.....	95
Figure 4-9: Movement of point P of the cutting edge of Figure 4-8 during conventional drilling	96
Figure 4-10: The motion path of point P shown in Figure 4-8 for two revolutions of twist drill in vibration assisted drilling for 5000 Hz frequency and 10 μm amplitude (the distance of point P is assumed to be 3 mm from the axis of rotation in this schematic).....	96
Figure 4-11: Motion path of point P shown in Figure 4-8 for two revolutions of twist drill in ultrasonic assisted drilling for 37220 Hz frequency and 10 μm amplitude.....	97
Figure 4-12: Part 1 – 2-flute twist drill in drilling action, Part 2- Enlarged axial projection of the twist drill shown in part 1. Part 3 – Visualization of the rake and clearance angles, feed velocity, resultant cutting velocity, and therefore the new reference plane π_{RWi} at an angle μ_i from the previous reference plane π_{RDj}	101

Figure 4-13: Visualization of mean and peak position of sinusoidal ultrasonic oscillations in UAD	103
Figure 4-14: Magnified portion of the chisel edge from the part-2 of Figure 4-12	105
Figure 4-15: Effective normal rake angle in CD and UAD at 10 m/min cutting speed and 0.05 mm/rev feed rate.....	107
Figure 4-16: Axial movement of a point on the cutting edge in CD and UAD (P.S. the positive values indicate drill going inside the material)	108
Figure 4-17: Axial movement of a point on the cutting edge in CD and UAD at 10 m/min cutting speed, 0.05 mm/rev feed rate, 40 kHz frequency and 5 μ m oscillation amplitude	108
Figure 4-18: Calculation of maximum effective rake angles obtained at various cutting speeds and amplitudes at 40 kHz frequency for a given tool geometry at the end point of cutting edge in UAD	109
Figure 4-19: Calculation of maximum effective rake angles obtained at various cutting speeds and amplitudes in CD for a given tool geometry at the end point of cutting edge.....	110
Figure 5-1: DMG/MORI SEIKI Ultrasonic-65 machine used in the experimental studies ...	113
Figure 5-2: Thrust force profile (94.2 m/min, 0.05 mm/rev) in UAD.....	115
Figure 5-3: Keyence amplitude measurement assembly having laser sensor head, controller, 24 V DC power supply and computer having LK Navigator 2 software for amplitude measurement.....	116
Figure 5-4: Keyence Laser sensor head with the drill tip located in such a way that the laser transmitted from the transmitter is reflected from the horizontal strip attached to the drill tip and received at the receiver further	117
Figure 5-5: Sinusoidal impressions on the internal cylindrical surface of aluminium at 100 mm/min cutting speed and 0.075 mm/rev feed rate (38760 Hz frequency and 4.7 μ m amplitude)	118
Figure 5-6: Sectioning of the workpiece material in 0°, 45° and 90° orientation.....	120
Figure 5-7: Sectioning of workpiece material in 135° orientation relative to 0° orientation shown in Figure 5-6.....	120
Figure 5-8: View of the material in the plane of sectioning at 0° shown in Figure 5-6	122
Figure 5-9: View of the material on the plane sectioned at 45° shown in Figure 5-6	122
Figure 5-10: View of the material on the plane sectioned at 90° shown in Figure 5-6.....	122
Figure 5-11: View of the material on the plane sectioned at 135° shown in Figure 5-6	122
Figure 5-12: Representation of carbon fibre orientations in every layer of the work piece material from entrance to exit of the hole during drilling with respect to the view of the workpiece in 0° plane of sectioning shown in Figure 5-8.....	123
Figure 5-13: Image of a drilled hole mentioning plane of sectioning for observing the machined surface	124
Figure 5-14: SEM image of the machined surface after sectioning the hole	124
Figure 5-15: ZEISS Sigma HV SEM	127
Figure 5-16: Polished and cleaned surface after polishing exhibiting damage propagation and fibre-matrix debonding	127
Figure 5-17: (a) Straight machined marks and the drilled hole, (b) centre identification and the dimensions of hole and marks in millimetres.....	129
Figure 5-18: An image of 3D scan of the hole exhibiting the machined marks around the hole and damage on the internal walls of the hole (282.6 m/min, 0.05 mm/rev).....	130

Figure 5-19: A schematic elaborating the horizontal and vertical CT scanning layers of a cylindrical specimen.....	130
Figure 5-20: Image of Vertical CT scanning layer on a diametrical plane visualizing the exit delamination (282.6 m/min, 0.05 mm/rev). P.S. the blank space between the two grey coloured CFRP material is the drilled hole.....	131
Figure 5-21: Fibre pull-out in side view of internal damage obtained from CT scanning in a vertical layer (P.S. the vertical layer is not on a diametrical plane)	132
Figure 5-22: A schematic displaying the drilling direction, drilling depth and CT scanning layers for exit delamination calculations	133
Figure 5-23: DICOM image of a horizontal CT scanning layer exhibiting the delaminated area in a loop near hole-exit for a 6 mm diameter hole (282.6 m/min, 0.05 mm/rev)	133
Figure 5-24: Delaminated area w.r.t. depth in drilling direction near hole-exit (282.6 mm/min, 0.05 mm/rev in CD).....	134
Figure 5-25: Schematic for Maximum radius of a CT scanned layer in horizontal direction	135
Figure 5-26: Maximum radius variation from entrance to exit in a hole (9.42 mm/min, 0.05 mm/rev).....	135
Figure 5-27: Schematic for representing off-centre sectioning of holes for mounting and SEM observation.....	136
Figure 5-28: Sectioned hole mounted in EpoCure 2 resin system and polished	136
Figure 5-29: Crack propagation and fibre pull out (9.42 m/min UAD). The diagram in the inset shows the location of the specific damage in a mounted sample. ...	137
Figure 5-30: Fibre pull out depth measurement (282.6 m/min cutting speed, 0.05 mm/rev, CD). The diagram in the inset shows the location of the specific damage in a mounted sample.....	138
Figure 5-31: Fibre dis-orientation (282.6 m/min cutting speed, 0.05 mm/rev, CD). The diagram in the inset shows the location of the specific damage in a mounted sample.....	139
Figure 5-32: Disorientation of fibres during drilling of CFRP (282.6 m/min, 0.05 mm/rev, UAD). The diagram in the inset shows the location of the specific damage in a mounted sample.....	139
Figure 5-33: Exit delamination depth measurement on the first side of the hole (0.942 m/min, 0.05 mm/rev CD). The diagram in the inset shows the location of the specific damage in a mounted sample.	140
Figure 5-34: Exit delamination depth measurement on the second side of the hole (0.942 m/min, 0.05 mm/rev CD). The diagram in the inset shows the location of the specific damage in a mounted sample.	141
Figure 5-35: Schematic displaying two perpendicular planes of sectioning for assessment of damage variation in a hole in the two respective planes of sectioning	142
Figure 5-36: Setup for recording tool flank wear. ZEISS camera was attached to the microscope in connection with a laptop for imaging.....	144
Figure 5-37: Flank surface width measurement at three locations in a new tool	145
Figure 5-38: Flank surface width measurement at three locations in a worn tool	145
Figure 5-39: Flank area measurement in a new tool.....	146
Figure 5-40: Unworn flank area measurement in a worn tool.....	146
Figure 5-41: (a) Side and (b) front view of 3 flute twist drill used in current experimental study.....	148
Figure 5-42: Experimental set-up having dynamometer, fixture holding carbon fibre strip, ultrasonic tool holder and the 6 mm diameter drilling tool.....	149

Figure 5-43: A schematic representation of thermocouple setup for cutting temperature measurement.....	152
Figure 5-44: (a) Side and (b) front view of 1.5 mm diameter TiAlN coated Tungsten carbide 2-flute twist drill used in the current experiment for pilot-hole drilling.....	153
Figure 5-45: (a) Side and (b) front view of 6 mm diameter TiN coated HSS 2-flute twist drill used in the current experiment for drilling of main-hole and displaying chisel edge radius to be 748.88 μm	154
Figure 5-46: Drilling of a pilot hole with 1.5 mm diameter two-flute twist drill.....	155
Figure 5-47: (a) Localised disorientation in carbon fibres (b) disorientation of carbon fibres at drilling site.....	156
Figure 5-48: Top and side view of 2-flute twist drills used in the experiment.....	158
Figure 5-49: Margin angle measurement of twist drill through optical microscopy.....	158
Figure 5-50: Schematic of rake, margin and clearance angles in side view of drill.....	159
Figure 5-51: (a) top and (b) side views of two 2.5 mm diameter flute twist drills used for pilot holes.....	160
Figure 5-52: Experimental setup for pilot-hole drilling using tungsten carbide drill in Phase-3.....	162
Figure 6-1: Plots of effective normal rake angles calculated at (a) 0.942, (b) 9.42 (c) 94.2 and (d) 282.6 m/min cutting speeds in CD and UAD.....	165
Figure 6-2: Plots of axial clearance angles calculated at (a) 0.942, (b) 9.42 (c) 94.2 and (d) 282.6 m/min cutting speeds in CD and UAD.....	166
Figure 6-3: Thrust force profile at 282.6 m/min cutting speed in CD.....	168
Figure 6-4: Thrust force profile at 282.6 m/min cutting speed in UAD.....	169
Figure 6-5: Thrust force profile at 94.2 m/min cutting speed in CD.....	169
Figure 6-6: Thrust force profile at 94.2 m/min cutting speed in UAD.....	169
Figure 6-7: Thrust force profile at 9.42 m/min cutting speed in CD.....	170
Figure 6-8: Thrust force profile at 9.42 m/min cutting speed in UAD.....	170
Figure 6-9: Thrust force profile at 0.942 m/min cutting speed in CD.....	170
Figure 6-10: Thrust force profile at 0.942 m/min cutting speed in UAD.....	171
Figure 6-11: Image of tool displaying chip-out near chisel edge after drilling at 0.942 m/min cutting speed in UAD.....	171
Figure 6-12: Average thrust force variation in CD and UAD at all the cutting speeds with new tool.....	172
Figure 6-13: Thrust force plot for conventional drilling and UAD, obtained from worn tool (error bars indicate maximum and minimum values of forces during three times repetitions).....	174
Figure 6-14: Area delamination factor for the CT scanning samples.....	176
Figure 6-15: Variation of average fibre pull out obtained from CT scanning at all the cutting speeds.....	177
Figure 6-16: Maximum damage at the entrance of the holes obtained from worn tool at all the cutting speeds in CD and UAD.....	179
Figure 6-17: Average crack propagation at all the cutting speeds in CD and UAD with a new tool.....	181
Figure 6-18: Average fibre pull out in all the samples with a new tool.....	181
Figure 6-19: Variation of average damage depth at the internal cylindrical machined surface (internal damage) obtained from worn tool in CD and UAD at all the cutting speeds.....	183
Figure 6-20: Exit delamination at all the cutting speeds in CD and UAD with a new tool....	184
Figure 6-21: Maximum damage depth at exit obtained from worn tool in CD and UAD at all the cutting speeds.....	185

Figure 6-22: Visualisation of fibre-matrix debonding and crack propagation across the laminates near exit around the hole drilled at 9.42 m/min cutting speed and 0.05 mm/rev feed rate in CD	186
Figure 6-23: Machined surface, CD (0.942 m/min, 0.05 mm/rev)	187
Figure 6-24: Machined surface, UAD (0.942 m/min, 0.05 mm/rev).....	188
Figure 6-25: Machined surface, CD (282.6 m/min, 0.05 mm/rev)	188
Figure 6-26: Machined surface, UAD (282.6 m/min, 0.05 mm/rev).....	189
Figure 6-27: Plastic deformation of the smeared matrix on the machined surface after CD at higher magnification (0.942 m/min, 0.05 mm/rev).....	190
Figure 6-28: Plastic deformation of the smeared matrix on the machined surface after UAD at higher magnification (0.942 m/min, 0.05 mm/rev)	190
Figure 6-29: Sharp cracks in CD (9.42 m/min, 0.05 mm/rev)	191
Figure 6-30: Machined Matrix in UAD (9.42 m/min, 0.05 mm/rev).....	192
Figure 6-31: Machined matrix surface in CD (94.2 m/min, 0.05 mm/rev)	192
Figure 6-32: Machined matrix surface in UAD (94.2 m/min, 0.05 mm/rev).....	193
Figure 6-33: Cutting temperature measurement at various cutting speeds in CD and UAD.....	193
Figure 6-34: Large fragment of the chip obtained in CD (0.942 m/min, 0.05 mm/rev)	197
Figure 6-35: Large chip fragment found in UAD (282.6 m/min, 0.05 mm/rev).....	197
Figure 6-36: Long and short, broken chip-fragments in UAD (0.942 m/min, 0.05 mm/rev).....	198
Figure 6-37: Effective normal rake angle in CD and UAD at 100 m/min cutting speeds for the given tool geometry and UAD parameters	208
Figure 6-38: Effective axial clearance angle in CD and UAD at 100 m/min cutting speeds for the given tool geometry and UAD parameters	208
Figure 6-39: Thrust force profile in the case of CD without pilot-hole.....	210
Figure 6-40: Thrust force profile in the case of CD with pilot-hole	210
Figure 6-41: Side view of twist drill used in the present experiment.....	211
Figure 6-42: Schematic of full drill engagement in (a) without and (b) with pilot-hole drilling.....	212
Figure 6-43: Identification of the points of full drill engagement during drilling for the case of 1 st hole in conventional with pilot hole drilling and measurement of average thrust force between these two points in the software 'Dynoware'.....	213
Figure 6-44: Thrust force variation obtained in the cases of CD, UAD, with and without pilot hole.....	215
Figure 6-45: Average torque variation obtained in the cases of CD, UAD, with and without pilot hole	217
Figure 6-46: Variation of tool flank wear in the cases of CD, UAD with and without pilot holes.....	219
Figure 6-47: Chisel edge wear area after drilling of every hole in the cases of conventional and ultrasonic without pilot-hole drilling.....	220
Figure 6-48: SEM image of chisel edge displaying chisel edge condition in the case of CD without pilot hole drilling after drilling of 10 holes	221
Figure 6-49: SEM image of chisel edge displaying chisel edge condition in the case of UAD without pilot hole drilling after drilling of 10 holes	221
Figure 6-50: Maximum damage depth measurement in (a) side 1 and (b) side 2 of 5 th hole in the case of CD with pilot. The overall maximum depth at entrance for this hole would be 2137.892 μm which is the maximum of the two measurements.....	223

Figure 6-51: Maximum damage depth at entrance for 1 st , 5 th and 10 th hole in all the cases of conventional, ultrasonic, with and without pilot-hole drilling	224
Figure 6-52: Plot of Maximum damage depth at exit for 1 st , 5 th and 10 th hole in all the cases of conventional, ultrasonic, with and without pilot-hole drilling	226
Figure 6-53: Depth of Fibre pull out measurement in the 1 st hole in the case of conventional drilling with pilot hole	227
Figure 6-54: Depth of Fibre disorientation measurement in the 5 th hole in the case of conventional drilling with pilot hole	227
Figure 6-55: Damage depth near entrance in the 1 st hole in the case of conventional with pilot-hole drilling.....	228
Figure 6-56: Damage depth near exit in the 1 st hole in the case of conventional with pilot-hole drilling.....	228
Figure 6-57: Plot of internal damage in 1 st , 5 th and 10 th holes in all the cases of conventional, ultrasonic, with and without pilot-hole drilling	229
Figure 6-58: Burnt matrix in 5 th hole of conventional without pilot-hole drilling.....	231
Figure 6-59: Traces of burnt matrix in 5 th hole of Ultrasonic without pilot-hole drilling.....	231
Figure 6-60: Burnt matrix in 10 th hole of conventional with pilot-hole drilling	232
Figure 6-61: Burnt matrix in 10 th hole of Ultrasonic without pilot-hole drilling	232
Figure 6-62: Chip fragments obtained at 100 m/min cutting speed in CD without pilot from 1 st hole	234
Figure 6-63: Chip fragments obtained at 100 m/min cutting speed in UAD without pilot from 1 st hole	234
Figure 6-64: Burnt matrix in the chip fragments at 100 m/min cutting speed in CD without pilot from 10 th hole	235
Figure 6-65: Burnt matrix in the chip fragments obtained at 100 m/min cutting speed and 0.05 mm/rev feed rate in UAD without pilot from 5 th hole	235
Figure 6-66: Effective normal rake angles obtained at 10 m/min cutting speed and 0.05 m/rev feed rate in CD and UAD (39740 Hz frequency and 7.6 μ m amplitude)	243
Figure 6-67: Effective normal rake angles obtained at 100 m/min cutting speed and 0.05 m/rev feed rate in CD and UAD (40300 Hz frequency and 6.8 μ m amplitude)	243
Figure 6-68: Effective axial clearance angles obtained at 10 m/min cutting speed and 0.05 m/rev feed rate in CD and UAD (39740 Hz frequency and 7.6 μ m amplitude)	244
Figure 6-69: Effective axial clearance angles obtained at 100 m/min cutting speed and 0.05 m/rev feed rate in CD and UAD (40300 Hz frequency and 6.8 μ m amplitude)	244
Figure 6-70: Thrust force profiles in CD and UAD (10 m/min, 0.05 mm/rev).....	246
Figure 6-71: Thrust force profiles in CD and UAD (100 m/min, 0.05 mm/rev).....	246
Figure 6-72: Thrust force variation at 10 m/min cutting speed and 0.05 mm/rev feed rate in all the cases of CD, UAD, with and without pilot holes.....	249
Figure 6-73: Thrust force variation at 100 m/min cutting speed and 0.05 mm/rev in all the cases of CD, UAD, with and without pilot holes	249
Figure 6-74: Thrust force from chisel edge in CD and UAD at 10 and 100 m/min and 0.05 mm/rev	251
Figure 6-75: Torque variation at 10 m/min cutting speed and 0.05 mm/rev feed rate in all the cases of CD, UAD, with and without pilot holes	254
Figure 6-76: Torque variation at 100 m/min cutting speed and 0.05 mm/rev feed rate in all the cases of CD, UAD, with and without pilot holes	254

Figure 6-77: Variation of average tool wear at 10 m/min cutting speed and 0.05 mm/rev feed rate for all the cases with respect to number of drilled holes	256
Figure 6-78: Variation of average tool wear at 100 m/min cutting speed and 0.05 mm/rev feed rate for all the cases with respect to number of drilled holes	257
Figure 6-79: Schematic showing rake angles in a (a) new and a (b) worn tool. It can be seen that the rake angle in a worn tool becomes negative if the uncut chip thickness becomes lower than the radius of curvature of cutting edge.....	259
Figure 6-80: Measurement of radius of curvature at the outer margin of cutting edge of tool through optical microscopy after drilling of 60 holes in 'UAD with pilot' at 10 m/min.....	260
Figure 6-81: Measurement of chisel edge thickness for the drill used in present experiment	261
Figure 6-82: Zero delamination damage at entrance at 10 m/min cutting speed in CD with pilot hole drilling in the first hole.....	263
Figure 6-83: Variation in maximum damage at entrance at 10 m/min cutting speed and 0.05 mm/rev feed rate in CD and UAD	265
Figure 6-84: Variation in maximum damage at entrance at 100 m/min cutting speed and 0.05 mm/rev feed rate in CD and UAD	265
Figure 6-85: Measurement of maximum depth of crack initiation and maximum damage depth in the case of conventional drilling without pilot at 10 m/min at 59 th hole (maximum depth of crack initiation = 364.06 μm and maximum damage depth = 718.95 μm).....	267
Figure 6-86: Plot of maximum depth of crack initiation at entrance at 10 m/min cutting speed and 0.05 mm/rev feed rate	267
Figure 6-87: Plot of maximum depth of crack initiation at entrance at 100 m/min cutting speed and 0.05 mm/rev feed rate	268
Figure 6-88: Zero delamination damage at exit at 100 m/min cutting speed in UAD with pilot hole drilling in the first hole.....	270
Figure 6-89: Variation in maximum damage at the exit at 10 m/min cutting speed and 0.05 mm/rev feed rate in CD and UAD	271
Figure 6-90: Variation in maximum damage at the exit at 100 m/min cutting speed and 0.05 mm/rev feed rate in CD and UAD	272
Figure 6-91: Measurement of damage height and depth in the case of conventional drilling without pilot at 10 m/min at 60 th hole (maximum depth of crack initiation = 728.12 μm and maximum damage depth = 1058.89 μm)	273
Figure 6-92: Plot of maximum crack initiation depth at exit at 10 m/min cutting speed and 0.05 mm/rev feed rate.....	274
Figure 6-93: Plot of maximum crack initiation depth at exit at 100 m/min cutting speed and 0.05 mm/rev feed rate	274
Figure 6-94: Variation of internal damage at 10 m/min and 0.05 mm/rev feed rate in all the cases of CD, UAD, with and without pilot holes.....	277
Figure 6-95: Variation of internal damage at 100 m/min and 0.05 mm/rev feed rate in all the cases of CD, UAD, with and without pilot holes.....	277
Figure 6-96: Chip fragments obtained in the hole number 1 at 10 m/min cutting speed in UAD.....	279
Figure 6-97: Chip fragments obtained in the hole number 1 at 100 m/min cutting speed in UAD	280

Figure 6-98: Effective normal rake angles at 10 m/min cutting speed and 26.5 mm/min feed rate in CD and UAD	289
Figure 6-99: Effective normal rake angles at 100 m/min cutting speed and 26.5 mm/min feed rate in CD and UAD	290
Figure 6-100: Comparison of percentage thrust force reduction due to ultrasonic assistance between 10 and 100 m/min cutting speeds and 26.5 mm/min feed rate in the case of 'without pilot hole' drilling.....	292
Figure 6-101: Comparison of percentage thrust force reduction due to ultrasonic assistance between 10 and 100 m/min cutting speeds and 26.5 mm/min feed rate in the case of 'with pilot hole' drilling	292

List of Abbreviations and nomenclatures

α	Rake angle
α_x	Axial rake angle
α_o	Orthogonal rake angle
α_n	Normal rake angle
α_{xW}	Axial rake angle in work reference system (effective rake angle)
α_{xDi}	Dynamic axial rake angle at a point 'i' of cutting edge in a twist drill
α_{xWi}	Dynamic axial rake angle at a point 'i' of cutting edge in a twist drill in work reference system
γ	Rake angle
γ_x	Axial rake angle
γ_o	Orthogonal rake angle
γ_n	Normal rake angle
γ_{xW}	Axial rake angle in work reference system (effective rake angle)
γ_{xDi}	Dynamic axial rake angle at a point 'i' of cutting edge
γ_{xWi}	Dynamic axial rake angle at a point 'i' of cutting edge in work reference system
δ	Wedge angle
θ	Helix angle of twist drill
λ	Inclination angle of cutting edge in a single point turning tool
λ_{Wi}	Dynamic inclination angle of cutting edge at point 'i' in a twist drill in work reference system
μ	Angle between reference plane in work reference system and original reference plane in single point turning tool
μ_i	Angle between π_{RD_i} and π_{RW_i} at point 'i' of cutting edge in a twist drill
μm	micro meter
π_R	Reference plane
π_x	Axial plane
π_o	Orthogonal plane
π_n	Normal plane
π_{RD_i}	Dynamic reference plane at point 'i' of cutting edge in a twist drill
π_{RW_i}	Dynamic reference plane at point 'i' of cutting edge in a twist drill in work reference system
ρ	Half cone angle of twist drill
Φ_{Di}	Dynamic cutting edge angle at point 'i' of cutting edge in a twist drill
Φ_S	Static cutting edge angle in a twist drill
Φ_{Wi}	Dynamic cutting edge angle in at point 'i' of cutting edge in a twist drill in work reference system
ψ	Chisel edge angle
ω	Oscillation angular frequency
$^\circ$	Degree
$^\circ C$	Degree Celsius
a	Oscillation amplitude
CCC	Carbon-carbon composites
CD	Conventional drilling
CFRP	Carbon fibre reinforced plastics

1: Introduction

cm^3	Cubic centimetre
CMC	Ceramic matrix composites
CMM	Coordinate measuring machine
CT	Computed tomography
d	Uncut chip thickness
f	Oscillation frequency
FRP	Fibre reinforced plastics
GPa	Giga Pascal
HSS	High speed steel
Hz	Hertz
kg	kilogram
kHz	kilo hertz
m	meter
m^2	Square meter
min	minute
mm	millimetre
mm^2	Square millimetre
MMC	Metal matrix composites
MPa	Mega Pascal
n	rotational frequency of drill per minute
N	Newton
N-cm	Newton centimetre
PCD	Poly crystalline diamond
PMC	Polymer matrix composites
r	Radius of twist drill
r_c	Chisel edge radius
r_i	Radial distance of a point 'i' of cutting edge from central axis in a twist drill
rev	revolutions
rpm	revolutions per minute
s	second
UAD	Ultrasonic assisted drilling
VAD	Vibration assisted drilling
V_c	Cutting velocity
V_{ci}	Cutting velocity at point 'i' of cutting edge in a twist drill due to its rotational motion
V_{cwi}	Resultant cutting velocity at point 'i' of cutting edge in a twist drill
V_f	Feed velocity in mm/min
V_{fi}	Resultant feed velocity at point 'i' of cutting edge
V_{fiCD}	Feed velocity component due to conventional feed motion at point 'i' of cutting edge in a twist drill
V_{fiUAD}	Feed velocity component due to ultrasonic oscillations at point 'i' of cutting edge in a twist drill
w	Half web thickness of twist drill
WC	Tungsten carbide
S_0	Feed rate in mm/rev
t	Time

1 Introduction

1.1 Background

Polymeric matrix composites (PMC), especially carbon fibre reinforced plastics (CFRPs), have been attractive as aircraft and aerospace structural components due to their superior properties (lighter weight and higher specific strength) compared to metals [1-4] which have led to greater weight savings resulting in greater payload, longer range and fuel saving [5].

In spite of curing to final shape, machining of CFRPs is required at several stages of production e.g., cutting and drilling of holes. The mechanical drilling process is one of the final processes in the manufacturing of the composite components and is required to generate holes in order to fasten the components together by bolts and rivets [1]. In a private communication [6], it was confirmed by BAE Systems that there are almost 3000 drilled holes required to drill for a single wing of F-35 aircraft and at present many resources and cost are required to produce the holes with minimum damage. Thus, drilling process plays an important role in the aircraft manufacturing for assembling the components through the use of rivets and bolts. Due to low thermal tolerance, heterogeneous, anisotropic and abrasive nature of CFRP material, workpiece damage is induced during conventional drilling (CD). Such damage includes matrix cracking, fibre pull-out on the internal cylindrical surface, thermal degradation of the matrix phase and delamination at the entrance and exit of drilled holes [3, 7-11]. Delamination during drilling has been reported to be the most detrimental damage which causes 60% of component rejection in the aircraft industry [12]. Such damage induced by drilling degrades the mechanical bearing strength of the component resulting in lower in-service life under fatigue

1: Introduction

loads [3, 11]. The avoidance of such drilling induced damage has been found to be impossible through CD and therefore, a tolerance criterion has been defined by the companies for acceptance of the damaged parts, for example, the criteria defined by BAE Systems for drilled CFRP parts is as follows –

- i. Delamination cannot extend beyond a depth of one structural ply
- ii. Any instance of a splinter for a hole or edge on external surfaces cannot be more than 3 mm wide
- iii. Any instance of a splinter for a hole or edge on external surfaces cannot be more than 3 mm long
- iv. No more than 10% of total edge of part length can be splintered (external surface)
- v. No more than 25% of the total circumference of a hole can be splintered (external surface)

In spite of such damage criteria, the production of even such low damage around holes is difficult and it requires a lot of resources and huge production cost (as communicated by BAE Systems in a private communication [6]). Therefore, avoidance of such drilling induced damage is a major concern for aircraft and aerospace industries and they are looking for alternative and efficient hole producing processes which could avoid the workpiece damage during drilling and reduce the production cost.

Several attempts have been made by researchers in order to reduce the damage during drilling of CFRP. There is a general consensus amongst researchers for reducing thrust force during drilling in order to reduce exit delamination [13]. The quantification and reduction of the damage on the internal cylindrical machined in a

hole (referred as ‘internal damage’ in the present research) is still a topic of research at present. The attempts by researchers for reducing the thrust force during drilling include optimisation of machining parameters, advanced drilling tool geometries and drilling using a pilot hole [13-22]. Other groups of researchers have attempted to reduce the damage during drilling through non-conventional manufacturing processes such as laser material processing, ultrasonic machining, water jet drilling and vibration assisted drilling [23-34]. Laser processing typically results in severe thermal damage (fibre swelling and matrix evaporation) [35] while water jet drilling causes matrix wash out and delamination near the exit [36, 37]. While ultrasonic machining did not cause any significant damage, it was found to be a slow process and hence not useful for drilling a large number of holes [31]. Authors have reported longer tool life and lower thrust force through the use of vibration assisted drilling [38]. Although the vibrations at low vibration frequencies in the range of 30 Hz to 600 Hz [30, 38, 39] caused a reduction in thrust force and exit delamination, the effects have been observed to be most effective when the frequency of vibrations was kept above 20 kHz. This type of drilling has been termed as ‘Ultrasonic Assisted Drilling (UAD)’ [27, 29].

Ultrasonic Assisted Drilling (UAD) is a process in which vibrations having an ultrasonic frequency (i.e. frequency in the access of 20 kHz) are imposed during drilling either on the workpiece or the drill in the axial direction. In the drilling of difficult-to-machine metals such as nickel-based superalloys and titanium alloys, UAD process has been found to cause a reduction in thrust and cutting forces and reduced length of exit burrs in the range of selected machining parameters [25-29]. To realise the effect of UAD on CFRP in a recent research, Makhdum et al. [40] have attempted UAD of CFRP with a new tool and reported 51% reduction in exit

delamination, 47% reduction in surface roughness and 90% reduction in thrust force due to ultrasonic assistance. Nevertheless, no justification has been provided by the authors for the selection of the specific parameters for drilling of both CFRP and metals. Other than drilling, ultrasonic assistance has also been applied to other processes such as turning and a reduction in cutting forces during machining has been reported [41-46]. The reason for such a reduction in cutting forces has been reported to be due to the intermittent cutting action of the tool. Patil et al. [47] have reported that during ultrasonic assisted turning process, the tool and material contact is disconnected in every ultrasonic oscillation cycle which causes variable stresses during each oscillation cycle. The mean stress per oscillation cycle has been reported to be lower than that in conventional machining and hence, the average machining force is reduced. The same phenomenon of intermittent cutting action has been surmised during UAD process and therefore, the reason for the reduction in cutting and thrust forces during UAD has been claimed to be intermittent cutting action of the drill without producing conclusive evidence [23-29, 40].

Though the importance and potential of UAD process has been recognised by the researchers yet this process has not been explored in detail with respect to machining parameters while drilling CFRP. The specific mechanism causing the beneficial effect of ultrasonic assistance still remains a mystery for the researchers. Therefore, there is a gap in the literature for developing a fundamental understanding of mechanism causing the beneficial effects of ultrasonic assistance in UAD of CFRP which would help in identifying the appropriate machining parameters resulting in minimum workpiece damage.

1.2 Aims and objectives

The research background motivates for the identification of appropriate machining parameters in UAD. The present research aimed at identifying the appropriate cutting speed in UAD resulting in minimum overall workpiece damage during drilling of CFRP. This aim was achieved through the following research objectives–

1. Determine the mechanism associated with cutting edges in a twist drill causing the reduction in machining forces in UAD of CFRP and its relationship with cutting speed.
2. Determine the underlying relationship in-between machining forces, overall workpiece damage (entrance/exit delamination and internal damage) and cutting speed in CD and UAD of CFRP.
3. Determine the influence of tool wear on the effectiveness of UAD with respect to cutting speed.

2 Introduction to CFRP

As the name suggests, carbon fibre reinforced plastics (CFRP) are the plastics which are “reinforced” with carbon fibres i.e., it is a specific type of composite material having carbon fibres as reinforcement and plastic as the matrix material surrounding carbon fibres [48]. CFRP is a type of specific class of composites – polymeric matrix composites (PMCs). Therefore, before discussing the importance of CFRP, it is necessary to have a general overview of the composite material itself. Thus, the current chapter overviews composite material and its types, discusses PMCs thereby explaining the effectiveness of CFRP and its applications.

2.1 Overview of composite materials

According to Sheikh-Ahmad [49], “*Composite materials, thus far can be defined as materials consisting of two or more constituents (phases) that are combined at the macroscopic level and are not soluble in each other.*” A composite material has two distinct constituents (phases) known as – the reinforcement and the matrix.

2.1.1 Reinforcement

The reinforcement is the part of the composite which carries the load. The main purpose of the reinforcement is to distribute and sustain with the load [50]. There are mainly three types of the reinforcements currently in use – fibres, whiskers and particulates. Fibres have a long axis, length and diameter ratio (i.e. aspect ratio) compared to that in particles [48, 49]. According to Kalpakjian and Schmid [51], the aspect ratio of long continuous carbon fibres varies between 200 – 500. All these reinforcements can be incorporated into a matrix material to form a composite either in continuous lengths or in chopped (discontinuous) lengths based upon the requirements of the mechanical properties. Whiskers are fibrous single-crystal

structures in the classification of discontinuous reinforcements. Whiskers have small diameters of 0.1 to 2 μm as compared to their length. There is a disagreement between the aspect ratios of whiskers amongst the authors. According to Schwartz [50], the aspect ratio of whiskers ranges between 50 – 100 while Kalpakjian and Schmid [51] report it to be between 100 – 15000 which is even larger than that of continuous long fibres. Particulates are the most common and cheapest discontinuous reinforcement. Particulates are generally used for producing isotropic metal matrix composite. Particulates do not have any definite orientation and vary between 2 – 40 μm in size [50, 52]. Most common types of particulates are aluminium oxide, silicon carbide, titanium carbide and tungsten carbide [50]. The reinforcement in a composite material is oriented in various directions. In addition, the distribution of reinforcement in the composite is inhomogeneous in general. Therefore, the properties of a composite material are direction specific which makes them an anisotropic material. The nature of a composite tends to isotropic as the randomness of reinforcement increases and its size decreases, Figure 2-1 [49].

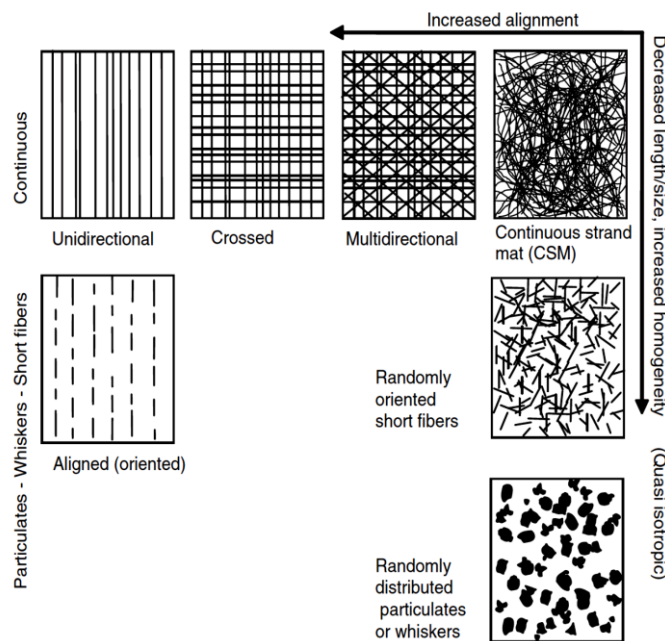


Figure 2-1: Property variation in composite materials with respect to size and shape of reinforcement [49]

2.1.2 Matrix

The matrix is the medium which surrounds and supports the reinforcements. The purpose of a matrix is to support and keep the reinforcement in the desired location and orientation and protect it from the environmental damage e.g. chemicals, humidity, and thermal effects [48, 50, 53]. The matrix transfers the load to the reinforcement and provides toughness and resistance to damage, impact and abrasion. The matrix provides lateral support to fibres against fibre-buckling under compressive load in fibre reinforced composites, in particular. The material of the matrix can be a polymer, a metal or a ceramic [2, 50, 54]. Composites are generally classified based upon the matrix material [49, 50, 54, 55]. Metal matrix composites (MMC) are the composites containing metal alloys as a matrix with reinforcement. The reinforcement can be short fibres in the form of single crystals or fine particles and continuous fibres. MMC have the ability to provide the required strength with minimum weight and volume which makes them useful for various structural and non-structural applications [50, 56, 57]. Ceramic Matrix Composites (CMC) are manufactured by reinforcing Silicon carbide (SiC) fibres into a Ceramic matrix such as Al_2O_3 , Si_3N_4 or SiC. Similar to MMC, the reinforcement can be a continuous fibre, short fibre or some discontinuous whisker platelets in CMC. CMC are useful for applications at higher temperature ranges above 1600°C due to their strength retention and corrosion and erosion resistance properties at elevated temperatures. CMC are used in furnace materials, gas turbines and heat engines [54, 58]. Polymer Matrix Composites (PMC) are formed by combining fibre reinforcements with organic polymer matrices. From the manufacturing point of view, PMC are much easier to manufacture than MMC and CMC because of relatively low processing temperatures required for fabrication [59]. PMC can be moulded into complex and

large shapes and hence are useful in various aircraft and aerospace applications [50, 59]. The advantage of MMC over PMC is the maximum operating temperature. For example, Boron/Aluminium MMC offers useful mechanical properties up to 510°C, whereas an equivalent Boron/Epoxy PMC composite is limited to about 190°C. In addition, MMCs such as Graphite/Aluminium, Graphite/Magnesium, and Graphite/Copper exhibit higher thermal conductivity because of the significant contribution from the metallic matrix [60]. However, MMC have a larger weight than PMC. The PMC are discussed in detail in Section 2.2. Carbon-Carbon Composites (CCC) contain carbon fibre reinforcements having a carbonaceous matrix. Manufacturing of CCC differs with that of PMC in a way that in CCC, the organic matrix material is heated till it gets converted into carbon. This type of material is applicable in the components where resistance to high temperature (more than 1370°C) and resistance to thermal shock is desired [50, 61, 62]. A relative comparison amongst the mechanical properties in fibre-axis direction of composite materials in various matrix systems is presented in Table 2-1.

Table 2-1: Mechanical properties of typical composite materials in the fibre-axis direction in various matrix systems, Note: ^aData from [60], ^bData from [63], ^cData from[64], ^dData from [65]

Type of composite	Material	Density (g/cm ³)	Young's Modulus (GPa)	Tensile strength (MPa)
MMC ^a	P100/6061Al Unidirectional	2.5	342.5	905
	Graphite/Al (GA 7-230), discontinuously reinforced	2.45	88.7	76.8
CMC ^b	C/SiC	1.8-2.8	30-150	80-540
CCC ^c	Carbon-Carbon	1.3-2.5	< 300	< 900
PMC ^d	CFRP (Unidirectional) High modulus	1.6	220	800

2.2 Polymer Matrix Composites (PMC)

PMC with fibre reinforcement are the most common form of composites used for commercial and high-performance applications due to a lighter weight to metals and higher strength to weight characteristics. These characteristics make PMC useful in many applications in the military, aircraft, aerospace and marine industries [12, 49, 66, 67]. The application of the PMC can be realised from the fact that PMCs occupy 50% by weight in the Boeing 787 aircraft [48]. The applications of PMC in various industries are summarised in Table 2-2.

Table 2-2: Applications of PMCs in various industrial areas [49]

Application area	Examples
Aerospace	Space structures, satellite antenna, rocket motor cases, high-pressure fuel tanks, nose cones, launch tubes
Aircraft	Fairings, access doors, stiffness, floor beams, entire wings, wing skins, wing spars, fuselage, radomes, vertical and horizontal stabilisers, helicopter blades, landing gear doors, seats, interior panels
Chemical	Pipes, tanks, pressure vessels, hoppers, valves, pumps, impellers
Construction	Bridges and walkways including decks, handrails, cables, frames, grating
Domestic	Interior and exterior panels, chairs, tables, baths, shower units, ladders
Electrical	Panels, housing, switchgear, insulators, connectors
Leisure	Tennis racquets, ski poles, skis, golf clubs, protective helmets, fishing rods, playground equipment, bicycle frames
Marine	Hulls, decks, masts, engine shrouds, interior panels
Medical	Prostheses, wheelchairs, orthofies, medical equipment
Transportation	Body panels, dashboards, frames, cabs, spoilers, front end, bumpers, leaf springs, drive shafts

2.2.1 Fibre Reinforcement for PMC

Glass, aramid and carbon fibres are the most common fibres used for the manufacturing of polymeric composite materials. **Glass fibres** are strong,

electrically nonconductive, corrosion resistant, amorphous and isotropic in nature. E-glass and S-glass are the two main categories of glass fibres out of which E-glass has lower cost and it is widespread for all the commercially available reinforcing fibres. S-glass has higher tensile strength as compared to E-glass and is used in aircraft components and missile casings [55].

Aramid fibres are manufactured by extrusion of the acidic solution of a polycondensation product of terephthaloyl chloride and p-phenylenediamine. Aramid fibres are used for tire cords and brake friction materials in the automotive industry. Aramid fibres are also used in many marine and aerospace applications where light weight, high tensile strength and resistance to impact properties are required. [48, 54].

Carbon and graphite fibres have a wide range of tensile modulus between 35 GPa (transverse) to 1000 GPa (fibre axis direction) [48]. Although low impact resistance is a disadvantage of carbon fibres, negative coefficient of thermal expansion ($-0.6 \times 10^{-6}/^{\circ}\text{K}$ [49]), high specific tensile strength (1377 kN-m/kg for high strength carbon fibre [68]) and high specific Young's modulus (127×10^6 N-m/kg for high strength carbon fibre [68]) in the axial direction as compared to metals (refer to Table 2-3 for metals) make carbon fibres useful for aircraft and aerospace industries where weight saving is more important than cost reduction [55]. Carbon fibres generally have the highest stiffness, strength and fatigue properties of all the fibres available for PMC [54]. Carbon fibres have lower carbon content (93% to 95%) as compared to the graphite fibres (more than 99%). The higher axial strength in the carbon fibre is the result of the strong covalent bonds (i.e., bond energy is 525 kJ/mol) along the basal planes in the graphite structures. However, since all the basal planes in the graphite structure are attached to each other with the weak van

Der Waal forces (bond energy is 10 kJ/mol), the strength transverse to the basal planes is less in the carbon fibres (1000 GPa modulus in axial direction and 35 GPa in transverse direction [48]). Figure 2-2 displays the covalent bond in a basal plane and van der Waals force amongst the basal planes. Hence, in order to manufacture good quality carbon fibres, alignment of all the basal planes along the axis of carbon fibre is important which increases its strength along the axis. This is generally performed by increasing the graphitization heat treatment temperature. The alignment of basal planes in the carbon fibre is shown in Figure 2-3 [59].

As mentioned by Sheikh Ahmad [49], out of glass, aramid and carbon fibres, carbon fibres have maximum Young's modulus of 400 GPa while glass fibres have minimum Young's Modulus of 80 GPa in the direction parallel to the fibre axis.

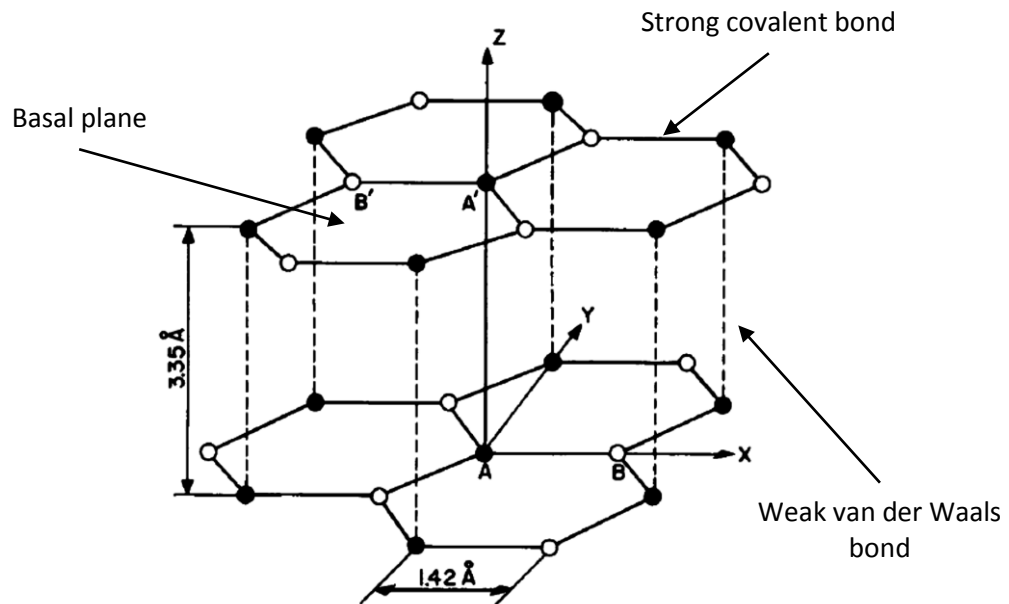


Figure 2-2: Strong covalent bonds in the basal planes and weak van der Waals bonds amongst the basal planes in the graphite structure [59]

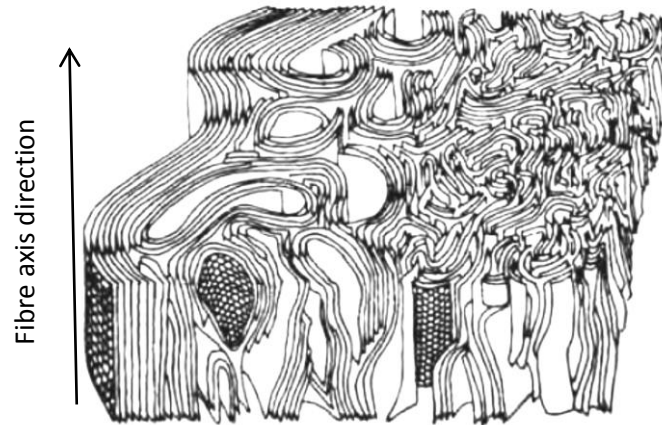


Figure 2-3: Alignment of basal planes in carbon fibres [69]

2.2.2 Matrix for PMC

Matrix materials for PMCS are broadly segmented into two main categories – thermoset and thermoplastics.

Thermosets are monomers which have low molecular weight and the low viscosity. These monomers when heated, are joined by cross links between them and converted into three-dimensional cross-linked infusible and insoluble structures due to a chemical polymerization reaction driven by the heat generated by the chemical reaction itself (an exothermic reaction) as shown in Figure 2-4. If necessary, heat is also added externally to accelerate the rate of polymerization. During the curing process, as the reaction progresses, the intermolecular volume decreases, the viscosity increases and a rubbery solid is produced. Further heating results in additional cross-linking of strong covalent bonds until the whole resin is cured [48, 55, 59]. Once the resin is cured, thermosets cannot be reshaped further by additional heating, instead additional heating results in thermal degradation. However, according to Mallick [55], if the cross-link density is less in thermosets, it may still be possible to soften them at elevated temperatures. Due to high cross link densities,

thermosets are inherently brittle unless some steps are taken to enhance their toughness.

The brittle nature of thermoset matrix creates a lot of challenges during its machining which are discussed in detail in Chapter 3. Also, cured thermoset polymers have a tendency to absorb moisture from the atmosphere. Moisture absorption softens the matrix and leads to poorer fibre-matrix adhesion and hence, the mechanical strength of the matrix of the composite material is affected [70, 71]. Moisture absorption property of thermosets also limits the application of cutting fluid during machining of thermosets. The moisture absorbed from the cutting fluid would affect the mechanical strength of the component being machined. Polyesters, vinyl esters, epoxies, bismaleimides, cyanate esters, polyimides, and phenolics are a few examples of the thermoset matrix materials. The processing temperature for thermoset epoxies for curing is in the range of 120 to 175°C [50]. Amongst the thermosets, epoxy and cyanate esters demonstrate low shrinkage after curing allowing high fabrication accuracy. Therefore, due to high dimensional accuracy, high glass transition temperature (e.g., 265°C for cyanate esters [55]), high strength and stiffness along with lighter weight compared to metal alloys, epoxies and cyanate esters are also used for aerospace applications such as wing box, wing panel, satellite antenna etc. [3, 48, 72] while polyamides, polybenzimidazoles (PBI), polyphenyl quinoxaline (PPQ), matrices are used in high-temperature aerospace applications in the range of 250°C to 400°C [54]. According to Campbell [48], the main disadvantage of thermoset matrix is their tendency to delaminate when impacted due to their low toughness and brittle nature.

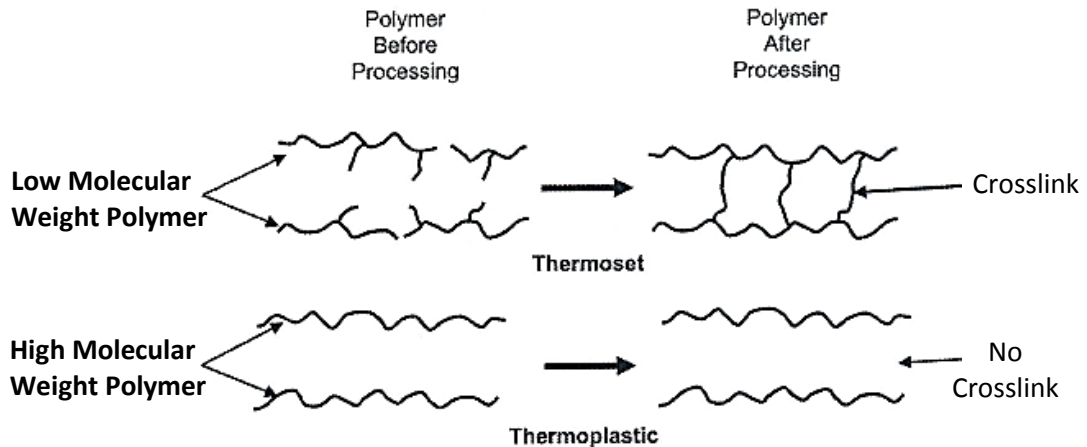


Figure 2-4: Curing process of thermoset and thermoplastic resins [48]

Thermoplastics are the long carbon chain polymers having high molecular weights with no chemical cross-linking between them and are fully reacted prior to thermal processing. These molecules are held together by weak intermolecular van der Waals forces and hydrogen bonding. Upon heating, these bonds are broken temporarily which allows relative movement of molecules leading to a reshaping of the object. Upon cooling the molecules freeze on their new places and the intermolecular weak van der Waals forces and hydrogen bonding are restored resulting in a new shape of the overall object. Thus the shape of thermoplastics can be altered as many times as required by heating them, unlike thermosets [2, 48]. Also, no chemical reaction takes place when thermoplastics are heated. Thermoplastics have a lower tendency of moisture absorption in comparison to thermosets. High-performance thermoplastics require temperature in the range of 260 to 465°C for thermal processing. Polyether ether ketone (PEEK), Polyether ketone ketone (PEKK), Polyether imide (PEI), Polyphenylene Sulfide (PSUL) and Polypropylene are a few examples of thermoplastic matrix materials [50]. Thermoplastic polymers like nylons, polyethylene terephthalate (PET), polycarbonate (PC) are used along with discontinuous fibres in the injection

moulded articles while thermoplastics like polyamide-imide (PAI), polyether ether ketone (PEEK), polysulfone (PSUL) and polyether imide (PEI) are used for high-temperature applications with continuous reinforced fibres [54].

2.3 Carbon fibre reinforced plastics (CFRP)

Carbon fibre reinforced plastics are a specific type of PMCs containing carbon fibres as reinforcement and thermosets or thermoplastics as matrix material. The orientation of fibres can be unidirectional, woven or multidirectional in the overall CFRP structure based upon the requirement of the component [73-77]. Table 2-3 compares the density, young's modulus, tensile strength, specific modulus and specific strength of CFRP to Aluminium and steel alloys. It can be seen from Table 2-3 that CFRP possesses higher tensile strength and young's modulus. In addition, it contains highest specific strength.

Table 2-3: Comparison of density, Young's Modulus, tensile strength, specific Modulus and specific strength of CFRP to metals, Note: ^adata from [67], ^bdata from [65]

Material	Density (g/cm³)	Young's Modulus (GPa)	Tensile strength (MPa)	Specific Modulus (x10⁶ N- m/kg)	Specific strength (kN-m/kg)
Aluminium alloys ^a (7075 T6)	2.8	71	572	25.36	204.29
Steel alloy ^a (1020 Cold drawn)	7.85	207	420	26.37	53.5
CFRP ^b (Unidirectional) High strength	1.6	145	1200	90.63	750
CFRP ^b (Unidirectional) High modulus	1.6	220	800	137.5	500

Figure 2-5 compares the specific strength and specific modulus of PMCs having glass, aramid and carbon fibres with those of metal alloys used in aerospace industry.

It is clear from Figure 2-5 that CFRP outperforms other aerospace metal alloys and PMCs when specific strength and specific modulus are compared. Thus, Table 2-3 and Figure 2-5 clearly illustrate the usefulness CFRP comparison to metal alloys for aerospace applications.

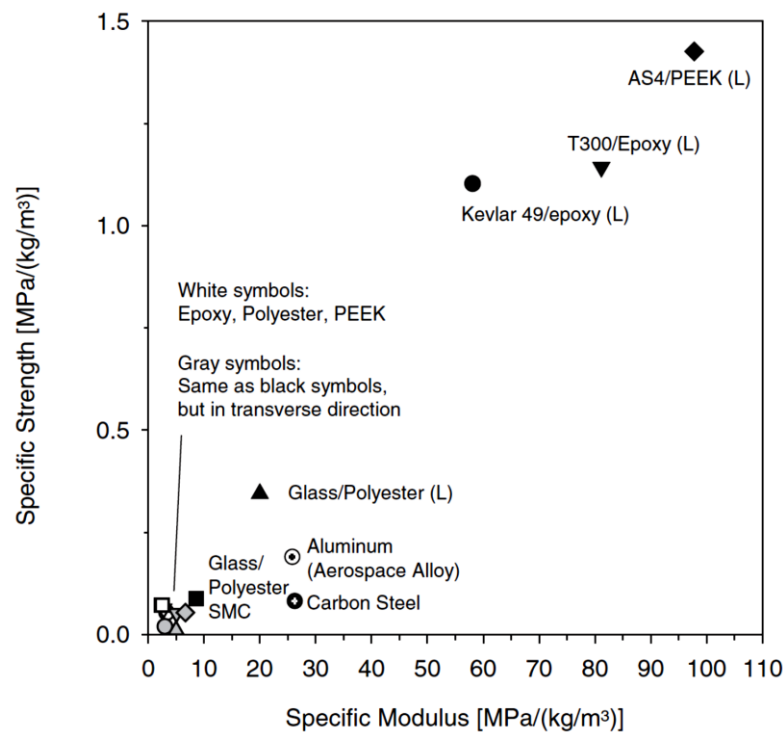


Figure 2-5: Comparison of specific strength and Specific Modulus of polymer composites and aerospace metal alloys, L- Longitudinal direction; AS4 and T300 are different varieties of carbon fibres [67];

2.4 Properties and applications of CFRP

Carbon fibres have a high modulus of 1000 GPa in the axial direction and 35 GPa in the transverse direction. This results in lower tensile strength in the transverse direction (38 MPa for carbon/epoxy [69]) in comparison to that in the axial direction (1400 MPa for carbon/epoxy [69]) in CFRP laminates which makes CFRP an anisotropic material having higher strength properties in the axial direction. To compensate for this, multidirectional CFRP are fabricated for use [73]. The applicability of CFRP laminates in aircraft industry has been well described by Schwartz [54] – Carbon/epoxy composites are used to fabricate wings, fuselages, air

brakes, doors, floors and cowlings. Carbon/bismaleimide composites are used for wing and fuselage skins, engine casings, and wing flaps where high-temperature application is required (because of glass transition temperature of bismaleimide matrix being in 220 to 315°C temperature range [48]). In addition, CFRP contains low coefficient of thermal expansion (CTE) as compared to metals, see Table 2-4. This makes CFRP more dimensionally stable over a wide range of temperatures [55]. In the aerospace industry, near-zero coefficient of thermal expansion property of CFRP has been found to be useful in order to maintain the separation and alignment of the primary and secondary mirrors on the Hubble telescope.

Table 2-4: Comparison of thermal properties of CFRP to metals [55]

Material	Density (g/cm³)	Coefficient of thermal expansion (10⁻⁶/°C)	Thermal conductivity (W/mK)
Plain carbon steels	7.87	11.7	52
Copper	8.9	17	388
Aluminium alloys	2.7	23.5	130–220
Ti-6Al-4V titanium alloy	4.43	8.6	6.7
K1100 carbon fibre– epoxy matrix	1.8	-1.1	300 (in axial direction)

In addition, satellite dish reflectors, deployment arms, struts and solar array panels are also made of CFRP composite. Carbon/PEEK composite has been used instead of Aluminium to save weight as the main structural in scientific space satellite as almost \$120,000/kg wt. was the cost of the launch of the satellite [54]. CFRP has been useful for engine components and blades of unducted fan engines (carbon fibre/ high toughened epoxy matrix) which have been introduced by General Electric Company [54]. In the automobile industry, screw rotors for compressors, automobile turbo chargers, and drive shafts made of carbon/epoxy composite have

been used [54, 69]. Thus, CFRPs have been useful in various components of an automobile, aircraft and aerospace industries as structural components with lower weights.

Due to the tendency of moisture absorption in polymeric matrices [48, 70, 71], glass transition temperature of CFRP gets reduced in a moist atmosphere, (the glass transition temperature of carbon/epoxy composite falls to 120°C in the moist atmosphere from 197°C in dry conditions [71]). Therefore, CFRP materials cannot be used where its strength properties are required to be retained at higher service temperatures in moist atmospheres.

In aircraft and aerospace applications, thermoset matrix are used in CFRP due to due to high dimensional accuracy, high glass transition temperature (e.g., 265°C for cyanate esters [55]), high strength and stiffness along with lighter weight compared to metal alloys (See, Figure 2-5 and Table 2-4). Since machining is required at several stages of production, unfortunately, CFRP gets damaged during machining and the abrasive nature of carbon fibre increases tool wear which increases production cost [78, 79]. Such machining induced damage is a major concern for aircraft and aerospace industries. The machining induced damage in CFRP is discussed in detail in Chapter 3.

3 Literature review of the drilling of CFRP

As demonstrated by Eneyew and Ramulu [75], when drilling of CFRP material is performed, the cutting edges of the drill have to machine all the relative fibre orientations with respect to cutting direction within one revolution of the drill as shown in Figure 3-1. Therefore, the machined surface generated by drilling will contain damage from the machining of all the relative fibre orientations. Thus, it becomes important to develop an understanding of the damage generated during the machining of the relative orientation of carbon fibres in CFRP before developing an understanding of the damage during drilling of CFRP.

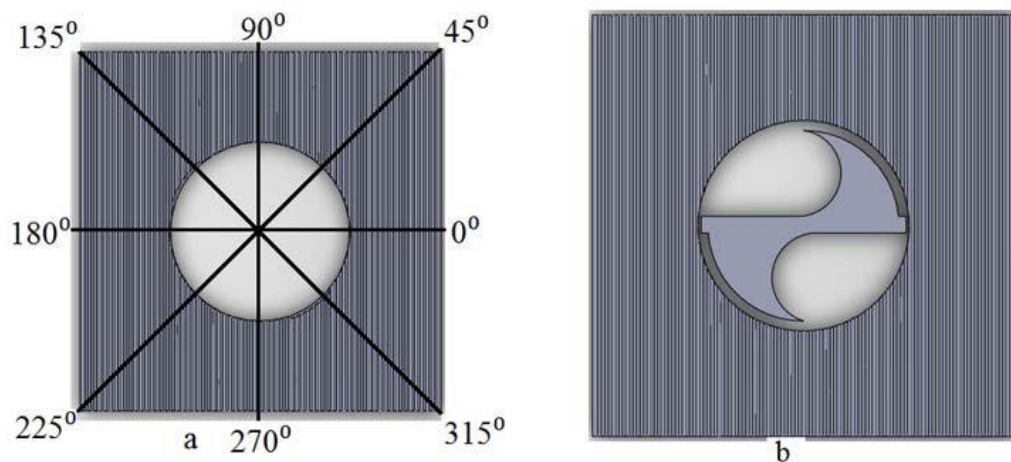


Figure 3-1: (a) Relative fibre orientations during one rotation of twist drill and (b) representation of twist drill with unidirectional CFRP material shown by Eneyew and Ramulu [75]

3.1 Mechanism of chip formation and damage during machining of CFRP in several relative orientations

The chip formation mechanism in machining of CFRP material is dependent on the relative orientation of the carbon fibres with respect to the cutting direction [74, 80-82]. A schematic for the relative orientations of carbon fibres in the CFRP

material with respect to the cutting direction is shown in Figure 3-2 and the same notation has been followed the current research work.

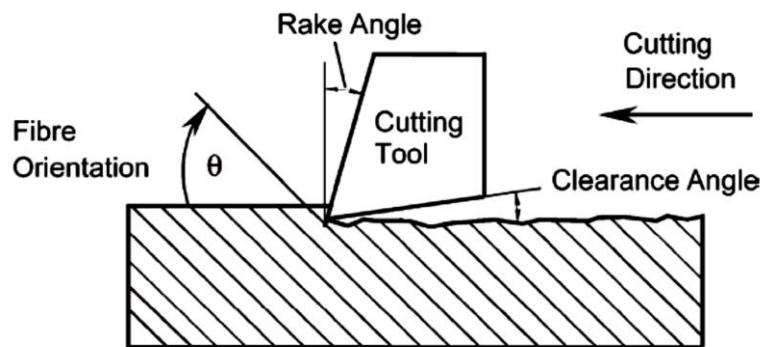


Figure 3-2: Machining notations in the study of Wang and Zhang [82]

The relative orientation of carbon fibres with respect to cutting direction has been segmented in 0° , 45° , 90° and 135° and the same orientations of carbon fibres in CFRP material were studied for machining by the researchers for chip formation mechanism and damage generation [74, 81].

When 0° relative orientation of fibres is machined with positive rake angle, the tool applies pressure on the work piece, Figure 3-3. As a result, a crack initiates ahead of the tool-tip resulting in peeling fracture and delamination of fibres. With the tool advancement, the crack propagates further ahead of the tool tip and fibres continue bending and flowing up on the rake face of the tool until bending of fibres causes bending induced fracture in a perpendicular plane to fibre direction producing small and distinct chips. When machining with negative rake angles, fibre failure happens because of micro-buckling and in-plane shear [74, 80, 81], Figure 3-3.

With the machining of 0° orientation of fibres, the damage on the machined surface has been found to be small sub-surface cracks reaching to only one or two fibre diameters as examined by Koplev et al [81]. The process of peeling, bending and bending induced fracture of fibres continues as the tool advances to machine further. Large fluctuations in the cutting forces have been found by the researchers during

the process of chip formation in the machining of 0° relative fibre orientation because of the particular processes of peeling, bending and bending induced fracture of fibres. [74, 80].

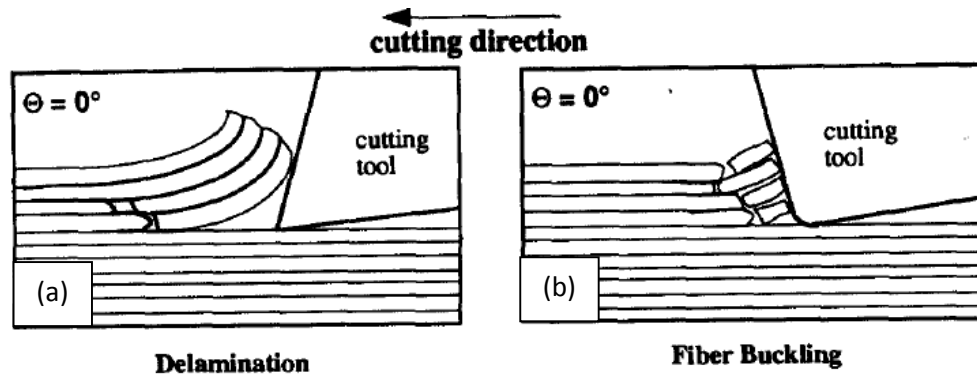


Figure 3-3: Machining of 0° relative fibre orientation with (a) positive rake angle (b) negative rake angle [74]

When 45° relative fibre orientation is machined, Figure 3-4, the forward motion of the tool compresses the fibres producing in-plane shear and tensile stress in the fibres which further causes tensile failure in the fibres. The chip formation consists of tensile failure of carbon fibres and in-plane shearing between the fibres. Because of in-plane shearing between the fibres and at the fibre-matrix interface, the chips generated for 45° relative orientation have been found to consist more of broken fibres and dust instead of discrete chip fragments [74, 80]. Because of uncertainty in the location of tensile fracture in the fibres, the machined surface generated after machining of 45° relative fibre orientation has been found to be more irregular than that after machining of 0° relative fibre orientation [73, 74]. According to Iliescu et al. [80], after fibre failure and chip ejection, the remaining fibres on the machined surface elastically return to their original position. This elastic returning of fibres causes rubbing on the tool-flank face which causes “highest” tool wear out of all the other relative fibre orientations.

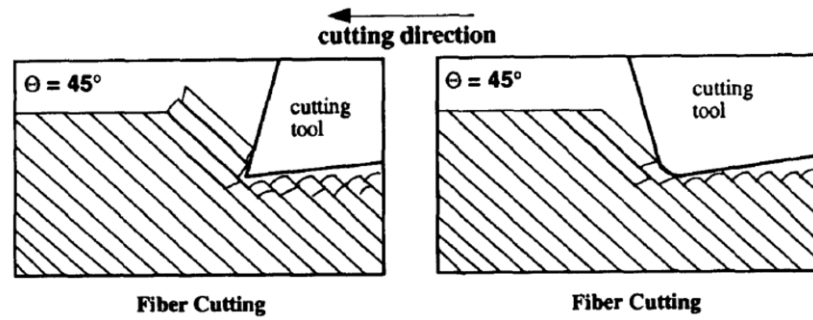


Figure 3-4: Orthogonal machining of 45° relative orientation by (a) positive rake angle and (b) negative rake angle tool [74]

When 90° relative orientation of fibres are machined, the workpiece is pressed by the tool and severe bending of the fibres is caused by the forces coming from forward motion of the tool. Because of bending of fibres, in-plane shear between fibres and mode-I (opening) failure of fibres happens on the machined surface which propagates a crack inside the machined surface, Figure 3-5. In the work of Koplev et al. [81], these cracks were found to be within 0.1 to 0.3 mm depth under machined surface. The chip formation takes place because of bending induced fracture in the carbon fibres similar to that in the machining of 45° orientation [74, 81].

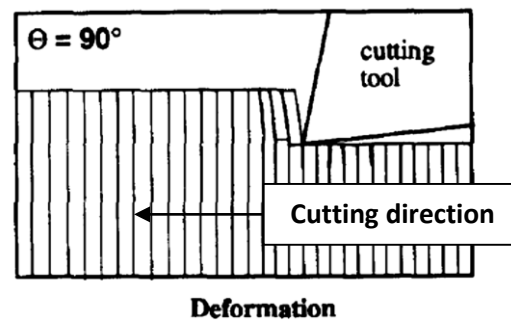


Figure 3-5: Deformation and bending of the fibres in the cutting direction of tool found in the orthogonal machining of 90° relative orientation of carbon fibres [74]

The material removal during machining of 90° relative orientation fibres takes places by the failure of fibres in the plane perpendicular to fibre orientations during bending [80, 81]. After failure and chip formation, the remaining bent fibres elastically recover their original position and rub the tool-flank face causing abrasive tool wear. The elastic recovery of fibres also reduces the effective depth of cut [67,

80]. As explained by Koplev et al. [81] for the machining of 90° relative orientation, “The forward motion of cutting tool presses the composite in front of it causing the composite to fracture and create a chip. At the same time, the downward pressure from the tool on the composite below the tool produces the crack at fibre-matrix interface”. In addition Wang and Zhang [83] and Koplev et al. [81] reported smearing of the matrix during orthogonal machining of 90° relative orientation fibres and the machined surface being covered by the smeared matrix hiding the fibres from the top view of the machined surface as shown in Figure 3-6.

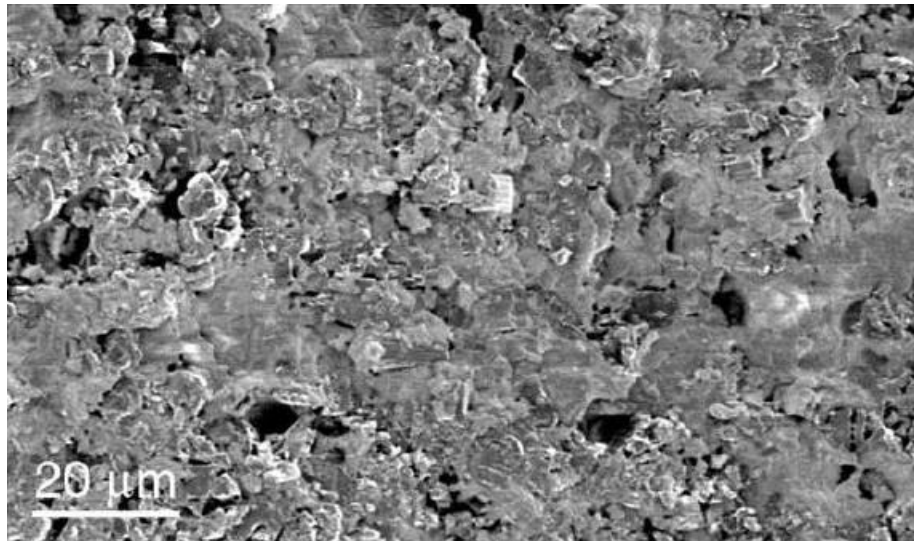


Figure 3-6: SEM image displaying smearing of matrix in the orthogonal machining of 90° relative orientation fibres covering fibres from the top view of machined surface in the work of Wang Zhang [83]

When 135° relative orientation of fibres are machined, because of forward and downward force from the tool, a crack is developed at the tool-tip on the work-piece causing fibre-matrix debonding, delamination and severe bending of the fibre-bundles. The failure of the fibres happens in a perpendicular plane to the fibre axis caused by severe bending induced fracture due to the forward motion of cutting tool, Figure 3-7. The amount of bending of fibres at 135° relative orientation was found to be more than that in 90° relative orientation. Chip formation takes place by bending of fibre bundles and pull-out leading to large discontinuous chips and irregular

machined surface. It has been found by the authors [80, 83] that 135° and higher relative fibre orientations undergo maximum sub-surface damage during orthogonal machining in comparison to the relative orientation between 0° - 90° , Figure 3-8.

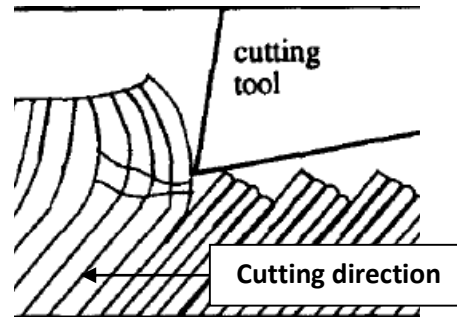


Figure 3-7: Bending of the fibres and irregular surface formation during orthogonal machining of 135° relative orientation of carbon fibres demonstrated by Wang et al. [74]



Figure 3-8: SEM image of fibre pull-out and sub-surface damage on the machined surface during orthogonal machining of 150° relative fibre orientation reported by Wang and Zhang [83]

Also, according to Wang et al. [74], the cutting forces required for machining were found to be higher in the cases of 90° and 135° (~ 800 N) as compared to those in the case of 0° and 45° (~ 200 N) relative fibre orientations because in the case of 90° and 135° relative orientations, the severe bending of fibres required more cutting force to be applied. Also, the force perpendicular to cutting direction during machining of 90° and 135° was found to be lower (~ 200 N) than that in the machining of 0° and 45° (~ 250 N) because in the machining of 90° and 135° the

elastic returning of fibres applied an upward vertical force on the tool flank face resulting in reduction in the force perpendicular to cutting direct required for machining.

3.2 Damage during conventional drilling

The damage generated on the material during conventional drilling has been segmented by authors in two categories – Entrance/exit delamination and damage on the internal cylindrical machined surface which includes fibre/matrix debonding, thermal damage to the matrix, fibre pull-out and interlaminar cracking [84, 85].

3.2.1 Entrance and exit delamination

When the drill starts penetrating the CFRP material at the entrance of the hole, the cutting force coming from cutting edges of the drill forces the material to propagate along its flutes before effectively cutting the material which causes a “peeling” action for the laminates at the entrance of the hole. The crack propagation due to this peeling action causes the top laminates at the entrance to separate from the rest of the laminates creating delamination at the entrance of the hole [84, 86], Figure 3-9. Since this delamination takes place because of “peel-up” action of the drill, it is also known as “peel-up” delamination.

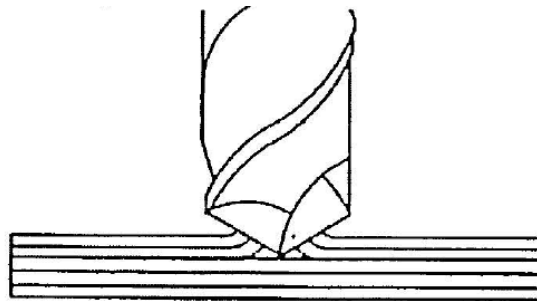


Figure 3-9: Entrance or Peel-up delamination during conventional drilling [86]

When a drill progresses into the material while drilling, an axial force in the direction of feed motion of drill is exerted by the drill on the material. This axial

force is known as thrust force. Because of the thrust force, laminates under drill have a tendency to be pushed away from rest of the upper laminates. As long as the thrust force lies below the interlaminar strength, the laminates do not separate from each another. In the region near the exit, the thrust force exceeds the interlaminar strength of the laminates, therefore, laminates start to be separated from each other creating exit delamination. This type of delamination happens because of “pushing the laminates down” action of the drill to the material, therefore, it is also known as push-out or push-down delamination, Figure 3-10 [84-86].

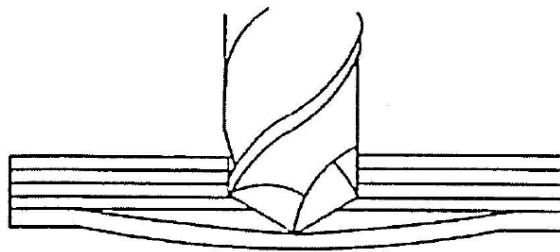


Figure 3-10: Push-out or exit delamination during conventional drilling [86]

3.2.2 Damage on the machined surface

As mentioned in Section 3, during drilling of CFRP, the cutting edges of the drill have to machine all the relative orientations within one rotation of the drill. Therefore, the machined surface generated by drilling contains the machined surface and damage on the surface generated in all the relative orientations of carbon fibres. This phenomenon is further explained in Section 3.4.3, later in this chapter.

3.3 Concept of critical thrust force and delamination

As mentioned in Section 3.2.1, the exit delamination happens when the forces from the chisel and cutting edges of drill exceed the interlaminar strength of the CFRP, laminates start to be separated from each other. The minimum thrust force required to delaminate the laminates is known as critical thrust force. There is good agreement amongst researchers that the exit delamination happens when the thrust

force during drilling exceeds the critical thrust force [87-90]. Therefore, in order to reduce exit delamination, researchers attempted to determine the critical thrust force theoretically and experimentally and keep the thrust force below this critical force by controlling the feed rate to avoid exit delamination.

To assess the value of critical thrust force for a given CFRP laminate, researchers have developed theoretical models. The simplest model for critical thrust force for exit delamination was proposed by Ho-Cheng and Dharan [87] applying linear elastic fracture mechanics with the assumption that delamination at the exit spreads homogeneously to a circular region having radius 'a'. It was suggested that the critical thrust force was a function of remaining depth under the drill during drilling. The critical thrust force reduces during drilling as the drill proceeds further into the material and for the last laminate just before the exit of the hole, critical thrust force would be lowest. Hence, care must be taken while penetrating the last laminate just before the exit of the hole in order to avoid the exit delamination. Jain and Yang [88] argued for exit delamination to be elliptical in shape for unidirectional composites because the extent of exit delamination would be higher in the direction of fibres as CFRP laminates are anisotropic in their model. Hocheng and Tsao. [13, 91] developed a theoretical critical thrust force model for identifying the critical thrust force for different types of drills such as saw drill, core drill, candle stick drill and step drill.

3.4 Methodologies to assess and quantify the damage around a drilled hole

Through hole drilling of CFRP with a conventional drill results in a hole having damage around it in the workpiece. The nature of the damage to the material which

is generated during drilling is related to its anisotropic brittle nature, fibre-matrix debonding and low thermal conductivity resulting in the fibre pull out, chipping, fuzzing and delamination. This section is an attempt to explain various methodologies adapted by other authors to identify and quantify damage in drilled holes in CFRP material in detail. In most of the researches, the damage has been segmented into two major types:

- Delamination at the entrance and exit of the hole
- Surface roughness of the internal machined surface of the hole

Based on the type of damage (delamination or internal damage in a hole), the specific methodologies to identify the damage are explained Sections 3.4.1 and 3.4.2.

3.4.1 Entrance and exit delamination

3.4.1.1 Optical Microscopy

Visual inspection through an optical microscope is the most common technique used by researchers in order to detect the damaged zone and quantify delamination [16, 92-98]. In this methodology, the entrance and the exit of the drilled holes are viewed through an optical microscope which is connected to a computer. The digital image of the affected region is captured by a camera attached to the microscope and processed further in imaging software. Some researchers have applied image processing based on pixel count to quantify the damage [93, 99], Figure 3-11. Other researchers have used imaging software like Omnimet [96, 98, 100] to measure the area or diameter of the affected zone depending upon the area or diameter delamination criteria, Figure 3-12.

3: Literature review of the drilling of CFRP

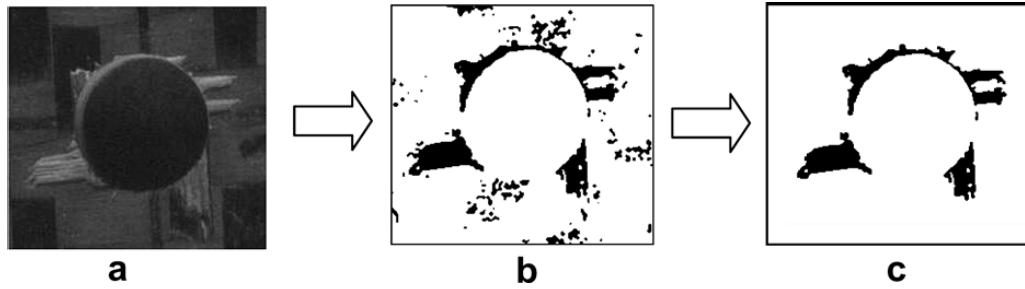


Figure 3-11: Image processing using ImageJ software technique to identify the delaminated diameter and area around a 5 mm diameter hole after capturing the digital image through the Mitutoyo microscope developed by Davim et al. [93]

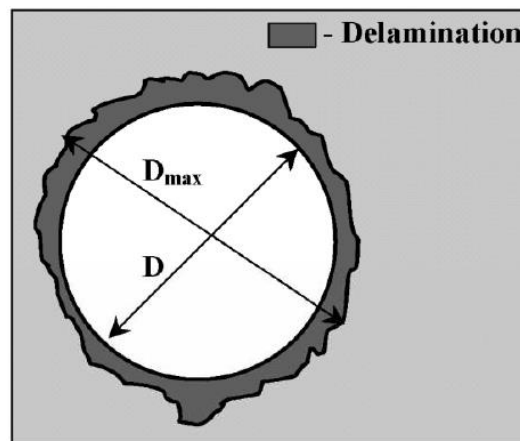


Figure 3-12: Measurement of the maximum diameter of exit delamination through visual inspection in Mitutoyo TM 500 toolmakers' microscope used by Davim and Reis [96]

Although this method of measuring the damaged area or diameter is quick, however, there are some difficulties associated with this technique reported by researchers. The most challenging problem with this technique reported by the researchers is the difficulty in identifying the extent of the subsurface damage at the exit of the hole. Since, the CFRP material is opaque, so the delamination between the internal layers near to the exit of the hole is not visible from the outside. It has been observed in a recent research [101-103] and also reported by other authors [104, 105] previously that the maximum extent of the damage during drilling may not be at the last layer of hole-exit but a few layers before the exit-layer of the hole in the CFRP laminates. Therefore, the maximum extent of the damage may not be reported accurately by visual inspection. The same has been reported recently by Kourra et al.

[101]. In their work, the holes were scanned through X-ray computed tomography (Discussed in section 3.4.1.4 in detail) to find out the delamination extent near hole-exit. It was found that the maximum damage extent was in the plies near hole-exit but not exactly in the last ply at the hole-exit as shown in Figure 3-13. This type of delamination is not detected by visual inspection due to CFRP material being opaque.

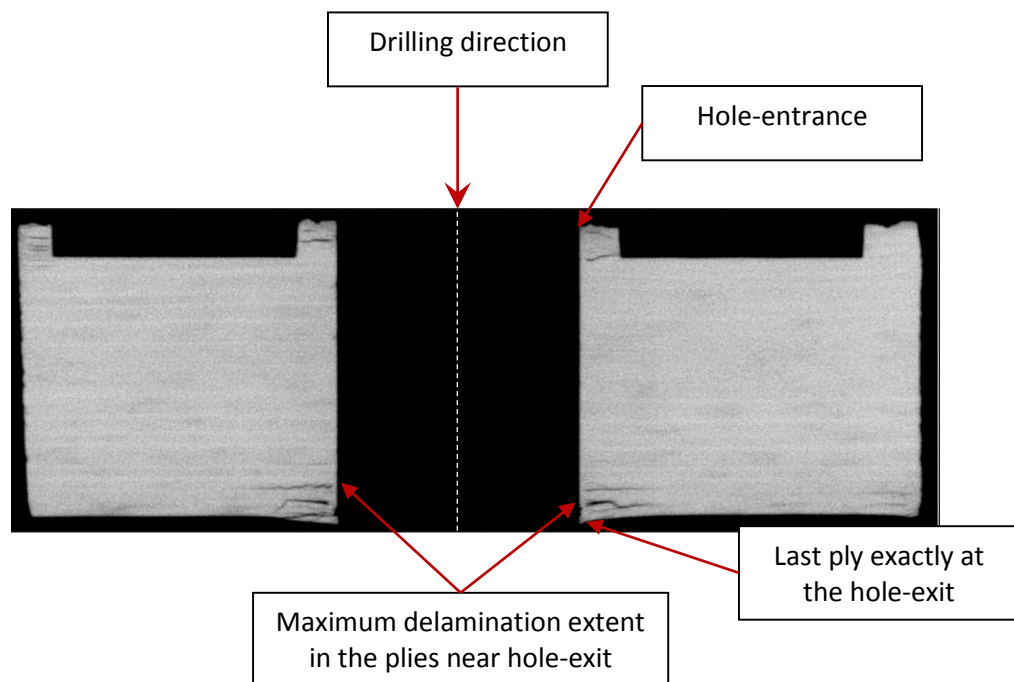


Figure 3-13: Side view of a drilled hole in a CT scanned image displaying maximum delamination in the plies near to the exit but not exactly at the exit ply around a 6 mm diameter hole in CFRP, reported by Kourra et al. [101].

In addition, while measuring the diameter or area of the damage manually in the imaging software, measurement is often subjective to the specific human being who is actually measuring the damage. Therefore, the data measured by this technique can be variable even if the same damage extent is measured by different people in the same microscope measurement setup.

3.4.1.2 Ultrasonic C-Scan

Ultrasonic scanning is a non-destructive technique for damage detection being used widely in the composite materials, electrical and electronics industries for

detection of voids and damage inside the manufactured materials and components [104, 106]. Ultrasonic C-scan is performed submerging the specimen along with the transducer and receiver in a fluid (water in most cases [107]). The ultrasonic pulses are transmitted from the transducer to the specimen, the waves get attenuated where a void or a damage inside the specimen is present because of change in the density of the material at the voids and damage. The reflected attenuated waves from the specimen top surface, damage inside the specimen and the bottom surface of the specimen are received at the receiver and hence, the size and location of the damage are detected inside the specimen through pulse travel time and detected amplitude [107]. The images of the damage inside the specimen are recorded on the plan view of the specimen. Once the damage is accessed, image processing is performed further to quantify the damage as performed by other researchers [13, 104, 108-111].

Although, this technique is capable of identifying the actual extent of the damage at the entrance and exit of the hole, however, in this methodology, the specimen is required to be submerged in water completely which promotes moisture absorption in the CFRP material. Moisture absorption softens the matrix and leads to poorer fibre-matrix adhesion and hence, the mechanical strength of the matrix of the composite material is affected [70, 71]. Therefore, drilled material cannot be tested further for its mechanical properties after ultrasonic C-scan because its strength would have been compromised by the absorbed moisture during ultrasonic C-scan. In addition, the voids present in the heterogeneous CFRP material cause scattering of the ultrasonic wave and acoustic attenuation instead of the delamination itself which creates difficulty in assessment of the delamination [112].

3.4.1.3 *X-ray enhanced radiography*

When a specimen is kept between the x-rays and photographic film, x-rays pass through the specimen, get attenuated and some energy of x-rays gets absorbed into the specimen itself [107, 113]. The attenuated x-rays and unabsorbed x-rays in the specimen reach to the photographic film and react with it, creating a 2D grey shadow of the specimen onto the photographic film. The grey intensity shadow on the photographic film depends on the absorption cross section of the specimen because a material having higher absorption cross section absorbs and attenuates x-rays up to a higher extent. CFRP has low absorption cross-sections and this is why a coating of absorbers like Zinc iodide, dibromomethane, tetrabromomethane, di-iodomethane etc. is required to enhance the extent of attenuation and thereby contrast on the radiographic film. It is performed by submerging CFRP in absorber solutions for sufficiently long time [10, 16, 104, 107]. The location and size of the damage and voids in the material are identified by analysing various grey intensity levels of shadow in the affected photographic plate due to x-rays. This technique is known as conventional x-ray radiography [107]. This technique has been used by several researchers in order to find out the actual extent of entrance and exit delamination [10, 104, 113-115]. After acquiring the radiographs of the drilled materials, image processing was performed to quantify exit delamination as shown in Figure 3-14. However, similar to ultrasonic C-scan, the samples are soaked in the wet solution which promotes the moisture absorption preventing the samples to undergo any mechanical property testing further [70, 71].

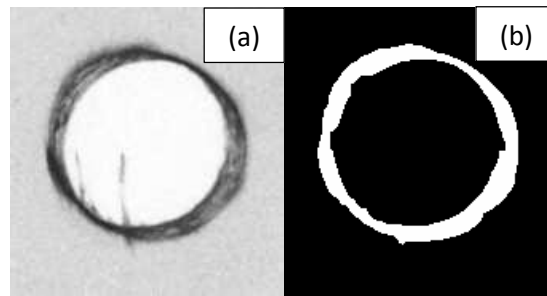


Figure 3-14: (a) X-ray radiograph of exit delamination and (b) processed image for damage quantification for a 6 mm diameter hole in the work of Durao et al. [104]

3.4.1.4 X-ray computed tomography (CT)

X-ray CT scanning is a non-contact and non-destructive methodology used by researchers to identify the damage inside a drilled hole. In this technique, the specimen is rotated 360° between the x-ray source and photographic detector such that numerous two-dimensional radiographs are collected at the detector caused by the attenuation of the X-rays by the specimen, Figure 3-15. Using all the radiographs collected from various projections of the specimen, the object is digitally reconstructed using back projection algorithms in a computer in 3D which consists outer and inner parts of the specimen [101, 112, 116], Figure 3-16. These algorithms digitally reconstruct the part in a 3D virtual environment exporting the grey scale value of a 2D pixel in the radiograph (resulting from attenuation of X-rays) to a 3D voxel. Therefore, digitally reconstructed specimen in the computer is created by voxels (which is a 3D representation of a pixel of a 2D radiograph). The 3D reconstruction of the specimen in the computer depends on the resolution of the voxel size which ultimately depends on the resolution of the pixels at the detector. The resolution of 2D radiographs is a function of sample size and the relative distance between the sample and detector. In a later step, the part is measured by a coordinate measuring machine (CMM) for scaling the voxel size proportional to the physical dimensions of the specimen. The 3D voxels constitute layers of the

3: Literature review of the drilling of CFRP

specimen having a thickness of a voxel size in the 3D reconstructed model. These layers can be exported as two-dimensional images in order to analyse internal defects in a part by analysing each image [101]. Some of the material used in the present research was used for developing the CT scanning technique reported in the work of Kourra et al. [101]. The entire CT scanning methodology used in the present research is explained in detail in Section 5.3.

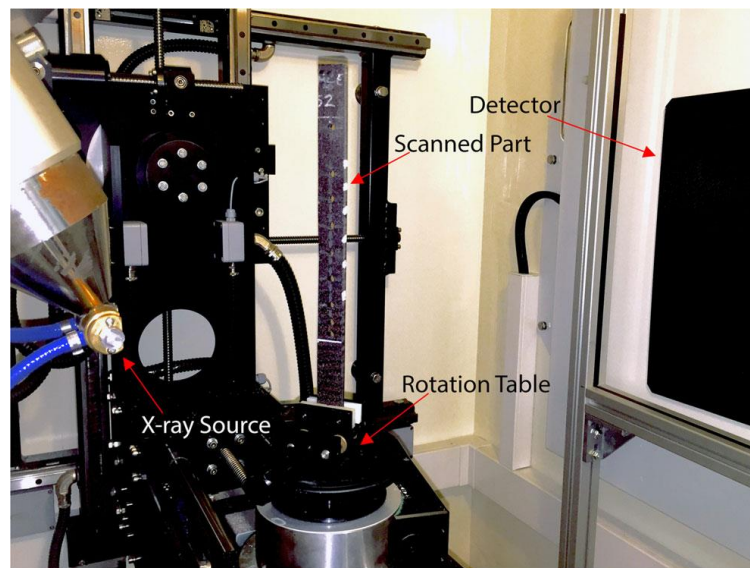


Figure 3-15: X-ray CT scanning setup used by Kourra et al. [101]

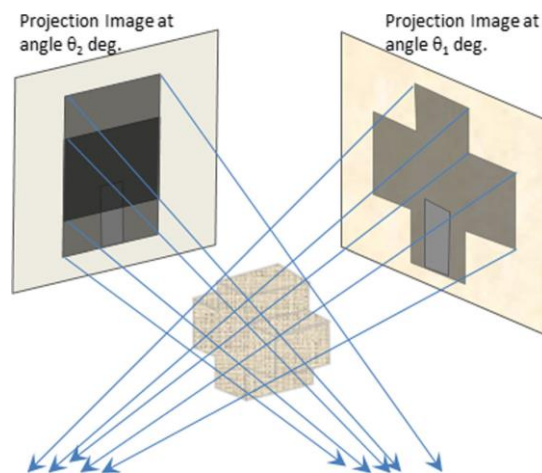


Figure 3-16: 3D reconstruction of specimen using back projection algorithms in X-ray CT scanning technique [101]

3: Literature review of the drilling of CFRP

Using this technique, researchers have identified and quantified the entrance and exit delamination in the drilled holes in CFRP material. Tsao and Hocheng [112, 116] compared the effects of various special geometry drills on the exit delamination during the drilling of CFRP material and compared the exit delamination data obtained from ultrasonic C-scan and X-ray CT scanning techniques by using image processing for delamination quantification. It was found that with the use of X-ray CT scanning, the delamination area was detected in greater details compared to that in ultrasonic C-scan, Figure 3-17. For a quantitative comparison, exit delamination extent by Ultrasonic C-scan was found to be 0.25 mm while in the case of CT scan, it was found to be 0.5 mm for twist drill of 10 mm diameter at same machining parameters of 31.4 m/min cutting speed and 0.003 mm/rev feed rate. Similarly, with the other drills and other machining parameters, X-ray CT scanning was found to be providing greater details of the damage as compared to that in Ultrasonic C-scan in their work. Persson et al. [114] compared X-ray radiography and X-ray CT scanning techniques for identifying the extent of damage propagation around a hole in CFRP material and found X-ray CT scanning to be providing “higher” resolution and greater detail of the damage in the holes as compared to that in X-ray radiography, however, the quantitative values were not provided in their work.

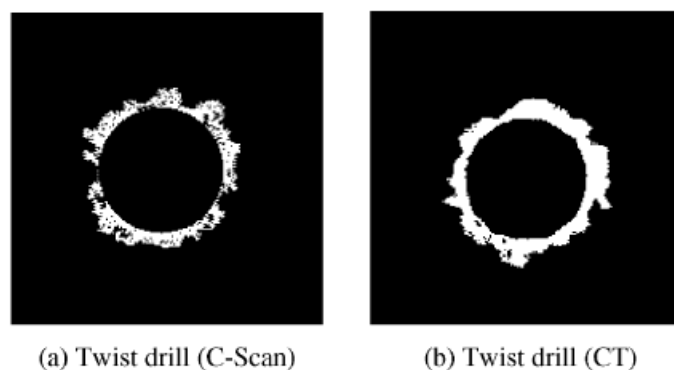


Figure 3-17: Detection of delaminated region through (a) ultrasonic C-scan and (b) X-ray CT scanning for a 10 mm diameter hole in the work of Tsao and Hocheng [112]

Greater details of the damage inside a hole can be obtained with x-ray CT scanning technique, however, this technique is relatively time-consuming compared to other damage evaluation techniques of X-ray radiography, ultrasonic C-scans and visual inspection. Persson et al. [114] mentioned that the time required for CT data collection by rotating the specimen 360° and further reconstructing it in the computer is comparatively longer as compared to the time required for the development of X-ray radiographs. However, the quantitative comparison of the respective intervals was not mentioned in their work. Also, it is important to consider the resolution of the images obtained. In the work of Persson et al. [114], the resolution of the pixels in CT scanning images was $36\ \mu\text{m}$ and in the work of Kourra et al. [101], the resolution of the pixels in CT scanning images was $15\ \mu\text{m}$. Therefore, the cracks having dimensions less than $15\ \mu\text{m}$ would not be visible in the CT scanning images in the work of Kourra et al. [101] and the cracks and damage inside the material having dimensions less than $36\ \mu\text{m}$ would not be visible in the work of Persson et al. [114].

Thus, a lot of techniques have been developed in order to assess entrance and exit delamination around a hole by the authors. However, all the technique have some disadvantages. Optical microscopy is the easiest technique however it is not useful for CFRP due to CFRP being opaque material and therefore maximum damage extent not being visible. Ultrasonic C-scan and X-ray radiography require CFRP to be submerged in liquid solutions which cause moisture absorption affecting its strength which makes it unworthy for further testing of mechanical properties. Although CT scanning provided more information of damage than other techniques, however, its slow processing time makes it useful for examination of selective holes only. In addition, CT scanning is also dependent on the resolution of images.

3.4.2 Quantification of entrance and exit delamination

Quantification of delamination in a hole was necessary for researchers in order to analyse the behaviour of damage with respect to machining parameters and tool geometry in order to achieve minimum damage around the drilled hole. In most of the research, delamination at the entrance and exit of a hole has been quantified by measuring the diameter of maximum extent of the damage as shown in Figure 3-18. In Figure 3-18, D_{max} is the diameter of the maximum extent of damage and D_o is the diameter of the originally intended hole. However, the maximum diameter of a damage extent is specific to a particular diameter of a drill. In order to compare the damage obtained from various diameter drills, the maximum diameter of delamination extent was normalised by dividing it by the diameter of originally intended hole and a standard non-dimensional parameter for delamination was defined as Delamination factor, Equation (3.1). Thus, normalised delamination factor was reported in most of the researches [16, 96, 98, 100, 117].

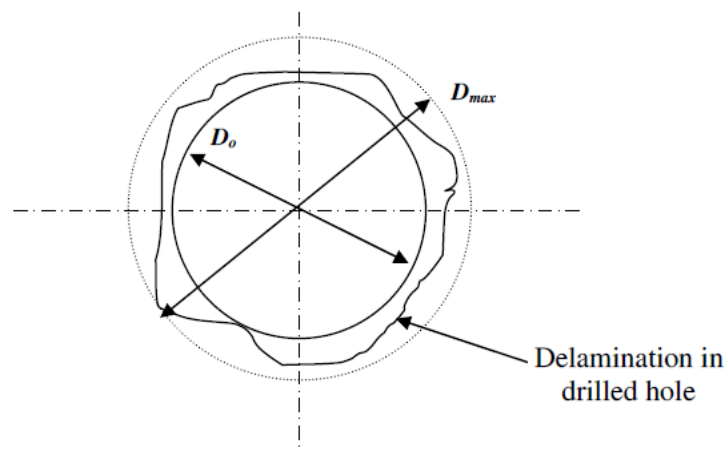


Figure 3-18: Identification of maximum diameter of delamination in drilled hole in the work of Karnik et al. [16]

$$\text{Delamination factor } (F_d) = \frac{D_{max}}{D_o} \quad - \text{Equation (3.1)}$$

In addition to this approach of considering the maximum diameter, some researchers like Enemuoh et al. [118] considered the maximum damage width and maximum damage depth in the whole periphery of the hole as a delamination criteria in their research . These authors [118] found damage depth and delamination to be reducing with cutting speed and increasing with respect to feed rate. However, the reason behind such variation was not explained in their work.

Similarly, Faraz et al. [119] considered maximum width and height of delamination as a damage criteria in their work, Figure 3-19. However, the maximum width of delamination (D_w) in their work coincides with the Damage depth (D_a) in the work of Enemuoh et al. [118]. Both signify the difference between the radius of maximum extent of delamination and original radius of intended hole.

Instead of calculating a normalised delamination factor, Hocheng and Tsao [13, 111, 112, 116] reported the difference between the diameter of maximum damage extent and diameter of originally intended hole as delamination. However, in their other work [120], delamination factor (D_{max}/D_o) was reported instead of the difference between the diameter of maximum damage extent and diameter of originally intended hole as damage quantification criteria. Normalised delamination factor can be used for comparing the delamination data obtained from various diameter drills. Whereas the difference between the diameter of maximum damage extent and diameter of original intended is useful only for comparison with same diameter holes. Therefore the damage difference data from Hocheng and Tsao [13, 111, 112, 116] makes it useful only for comparing the damage obtained around 10 mm diameter drills.

3: Literature review of the drilling of CFRP

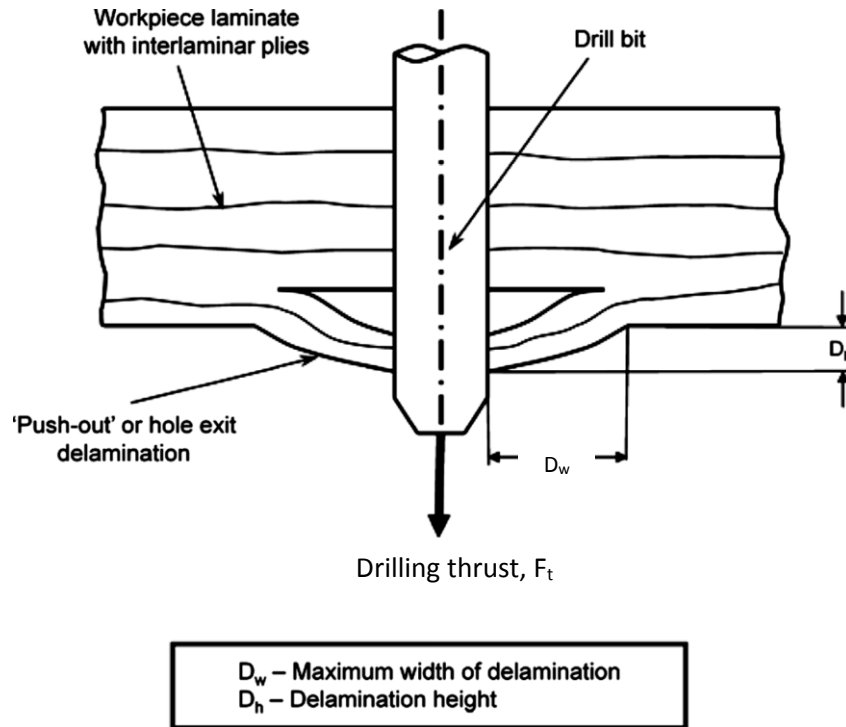


Figure 3-19: Delamination height and width considered as damage criteria in the work of Faraz et al. [119]

Some authors argued for considering the area of maximum damage as a parameter for delamination, because when considering the diameter of maximum delamination, it is assumed that the entire circular area inside that maximum diameter circle is damaged which may not be accurate. It would be accurate only when the entire circular area inside maximum diameter of damage is affected due to delamination. Therefore, authors proposed to measure the exact damaged area instead of diameter for maximum extent of damage and normalised it by dividing it by the circular area of the originally intended hole as shown in Equation 3.2 and in Figure 3-20 [95, 99]

$$\text{Delamination factor} = \left(\frac{A_{del} - A_{nom}}{A_{nom}} \right) \% \quad \text{Equation (3.2)}$$

Where, A_{del} is the exact damaged area and A_{nom} is the circular area of originally intended hole, Figure 3-20.

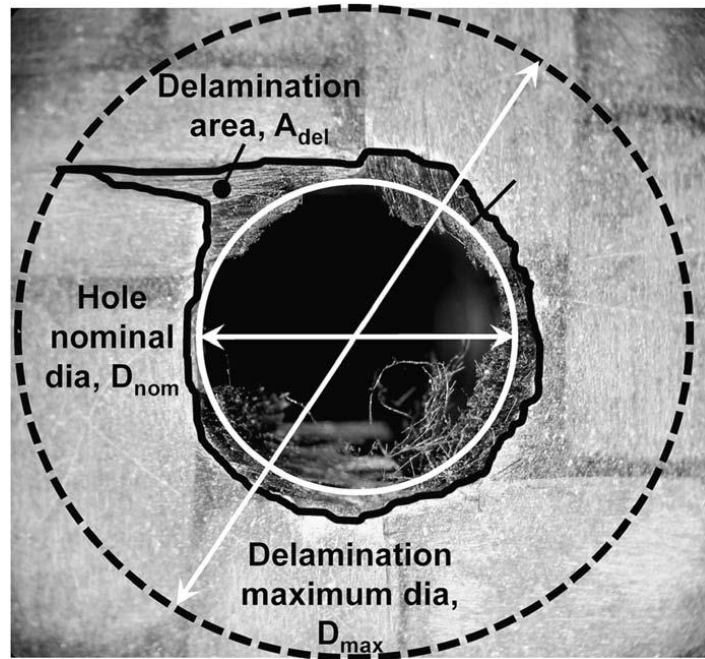


Figure 3-20: Area delamination measurement around 4 mm diameter hole in the work of Faraz et al. [95]

Davim et al [93] considered delamination to be falling between two extreme cases of fine crack and uniform delamination, Figure 3-21. They reported that actual delamination has an irregular shape lying in between the two cases of fine cracks and uniform delamination cases. Therefore, to calculate delamination factor more accurately, both diameter and area delamination factors would have to be taken into account.

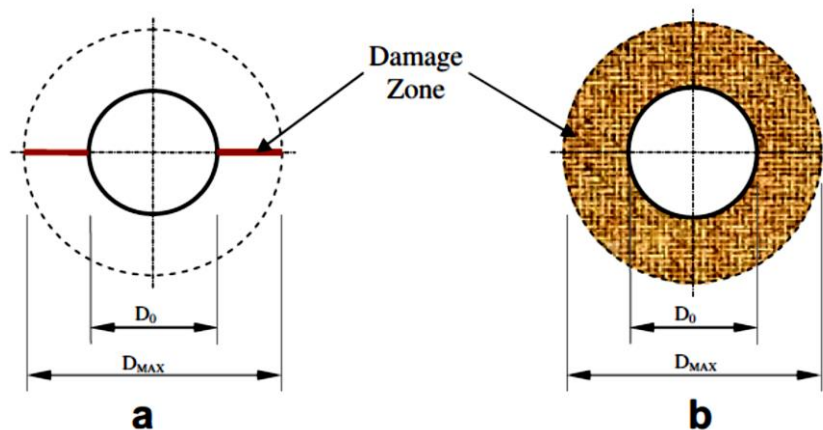


Figure 3-21: Two extreme cases of (a) Fine cracks (b) uniform delamination considered in the work of Davim et al. [93].

Davim et al. [93] proposed a new parameter of adjusted delamination factor (F_{da}) by merging the area delamination factor and the diameter delamination factors together to find out the more accurate delamination factor as compared to individual diameter and area delamination factors. If F_{da} is the adjusted delamination factor, A_d is damage area, A_{max} is the circular area corresponding to the maximum diameter (D_{max}) of the damage around the hole and A_0 is the nominal hole area then according to Davim et al. [93], delamination factor F_{da} was defined as according the Equation 3.3–

$$F_{da} = F_d + \frac{A_d}{(A_{max} - A_0)} (F_d^2 - F_d) \quad \text{- Equation (3.3)}$$

Davim et al. [93] calculated the delamination factors by applying image processing on the photographs of delaminated areas and compared all the definitions of the delamination factors, Figure 3-22. In Figure 3-22, it can be seen that that for delamination at the entrance, diameter delamination factor (F_d) is 1.15 while adjusted delamination factor (F_{da}) is 1.16. At the hole exit, F_d is 1.76 and F_{da} is 1.88. Although F_{da} provides a different data due to combining area and diameter information in a single parameter, it cannot be argued that it is more accurate than F_d .

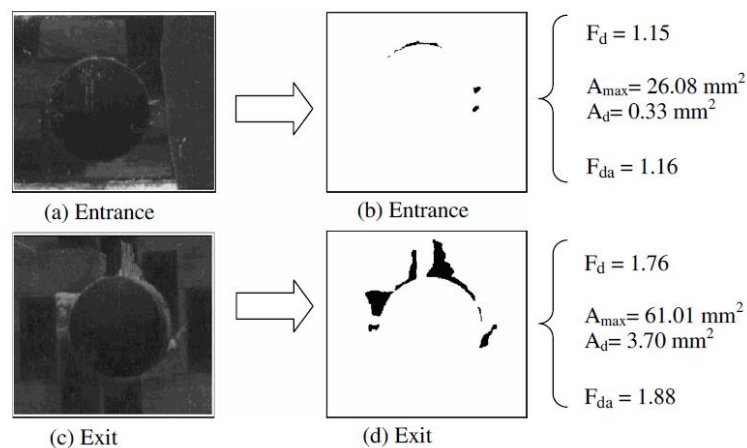


Figure 3-22: Diameter delamination factor (F_d) and adjusted delamination factor (F_{da}) calculated around 5 mm diameter hole in the work of Davim et al. [93].

Thus, exit delamination has been quantified by several parameters out of which area and diameter delamination factor has been the most commonly used parameters by the authors so far.

3.4.3 Assessment and quantification of internal damage in a drilled hole

The damage on the internal cylindrical machined surface in a hole has been termed as ‘Internal damage’ in the present research. Thorough assessment and quantification of internal damage is still a subject of ongoing research [75]. At present, fibre pull-out on the internal machined surface in a hole is the only quantifiable internal damage discussed by other researchers and surface roughness has been used as a parameter to quantify the fibre pull-out in a hole [7, 75, 83, 118, 121-126]. The most common approach to measure the surface roughness has been using a stylus-based measurement system in which a stylus is touched to the test-surface and moved to a predefined distance. Parameters like average surface roughness (R_a), root mean square (RMS) surface roughness (R_q), peak-to-valley roughness (R_y) etc. are used for a 2D surface roughness measurement [127]. Following this approach, some researchers [7, 118, 122, 125, 126] measured surface roughness in a single direction on a particular selected line on the cylindrical surface of a drilled hole in order to analyse the variation in surface roughness with respect to machining parameters (cutting speed, feed rate) and tool geometries. Using this method did not result in a consensus amongst the authors – for example, Davim et al. [122] and Tsao [126] reported decrease in surface roughness with increasing cutting speed in the selected range of respective cutting speeds (55, 71 and 86 m/min for Davim et al. [122] and 23.5, 29.8 and 36.1 m/min for Tsao [126]) whereas Zitoune et al. [125] reported no significant difference with respect to cutting speed (4 to

69 m/min cutting speed range). Although the authors [122, 125, 126] agreed upon increasing surface roughness with increasing feed rate as shown in Figure 3-23.

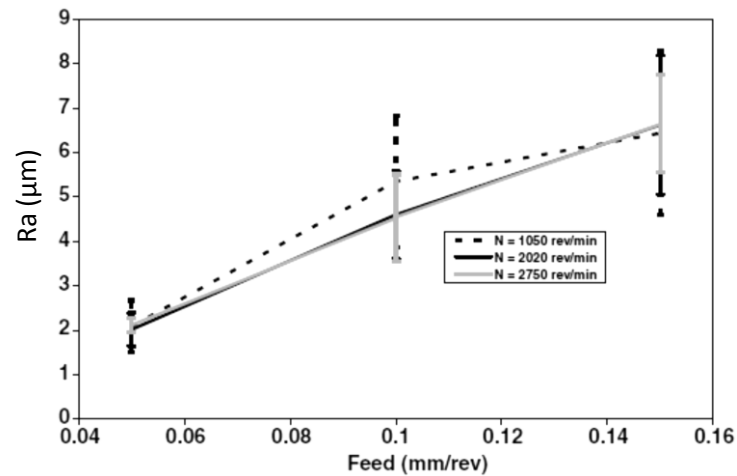


Figure 3-23: Increase in the average surface roughness of carbon fibre composite with increase in feed rate in the work of Zitoune et al. [125]

In addition, Shyha et al. [7] reported an increase in average surface roughness from 0.5 μm in the first hole to 5 μm after drilling of 310 holes with increasing tool wear (0.3 mm flank wear) on CFRP surface at 40 m/min cutting speed and 0.05 mm/rev feed rate. Enemouh et al. [118] reported 118° to be the optimum point angle (out of 75°, 95°, 118°, 140° and 160° point angles) of a two flute twist drill for minimum surface roughness. However, none of the authors provided a scientific justification for such variation of fibre pull-out (surface roughness) with respect to machining parameters and tool geometries. In addition, measuring surface roughness on the internal cylindrical wall of a drilled hole having small diameters like 4, 6 and 10 mm has been a challenging task for researchers because most of the devices available for surface roughness quantification are for use when the surface under consideration is flat. Also, the location of maximum fibre pull out depends on upon the relative orientation of the fibres with respect to cutting speed directions in throughout the periphery of the hole [75]. Therefore, measuring a surface roughness

in one direction on a randomly selected line on the cylindrical surface of a hole cannot provide the accurate fibre pull out information. To overcome this challenge and develop a thorough understanding on machining of carbon fibre composites during the drilling, Eneyew and Ramulu [75] measured the surface roughness on six angular cross-sectional positions of 45° , 90° , 135° , 225° , 270° and 315° as shown in Figure 3-24.

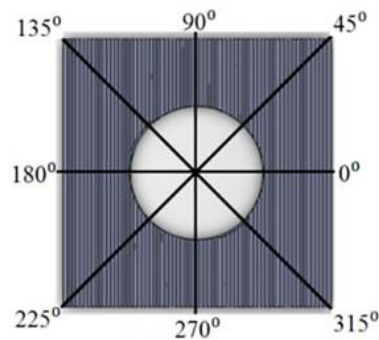


Figure 3-24: (a) Angular positions of surface roughness measurement in the work of Eneyew and Ramulu [75]

This method in the work of Eneyew and Ramulu [75] did reveal that the maximum damage in the machining of unidirectional CFRP material during drilling happens at the locations of 135° and 315° and fibre pull-out depth increases with increasing cutting speed. In addition, out of average surface roughness (R_a), maximum peak-to-valley height (R_t), root mean square roughness (R_q) and ten point average surface roughness (R_z), R_a and R_t showed similar variation regardless of cutting speed and feed rate parameters whereas value of surface roughness in R_t was relatively higher as compared to R_a . Thus, maximum peak-to-valley height surface roughness (R_t) was reported to be the best-describing parameter for fibre pull out information, Figure 3-25.

3: Literature review of the drilling of CFRP

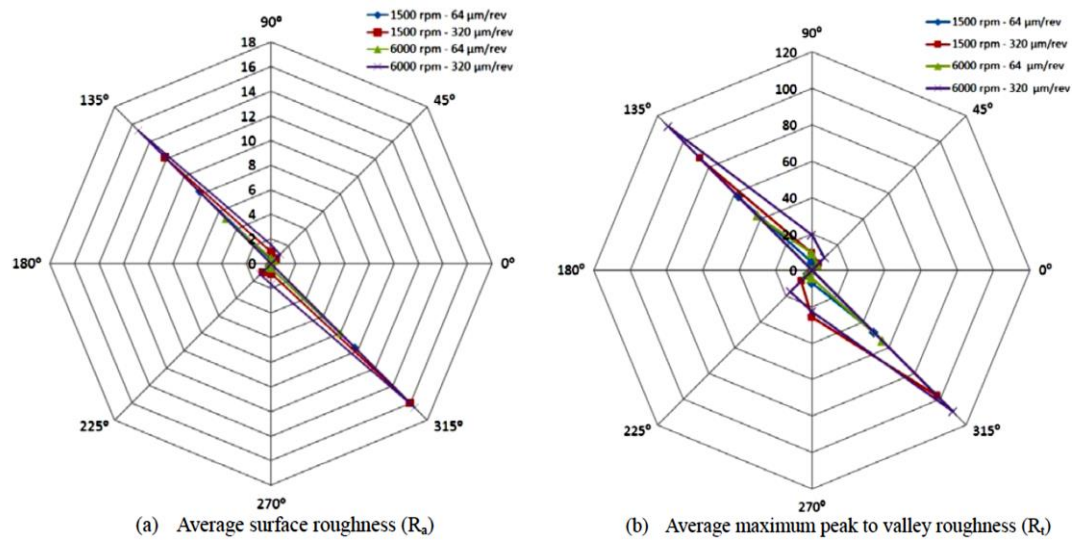


Figure 3-25: (a) Average and (b) maximum peak-to-valley surface roughness variation at various angular locations in the work of Eneyew and Ramulu. [75]

Measurement of fibre pull-out through a stylus is dependent upon the size of the stylus in contact with the surface. If the size of damage is larger than the size of the stylus, the stylus would not be able to record the accurate depth of fibre pull-out. Therefore, in a recent research, Wang et al. [8] proposed the use of confocal microscope (a non-contact and non-destructive method) to measure the surface roughness of the machined surface in the drilling of CFRP material and compared the results obtained from confocal microscope to those obtained with the help of a surface profilometer. The drilling test was conducted on the cutting speeds between 23.2 m/min to 171.2 m/min and feed rates between 0.05 to 0.23 mm/rev. The surface profilometer results in the work of Wang et al. [8] were found to be in the agreement with those in the work of Eneyew and Ramulu [75], i.e. peak-to-valley height (R_y) was found to be more accurate than average surface roughness (R_a) for fibre pull-out information and fibre pull out was found to increase with increase in cutting speed in the work of Wang et al. [8]. However, it was reported that the fibre pull-out measurement obtained from confocal microscope was “almost” two times to the results obtained from surface profilometer and results from both methods agreed on

the conclusion that the fibre pull out increases with increase in cutting speed and feed rate values, Figure 3-26. This result contradicts the findings of Davim et al. [122] and Tsao [126] where fibre pull-out was found to reduce with increasing cutting speed when measuring a linear surface roughness on a randomly selected line on the cylindrical surface of a hole.

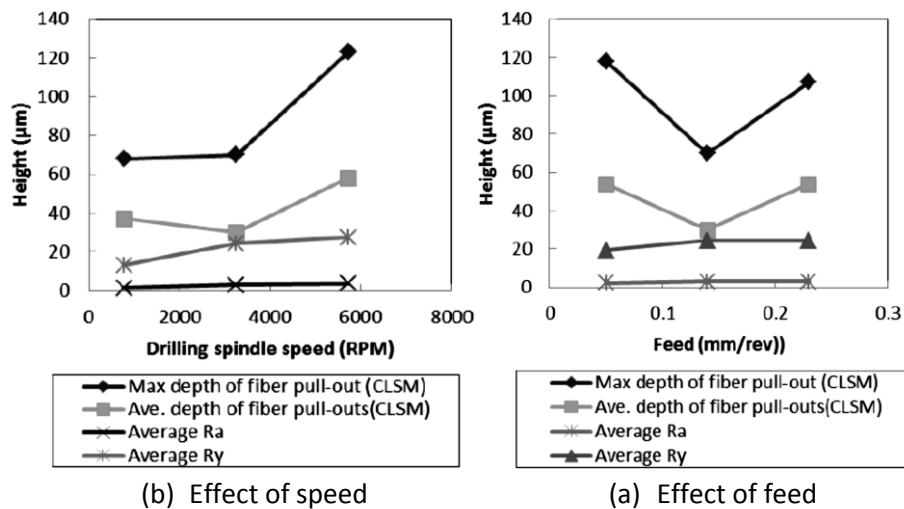


Figure 3-26: Comparison between the fibre pull-out information obtained from confocal laser microscope and surface profilometer in the work of Wang et al. [8]. In addition, Increase in surface roughness with increase in (a) cutting speed (b) feed rate (Ra = average surface roughness and Ry = peak-to-valley height)

The results in the work of Wang et al. [8] suggest that confocal microscope does provide greater information of fibre pull-out as compared those obtained from surface profilometers, however, the accuracy of damage quantification (depth of fibre pull-out into the material) on the internal machined surface of a drilled hole is still under research. In addition, none of the authors have explained the reason for such behaviour of increasing (or decreasing) depth of fibre pull out with respect to machining parameters. Therefore, it requires more rigorous research to develop a thorough understanding of the types and causes of internal damage during drilling of CFRP and its behaviour with respect to machining parameters which is a subject of ongoing research [8, 75].

It can also be observed through the discussion in Section 3.4 that the internal damage and entrance/exit delamination are assessed and quantified with different techniques and equipment. Each technique possesses its own disadvantage. There is no universal technique developed at the moment which could intimate all the damage around a hole in CFRP accurately at once.

3.5 Attempts to minimise the damage through conventional drilling of CFRP

3.5.1 Machining parameters

Identifying the appropriate machining parameters is necessary for achieving a good surface finish in machining. In the conventional drilling of CFRP, cutting speed and feed rates of the drill are the process parameters which can be controlled by the machining operator.

Regarding the cutting speed, in some experiments, exit delamination was found to increase with increasing the cutting speed [93, 96, 100, 128] while conversely, some authors found the exit delamination to be decreasing while increasing the cutting speed [14-16]. The argument behind the reduction of the delamination with increasing cutting speed was given that the cutting temperature at the tool-material interface increases as the cutting speed is increased because of higher friction between tool-cutting edge and the workpiece. Therefore, the matrix in the CFRP material gets softened at a higher cutting temperature which requires less cutting and thrust forces to be machined. Thus lower thrust force causes lower delamination at higher cutting speeds. However, no argument was presented by the authors for increasing the delamination while increasing cutting speed.

For feed rates, there is a general agreement amongst the researchers on increasing the delamination with increasing feed rate [15, 92, 100, 105, 126, 129, 130]. This happens because thrust force during drilling increases linearly as the feed rate is increased. Thus higher thrust force causes higher exit delamination. As reported by Tsao et al. [13], the extent of delamination was found to be enlarged upon increasing feed rate due to increase in thrust force in and delamination was found to increase linearly in their work in the selected range of parameters.

3.5.2 Pilot holes

According to Jain et al. [131], there are three sources of thrust force during drilling, Figure 3-27:

- i. Thrust force from primary cutting edges,
- ii. Thrust force from secondary cutting at outer chisel edges
- iii. Thrust force coming from indentation process at the centre of chisel edge

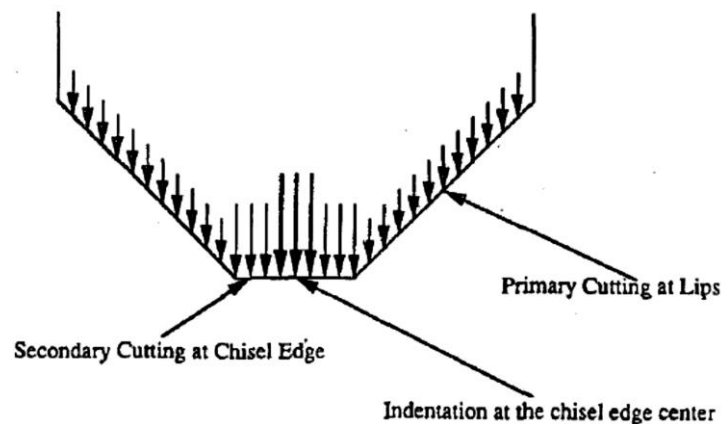


Figure 3-27: Sources of thrust force in a drill during drilling process and maximum thrust force coming from centre of chisel edge due to indentation [131]

Jain and Yang [131] mentioned that 40 to 60% of overall thrust force comes from chisel edge of the drill while drilling. As mentioned in section 3.3, exit delamination during drilling could be reduced by reducing the thrust force during drilling. Therefore, following the approach of reducing thrust force to reduce exit

delamination, researchers [18-21] proposed to drill a pilot hole having an equivalent diameter to chisel edge and remove the material in front of the chisel edge so that when drilling actual concentric hole with larger diameter, the large force coming from chisel edge indentation could be avoided and thus exit delamination could be reduced. Jain and Yang [131] conducted a test to find out the effect of the chisel edge during drilling. They drilled holes at 24 m/min cutting speed and 0.035 mm/rev feed rate and found that when drilling after producing a pilot hole having an equivalent diameter to the chisel edge (20% of drill diameter), a reduction of ~100 N in thrust force was observed as compared to that in drilling without pilot hole for 6.35 mm diameter of holes. Won and Dharan [20] also performed the experimental study to develop an understanding of the effect of pilot holes on thrust force. In their work the holes were drilled with diameters of 6.35 mm and 7.8 mm at 1000 rpm spindle speed (19.9 m/min and 24.5 m/min cutting speeds respectively) with the feed rates from 0.1 to 0.7 mm/rev. In their work also the thrust force in the case of with-pilot hole was found to be lower than that without a pilot hole, Figure 3-28. It was found that with pilot holes, the thrust force was not affected by increment in the feed rate as shown in Figure 3-29. This suggests that higher feed rates could be used increasing production rate keeping the forces constant when using pilot holes. Also, the torque values were found to be unaffected by using pilot holes in their work as the majority of torque is generated from cutting forces which come from cutting edges and pilot hole drilling removes the effect of chisel edge only.

Tsao and Hocheng [21] developed a theoretical model for critical thrust force for the case of with-pilot hole and performed an experimental study with 10 mm diameter high speed steel (HSS) drill at 31.4 m/min cutting speed, 8-12 mm/min feed rates with 1.5 and 2 mm diameter pilot holes to find out the effect on thrust force,

3: Literature review of the drilling of CFRP

Figure 3-30. The work found that the critical thrust force for the onset of delamination was reduced slightly (11%) in the case of with-pilot as compared to that in the case of without pilot hole. However, the reduction in thrust force by using a pilot hole was found to be in the range of 25-50%. Thus, the thrust force was found to be reduced effectively even if the critical thrust force was increased slightly in the case of with-pilot hole drilling. It was also found that thrust force in the case of without pilot increased with increasing chisel edge length, however, the reason for such behaviour was not explained in their work, Figure 3-30.

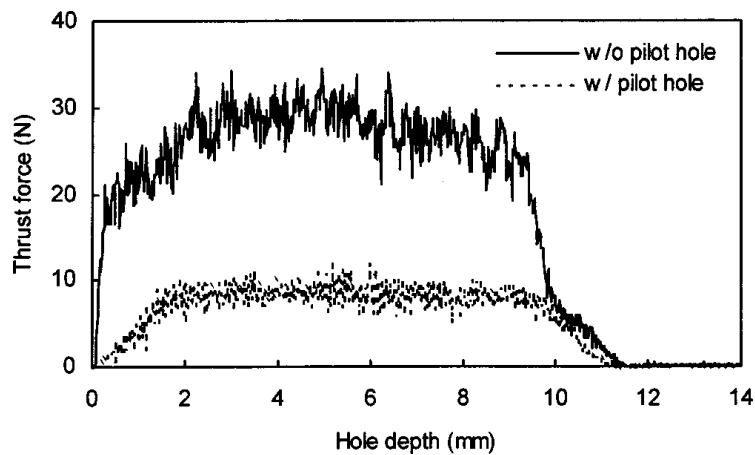


Figure 3-28: Lower thrust force obtained in the case of with-pilot hole than that in the case of without-pilot hole drilling in the work of Won and Dharan [20]

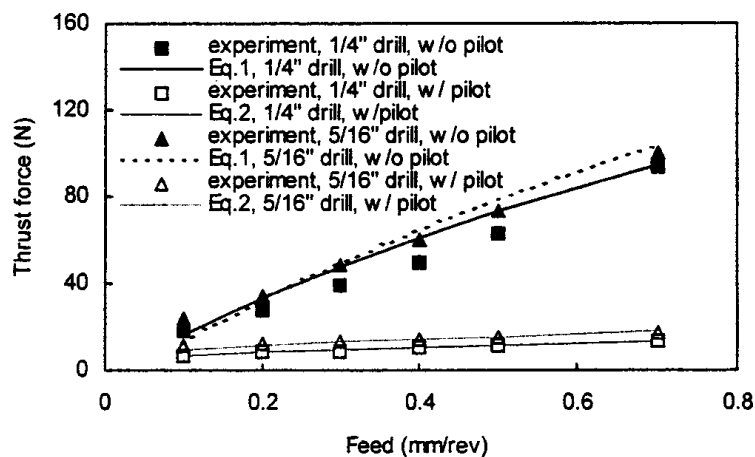


Figure 3-29: Effect of feed rate on thrust force when using pilot holes in the work of Won and Dharan [20]

3: Literature review of the drilling of CFRP

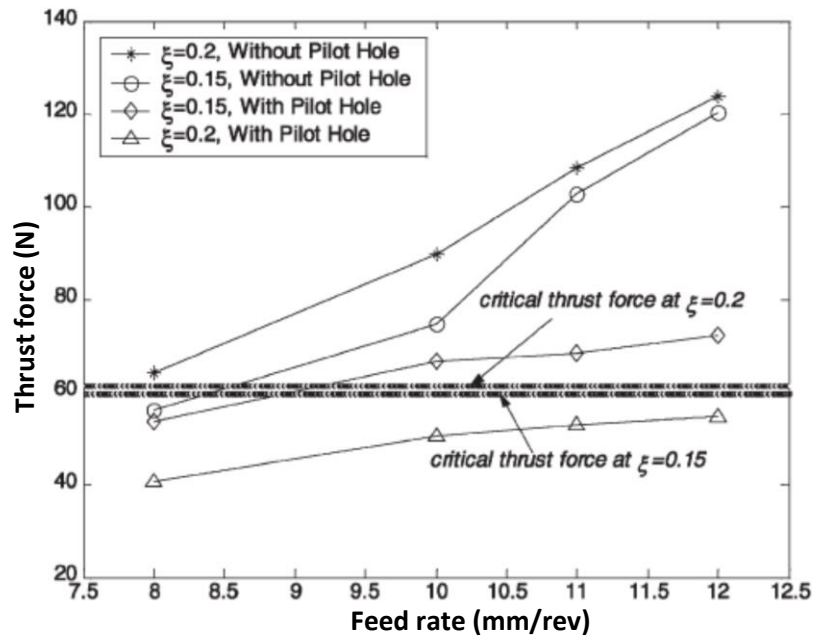


Figure 3-30: Thrust force in the cases of with and without pilot holes with 10 mm diameter drill at various feed rates and 1000 rpm spindle speed in the work of Tsao and Hocheng [21] (ξ = chisel edge length to diameter ratio)

In addition, Tsao and Hocheng [21] predicted a range of chisel edge length to diameter ratio theoretically in which a delamination free drilling could be achieved however, it was not verified experimentally. To determine the effect of pilot holes on entrance and exit delamination with different geometries drills, Faraz and Biermann [99] conducted an experimental study on 10 mm thick woven CFRP/epoxy laminates with two uncoated cemented carbide twist drills having 118° and 85° point angles, 26° and 0° rake angles and 8 mm diameter, at 80 m/min cutting speed and 0.05 and 0.35 mm/rev feed rates. The diameters of pilot holes were 4 mm and 5.5 mm respectively. The machining parameters and drill used to drill pilot holes were not mentioned in their work. Also, it was not clear in their work whether the diameter of the pilot hole was equivalent to chisel edge length or otherwise.

Similar to previous researches, Faraz and Biermann [99] also found thrust force to be reduced by 50% in both the cases of drills when 4 mm diameter pilot holes were used as compared to the case of without pilot hole. With the use of higher

3: Literature review of the drilling of CFRP

diameter of 5.5 mm for pilot hole, the thrust force was found to be reduced by 70% due to the less remaining material to be drilled in the subsequent drilling. However, the entrance delamination was found to be unaffected by pilot holes and exit delamination was found to increase when using pilot holes. Also, with an increase in the diameter of pilot holes (5.5 mm), the exit delamination was found to increase even more for 118° point angle drill in spite of large 70% reduction in thrust force as shown in Figure 3-31. It was suspected that the critical thrust force for the onset of exit delamination was reduced “much significantly” after drilling pilot holes. Also, across the periphery at the exit, the fibres were more prone to bend instead of cutting under the action of cutting edges of twist drill propagating at the exit. Therefore, the exit delamination was not reduced even if a large reduction in the thrust force was observed in their work. Work of Faraz and Biermann [99] also suggests further that effective tool geometries need to be researched instead of focusing on chisel edge effects in order to reduce exit delamination in drilling of CFRP material.

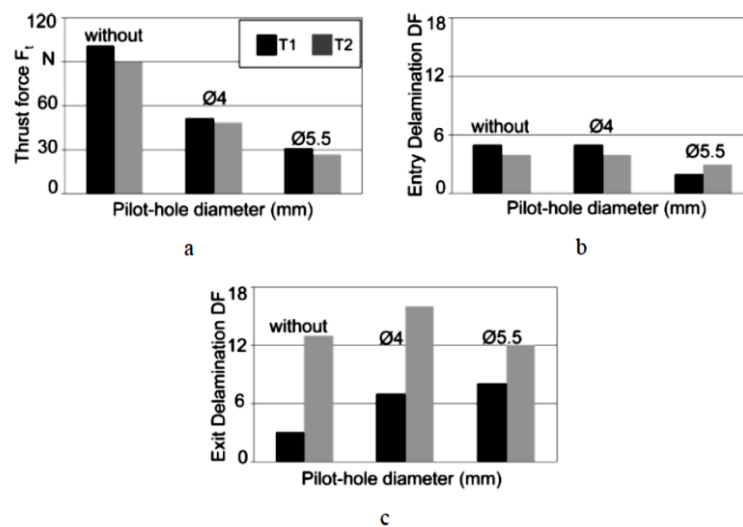


Figure 3-31: Effect of pilot hole drilling at (a) Thrust force, (b) entrance delamination and (c) exit delamination in the work of Faraz and Biermann [99]

3.5.3 Tool geometry

In addition to machining parameters, tool geometry plays an important role in the drilling of CFRP material. Researchers have proposed many of alternative tool geometries (other than conventional two flute twist drills) which cause lower thrust force and hence reduce delamination during drilling [13, 17, 79, 91, 108, 116, 132]. Although, the researchers did not propose any geometry which could reduce the internal damage (fibre pull-out, matrix cracking, fibre-matrix debonding) in the hole.

Gaitonde et al. [94] conducted the experiment to identify the effect of cutting speed, feed rate and the point angle of the two flute twist drill on the entrance delamination factor based upon response surface methodology with three-level full factorial design and developing a second order regression model. They conducted the experiment with the levels of 60, 120 and 600 m/min cutting speeds, 1, 3 and 6 m/min feed rates and 85° , 115° and 130° point angles. It was found that the entrance delamination could be reduced by using a low point angle. Delamination factor at the entrance was found to increase from 1.4 to 2.2 when point angle was increased from 85° to 130° . Thus, low point angle was recommended for reducing the entrance delamination. The exit delamination was not a focus in their work.

Chen [10] conducted an experimental study at 21.5 m/min cutting speed, and 0.1 mm/rev feed rate with 5 mm diameter HSS drill to study the effect of tool geometry (point angle, helix angle, chisel edge rake angle and web thickness) on delamination. It was found that increasing point angle from 90° to 140° caused a reduction in torque from 16 to 6 N-cm. The reason behind this was explained as increasing the point angle caused an increase in the orthogonal rake angle at each point on the primary cutting edge which led to the lower cutting force resulting in a reduction in torque. However, due to increase in thrust force from 40 to 100 N with

increasing point angle from 90° to 140° , lower point angle was recommended for lower delamination. As increasing helix angle causes an increase in the orthogonal rake angle at the primary cutting edges, therefore a reduction in thrust force with increasing helix angle was found in their work. It was reported that thrust force was reduced by 5 N when the helix angle was increased from 24° to 40° in their work. However, in practice, 5 N is a small force to be claimed as a reduction in thrust force. As most of the drilling force comes from chisel edge, Chen [10] reported increasing chisel edge rake angle from 40° to 60° causing a reduction of 10 N in thrust force, as larger the chisel edge rake angle imposes smaller chisel edge length and hence smaller thrust force being produced during drilling. They also noted that increasing the web thickness of a drill from 0.6 mm to 1.1 mm resulted in 40 N additional thrust force. It was explained that increasing web thickness increased chisel edge length and hence, the thrust force increased. Therefore, lower web thickness in a drill was recommended for lower delamination during drilling of CFRP.

Durao et al. [129] conducted an experimental study to identify the effect of drill geometries of twist drills having 120° and 85° point angle in addition to brad drills, dagger drills and step drills on thrust force, exit delamination and internal surface roughness in the drilled holes. All drills had 6 mm diameters in their study. The cutting speed was 53 m/min and feed rates were 0.02, 0.06 and 0.12 mm/rev. It was found that out of all the drills, even though the thrust force was maximum in the case of twist drill having 120° point angle, Figure 3-32, the exit delamination was reported to be minimum. Maximum exit delamination was found in the case of brad drill as shown in Figure 3-33. Therefore, for minimum damage in the drilled hole,

the twist drill having 120° point angle was recommended in their work for drilling of CFRP material.

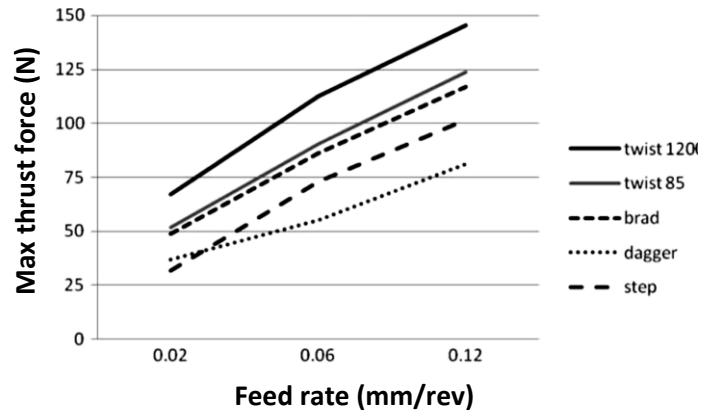


Figure 3-32: Thrust force generated in the cases of twist, brad, dagger and step drills used in the work of Durao et al. [129]

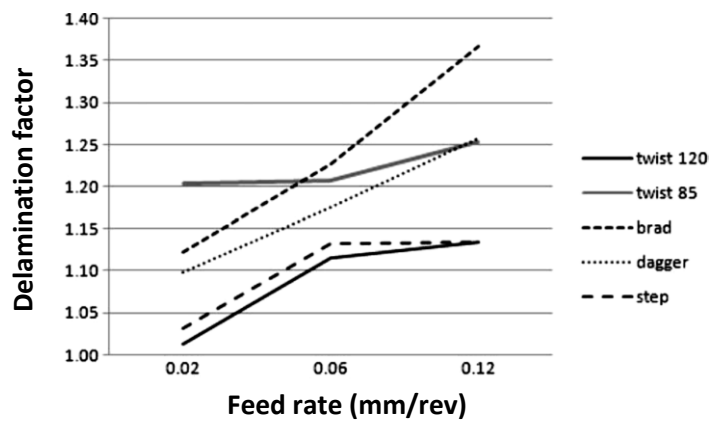


Figure 3-33: Comparison of exit delamination from the twist, brad, dagger and step drills used in the work of Durao et al. [129]

Piquet et al. [79] proposed an alternative geometry of a twist drill for drilling of thin CFRP plates of 3 mm thickness. In the new geometry, the cutting edge of a twist drill was trimmed further and minor cutting edges were produced making a pointed and bullet shaped drill, Figure 3-34.

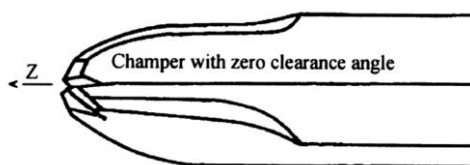


Figure 3-34: A bullet shaped drill geometry proposed by piquet et al. [79]

3: Literature review of the drilling of CFRP

The effectiveness of the tool lies in the specific geometry of the tool in which tip (AB in Figure 3-35) of proposed drill (OP1 in Figure 3-35) drill has reached to the hole exit during drilling while the nominal diameter (D) of OP1 drill did not reach to the hole entrance unlike conventional two flute twist drill (F2 in Figure 3-35) where the whole cutting edge is near to the hole-exit. According to Piquet et al. [79] this allowed thrust force to be distributed along the entire drilling depth instead of concentrating at the last few laminates near hole exit in the case of conventional two flute twist drill which led lower delamination in the case of proposed tool-geometry. The thrust force was found to be 37% less in the case of proposed drill as compared to that in the case of conventional two flute twist drill when drilling with 18 m/min cutting speed and 0.05 mm/rev feed rate. However, the quantitative comparison between the damage generated in the case of two drills was not presented in their work.

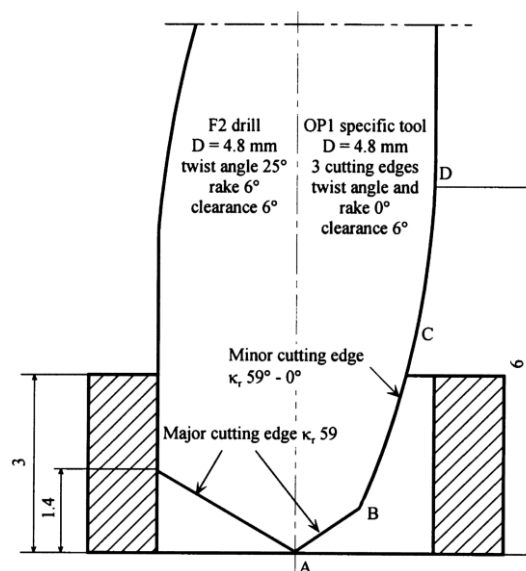


Figure 3-35: Comparison between the cutting mechanism of 2-flute twist drill and the proposed geometry of bullet shaped drill in Figure 3-34 by Piquet et al.[79] (F2 = conventional 2-flute twist drill, OP1 = proposed geometry of 3-flute drill).

Tsao and Hocheng [13, 17, 91, 116, 132] conducted theoretical and experimental research to study and compare the effect of twist, saw, candle stick and step drill

geometries on thrust force and exit delamination, Figure 3-36. They found experimentally that critical thrust force during drilling varied with individual drill geometries. They conducted drilling tests at 28.3 and 31.4 m/min cutting speeds and feed rates between 0.003 to 0.0133 mm/rev for each type of drill (made of HSS) to determine the effect of the various drill geometries on thrust force. Out of all the drills, the minimum thrust force in the range of selected drilling parameters was found for candle stick drill because candle stick drill has a smaller and pointed chisel edge which punches through the last ply and eliminates the effect of chisel edge during drilling as compared to twist drill and hence the thrust force is reduced, Figure 3-37. In addition, based upon experimental critical thrust force value for each drill, they identified the critical feed rate (feed rate above which thrust force exceeds critical thrust force and delamination takes place at the exit of the hole) for each drill geometry. Maximum thrust force and minimum critical feed rate of 0.0047 mm/rev were found for the case of twist drill, Figure 3-37. The maximum critical feed rate of 0.0075 mm/rev was found in the case of core drill. This means that the holes could be drilled at largest feed rate with core drill in order to avoid the exit delamination. This was reported to be because core drills have a different machining mechanism to twist and candle stick drills. It consists of small diamond grains on the periphery of the hollow drill which remove the material during drilling through abrasive machining similar to material removal process in grinding operation. However, due to core drills being hollow, chip clogging inside the hollow drills was found to be a cumbersome problem in drilling with a core drill.

3: Literature review of the drilling of CFRP

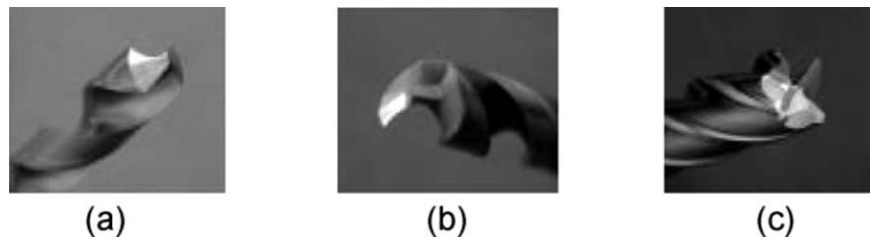


Figure 3-36: (a) Twist drill, (b) Candle stick drill and (c) saw drill having 10 mm diameter used in the work of Hocheng and Tsao [13, 17]

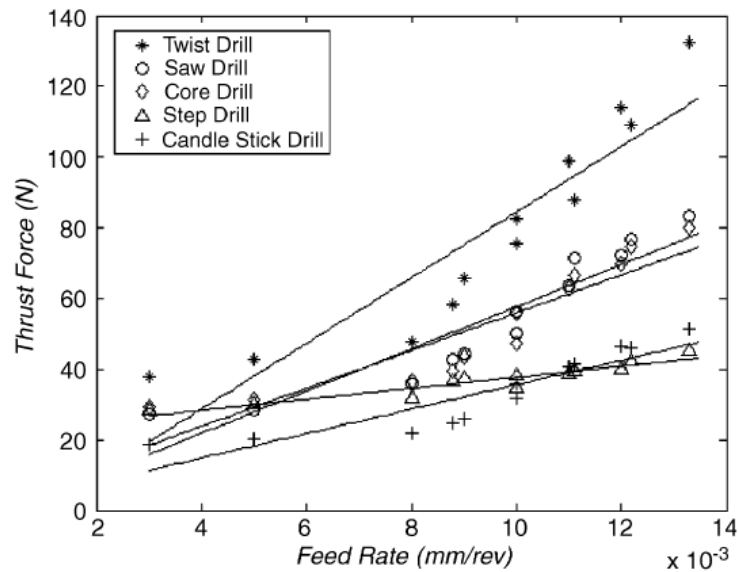


Figure 3-37: Thrust force data for various drills in the work of Hocheng and Tsao [13]

Once it was determined that maximum critical feed rate was in the case of core drills then further work was needed in order to facilitate chip removal easier through core drills. In a later work Tsao and Chiu [108] proposed special geometries of core drills which were the combination of conventional and core drills as shown in Figure 3-38. Also, the cutting velocities and rotational directions of the two (internal and external) parts of special core drills were independent. It was found that the maximum reduction in the thrust force was found when the rotational direction of internal and external parts of special core drills was in opposite direction because according to Tsao and Chiu [108] rotation in opposite direction caused a reduction in uncut chip thickness and chip removal became easier. Also, out of all the special

geometry drills, the core-saw drill was found to cause lowest thrust force due to thrust force being distributed on the cutting edges of saw drill instead of the centre of the drill as in the case of a twist drill. However, quantitative comparison amongst the damage generated through various drill bits was not presented in their work.

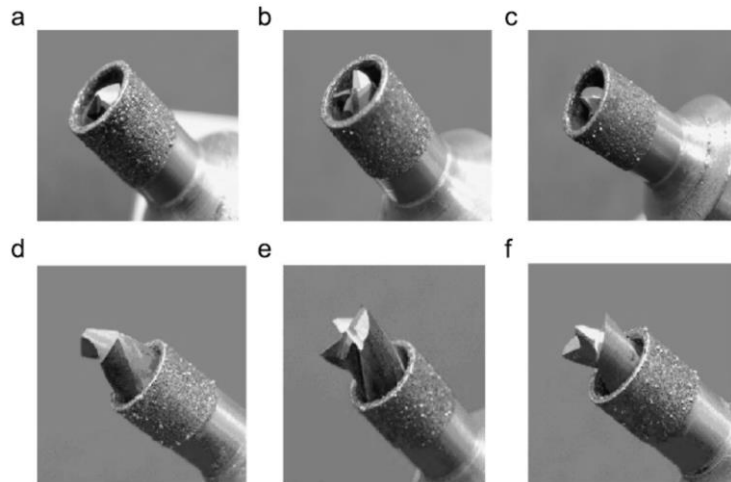


Figure 3-38: (a) core twist drill, (b) core saw drill, (c) core candle stick drill (d) step core twist drill, (e) step core saw drill and (f) step candle stick drill having 10 mm outer drill diameter experimented in the work of Tsao and Chiu [108]

In addition to the pilot holes and tool geometries, use of a backup plate at the exit of a hole has been advised by the authors in order to reduce exit delamination. According to Tsao and Hocheng [133], use of a backup plate causes an increase in the theoretical critical thrust force required for delamination. If the thrust force during drilling is kept below the theoretical critical thrust force, the delamination free holes could be achieved. Tsao and Hocheng [133] proposed a mathematical model for using a backup plate during drilling. It was found that using a backup plate increased theoretical critical thrust force for delamination, Figure 3-39. The experiment was performed at 31 m/min cutting speed and 8, 12 and 16 mm/min feed rates with 10 mm diameter HSS drills. It was found that although using a backup plate caused an increase in the thrust force, however, the theoretical critical thrust force was increased to a much larger extent as shown in Figure 3-39. This is why it

was proposed that the holes could be drilled with a larger feed rate when using a backup plate. However, the quantitative comparison between the damage generated during with and without backup plate was not presented in their work. In addition, it was mentioned that the use of a backup plate is well known to the industries.

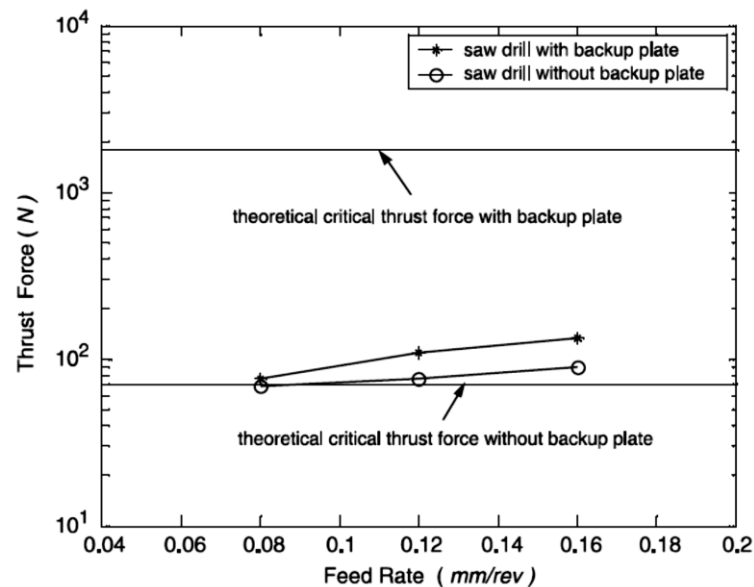


Figure 3-39: Thrust force variation with respect to feed rate with and without a backup plate in the work of Tsao Hocheng [133], Although experimental thrust force with backup plate increased but it was lower than the theoretical critical thrust force required for delamination.

3.5.4 Tool wear and material

Tool wear is an important aspect during drilling of CFRP. Authors have reported thrust force to be increasing with increasing tool wear [78, 95, 134, 135]. As CFRP material is abrasive in nature, tool material and tool wear play an important role in the drilling of CFRP. Due to abrasive nature of CFRP, the tool wears rapidly which shortens tool life and increases the cost of production [10]. In addition, during any machining operation, as the wear at flank surface increases, area in the flank surface exposed for friction between flank surface face and workpiece increases. Due to increase in friction forces, cutting temperature increases [136]. Increasing cutting temperature is detrimental to the matrix of CFRP and it causes thermal damage

3: Literature review of the drilling of CFRP

during drilling, resulting in the reduction of fibre-matrix interfacial shear strength and deteriorated machined surface [136, 137]. Thus, increase in tool wear during drilling of CFRP is not desired during drilling. For an uncoated tungsten carbide tool, a cutting edge rounding due to abrasive wear as a result of drilling CFRP has been reported [95, 138], Figure 3-40. In order to minimise the damage, low cutting speed and low feed rate have been suggested by the authors to use since it results in low tool wear [3, 10, 135].

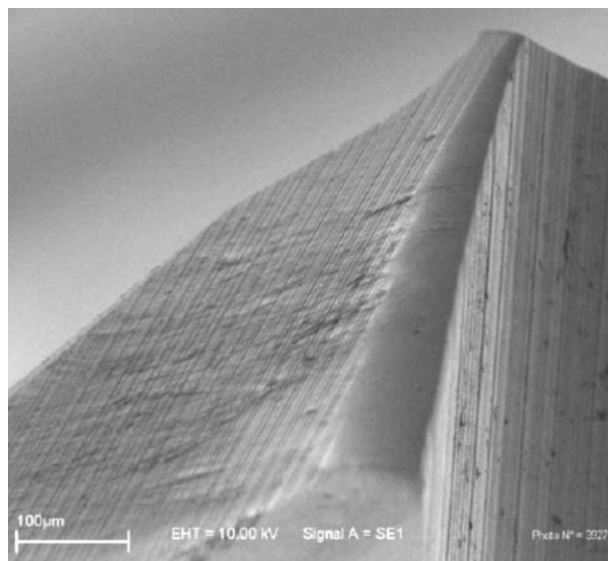


Figure 3-40: SEM Image of cutting edge rounding due to at the cutting edge of uncoated tungsten carbide tool in the work of Lliescu et al. [138].

Since machining of CFRP is wear dominated, therefore, appropriate selection of tool material having more resistance to wear would be required which could retain its geometry for larger machining time and hence, machining damage and production cost could be reduced [72]. The authors have compared the tool materials of HSS, Tungsten carbide (WC), poly crystalline diamond (PCD) and have concluded that PCD tool results in lowest tool wear and longest tool life whereas, tool made of HSS had the maximum tool wear and lowest tool life during machining of CFRP [72, 100, 139-141]. Thus, drills made of HSS cause higher delamination as compared to those

made of WC and PCD because WC and PCD material is less affected by the abrasive nature of CFRP in comparison to HSS material [100, 139]. In addition, in order to protect the tool-material from the abrasive workpiece and the extreme conditions of the machining environment during machining, tool coatings having higher resistance to abrasion wear have been recommended by the authors [138]. Titanium nitride (TiN), Titanium aluminium nitride (TiAlN), diamond coating are a few examples of tool coatings. Out of these, the diamond coating contains maximum resistance to wear and lasts for the longest duration of time during machining [142-144]. Although as reported by Teti [72], PCD tool material contains greater resistance towards tool wear as compared to diamond coating. Therefore, PCD tool is recommended for CFRP drilling. At the moment, dagger drills having PCD inserts are used as the current state-of-the-art for drilling of CFRP in BAE Systems. The machining parameters for a 6.35 mm diameters are 5000 rpm spindle speed (100 m/min cutting speed) and 300 mm/min feed rate [6]. For a 6 mm diameter, diamond coated twist drill, 100 m/min cutting speed and 0.03 mm/rev feed rate has been recommended by the tool manufacturer SGS Solid Carbide Tools [145].

Thus, through conventional drilling, authors have recommended high cutting speed and low feed rate for low delamination. However, high cutting speed causes higher tool wear and hence reduces the tool life which increases the cost of production. Alternate tool geometries (other than twist drills) have been attempted to lower the damage. Nevertheless, the damage has not been ruled out completely through conventional drilling methods. In addition, the internal damage in a hole has not been studied in detail during conventional drilling and it is still a current topic of research amongst the researchers.

3.6 Attempts to minimise the damage during drilling of CFRP through non – conventional manufacturing processes

When even after using advanced geometry drills, the delamination and damage on the internal cylindrical machined surface of a hole could not be avoided during drilling, researchers attempted to find alternative and non-conventional manufacturing processes through which delamination and damage in a hole could be avoided. In the non – conventional machining processes laser processing, water and abrasive water jet machining, ultrasonic machining and vibration assisted machining have been used in most of the studies.

3.6.1 Laser Processing

Laser processing is a non-contact and non-polluting process which has the advantage of intense heat to evaporate and cut the materials. A high-energy beam of the laser is focused in a 0.1 to 1 mm diameter area of the material which causes melting, vaporisation and thermal degradation through the depth of the material. The molten and evaporated material is blown away from the machined surface by the external pressure of inert gas atmosphere coaxial to laser beam [31]. During laser drilling, there is no direct contact between cutting tool and laminates of CFRP, therefore, the exit delamination does not take place [31]. However, in order to melt and sublimate CFRP, the laser power is set in such a way that the temperature of heat affected zone (HAZ) is more than the vaporization temperature of carbon fibres. Due to different evaporation temperatures of carbon fibre and matrix (3900°C and ~800°C respectively [146]), The carbon fibre being conductor of heat (50 W/mK) conductivity in fibre axis direction [146]), conducts the heat to surrounding matrix in the heat affected zone. This affects the surrounding matrix and thermal damage i.e. thermal degradation, fibre swelling and matrix burning take place, leading to a loss

in strength of CFRP [31, 35, 147]. Therefore, due to the thermal damage, laser processing is not recommended for drilling of CFRP. These challenges require other manufacturing processes for achieving comparatively lower damage in the drilling of CFRPs.

3.6.2 Water jet and Abrasive water jet machining (WJM and AWJM)

In water jet machining (WJM), a pressurised water jet (up to 3800 bar) is released through a small nozzle (0.12 – 0.33 mm diameter) directed at the work piece which impacts the surface with high velocity (~870 m/s) and hence, the cutting and drilling is performed by the localised shearing, fracture and erosion of the material and machined chips are flown away by water [31-34]. In order to increase the cutting efficiency to machine the hard materials, the abrasive slurry is mixed with the water jet and the combined process itself is known as abrasive water jet machining (AWJM). Unlike laser machining, AWJM results in minimum thermal or mechanical stress being induced and it is comparatively inexpensive [32, 36, 148]. Similar to conventional drilling, exit delamination during water jet drilling is also found due to thrust jet force exerted by water jet onto composite laminates. As the water jet approaches towards the exit of a hole, the support under the laminates reduces and laminates tend to be pushed away. When the thrust jet force exceeds the critical thrust force at the exit, exit delamination takes place [149]. Disadvantages such as delamination at the jet exit side due to the perpendicular force of the jet on the workpiece surface, absence of the matrix material due to being washed out by jet as it is softer than fibres and cracking and chipping at the exit side due to the reduction in the power density of the water jet over the layers of the laminate make WJM difficult for drilling of CFRP [36, 37].

3.6.3 Ultrasonic machining

In ultrasonic machining (USM), there is a vibrating tool with ultrasonic frequency e.g., 20 kHz attached with the ultrasonic vibration generator having a power of ~250 W [150] and an abrasive slurry between the tool and the work piece. The material is removed by the “hammering” of the vibrating tool to the abrasive particles which in turn impact the workpiece material. Material removal is performed by the erosion of the material from the surface of the workpiece. Ultrasonic machining is suitable for the brittle material which can be eroded easily and it is free from delamination [4, 150-152], Figure 3-41. It has been reported that there is no exit delamination during ultrasonic drilling of CFRP [152]. However, this process is not recommended for mass production due to its much slower material removal rate i.e. a few minutes for a hole compared to other hole-making processes [31].

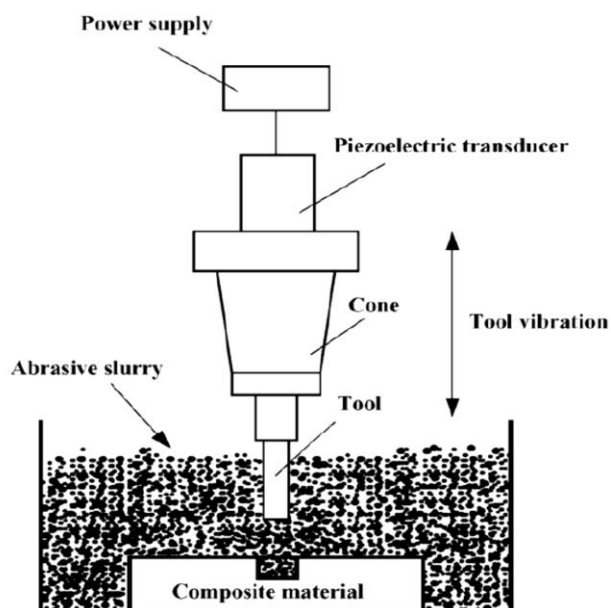


Figure 3-41: Schematic of ultrasonic machining [31]

3.6.4 Rotary ultrasonic machining

Some researchers imposed ultrasonic vibrations in the axial direction having constant axial feed rate using the rotating core drills with metal bonded diamond abrasive grits on it and defined it as ‘rotary ultrasonic machining (RUM)’ process. It

is a non-traditional manufacturing process which combines the material removal mechanism of diamond grinding and ultrasonic machining [153]. In RUM, the tool rotates and the chip removal is performed by the abrasive diamond grits bonded with the tool during diamond grits-material interaction in the rotating tool. The coolant is flown through the centre of the drill which keeps the drill cool and takes away all the chips generated during machining [153-156]. Although some authors have found zero delamination [157] with this process but similar to ultrasonic drilling, this process took 3.5 minutes to drill a hole and therefore not useful for mass production. Upon increasing the feed rate edge chipping has been reported by authors similar to as shown in Figure 3-42 when drilling the holes with this process which is still a challenge to be solved with this process. In addition, with the use of cutting coolant, this process would not be recommended for machining of carbon fibre composites as in the machining of carbon fibre composites, the use of coolant is not recommended by the researchers due to moisture being absorbed into the matrix of CFRP and hence reducing its strength [70, 71].

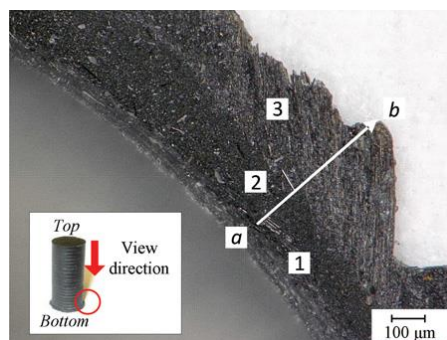


Figure 3-42: Edge chipping at the exit of the hole during RUM in the work of Feng et al. [156]. The distance between 'a' and 'b' was found to be 600 μm defined as chipping size in their work. The maximum thickness of the edge chipping was 207.9 μm in their work.

3.6.5 Vibration assisted machining

As mentioned in section 3.5, researchers made several attempts to reduce cutting and thrust forces in order to reduce damage in the drilling of CFRP by implementing

the techniques of pilot hole drilling, modifying geometries of drills and optimizing machining parameters. A group of other authors has reported cutting forces being reduced when vibrations are implemented on cutting tool or on workpiece due to its intermittent cutting action (explained in section 3.6.5.1) [40-47]. Some other researchers attempted imposing vibrations during drilling of CFRP and found a reduction in exit delamination due to reduction in thrust force [40, 158, 159]. However, the only damage considered in the work so far is exit delamination. There is little literature available in detail which could explore the effect of vibrations on the entire damage in a workpiece hole during vibration assisted drilling.

Vibration assisted drilling is a specific process of vibration assisted machining process. In vibration assisted machining, the vibrational motion is imposed on machining tool or workpiece during machining. Vibrations can be applied on the tool either in the direction of the cutting motion or feed motion or in both. One directional vibration implemented on a cutting tool results into a linear path and two-dimensional vibrations result into an elliptical path of cutting tool during machining. [160, 161]. Vibrations can also be implemented on the workpiece instead of cutting tool during machining [161, 162].

3.6.5.1 Concept of intermittent cutting during vibration assisted machining

As mentioned earlier, intermittent cutting action has been recognised by authors causing a reduction in cutting forces during VAM. To understand the intermittent cutting action in vibration assisted machining, the tool material interaction during vibration assisted machining is required to be visualized. As explained by Brehl and Dow [161], the vibration assisted machining contains four stages as shown in Figure 3-43.

3: Literature review of the drilling of CFRP

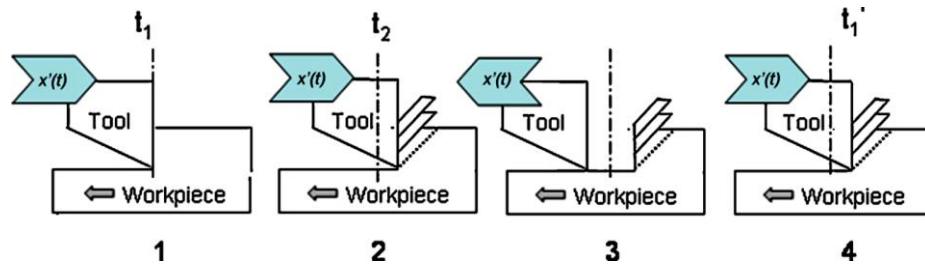


Figure 3-43: Intermittent cutting action of cutting tool explained by Brehl and Dow [161]

In part 1 of Figure 3-43, the tool approaches to the workpiece having the direction of motion in the opposite direction of workpiece motion with the relative velocity with respect to workpiece greater than zero at time instant t_1 . After this, the tool starts machining and chip formation until its relative velocity becomes zero with respect to the workpiece which is shown in part 2 of Figure 3-43 at time instant t_2 . Because of the continuation of the vibrational cycle and changing its direction, the tool reverses its direction of motion and moves in the direction of the workpiece as shown in part 3 Figure 3-43. The tool moves further in the same direction until its velocity becomes zero and then the tool again reverses its direction of motion in the opposite direction of workpiece motion and is ready for another vibration cycle. The step 3 shown in Figure 3-43 is the critical step in which the tool can separate from workpiece if its velocity in the direction of workpiece motion is greater than that of workpiece itself.

If the vibrations are imposed in the direction of cutting speed (V), for a given vibration frequency (f) and amplitude (A), there exists a critical cutting velocity below which the cutting tool breaks contact with the material during machining in one oscillation cycle. As shown in Figure 3-43, the vibrations are applied to the cutting tool and cutting velocity is given to the workpiece. The location of the cutting tool ($X_I(t)$) in the sinusoidal oscillations of the tool can be represented by:

$$X_I(t) = A \sin(\omega t) \quad \text{- Equation (3.4)}$$

In Equation (3.4), angular frequency $(\omega) = 2\pi f$

Because of the linear cutting velocity, the location of workpiece $(X_2(t))$ would be,

$$X_2(t) = Vt \quad \text{- Equation (3.5)}$$

The cutting motion of cutting tool during chip formation in the vibration assisted machining would be the resultant relative motion of cutting velocity and vibrational motion between them. Therefore, the relative location of the tool with respect to work piece $(X(t))$ would be

$$X(t) = X_1(t) + X_2(t) = A \sin(\omega t) + Vt \quad \text{- Equation (3.6)}$$

And relative velocity of the cutting tool with respect to work piece $(X'(t))$ would be

$$X'(t) = \frac{d}{dt}[X(t)] = A\omega \cos(\omega t) + V \quad \text{- Equation (3.7)}$$

Going back to step 3 of Figure 3-43, the tool-workpiece detachment is possible if the tool has a greater velocity than that of the workpiece. In mathematical terms, if $X_1'(t) > X_2'(t)$ at step 3, the tool will lose the contact with the workpiece. This means, in order to lose contact between tool and workpiece,

$$A\omega \cos(\omega t) > V \quad \text{- Equation (3.8)}$$

The maximum value of $\cos(\omega t)$ is 1. Therefore, in absolute terms if $V < A\omega$, i.e. $V < 2\pi fA$, the tool and workpiece will have a periodic separation in step 3 of Figure 3-43 in every vibration cycle. This periodical cutting by cutting tool and tool-workpiece separation in every vibration cycle is known as the **intermittent cutting action of cutting tool**. Thus, unlike conventional machining where chip formation happens due to the continuous interaction between tool and workpiece, the chip formation in vibration assisted machining happens due to intermittent tool-workpiece

interactions during machining in every vibration cycle. Most researchers have reported this intermittent cutting to be responsible for reduced cutting forces during vibration assisted machining of various materials as compared to those in conventional machining [40-44, 47].

3.6.6 Vibration assisted drilling (VAD) of CFRP

Some researchers have implemented low vibration frequencies in the range of 30 Hz to 600 Hz [30, 38, 39] during drilling of CFRP material and found a reduction in exit delamination compared to CD.

Sadek et al. [30] performed an experimental study at cutting speeds of 113, 169 and 226 m/min and feed rates of 0.025, 0.05 and 0.075 mm/rev. The vibrational parameters in their work were 30 and 60 Hz frequency and amplitude was varied from 25 μm to 800 μm in such a way that axial speed ratio (ASR) of vibrational speed and conventional feed speed ($A\omega$ and V respectively in Equation 3.8) had consistent values of 3.3, 6.7 and 10 at every cutting and feed rate combination. Therefore, they observed the thrust force variation with respect to reducing intermittent contact between tool and workpiece with increasing frequency and amplitude. As the intermittent contact between tool and workpiece was reduced with increasing ASR, thrust force was found to increase, Figure 3-44. It can be seen Figure 3-44 that with in increasing ASR the thrust force in VAD increased at all the cutting speeds. In addition, it was reported that lower thrust force in VAD in comparison to CD was obtained when the amplitude of oscillations was low and frequency was high. The reason behind this was explained as the depth of cut to be smaller at the maximum tool-material engagement at low amplitude. Also, at high frequency, the tool-material engagement time would reduce which subsequently reduce the MRR per oscillation cycle resulting in reduction in cutting forces. The

3: Literature review of the drilling of CFRP

cutting temperature was also measured in their work and no thermal damage was found even if the cutting temperature of 380° exceeded the thermal degradation temperature of epoxy (320°) unlike in their CD work. The authors explained this in terms of an air gap between tool and workpiece during intermittent cutting proposing that the heat was convected away from the tool by air-gap flow between tool and workpiece which did not occur in CD. The exit delamination was measured by observing the exit of the hole through a Winslow 560 video tool and it was claimed to achieve zero exit delamination at 0.025 mm/rev feed rate although no pictorial evidence was produced to support this. The hole surface roughness was measured by a contact surface profilometer and was found to increase from 2 to 6 μm as cutting speed increased from 113 to 226 m/min at each feed rate with the VAD process. In CD, the surface roughness was found to be 1.5 to 3 μm . Therefore, at highest cutting speed and feed rate the surface was found to be deteriorated in VAD as compared to that in CD. The reason was suspected to be increasing the depth of cut at high amplitude maximum cutting tool engagement.

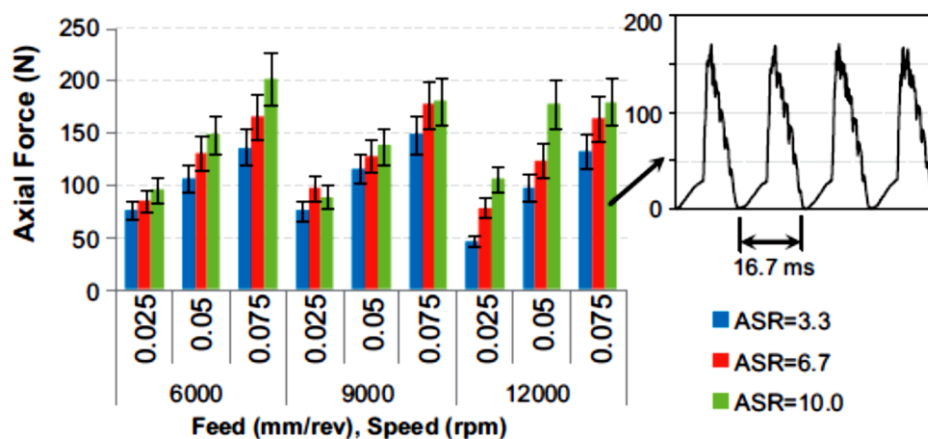


Figure 3-44: Thrust force variation in VAD at various cutting, feed speeds and ASR at 30 Hz frequency in the work of Sadek et al. [30]

Since the critical thrust force reduces rapidly during drilling, therefore, lower feed rate could be used near the exit of a hole in order to avoid the exit delamination during drilling in the case of constant drilling parameters. To solve this problem, Linbo et al. [39] proposed the concept of hybrid variation vibration assisted drilling with three steps of constant-variation-constant parameters to control thrust force during drilling and keep it below the critical thrust force, Figure 3-45. The first step of constant parameters was used at the entrance of the hole when chisel edge is about to penetrate the surface as according to Linbo et al. [39], the entrance delamination could be avoided using high cutting speed. The second step of variation in vibration drilling parameters was used at the moment when the chisel edge of the drill was about to penetrate the last laminate. At this step, the vibration parameters of feed rate, vibration frequency and amplitude were optimized in such a way that the resultant thrust force was lower than the instantaneous critical thrust force. Further, as the chisel edge penetrated the last laminate, constant vibration parameters were used to avoid the exit delamination. This step involves the optimization of the vibration parameters and calculation of the critical thrust force. They performed the simulation for the thrust force and verified it with the experimental observations with a 2.0 mm diameter drill at 138 m/min cutting speed and feed rates between 15 to 300 mm/min. The vibration frequency was varied from 100 to 600 Hz and amplitude was varied from 1 to 10 μm . With this method, the authors reported that they could control the thrust force during drilling and because of variation in the drilling parameters in the second step of variation, the thrust force was found to be reducing as shown in Figure 3-45.

3: Literature review of the drilling of CFRP

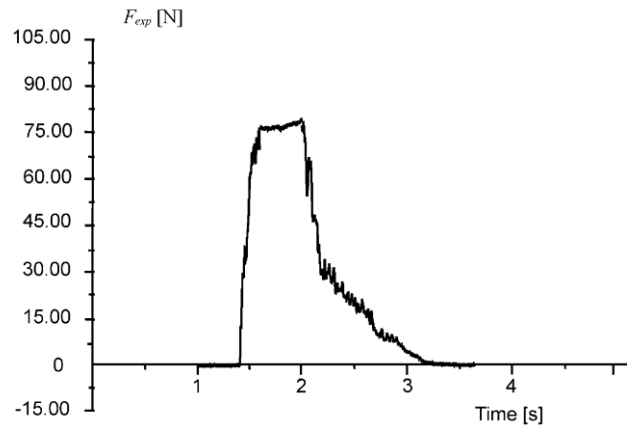


Figure 3-45: Thrust force variation in the hybrid variation drilling [39]

As reported by Linbo et al. [39], the exit delamination was found to be reduced “significantly” with this method. However, there was no quantitative comparison of damage during drilling in their work.

Wang et al. [38] performed experiments to investigate the thrust force in VAD of – glass fibre reinforced plastics (GFRP), CFRP and printed circuit board (PCB) with a 0.5 mm diameter HSS and tungsten carbide drills having 35 m/min cutting speed with the feed rates of 50, 150 and 250 mm/min. The vibration frequencies were 100, 300 and 500 Hz and amplitudes were 2, 6, 10 μm . In this work, the thrust force was found to increase with respect to drilling depth from the entrance to exit when HSS drills were used. This phenomenon was explained as HSS drill has less wear resistance as compared to tungsten carbide drills, therefore, the HSS drill wears out rapidly while drilling a hole in CFRP as compared to tungsten carbide drill. Therefore, the thrust force was found to be increasing with respect to drilling depth due to increasing tool wear in HSS drill. It is reasonable as observed by other authors [100, 139]. The thrust force was found to be gradually reducing with respect to drilling depth from the entrance to exit in a hole when drilling with tungsten carbide drill in the conventional drilling of CFRP. It was explained that while drilling due to

epoxy being non-conducting, accumulation of heat took place near the cutting edge of the drill, which softened epoxy, therefore, thrust force was reduced as the drill progressed during drilling in the case of tungsten carbide drill. This was verified by drilling a hole in the epoxy matrix without carbon fibres and thrust force was found to be reducing with respect to drilling depth. The intermittent cutting action was surmised to cut the fibres abruptly during to-and-fro oscillatory motion of cutting edge which changed the forming mechanism of chips compared to CD. The thrust force in VAD was found to be lower as compared to that in conventional drilling [38], Figure 3-46. The reason for the reduction in thrust force in VAD was proposed as the reduction in friction between rake face and chips due to frequent oscillatory motion resulting in a relative time of contact being shortened as compared to CD. The effect of reduced thrust force on damage in drilling was not a focus in their work. With amplitudes above $6\ \mu\text{m}$, the thrust force in VAD was found to be more than that in CD. The reason for this was explained as the increasing impact force in the material during VAD due to oscillations of the drill. However, there has been no evidence produced to support this.

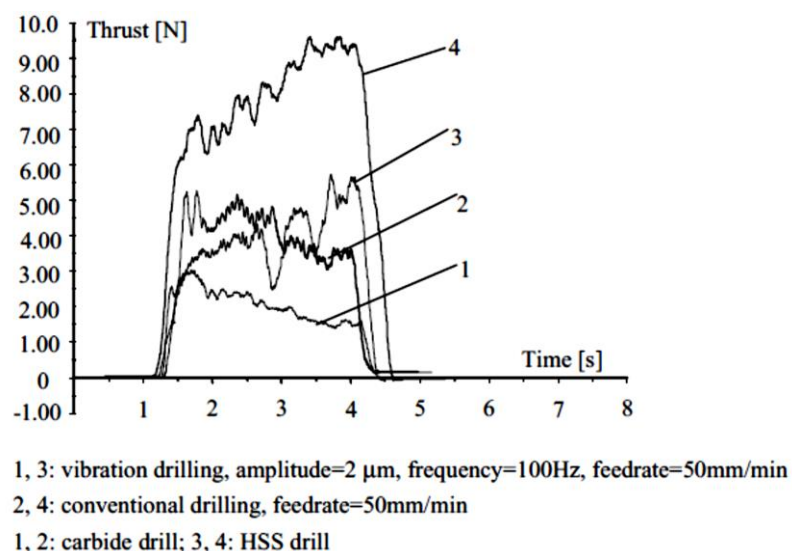


Figure 3-46: Thrust force reduction due to VAD of CFRP in the work of Wang et al. [38]

3.6.7 Ultrasonic assisted drilling (UAD) of CFRP

As reported by Sadek et al. [30], low vibration amplitude and high frequency resulted into a reduction in thrust force during drilling as compared to that in CD in their work. To realize the effect of higher frequencies on metals, other researchers applied higher frequency which falls in the range of ultrasonic frequencies (20 kHz to 60 kHz in general used by the researchers) to see its effect in the drilling of metals [23-29]. Better results (lower thrust force, longer tool life and the smaller chips) were obtained when the cutting of the material was intermittent during the drilling when the frequency of oscillations fell in the ultrasonic range [29] as compared to that in conventional drilling. This particular type of drilling is known as **ultrasonic assisted drilling (UAD)**.

The research is still in its initial phase of the drilling of CFRP with UAD and researchers are making an attempt to meet the challenges (minimizing the entrance/exit delamination and the internal damage) during the through hole drilling of CFRP. In a recent research, Makhdum et.al [40, 158, 163-165] have conducted two sets of experimental studies on UAD of CFRP and developed a finite element model to predict the thrust force, torque and exit-delamination in CD and UAD. The focus of their research was to identify the effectiveness of ultrasonic oscillations for reducing thrust force, torque and exit delamination. In the first experimental study [163, 165], the focus was on the reduction of thrust force and torque because of ultrasonic oscillations. The cutting speed was varied from 4.0 to 32 m/min (260 rpm to 1700 rpm) keeping the feed rate constant at 50 mm/min. The reduction in the thrust force due to ultrasonic oscillations (32.2 kHz frequency and 10 μ m amplitude), as compared to that in CD was found to increase from 15.8% to 31.1% with the increasing cutting speed at constant feed rate. The maximum reduction in

3: Literature review of the drilling of CFRP

the thrust force (31.1%) was found at the highest cutting speed of 32 m/min (1700 rpm). Further, with an improved setup (31.7 kHz frequency and 6 μ m amplitude), Figure 3-47, 91% reduction in the thrust force and 0 N-cm average torque at 0.75 m/min (40 rpm) cutting speed and 8 mm/min feed rate were found. Although, in practice, zero torque does not seem to be accurate i.e. machining is not possible without the cutting forces. In addition, the reason for selecting such machining parameters was not explained in their work. Longer chips and fusion of carbon fibres into the matrix in the chips in UAD were reported in their study, Figure 3-48.

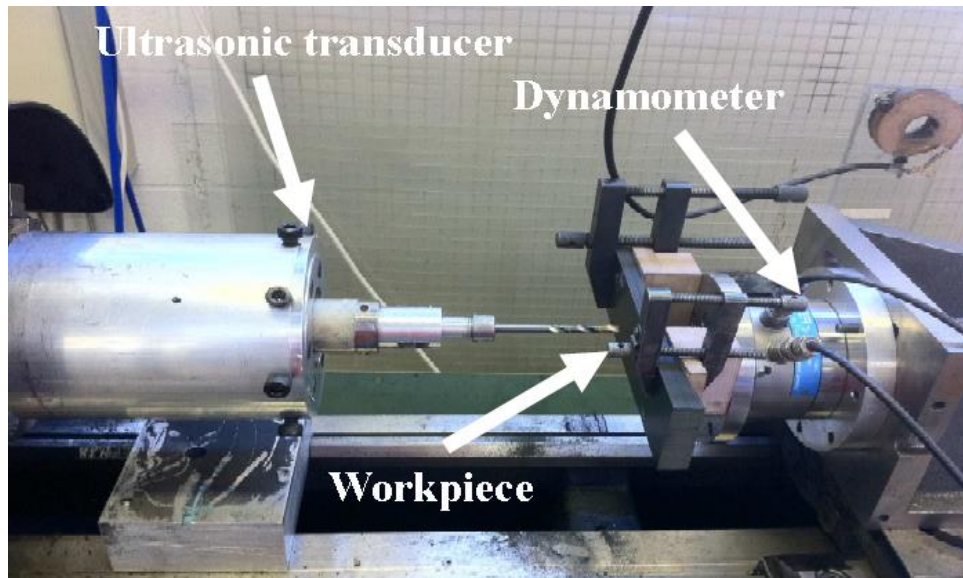


Figure 3-47: Experimental setup of Makhdum et al. for UAD of CFRP [163]



Figure 3-48: Longer spiral chip formation in UAD in the work of Makhdum et al. [164]

In the second experimental study of Makhdum et al. [40], the feed rate was varied from 4 to 20 mm/min at a constant cutting speed of 0.38 m/min (40 rpm) at 27.8 kHz frequency and 6 μ m oscillation amplitude observing the thrust force, torque, exit delamination, cutting temperature and tool wear. As the feed rate was increased from 4 to 16 mm/min, the reduction in the thrust force due to ultrasonic oscillations was found to be increasing from 229 N to 356 N however, at 20 mm/min feed rate the thrust force and torque in the conventional drilling and UAD were found to be similar (511 N and 508 N respectively). Similarly, the exit delamination factor was found to be reduced in UAD as compared to that in CD at all the feed rates except 20 mm/min. The reduction in the exit delamination factor increased from 1.18 to 2.6 as the feed rate increased from 4 mm/min to 16 mm/min but at 20 mm/min the exit delamination factor was found to be similar in CD and UAD (5.83 and 5.86 respectively). The reason for this was speculated to be the absence of the ultrasonic intermittent cutting action at the higher feed rate of 20 mm/min. However, no evidence was produced to support this argument. Now, an interesting phenomenon can be observed at the feed rate of 20 mm/min when comparing to this work of UAD of CFRP [40] and the previous work by Alam et al. [23] in the UAD of cortical bone, Figure 3-49. In both the works, the feed rate was 20 mm/min ('V' in Equation 3.8). The actual maximum ultrasonic assisted velocities were 75360 mm/min (20 kHz frequency and 10 μ m amplitude) and 62850 mm/min (27.8 kHz frequency and 6 μ m amplitude) respectively (' $a\omega$ ' in Equation 3.8). In the work of Alam et al. [23], it was argued that the maximum velocity of 75360 mm/min was "very high" as compared to the feed rate of 20 mm/min and therefore the reduction in thrust force was obtained. While in the work of Makhdum et al. [40], it was speculated that the intermittent cutting action was absent at 20 mm/min and

3: Literature review of the drilling of CFRP

therefore the reduction in thrust force was not obtained. Although the maximum velocity of 62850 mm/min was “very high” as compared to 20 mm/min feed rate in the work of Makhdum et al. [40]. However, no evidence was produced in support of the argument in both the works and materials being machined were different i.e. cortical bone and CFRP respectively (Nevertheless, both are composite materials).

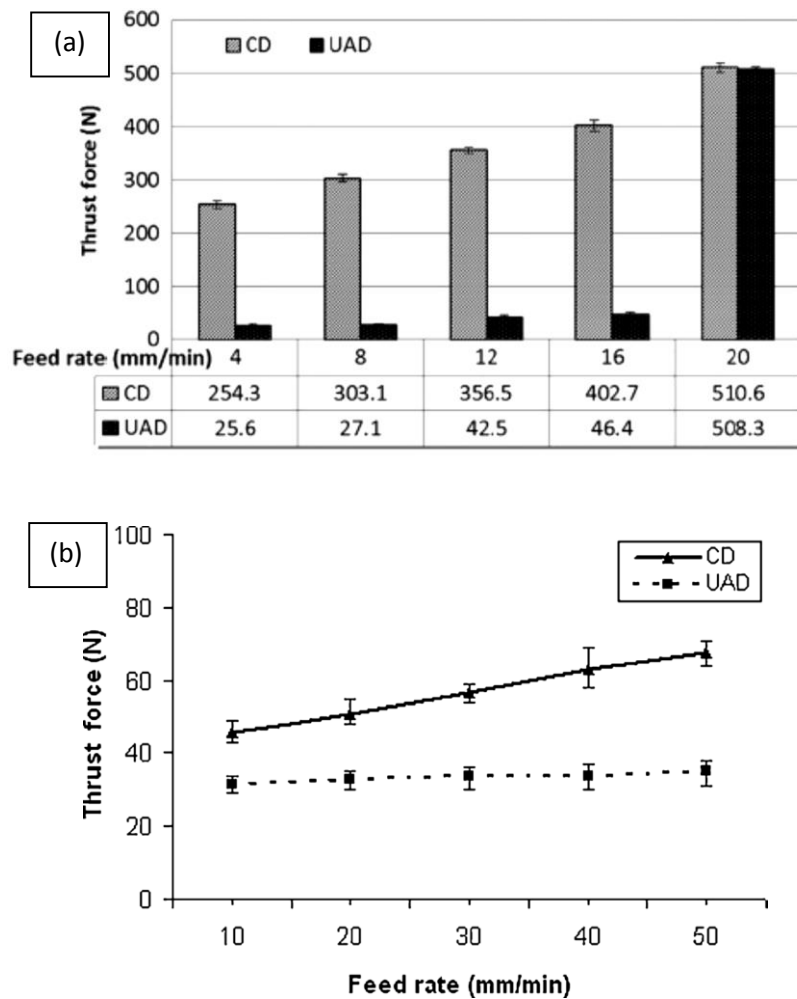


Figure 3-49: Thrust force from (a) CD and UAD of CFRP by Makhdum et al. [40] and (b) CD and UAD of cortical bone by Alam et al. [23]

Comparing the two cases [40] and [23], raises the suspicion on the intermittent cutting action being dependent on the configuration of the specific material being drilled and ultrasonic parameters even at similar cutting speed and feed rates.

3: Literature review of the drilling of CFRP

Furthermore, even though the thrust force was not found to be reduced at 20 mm/min feed rate in UAD in the work of Makhdum et al. [40], the internal surface roughness in UAD was found to be lower than that in CD (2.48 μm and 1.72 μm respectively). The reason for this was not explained in their work and it was asserted as the “effectiveness” of ultrasonic assistance. No correlation between the feed rate and the exit delamination in UAD was found in their work. Also, in both experimental studies [163, 165] and [40], the reason for selecting the specific machining parameters was not provided. The reason behind larger chips generated in UAD was given as transition of CFRP material from brittle to ductile. The cutting temperature was measured by a thermal camera focusing at the entrance of the hole, therefore, the exact temperature at the chip-tool interface could not be captured in their study (unlike the cutting temperature measured by Weinert and Kempmann [136] by attaching the thermocouple at the flank face of the drill). Therefore, it raises a possibility of an alternative theory that the cutting temperature at the chip-tool interface would have risen until the glass transition temperature of the matrix and hence softening of the matrix material resulting in the larger chips. The same thing was attempted to be verified in their work through thermo-gravimetric analysis (TGA) and it was shown that the epoxy started to decompose at $\sim 360^\circ\text{C}$. TGA detects the change in mass with respect to temperature but it does not detect the temperature at which the matrix starts softening [166]. Therefore, the temperature detected in TGA is the temperature at which the matrix started decomposing and losing its mass. So, it is questionable that the claimed transition from brittle to ductile could have been actually the matrix softening because of higher cutting temperature. The cutting temperature was found to be more than 260°C in UAD while it varied from 67 to 90°C in CD as the feed rate was increased from

4 mm/min to 20 mm/min. At 20 mm/min the cutting temperature in UAD was also found to be 90° C. The reason for the higher cutting temperature in UAD was reported to be the localized ultrasonic impacts in UAD in each ultrasonic oscillation cycle. At 20 mm/min, it was speculated that there was no ultrasonic impact action, so no rise in the cutting temperature was found. Also, the effect on internal damage in a hole during UAD was not a focus in their work.

There is no other research work available in the literature which could explain the effects of UAD on CFRP other than Makhdum et al. [40, 163, 164] and Phadnis et al. [159, 165] at the moment. Although to investigate the importance of UAD drilling induced delamination in fibre reinforced plastics (FRPs), Mehbudi et al. [167] did attempt UAD on drilling of 'glass fibre reinforces plastics (GFRP)' material through Taguchi L9 orthogonal arrays with the machining parameters of 5.5, 11.1 and 15.7 m/min cutting speeds and 50, 80 and 110 mm/min feed rates. The ultrasonic parameters were 22 kHz frequency and 5, 10 and 15 μm amplitude. On average, a reduction of 20 N in thrust force was reported in their work in UAD as compared to that in CD which resulted in almost 30% reduction in exit delamination in UAD compared to in CD. Feed rate and oscillation amplitude were found to be the most significant parameters for thrust force and hence, exit delamination. Increasing amplitude from 5 to 15 μm resulted in a reduction of thrust force from 30 N to 15 N and exit delamination factor from 1.4 to 1.25 while increasing feed rate from 50 to 110 mm/min resulted in an increase in thrust force from 15 to 35 N and exit delamination factor from 1.25 to 1.40. With this experiment, Mehbudi et al. [167] could report that the effect of cutting speed in UAD was lowest on thrust force and exit delamination compared to feed rate and oscillation amplitude in the selected machining parameter range for the drilling of FRPs. This information was not a

focus in the work of Makhdum et al. [40, 163, 164] and Phadnis et al. [159, 165]. In addition, the reason behind selecting the specific parameters was not mentioned and damage on the internal surface of the drilled hole was not a focus of the work of Mehbudi et al. [167].

Thus, UAD has not been explored in a great detail for the feasibility of drilling of CFRP in relation to forces and damage generated during drilling. In addition, it can also be observed that the reason for selecting the specific machining parameters for the experiment was not mentioned in most of the cases.

3.7 Conclusions from the review

From the literature review, it is evident that several techniques have been investigated by the researchers in order to reduce the damage generated during drilling of CFRP. Most of the researchers' emphasis was on a reduction of thrust force while drilling so that the exit delamination could be reduced. Therefore various techniques for reducing thrust force in CD have been proposed including optimization of machining parameters, using pilot holes and using special geometry drills to change the cutting mechanism. However, damage still remains in a conventionally drilled hole in CFRP and researchers are making attempts to further reduce this damage.

It can also be noted that the accurate assessment and estimation of damage in a drilled hole has been a challenge itself for researchers. Exit delamination has been assessed by using techniques of optical microscopy, ultrasonic C-scan, X-ray enhanced radiography and X-ray computed tomography while internal damage in a hole has been assessed by using contact based surface profilometers in most of the research and surface roughness was used in order to quantify the damage of the

internal cylindrical surface of a hole. However, through the use of confocal microscopy, it has been shown that contact based surface profilers do not obtain accurate values of fibre pull out data from a machined surface in a drilled hole. There has not been a single universal technique which could report all the damage in a hole without destructive sectioning and research is still in progress to develop the techniques which could identify damage more accurately in a drilled hole in CFRP.

In another approach, researchers have investigated different non-traditional manufacturing processes such as Laser processing, AWJM, ultrasonic machining, RUM and VAD. Laser processing is a fast process but it burns the material and forms a heat affected zone. In contrast, AWJM has a good material removal rate ($150\text{mm}^3/\text{s}$) and does not produce any heat affected zone but it creates delamination and an irregular kerf width. Ultrasonic machining does not have any delamination and thermal effects but this process is slow having low material removal rates ($10\text{mm}^3/\text{s}$). RUM offers zero delamination as claimed by the authors but it involves cutting coolant similar to ultrasonic machining and both the processes are not recommended to be used to drill CFRP because of moisture absorption and reduction in the matrix strength unless an inert cutting fluid could be used during drilling (similar case with AWJM). With the help of intermittent cutting action of the drill in VAD, the reduction in thrust force has been reported by researchers. However, there has not been any evidence produced achieving zero damage in a drilled hole in VAD. Ultrasonic frequencies have been used by the researchers in UAD for drilling of difficult to machine metals like titanium and nickel-based superalloys and reduction in thrust force, reduced size of exit burrs and small and broken chips due to intermittent cutting action of drill have been achieved through UAD. There has been little research for drilling of CFRP through UAD. A recent research of Makhdam et

al. [164] reported lower exit delamination due to lower thrust force at 0.75 m/min (40 rpm), longer chips from CFRP being produced by UAD and it has been proposed that the reason for longer chips is the transition from brittle to ductile of epoxy matrix in CFRP. However, the evidence presented in support of the argument is required to be investigated further. No research has been reported which could explain the effect of ultrasonic oscillations on the internal damage of the cylindrical machined surface in a hole like fibre pull out and disorientation of fibres. In addition, it can also be noted that UAD of CFRP has not been investigated in relation to machining theory and the only reason for the reduction of thrust force has been proposed as intermittent cutting action during drilling. However, no conclusive evidence of intermittent cutting action during drilling has been produced. It can also be noted that none of the authors explained the reasons for the selection of specific machining parameters at which ultrasonic assistance was found to be “effective”.

Thus, it can be concluded from the literature review that UAD has been reported to reduce the thrust force, however, it has not been explored in detail with respect to machining parameters (in particular, cutting speed). In addition, the mechanism producing the advantageous effects of UAD during drilling of CFRP has not been investigated in relation to machining theory. Therefore, there is a gap in the literature for determining the mechanisms in UAD of CFRP causing its beneficial effect in relation to machining theory which would help in identifying the appropriate machining parameters in UAD at which the damage generated during drilling of CFRP is minimum.

4 Effective rake and clearance angles in CD and UAD for a twist drill geometry

Before investigating the effective rake angles in a twist drill geometry, it is important to have an overview of machining fundamentals relating to cutting tool geometry which helps in understanding the complicated geometry of a twist drill and visualising the effective rake angles. Therefore, this chapter is dedicated to the fundamentals of the conventional machining process and subsequently the calculation of the effective rake angle for a twist drill geometry.

4.1 Conventional machining

According to Chattopadhyay [168], “*Machining is a gradual material removal process in which layers of excess material are removed from an object (called workpiece) with the help of a tool in the form of chips in order to achieve the desired shape, dimensional accuracy and surface finish in the workpiece*”. Trent [169] referred to metal cutting as the operations in which a thin layer of metal is removed by a wedge-shaped tool in the form of chips.

As explained by Trent [169], the surface of a cutting tool over which chip flows during machining is known as rake surface. The cutting edge of a cutting tool is formed by the intersection of rake and flank (clearance) surfaces. The cutting tool is designed in such a way that the clearance surface should not rub against the finished surface [169]. Clearance angle is provided to avoid rubbing of flank face against the finished machined surface during machining and damaging machined surface and tool itself. Therefore, clearance angle is always recommended to be positive by the

4: Effective rake and clearance angles in CD and UAD for a twist drill geometry

authors. The angle between the rake and flank surface is known as ‘wedge angle (δ)’ [168].

The angle between the rake surface and the plane perpendicular to the cutting direction is known as ‘rake angle (γ)’ in a cutting tool. The angle between the flank surface and finished surface is known as ‘clearance angle (α)’ of a cutting tool. Some authors have also defined clearance angle as ‘relief angle’ [170]. The plane perpendicular to the cutting speed is also known as ‘reference plane (denoted as π_R in the current research)’ [168, 171, 172]. The machining action, the rake and clearance angles, rake and flank surfaces of a cutting tool during machining and chip formation during the shaping process are shown in a diagram in Figure 4-1.

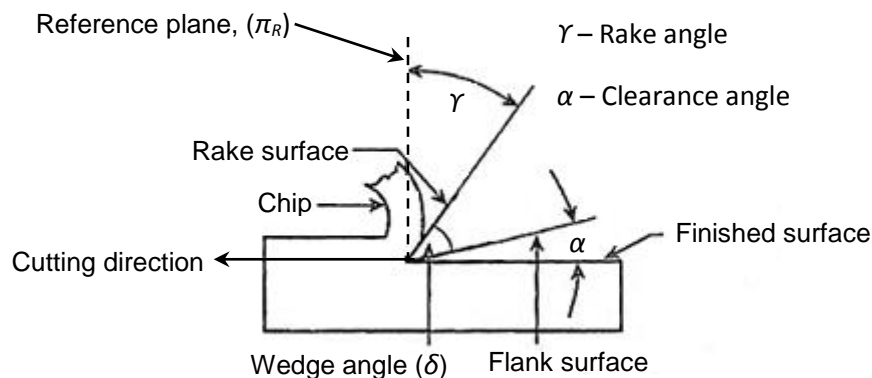


Figure 4-1: Machining action of a cutting tool in a shaping process (borrowed from [168])

From Figure 4-1, it can be concluded that:

$$\gamma + \alpha + \delta = 90^\circ \quad \text{- Equation (4.1)}$$

Equation (4.1) is helpful for assessing the rake and clearance angles of a cutting tool in case any one of rake, clearance or wedge angle is not provided by the tool manufacturer.

4.2 Orthogonal and oblique cutting

Orthogonal cutting is a type of cutting where the cutting edge of cutting tool is oriented at right angles to the cutting direction. In the oblique cutting, the cutting edge of cutting tool is not at the right angles to the direction of cutting. The cutting edge is inclined at an angle of λ_s from the cutting edge orientation in orthogonal cutting. The angle with which the cutting edge is inclined from the orthogonal cutting edge is known as inclination angle (shown as λ_s in Figure 4-2(b)) of cutting edge. Figure 4-2 demonstrates clearly the orthogonal and oblique machining conditions [168, 173]. Authors have proposed orthogonal machining at chisel and oblique machining at cutting edge in a twist drill [174].

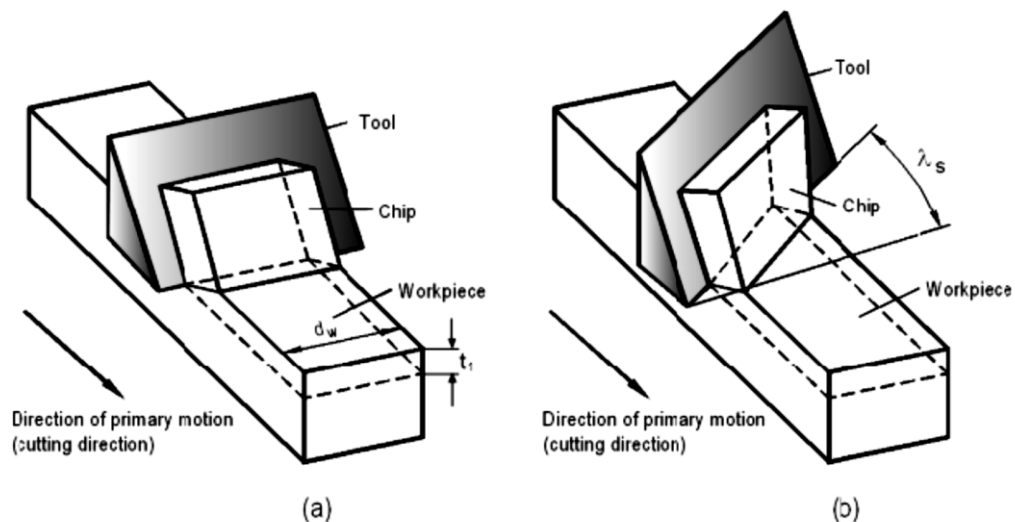


Figure 4-2: Demonstration of (a) orthogonal and (b) oblique cutting [171]

4.3 Cutting tool geometry

The geometry of a cutting tool has been explained by many authors [168, 170, 171, 173, 175, 176] which express similar explanations in different nomenclatures. In general, the tool geometry has been considered in three systems:

4: Effective rake and clearance angles in CD and UAD for a twist drill geometry

- Tool-in-hand
- Tool-in-machine (machine reference system [168, 170])
- Work reference system (tool-in-use)

According to Watson [170], tool-in-hand system was introduced to facilitate the tool manufacturer and inspection of the tool. However, when a tool is fixed within the machine, its orientation is defined with respect to the machine tool. This system is known as tool-in-machine system [170, 173]. Work reference system (Tool-in-use) identifies the geometry of a cutting tool when the tool is actually involved in a machining operation, unlike the other systems. According to the authors [168, 170, 172, 173], when the tool is actually involved in machining, the actual tool path can be different from the assumed tool path considered in the other systems due to multiple motions (cutting and feed motions) being implemented on the tool and workpiece. The study of tool geometry in this system becomes important because the value of effective rake angle is affected due to relative motion between the tool and workpiece during machining [171]. It is discussed further in Section 4.3.2.

4.3.1 Various rake and clearance angles in a cutting tool geometry

According to The International Organization for Standardization (ISO), three types of rake angles have been defined for a cutting tool – Axial rake angle, orthogonal rake angle and normal rake angle [170]. Correspondingly, the clearance angles are also three types – axial, orthogonal and normal clearance angles. The axial, orthogonal and normal rake angles for a single point turning tool are shown in a schematic in Figure 4-3. The respective angles are visualized along the cross section of the tool in sections AA', BB', CC' and DD' at an arbitrary point O of the cutting edge for tool-in-hand system [170, 173, 177]. As a general definition, the

4: Effective rake and clearance angles in CD and UAD for a twist drill geometry

rake angle is defined as the angle between the rake surface and reference plane (π_R) in a cutting tool. The clearance angle is defined as the angle between the flank surface and cutting plane. However, when visualizing these angles in the specific planes of references (i.e. the cross-sections AA', BB' and DD' in Figure 4-3) their values differ [168].

To explain and understand the respective (axial, orthogonal and normal) rake angles clearly, the schematic in Figure 4-3 is divided into 5 parts. Part 1 is the top view of the single point turning tool along reference plane (π_R) in which the rest of the cross sections (AA', BB' and DD') are defined along which the respective rake and clearance angles would be visualized. The assumed direction of cutting speed is perpendicular to the reference plane (π_R), coming out of the plane of the paper.

Part 2 is the cross-section view of the tool along section AA' and it is known as the axial projection of the tool. The plane along section AA' is known as Axial plane (π_x). Axial rake angle is defined as the angle between rake surface and reference plane measured on axial plane which is defined as γ_x and the corresponding axial clearance angle is defined as α_x [168, 170, 173, 177].

Similarly, orthogonal rake angle is defined in the cross-sectional view of cutting tool perpendicular to the reference plane (π_R) along section BB' which is shown in part 3. The plane along section BB' has been defined as orthogonal plane (π_o). The orthogonal rake angle is shown as γ_o and orthogonal clearance angle is shown as α_o .

The inclination of cutting edge with reference plane is defined as inclination angle which is shown as (λ) along the Section CC' in part 4. The plane along section CC' has been defined as cutting plane [168]. Furthermore, normal rake angle is defined as the angle of inclination of rake surface with the reference plane measured

4: Effective rake and clearance angles in CD and UAD for a twist drill geometry

along the plane normal to the cutting edge (Section DD'). The plane normal to the cutting edge is termed as normal plane (π_n). To visualize normal rake and clearance angles, the projection of cutting tool along section DD' is drawn in Part 5 of Figure 4-3. The normal rake angle is shown as γ_n and normal clearance angle is shown as α_n in Figure 4-3. The plane along section DD' is normal plane (π_n) [168, 170, 173, 177]. In an earlier research of Brown and Armarego [178], it was found that normal rake angle is the most important angle out of axial, orthogonal and normal rake angles for influencing the cutting forces during oblique machining. When increasing the normal rake angle from -10° to 20° keeping axial and orthogonal rake angles constant, the cutting force was found to reduce from 200 to 100 N in their work. Whereas when axial rake and orthogonal rake angles were varied keeping normal rake angle constant, the cutting forces did not show a difference. Thus, normal rake angle was found to be most influencing rake angle for cutting forces during machining.

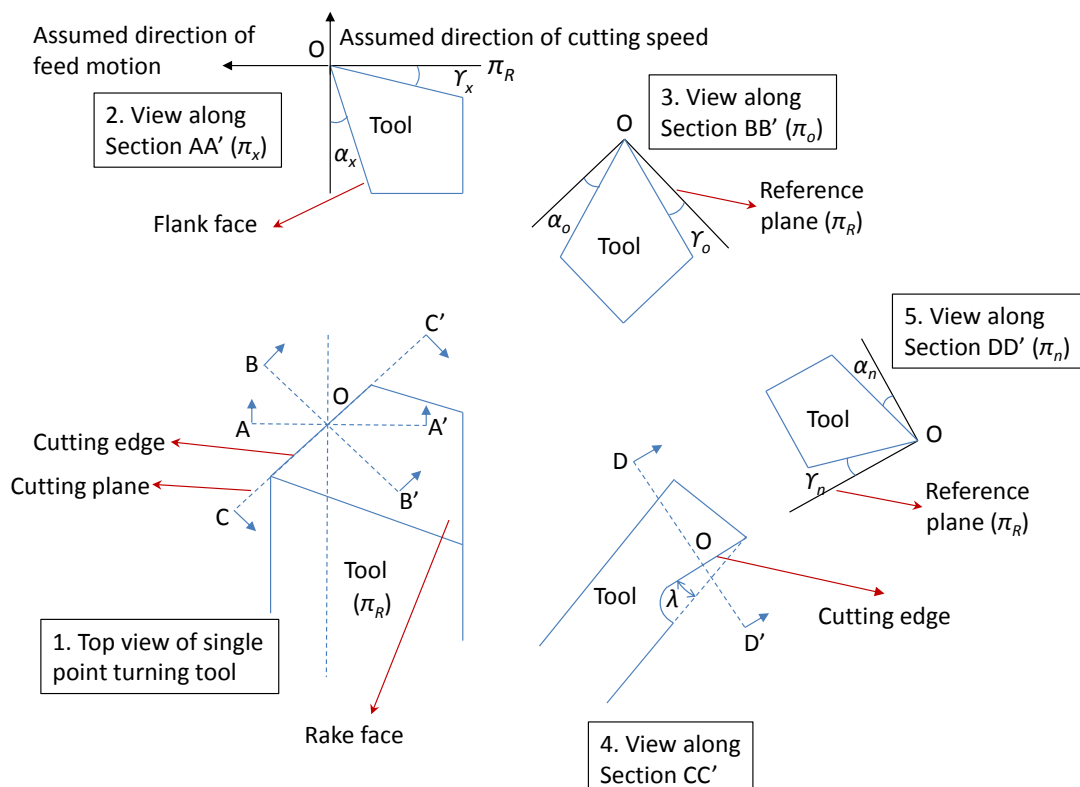


Figure 4-3: Schematic to visualize axial, orthogonal and normal rake angles in a single point turning tool

4.3.2 Importance of work reference system

An example of cutting and feed motions implemented on cutting tool in threading process is shown in Figure 4-4, in which a threading tool is involved in the threading operation. As it can be seen in Figure 4-4 in the axial projection along section ‘A-A’ that the threading tool contains two speeds – cutting speed (V_c) and feed rate (V_f). When feed rate was zero, the original reference plane (π_R) was perpendicular to the cutting speed (V_c). As feed motion (V_f) is introduced to threading tool in the axial direction of threading, the resultant cutting velocity of V_c and V_f becomes along the velocity vector, V_R , which makes an angle of μ with the original cutting velocity, V_c . However, the reference plane is fundamentally defined to be perpendicular to the resultant cutting velocity during machining [168, 170, 173]. Therefore, the reference plane in work reference system becomes π_{RW} instead of π_R and the angle between the original reference plane π_R and π_{RW} becomes μ . γ_x and α_x are the axial rake angles in the axial projection of threading tool in Figure 4-4.

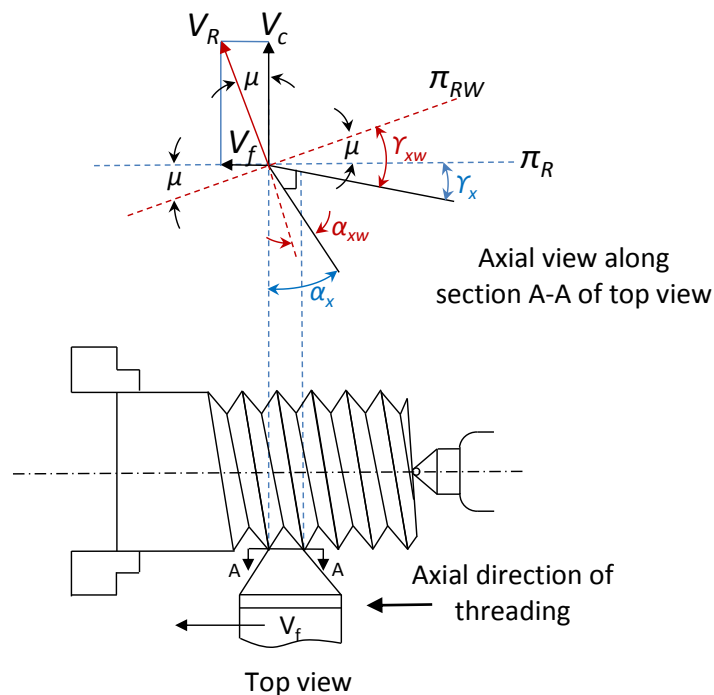


Figure 4-4: Visualization of rake and clearance angles in work reference system in threading operation (borrowed from [168])

4: Effective rake and clearance angles in CD and UAD for a twist drill geometry

The introduction of angle ' μ ' in Figure 4-4 affects the values of rake and clearance angles in work reference system. Therefore, the effective rake angle (γ_{XW}) in work reference system in Figure 4-4 becomes [168, 170, 173]–

$$\gamma_{XW} = \gamma_X + \mu \quad \text{- Equation (4.2)}$$

Effective clearance angle (α_{XW}) in work reference system becomes –

$$\alpha_{XW} = \alpha_X - \mu \quad \text{- Equation (4.3)}$$

Where, value of μ can be determined from the axial view along section A-A as –

$$\tan \mu = \frac{v_f}{v_c} \quad \text{- Equation (4.4)}$$

Thus, during machining (when the tool is actually being used), the effective rake angle is higher than the original rake angle of the tool while effective clearance angle becomes lower than the original clearance angle of cutting tool due to the relative motion of cutting tool and workpiece.

4.4 Geometry of two flute twist drill in work reference system

The twist drill is a tool which is commonly used for the hole-making (drilling) process. The salient features of a two flute twist drill are shown in Figure 4-5.

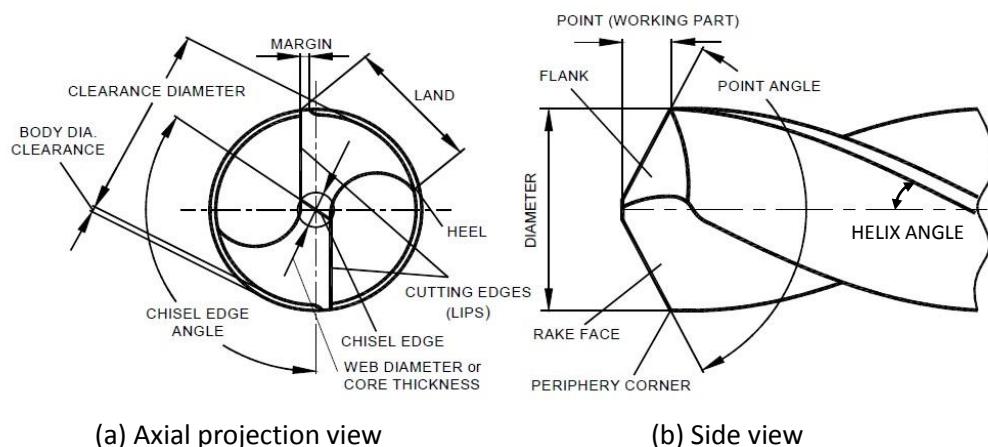


Figure 4-5: Salient features of a two flute twist drill in (a) axial projection and (b) side view [171]

4: Effective rake and clearance angles in CD and UAD for a twist drill geometry

Compared to the geometry of single-point turning tools, the geometry of a twist drill is more complex. In a two flute twist drill, two sharp cutting edges are connected to a relatively small and pointed chisel edge in a twist drill unlike that in single point turning tool. In the twist drill, the cutting velocity vector along the cutting edge changes continuously in both magnitude and direction as shown in Figure 4-6. The axial projection view of a two flute twist drill is shown in a schematic in Figure 4-6. It can be seen in Figure 4-6 that the direction of cutting velocity vectors V_{c1} , V_{c2} and V_{c3} at points 1, 2 and 3 of cutting edge are different from each other due to the direction of cutting motion being perpendicular to its radial direction which keeps on changing from point to point in cutting edge. In addition, the magnitude of cutting velocity vector increases as we move away from the centre of twist drill along its cutting edge [168].

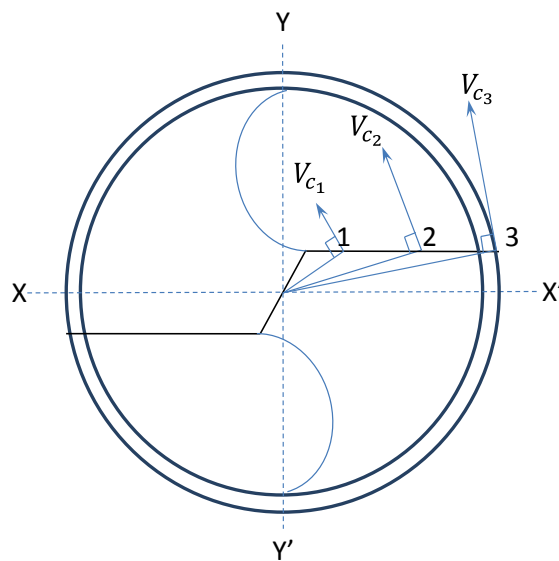


Figure 4-6: Schematic displaying the variation in velocity along the cutting edge in axial projection view

Zero cutting velocity at centre and chisel edge makes a complicated material removal mechanism near the centre. According to some authors, the material

removal at chisel edge happens due to extrusion instead of machining due to nearly zero cutting velocity [179].

4.5 Ultrasonic assistance on a twist drill during drilling

Before considering the effect of ultrasonic oscillations during drilling of the workpiece, it is necessary to understand and visualize the movement of the cutting edge of the drill. Vibrations applied are sinusoidal in nature because of sinusoidal vibrations are generated in the piezo-electric crystal of ultrasonic actuator in reverse piezoelectric effect. In this research, the vibrations were applied in the axial direction of the drill. Figure 4-7 shows all the motions applied on a two flute twist drill. As shown in Figure 4-7, there are three simultaneous motions applied to the drill– first is the axial feed motion which comes from the feed rate, second is a rotational motion coming from the spindle and third is a vibrational motion due to axial vibrations of the drill.

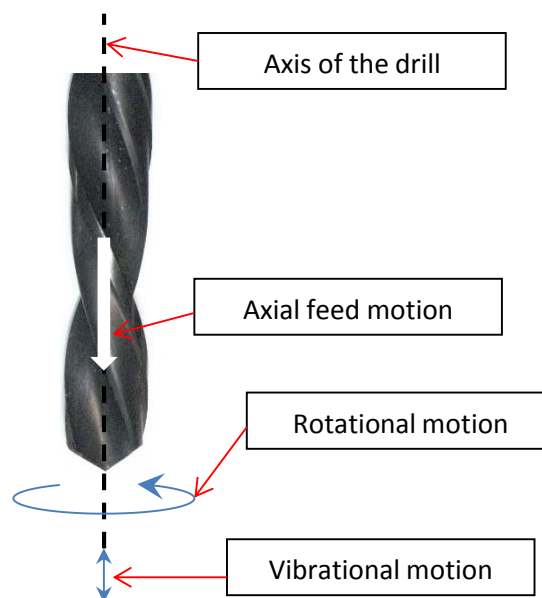


Figure 4-7: Rotational, vibrational and feed motions of the drill during vibration assisted drilling

To identify the specific effect of axial vibrations on the machining, the effect on the motions of cutting edges needs to be visualised further. A closer observation of

4: Effective rake and clearance angles in CD and UAD for a twist drill geometry

the cutting edges is shown in Figure 4-8, displaying two-dimensional projection of the cutting edges of the twist drill in Figure 4-7 on the plane of the paper. The projections of cutting edges of twist drill are shown as AB and A'B' in the schematic shown in Figure 4-8. The drill is assumed to be rotating about its axis OO' in the counter-clockwise direction and oscillating in the axial direction. The point P is an arbitrary point on the cutting edge of the drill having rotational, vibrational and feed motions. The direction of the rotational velocity of point P is perpendicular to the plane of paper going towards into the plane of the paper. It can be seen in Figure 4-8 that the motion of point P would be a resultant motion of the three individual motions involved, i.e. rotational, vibrational and feed motions. In the conventional drilling, i.e. in the absence of the axial vibrations, the locus of point P of the cutting edge of Figure 4-8 is shown in Figure 4-9, for two revolutions of the drill in counter-clockwise rotational direction. When the axial vibrations are implemented, the resultant motion of point P would be similar to as shown in Figure 4-10.

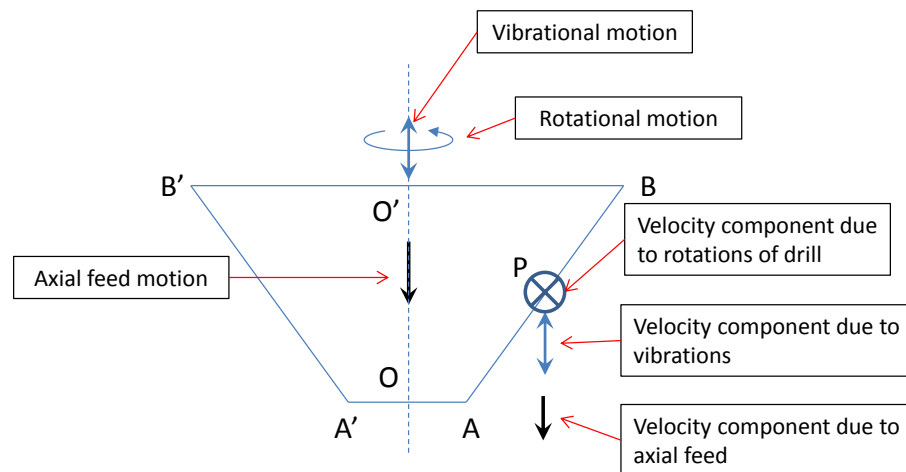


Figure 4-8: Schematic for the projection of the cutting edges of a twist drill on the plane of paper displaying the rotational and vibrational motions applied on the cutting edge

4: Effective rake and clearance angles in CD and UAD for a twist drill geometry

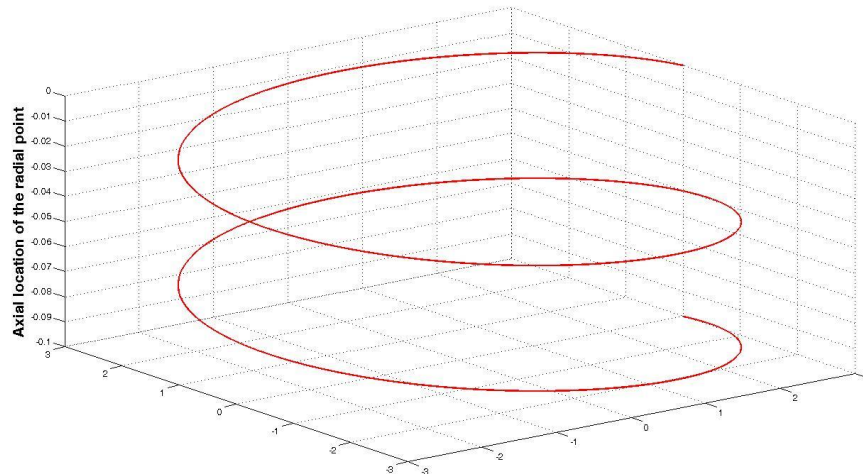


Figure 4-9: Movement of point P of the cutting edge of Figure 4-8 during conventional drilling

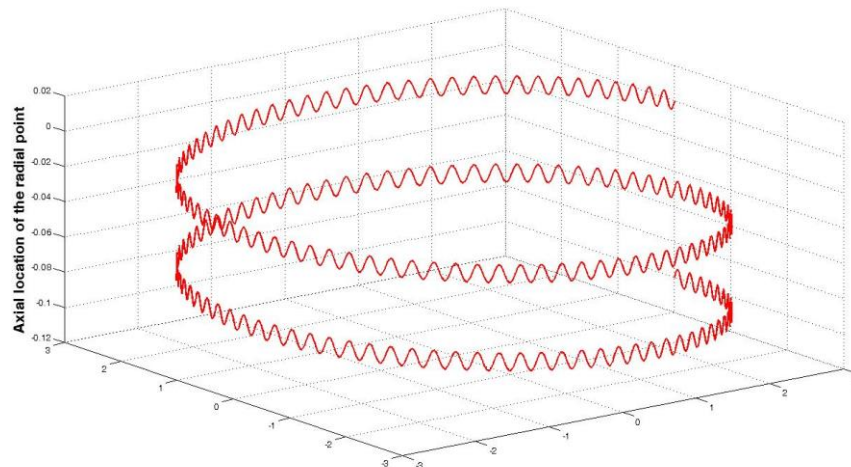


Figure 4-10: The motion path of point P shown in Figure 4-8 for two revolutions of twist drill in vibration assisted drilling for 5000 Hz frequency and 10 μm amplitude (the distance of point P is assumed to be 3 mm from the axis of rotation in this schematic)

When, the frequency of axial vibrations of the drill is increased such that it lies in the range of ultrasonic frequencies (20-200 kHz), the movement of point P of cutting edge shown in Figure 4-10 becomes denser due to the high ultrasonic frequency of oscillations. Such movement of point P is shown in Figure 4-11.

4: Effective rake and clearance angles in CD and UAD for a twist drill geometry

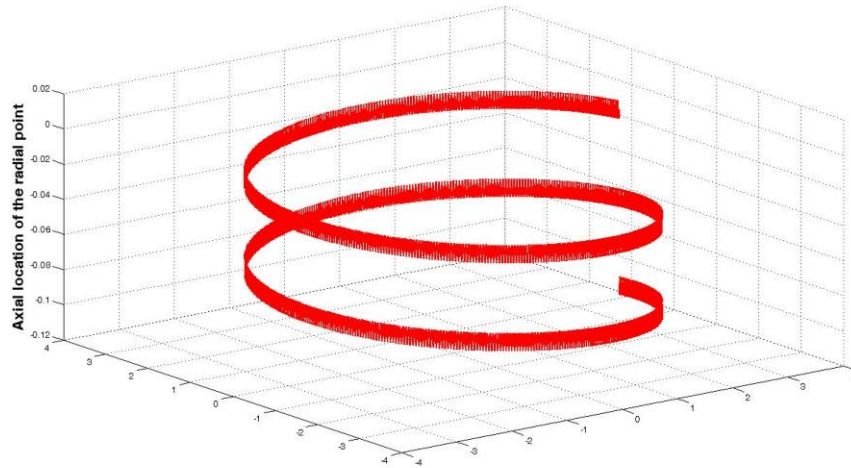


Figure 4-11: Motion path of point P shown in Figure 4-8 for two revolutions of twist drill in ultrasonic assisted drilling for 37220 Hz frequency and 10 μ m amplitude

The different cutting motion of a point on cutting edge in UAD, Figure 4-11, compared to that in CD, Figure 4-9, indicates different cutting mechanism in UAD which is to be investigated.

The rake angle has been found to be an important parameter in the machining (and hence material removal) of both metals [168, 169, 180] and CFRP [181]. In the machining of metals, higher rake angles are preferred for lower surface roughness and lower cutting forces [168]. While in the machining of CFRP, higher rake angles were found to break carbon fibres easily and helping in the localization of the damage generated in the orthogonal machining of CFRP [181]. According to Arola et al. [181], the damage in the machining of carbon fibre composites could be localised by increasing the rake angles during orthogonal machining of CFRP. Zhang et al. [182] have calculated the thrust force and torque analytically in the vibration assisted drilling (VAD) of composite materials. During the thrust force calculation, it was displayed that the effective rake angle (discussed in Section 4.6) at a point of cutting edge becomes variable if the vibrations are applied on the drill during drilling. A difference of 2° was found between rake angles in CD and VAD in

4: Effective rake and clearance angles in CD and UAD for a twist drill geometry

their work. However, their focus was on calculating the thrust force and torque during drilling and not the effect of variable effective rake angles on damage during drilling.

As mentioned in the literature review, damage during drilling (entrance and exit delamination, fibre pull out and fibre matrix debonding) has been found a major problem in the drilling of CFRP. Therefore, in the present research an attempt has been made to determine the effect of dynamically varying effective normal rake and clearance angles due to ultrasonic oscillations on the damage generated on the machined surface during drilling at various cutting speeds. The fundamental derivation of variation of the effective normal rake angles at a point of a cutting edge because of ultrasonic oscillations is visualized and discussed in Section 4.6.

4.6 Effective rake and clearance angles in CD and UAD for a twist drill geometry in work reference system

Similar to the cutting tool geometry explained previously in section 4.4, the geometry of a twist drill has also been analysed and explained by many authors which express similar explanations in different nomenclature [168, 170-172, 179, 183-185].

As explained in Section 4.3.2, the rake and clearance angles are affected if the feed motion becomes comparable to cutting speed in work reference system as the work reference system is required to be considered when the tool is actually involved in machining. To visualize the whole drilling process and the concept of effective rake angles, the twist drill in drilling action is shown in Figure 4-12. The complete drilling process and the geometry of a twist drill are explained in three parts:

4: Effective rake and clearance angles in CD and UAD for a twist drill geometry

Part 1 in Figure 4-12 shows the front view of the twist drill rotating about its axis of rotation and moving downwards through its feed motion.

Part 2 in Figure 4-12 displays the axial projection of the twist drill having centre O, the projection of chisel edge AA' and projections of cutting edges (AB and A'B'). The feed direction of the drill in part 2 is assumed to be perpendicular to the plane of the paper and coming outwards from it. The perpendicular distance between the cutting edge AB and the horizontal axis YY' is known as half chisel edge width ' t '. Point ' i ' is an arbitrary point on the cutting edge AB at a radial distance of r_i from its centre O, similar to point P shown in Figure 4-8. In the plane of axial projection, the velocity, V_{c_i} of point i due to the rotational motion of twist drill is directed in the perpendicular direction to its radial distance r_i . The radial distance r_i makes an angle of β_i from the central axis YY'. The plane perpendicular to the plane of paper and passing through the points O and i is known as dynamic reference plane, π_{RD_i} at point ' i ' of the cutting edge. The reference plane is fundamentally identified by the plane perpendicular to the cutting velocity [168, 173]. The feed rate direction is assumed to be in the direction of perpendicular to the plane of the paper and directing outwards from it.

Before determining the effective rake angles in drilling, it is necessary to visualize the rake angle in the twist drill geometry. The axial rake angle in a twist drill is the angle between rake surface and reference plane [168, 173], which is shown in Part 3 of Figure 4-12.

Part 3 of Figure 4-12 visualizes the rake surface and reference plane cross-sectionally in order to visualize the axial rake angle at point i , i.e. the projection of the drill along the plane XX' and perpendicular to the plane of axial projection. The

4: Effective rake and clearance angles in CD and UAD for a twist drill geometry

axial rake and clearance angles are shown as γ_{XD_i} (angle between the rake surface and the reference plane) and α_{XD_i} (angle between the flank face and the cutting plane [168, 170, 173]).

In part 3 of Figure 4-12, when the axial feed velocity, V_{f_i} , is imposed on the drill, the resultant cutting velocity becomes the resultant velocity of cutting and feed velocities, V_{cw_i} . Hence, the cutting velocity is changed from V_{c_i} to the resultant cutting velocity, V_{cw_i} , which makes an angle of μ_i to the original cutting velocity, V_{c_i} . Since, the reference plane is always identified by the plane perpendicular to the cutting velocity [168, 173], the new reference plane in work reference system would be π_{RW_i} , at an angle of μ_i from π_{RD_i} in such a way that the new reference plane of work reference, π_{RW_i} is perpendicular to the resultant cutting velocity, V_{cw_i} . The system of this type of reference is known as Work Reference System, in which the tool-geometry is visualized during its “working” action i.e. the tools are actually involved in machining process as explained in Section 4.3.2. The new reference plane π_{RW_i} is known as dynamic work reference plane at point ‘i’ of the cutting edge.

4: Effective rake and clearance angles in CD and UAD for a twist drill geometry

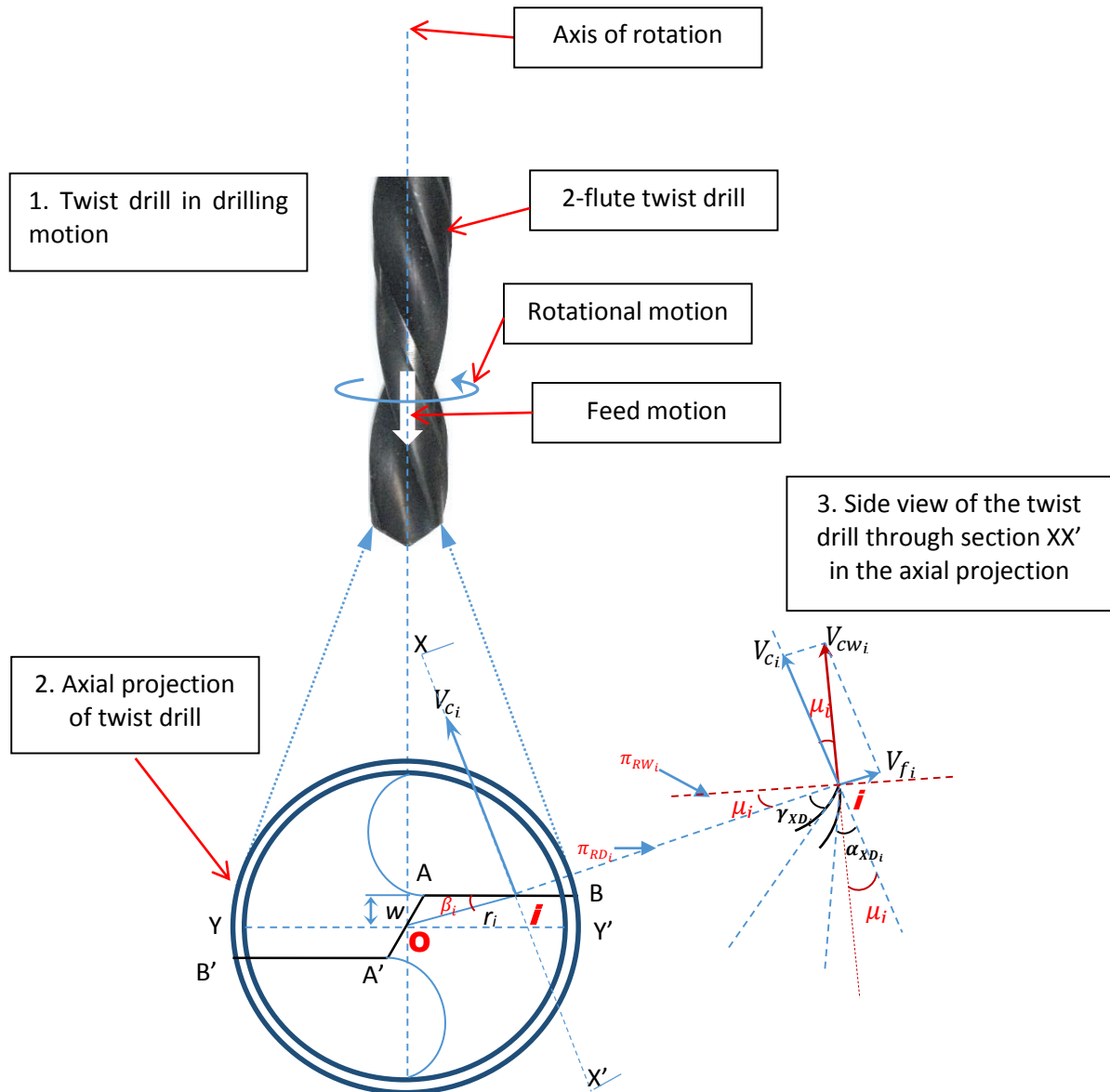


Figure 4-12: Part 1 – 2-flute twist drill in drilling action, Part 2- Enlarged axial projection of the twist drill shown in part 1. Part 3 – Visualization of the rake and clearance angles, feed velocity, resultant cutting velocity, and therefore the new reference plane π_{RWi} at an angle μ_i from the previous reference plane π_{RDi}

The effective rake angle at point ‘i’ in work reference system in Figure 4-12 would be [168, 170, 173]:

$$\gamma_{XW_i} = \gamma_{XD_i} + \mu_i \quad \text{- Equation (4.5)}$$

Similarly, the effective clearance angle in work reference system would be the resultant angle between the flank face and the new cutting plane. It is given in Equation (4.6):

4: Effective rake and clearance angles in CD and UAD for a twist drill geometry

$$\alpha_{XW_i} = \alpha_{XD_i} - \mu_i \quad \text{- Equation (4.6)}$$

$$\text{Where, } \mu_i = \tan^{-1} \left(\frac{V_{f_i}}{V_{c_i}} \right) \quad \text{- Equation (4.7)}$$

$$\text{The cutting speed at point } i, V_{c_i} = 2\pi r_i n \quad \text{- Equation (4.8)}$$

Where, 'n' is the rotational frequency of drill in revolutions per minute.

Hence, during the drilling operation, the effective axial rake angle becomes more than its original axial rake angle, while the effective axial clearance angle is lower than the original axial clearance angle of the drill. In order to calculate the effective rake angles in CD and UAD, the individual velocity components (V_{c_i} and V_{f_i}) are required to be calculated so that angle μ_i could be estimated from Equation (4.7) and hence effective axial rake angle γ_{XW_i} could be calculated from Equation (4.5).

If the axial feed rate for conventional drilling is S_0 mm/rev then the feed velocity component conventional drilling ($V_{f_{iCD}}$) is:

$$V_{f_{iCD}} = S_0 n \text{ mm/min}; \quad \text{- Equation (4.9)}$$

When the ultrasonic oscillations are imposed in the axial direction of the conventional drilling, the resultant feed velocity of point 'i' of the cutting edge would be the addition of conventional feed velocity and ultrasonic velocity. Ultrasonic oscillations generated through ultrasonic actuator are harmonic sinusoidal oscillations in nature [186]. Assuming ultrasonic oscillation amplitude = a , oscillation frequency = f , angular ultrasonic oscillation frequency = ω , the ultrasonic oscillatory displacement of twist drill at an arbitrary location 'y' between two extreme locations during sinusoidal oscillations is defined by the Equation (4.10) and the oscillations imposed in axial direction of twist drill are visualized in Figure 4-13.

4: Effective rake and clearance angles in CD and UAD for a twist drill geometry

$$y = a \sin \omega t \quad \text{- Equation (4.10)}$$

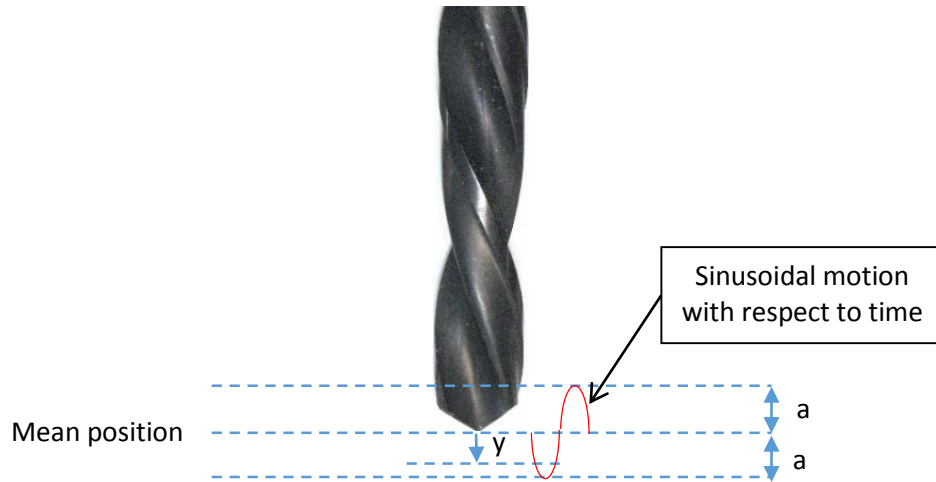


Figure 4-13: Visualization of mean and peak position of sinusoidal ultrasonic oscillations in UAD

Therefore, ultrasonic velocity component (V_{fiUAD}) would be,

$$V_{fiUAD} = \frac{dy}{dt} = \frac{d(a \sin \omega t)}{dt}$$

$$\Rightarrow V_{fiUAD} = a\omega \cos \omega t \quad \text{- Equation (4.11)}$$

The resultant feed velocity (V_{fi}) of the point 'i' of a cutting edge in Figure 4-12 in ultrasonic assisted drilling would be the summation of conventional axial feed velocity and velocity imposed by ultrasonic assistance as defined in the Equation (4.12),

$$V_{fi} = V_{fiCD} + V_{fiUAD} \Rightarrow V_{fi} = S_0 N + a\omega \cos \omega t \quad \text{- Equation (4.12)}$$

Thus, Equations (4.8) and (4.12) provide the values of velocity components (V_{ci} and V_{fi}) in order to calculate μ_i in Equation (4.7). The axial rake angle (γ_{XD_i}) in Equation (4.5) at a point 'i' on cutting edge and helix angle (θ) of twist drill are related by the Equation (4.13) (as defined by other authors, [168, 182]):

$$\gamma_{XD_i} = \tan^{-1} \left(\frac{r_i}{r} \tan \theta \right) \quad \text{- Equation (4.13)}$$

4: Effective rake and clearance angles in CD and UAD for a twist drill geometry

The machining mechanism at cutting edges of a twist drill is oblique machining due to the presence of inclination angle in cutting edges [183, 187] (denoted by angle of obliquity by Brown and Armarego [178]) in a twist drill geometry. In the research of Brown and Armarego [178], it was found that normal rake angle is the most influencing angle out of axial, orthogonal and normal rake angles for cutting forces. Therefore, effective normal rake angle in work reference system in CD and UAD is required to be calculated in order to get an indication towards cutting forces during machining. The value of effective normal rake angle in UAD ($\tan \gamma_{nW_i}$) is related to the orthogonal rake angle ($\tan \gamma_{oW_i}$) through Equation (4.14) [168],

$$\tan \gamma_{nW_i} = \tan \gamma_{oW_i} \cos \lambda_{W_i} \quad \text{- Equation (4.14)}$$

In Equation (4.14), λ_{W_i} is the inclination angle of cutting edge in work reference system, the orthogonal rake angle (γ_{oW_i}) and axial rake angle (γ_{xW_i}) in the work reference system are related are per the following Equation (4.15) [168]:

$$\tan \gamma_{oW_i} = \frac{\tan \gamma_{xW_i} + \tan \lambda_{W_i} \cos \phi_{W_i}}{\sin \phi_{W_i}} \quad \text{- Equation (4.15)}$$

ϕ_{W_i} in Equation (4.15) is the dynamic cutting edge angle in work reference system. Thus, in order to calculate the orthogonal rake angle in work reference system from Equation (4.15), the values of λ_{W_i} and ϕ_{W_i} are to be known.

In order to calculate ϕ_{W_i} , following two relations are mentioned [168] :

$$\tan \phi_{W_i} = \frac{\tan \phi_{D_i}}{\cos \mu_i} \quad \text{- Equation (4.16)}$$

$$\tan \phi_{D_i} = \frac{\tan \phi_s}{\cos \beta_i} \quad \text{- Equation (4.17)}$$

In Equations (4.16) and (4.17), ϕ_s is half cone angle of the twist drill which is generally provided by the tool manufacturer. The value of μ_i has been mentioned

4: Effective rake and clearance angles in CD and UAD for a twist drill geometry

already in Equation (4.7). From the part-2 of Figure 4-12, value of β_i can be calculated with the way mentioned in the Equation (4.18):

$$\beta_i = \sin^{-1}\left(\frac{w}{r_c}\right) \quad \text{- Equation (4.18)}$$

The portion of chisel edge from part-2 of Figure 4-12 is shown in Figure 4-14. In Figure 4-14, ' Ψ ' is the chisel edge angle of the twist drill (Figure 4-5 (a)) and ' r_c ' is the chisel edge radius.

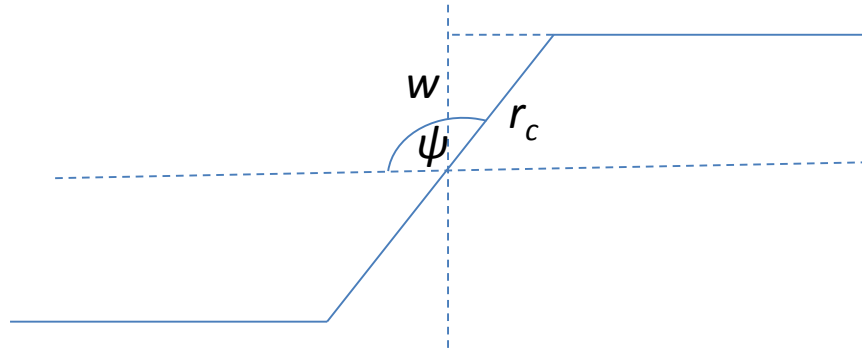


Figure 4-14: Magnified portion of the chisel edge from the part-2 of Figure 4-12

From Figure 4-14, it can be seen that, $\cos(\psi - 90) = \frac{w}{r_c}$ - Equation (4.19)

Thus, if ' Ψ ' and ' r_c ' are known, value of β_i , can be calculated from Equations (4.18) and (4.19). To calculate the value of λ_{W_i} , Watson [188] has provided a relation in the following Equation (4.20) –

$$\sin \lambda_{W_i} = \sin \beta_i \sin \phi_s \cos \mu_i + \cos \phi_s \sin \mu_i \quad \text{- Equation (4.20)}$$

Putting all these values in Equation (4.15), the orthogonal rake angle in work reference system for the UAD for point ' i ' of the cutting edge in Figure 4-12 becomes:

$$\tan \gamma_{oW_i} = \frac{\tan \left[\tan^{-1} \left(\frac{r_i}{r} \tan \theta \right) + \tan^{-1} \left(\frac{S_0 N + a \omega \cos \omega t}{2 \pi r_i N} \right) \right] + \tan \lambda_{W_i} \cos \phi_{W_i}}{\sin \phi_{W_i}} \quad \text{- Equation (4.21)}$$

4: Effective rake and clearance angles in CD and UAD for a twist drill geometry

Using Equations (4.21) and (4.14), the effective normal rake angle in CD and UAD can be calculated. This type of calculation has been performed earlier by Zhang et al. [182] during calculation of thrust force and torque in conventional and vibration assisted drilling, however, the calculations were more focused on thrust forces and torque instead of rake angles themselves. In addition, the effect on damage in the drilling of CFRP through the fundamental variations in rake and clearance angles in UAD has never been the focus of earlier research.

As an example, a rake angle calculation was performed for a 6 mm diameter standard two flute twist drill having 30° helix angle and 1.5 mm chisel edge diameter. The effective rake angle variation for three ultrasonic cycles was calculated for 10 m/min cutting speed and 0.05 mm/rev feed rate as shown in Figure 4-15. It can be seen in Figure 4-15 that the effective rake angle in CD attains a maximum value of 34° (constant value with respect to time) while that attains the maximum value of 63° in UAD and it oscillates periodically between 63° and -51° . In the work of Zhang et al. [182], because of using low vibration frequency of 130 Hz, they obtained a small difference of 4° between the effective normal rake angles in conventional and vibration assisted drilling, although their calculation was focused on the thrust force instead of rake angles variation and they did not mention the effective axial and normal clearance angles variation in their work.

4: Effective rake and clearance angles in CD and UAD for a twist drill geometry

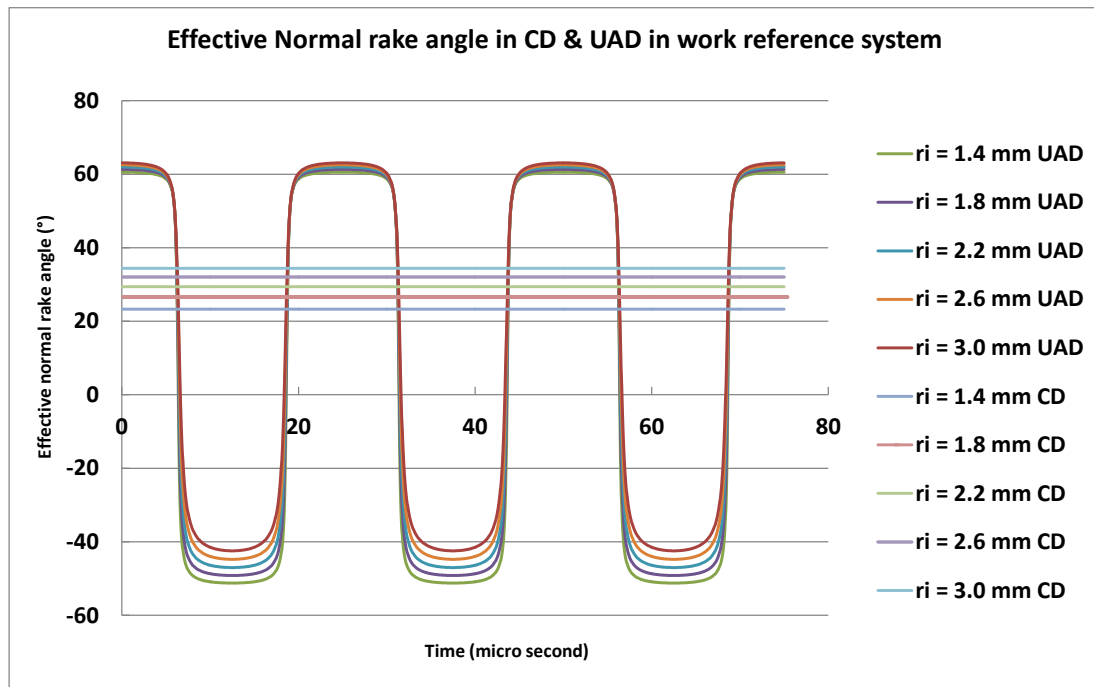


Figure 4-15: Effective normal rake angle in CD and UAD at 10 m/min cutting speed and 0.05 mm/rev feed rate

When examining the axial movement of the drilling tool in the same time interval of three ultrasonic oscillations of Figure 4-15, it would be similar to shown in Figure 4-16. Positive values in Figure 4-16 indicate the tool moving towards (into) the workpiece axially and negative values indicate the tool moving backwards (moving away from the workpiece) during ultrasonic oscillations. In Figure 4-16, it can be seen that the tool moves in a sinusoidal to-and-fro motion because of ultrasonic sinusoidal oscillations whereas in CD, the tool moves consistently into the workpiece. Although the movement in CD seems to be at a zero value in Figure 4-16. It is because of the low feed rate of 0.05 mm/rev (26.5 mm/min). This means that the tool would move only $26.5 \cdot 70 / (60 \cdot 1000) = 0.304 \mu\text{m}$ towards the workpiece in y-axis within 70 μs in CD whereas the tool oscillates between the range of $\pm 5 \mu\text{m}$ amplitude in UAD in the y-direction. Since 0.304 μm is negligible in comparison to 5 μm , the axial movement of the tool in CD seems to have zero movements in y-axis in Figure 4-16. The axial movement towards the workpiece in

4: Effective rake and clearance angles in CD and UAD for a twist drill geometry

CD can be clearly visualized when considering a larger duration of 100 ultrasonic cycles (2500 μs) in Figure 4-17.

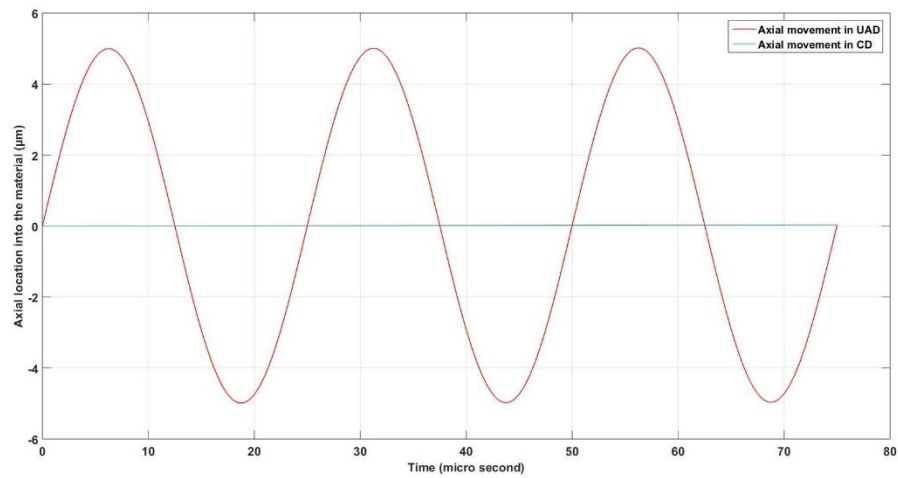


Figure 4-16: Axial movement of a point on the cutting edge in CD and UAD (P.S. the positive values indicate drill going inside the material)

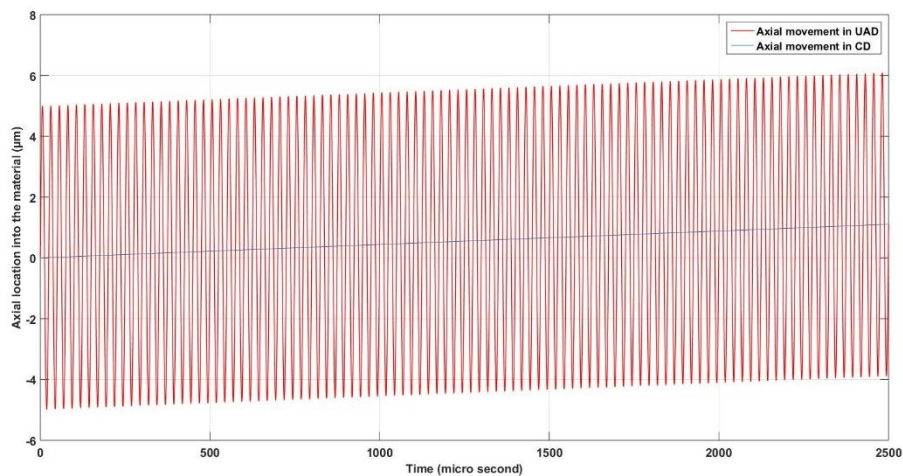


Figure 4-17: Axial movement of a point on the cutting edge in CD and UAD at 10 m/min cutting speed, 0.05 mm/rev feed rate, 40 kHz frequency and 5 μm oscillation amplitude

When considering Figure 4-15 and Figure 4-16 together, it can be seen that the rake angle is positive in the time duration when the tool is actually progressing “towards” the workpiece. During the time intervals when the effective rake angle is negative in UAD, the tool is actually moving backwards. Therefore, it can be inferred that the effective rake angle is always positive when the tool is actually

4: Effective rake and clearance angles in CD and UAD for a twist drill geometry

machining in UAD and it is larger than that in CD. Thus, the positive value of effective rake angle during ultrasonic oscillation is required to be considered in UAD as effective rake angle. This implies that the effective rake angle in UAD is 63° in Figure 4-15 for the time interval when the tool is actually involved in machining during UAD. Furthermore, when examining the variation of theoretical effective normal rake angles in UAD with respect to cutting speed and ultrasonic oscillation amplitude, Figure 4-18, it can be seen that the effective normal rake angle reduces with increasing cutting speed and it increases with increasing oscillation amplitude. When the variation of effective rake angle is examined in CD, it attains a constant value of 30° at all the cutting speeds in CD, Figure 4-19. Thus, effective rake angles attain larger value in UAD than those in CD at all the cutting speeds.

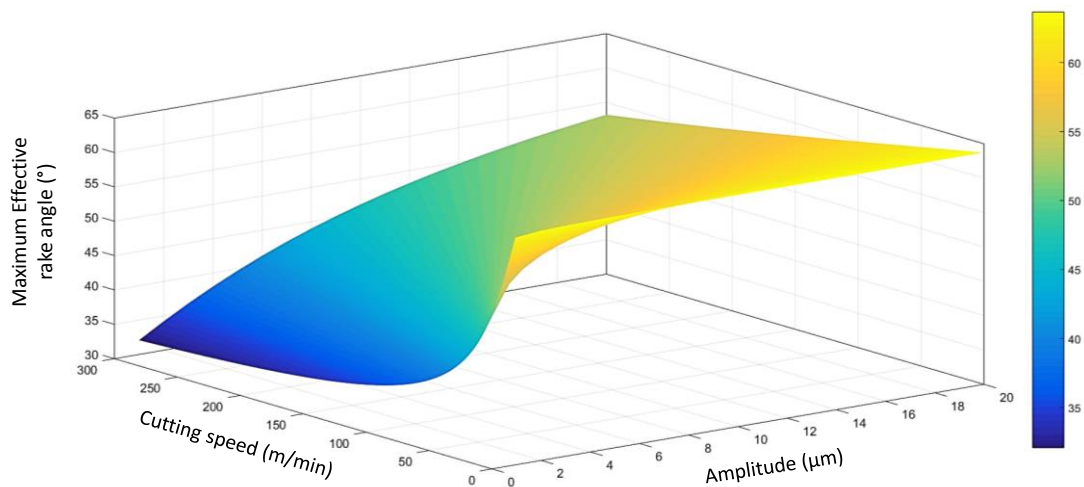


Figure 4-18: Calculation of maximum effective rake angles obtained at various cutting speeds and amplitudes at 40 kHz frequency for a given tool geometry at the end point of cutting edge in UAD

4: Effective rake and clearance angles in CD and UAD for a twist drill geometry

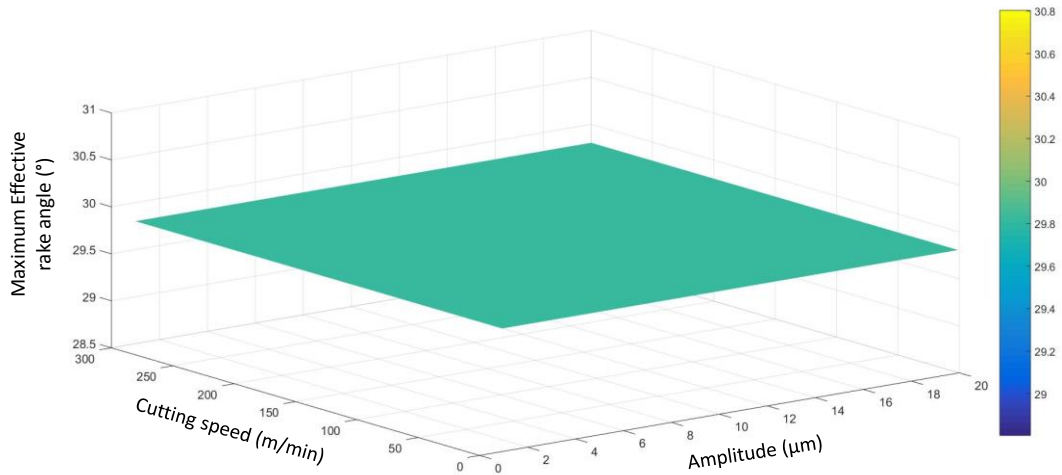


Figure 4-19: Calculation of maximum effective rake angles obtained at various cutting speeds and amplitudes in CD for a given tool geometry at the end point of cutting edge

Arola et al. [181] inspected the machined surface of unidirectional Graphite/epoxy composite material at 0° , 5° and 10° rake angles at cutting speeds of 4, 9 and 14 m/min and depth of cuts of 0.127, 0.254 and 0.381 mm. Low matrix smearing and lower average surface roughness was found in the case of 10° rake angle as compared to that at 0° rake angle at all the cutting speeds. Furthermore, periodicity of fracture events during chip formation was examined and it was found that the prevalent period of dynamic fracture events in trimming with a 10° rake tool was smaller than that with a 0° rake angle tool indicating smaller chip length and localised fracture within the contact zone resulting in improved surface texture in the case of 10° rake angle with respect to that with 0° rake angle tool. Thus, the damage was found to be localised using higher rake angle tool in their work.

As a general machining concept, higher rake angle results in lower machining forces and improved surface roughness [168, 169]. The effective normal rake angle in UAD is higher than those in CD, Figure 4-15. This suggests that the machining forces should be lower in UAD than that in CD. In addition, larger effective normal rake angle at lower cutting speeds in UAD should result in a larger reduction in the

4: Effective rake and clearance angles in CD and UAD for a twist drill geometry

machining forces in UAD when comparing CD and UAD as compared to those at higher cutting speeds, Figure 4-18. Therefore, the current research was performed in order to determine the effect of such high and rapidly varying effective normal rake angles on thrust force, torque and damage during UAD in comparison to those in CD of CFRP.

5 Experimental Methodology

5.1 Equipment

5.1.1 Machining centre

Drilling was performed on a DMG/MORI SEIKI ULTRASONIC 65 monoBLOCK® machine, Figure 5-1. The ultrasonic part of this machine works on the concept of the reverse piezoelectric effect, wherein the transmission of the electrical high-frequency signal from the fixed coil of the spindle to the piezo elements in the tool holder is executed without contact (inductive). Because of the reverse piezo-electric effect, an oscillation is generated in the axial direction and is superimposed on the conventional tool rotation and feed rate. This machine has a maximum spindle speed of 18,000 rpm and maximum 40,000 mm/min feed rate. The ultrasonic oscillation parameters depend on the tool and tool holder combination. Once the drilling tool is located within the tool holder, the resonance frequency and the *maximum* oscillation amplitude is fixed. The amplitude can be varied from 0% to 100% of the maximum oscillation amplitude of tool and tool holder combination. The power rating of the ultrasonic transducer in the machine was found to be a function of the specific tool and tool holder combination in the present research. The overall range of power rating was 90 – 105 W during the experimental trials.



Figure 5-1: DMG/MORI SEIKI Ultrasonic-65 machine used in the experimental studies

5.1.2 Force measurement

A dynamometer was used for thrust force and torque measurement during the experimental studies. For Phase-1 (Section 6.1), a Kistler dynamometer of ‘type 9257 B’ connected to charge amplifier of ‘type 5070’ was used. After the experimental trials conducted in Phase-1, the dynamometer (type 9257 B) became non-functional and it was sent for repairing. Therefore, the research after Phase-1, in the Phases-2 and 3 (Sections 6.2 and 6.3), was conducted with a Kistler dynamometer of ‘type 9271 A’ connected to charge amplifier of ‘type 5019’. The charge amplifier was connected to a computer in which the thrust force and torque measurement was recorded and evaluated by Dynoware software. The technical data for the dynamometers of type 9257 B and 9271 A are provided in Table 5-1 and Table 5-2 respectively. F_x , F_y and F_z in Table 5-1 and Table 5-2, are the forces applied on the dynamometer in the respective X, Y and Z directions respectively. M_z in Table 5-2 is the torque in the direction of Z-axis of ‘type 9271 A’ dynamometer.

5: Experimental Methodology

Table 5-1: Technical data of type 9257 B dynamometer

Characteristics		Values	Units
Range	Fx, Fy, Fz	(-5) to 5	kN
	Fz for (Fx and Fy) ≤ 0.5 Fz	(-5) to 10	kN
Overload	Fx, Fy, Fz	-7.5 / 7.5	kN
	Fz for (Fx and Fy) ≤ 0.5 Fz	-7.5 / 15	kN
Threshold		<0.01	N
Sensitivity	Fx, Fy	~ -7.5	pC/N
	Fz	~ -3.7	pC/N
Natural frequency	f(x,y,z)	3.5	kHz
Natural frequency (mounted on all flanges)	f(x,y)	2.3	kHz
	f(z)	3.5	kHz
Operating temperature range		0 to 70	$^{\circ}\text{C}$
Temperature coefficient of sensitivity		-0.02	$\% / ^{\circ}\text{C}$
Capacitance (of channel)		220	pF
Insulation resistance (20 $^{\circ}\text{C}$)		$>10^{13}$	Ω
Ground Insulation		$>10^8$	Ω
Weight		7.3	kg

Table 5-2: Technical data of type 9271 A dynamometer

Characteristics		Values	Units
Range	Fz	(-5) to 20	kN
	Mz	(-100) to 100	Nm
Overload	Fz	-7.5 / 30	kN
	Mz	-150 / 300	Nm
Threshold	Fz	~ 0.02	N
	Mz	~ 0.02	N-cm
Sensitivity	Fz	-1.8	pC/N
	Mz	-1.5	pC/N-cm
Natural Frequency		>3	kHz
Operating temperature range		0 to 70	$^{\circ}\text{C}$
Temperature coefficient of sensitivity		-0.02	$\% / ^{\circ}\text{C}$
Capacitance		~ 350	pF
Insulation resistance		>10	T Ω
Weight		2.9	kg

Average thrust force between entrance and exit was considered for analysis. An example of average thrust force measurement is shown in Figure 5-2. All the measurements for thrust force were rounded off to zero decimal places in the present research. Therefore, the average thrust force in Figure 5-2 = 171 N. The same was followed for torque values.

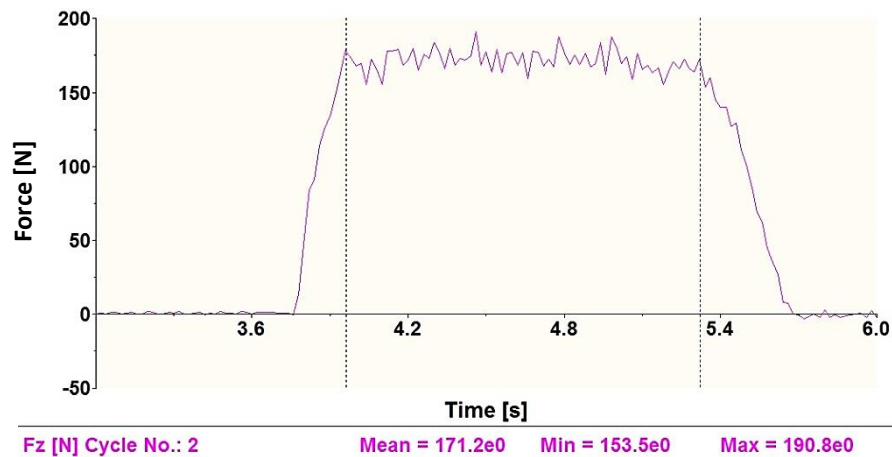


Figure 5-2: Thrust force profile (94.2 m/min, 0.05 mm/rev) in UAD

5.1.3 Ultrasonic amplitude measurement

Although the amplitude in the Ultrasonic 65 machine could be varied from 0% to 100% of the maximum amplitude (in the steps of 10%), the actual value of the 100% amplitude was not known for a drill and tool-holder combination when the drill is fixed into the tool holder. Therefore, the maximum amplitude had to be measured by an external instrument. A Keyence Laser sensor device was used for this purpose. The Keyence laser sensor is a device having a laser sensor head connected to a controller which is further connected to a laptop, Figure 5-3.

5: Experimental Methodology

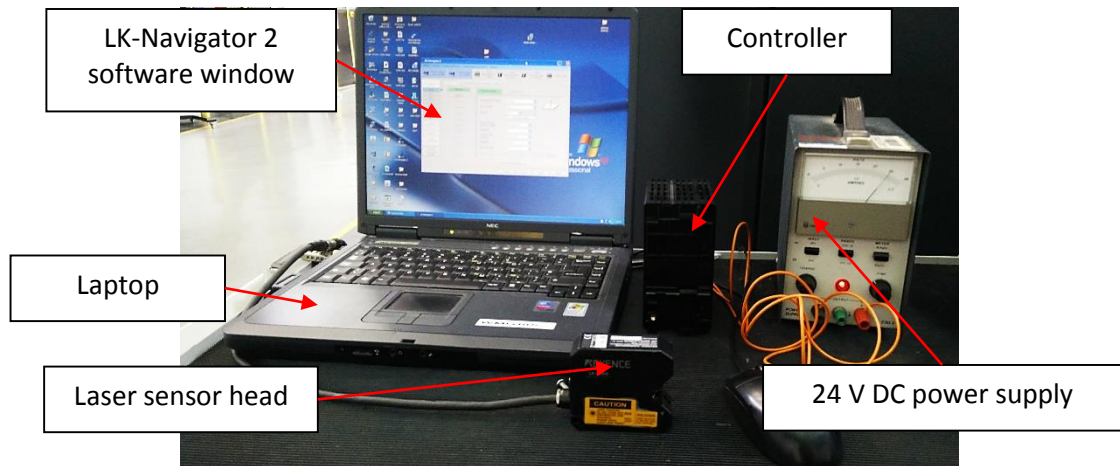


Figure 5-3: Keyence amplitude measurement assembly having laser sensor head, controller, 24 V DC power supply and computer having LK Navigator 2 software for amplitude measurement

The laser head has a laser transmitter and a laser receiver. The laser being transmitted from the transmitter is detected by the receiver after reflecting from a flat surface and thus detecting the location of the flat surface. Maximum data acquisition frequency of this particular equipment is 392 kHz which means that this equipment can detect the location of a surface having oscillation frequency lower than 392 kHz. Since, the Keyence laser device requires a horizontal surface to reflect laser, a small horizontal steel strip having dimensions of 5 mm x 5 mm x 0.15 mm was glued on the tip of the drill, with the help of Cyanoacrylate adhesive (commonly known as ‘super glue’), and it was left to dry completely for 4 hours. The setup is shown in Figure 5-4.

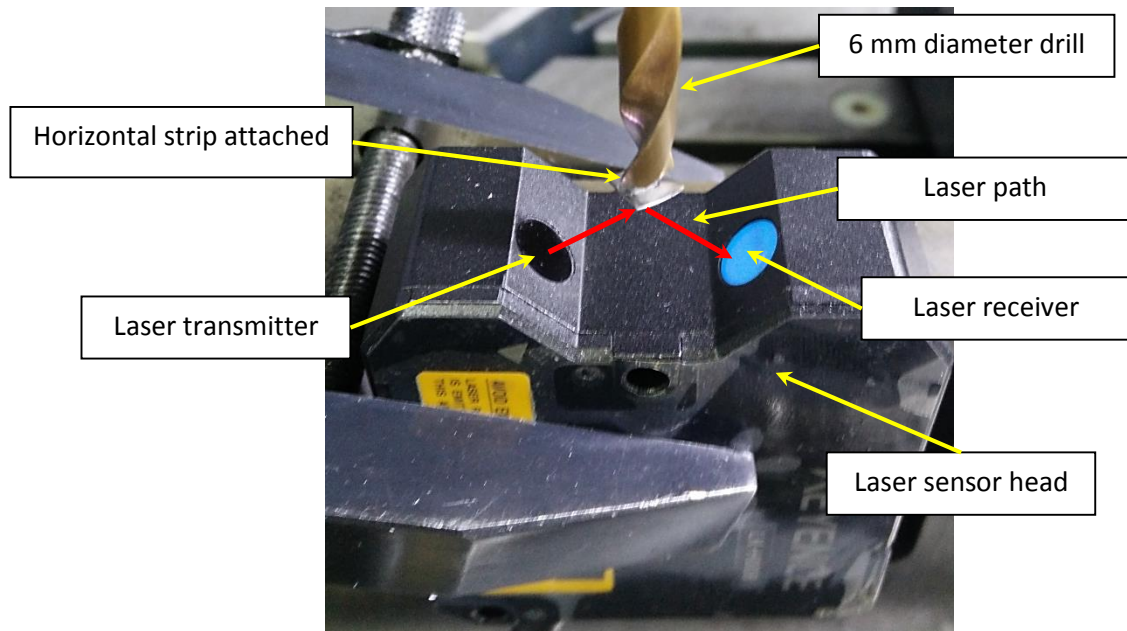


Figure 5-4: Keyence Laser sensor head with the drill tip located in such a way that the laser transmitted from the transmitter is reflected from the horizontal strip attached to the drill tip and received at the receiver further

Since the ultrasonic oscillation amplitude was measured in the air before machining in the present research (i.e. when the tool was not involved in machining), a possibility arises whether the amplitude of ultrasonic oscillation was same while the tool was actually involved in machining as that when it was measured in the air before machining. In order to examine this, a test hole was drilled in an aluminium alloy (7050 T7451) at 100 m/min cutting speed and 0.075 mm/rev feed rate (parameters recommended by BAE Systems). The ultrasonic frequency was 38760 Hz. The peak-to-peak ultrasonic oscillation amplitude measured in the air before the experiment was $4.7 \mu\text{m}$. Figure 5-5 displays the ultrasonic impressions on the internal cylindrical machined surface of the drilled hole in Aluminium alloy. It can be seen that the peak-to-peak amplitude measured on the impression at the machined surface was $4.689 \mu\text{m} \approx 4.7 \mu\text{m}$. Thus, this evidence proves indirectly that the amplitude of oscillations was not damped during machining in the present. However,

further research is ongoing at WMG to verify this phenomenon through more direct evidence.

The aluminium alloy was chosen for this test because such impressions like Figure 5-5 could not be obtained in CFRP material due to its properties being different to that of aluminium alloy. Therefore, this test was assumed to be the closest approximation to the amplitude variations in the UAD of CFRP and it was concluded that similar to aluminium alloy, the ultrasonic amplitude would be the same in the cases when measured in air and when the tool is actually involved in machining during UAD of CFRP.

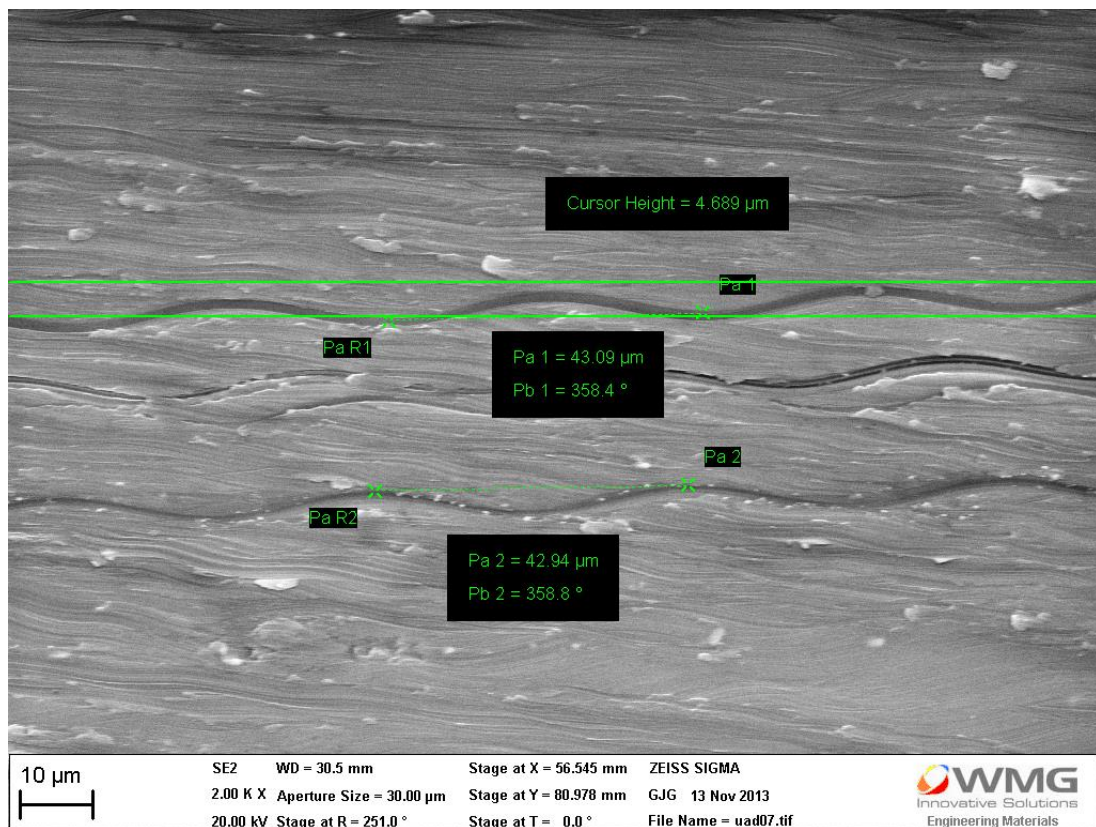


Figure 5-5: Sinusoidal impressions on the internal cylindrical surface of aluminium at 100 mm/min cutting speed and 0.075 mm/rev feed rate (38760 Hz frequency and 4.7 μm amplitude)

5.2 Workpiece material

The workpiece material used in the drilling experiments was a research grade version of HTM 552 and it was provided by BAE Systems Ltd. The material was a carbon fibre composite having Bismaleimide matrix. The properties of HTM 552 provided by BAE Systems are presented in Table 5-3.

Table 5-3: Properties of the HTM 552 material provided by BAE Systems

Resin density	1.25 g/cm ³
Fibre density	1.78 g/cm ³
Laminate density	1567 kg/m ³
Resin areal weight	68 g/m ²
Fibre areal weight	145 g/m ²
Prepreg areal weight	213 g/m ²
Prepreg resin content by weight	32 %
Prepreg fibre content by weight	68 %
Predicted laminate resin volume fraction	40.1 %
Predicted laminate fibre volume fraction	59.9 %
Cured ply thickness (CPT)	0.136 mm
Overall workpiece thickness	7.4 mm
Interlaminar shear strength at room temperature	90 MPa
Flexural strength at room temperature	1029 MPa
Flexural modulus	68 GPa

As the damage during the machining of carbon fibre is dependent on the carbon fibres' orientation ([80], [82], [81]), an understanding of the fibre orientation in the workpiece material was essential for the appropriate explanation of the drilling results. Therefore, in order to determine the orientation of carbon fibres in the workpiece material, the material was sectioned in the angular orientations of 0°, 45°, 90° and 135°, as shown in Figure 5-6 and Figure 5-7, mounted & polished using the methodology mentioned in the Section 5.3.1.

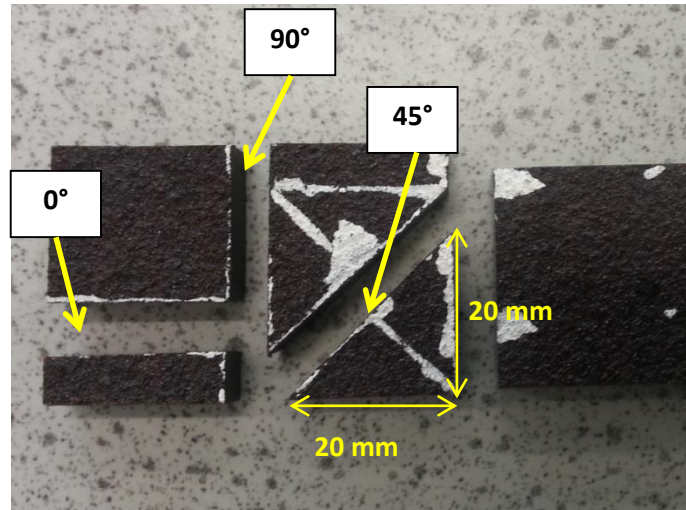


Figure 5-6: Sectioning of the workpiece material in 0°, 45° and 90° orientation

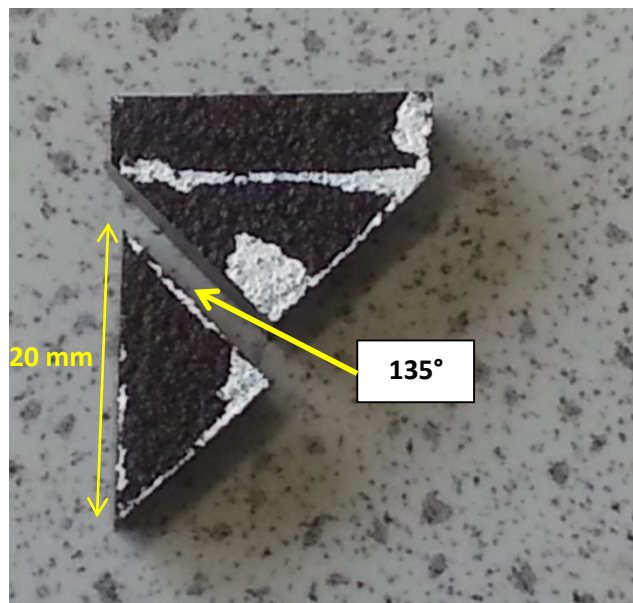


Figure 5-7: Sectioning of workpiece material in 135° orientation relative to 0° orientation shown in Figure 5-6

All sectioned orientations were observed further after mounting and polishing in the LEICA DM 4000 M microscope.

The images of these sectioned samples were captured using OmniMet software and are presented in Figure 5-8 to Figure 5-11. The most easily identifiable orientation of carbon fibres was found to be 0° in each plane of sectioning (because of clearly visible parallel lines). Therefore, after carefully examining each layer of fibres at all planes of sectioning, the orientation of each layer with respect to the 0°

plane of sectioning in Figure 5-6 is listed in Table 5-4. The oriented layers of the 0° plane of sectioning, shown in Figure 5-8, are correlated to their respective orientations of Table 5-4 with red coloured arrows in Figure 5-12. It was found that there were overall 49 layers out of which top and bottom layers were woven carbon fibres while the intermediate layers were unidirectional. Unlike the materials reported in the in several studies in the literature, the multidirectional layers were not found to have a repeatable pattern; however, there exists a layer having 0° orientation in the middle of the workpiece material around which the rest of the layers are mirrored except two specific layers having 0° and 135° orientations as shown in Figure 5-12. The thickness of the workpiece was measured with the help of Vernier callipers and it was found to be 7.4 mm. The workpiece was kept same in all the experimental studies so that the results would not be affected because of variation in the workpiece in the subsequent experimental studies.

5: Experimental Methodology

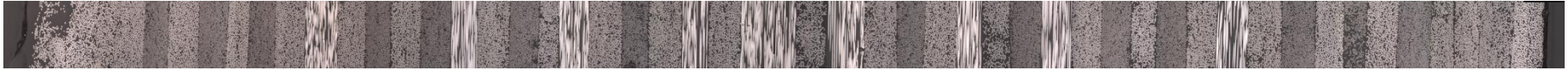


Figure 5-8: View of the material in the plane of sectioning at 0° shown in Figure 5-6



Figure 5-9: View of the material on the plane sectioned at 45° shown in Figure 5-6



Figure 5-10: View of the material on the plane sectioned at 90° shown in Figure 5-6



Figure 5-11: View of the material on the plane sectioned at 135° shown in Figure 5-6

5.3 Sample preparation and inspection methodologies

5.3.1 Sectioning, mounting and polishing of the samples

To visualize the machined surface after drilling, and to analyse the damage and cracks in the machined material underneath the machined surface, it was necessary to section the samples as shown in Figure 5-13 and Figure 5-14. The reason for selecting the specific plane of sectioning in Figure 5-13 is explained in detail in Section 5.5.

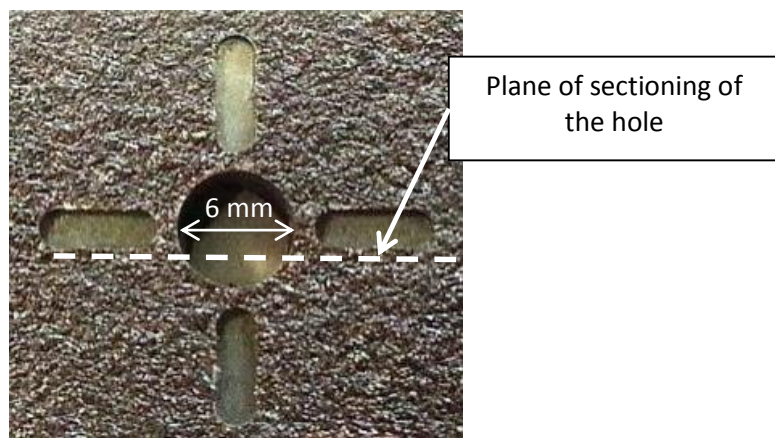


Figure 5-13: Image of a drilled hole mentioning plane of sectioning for observing the machined surface

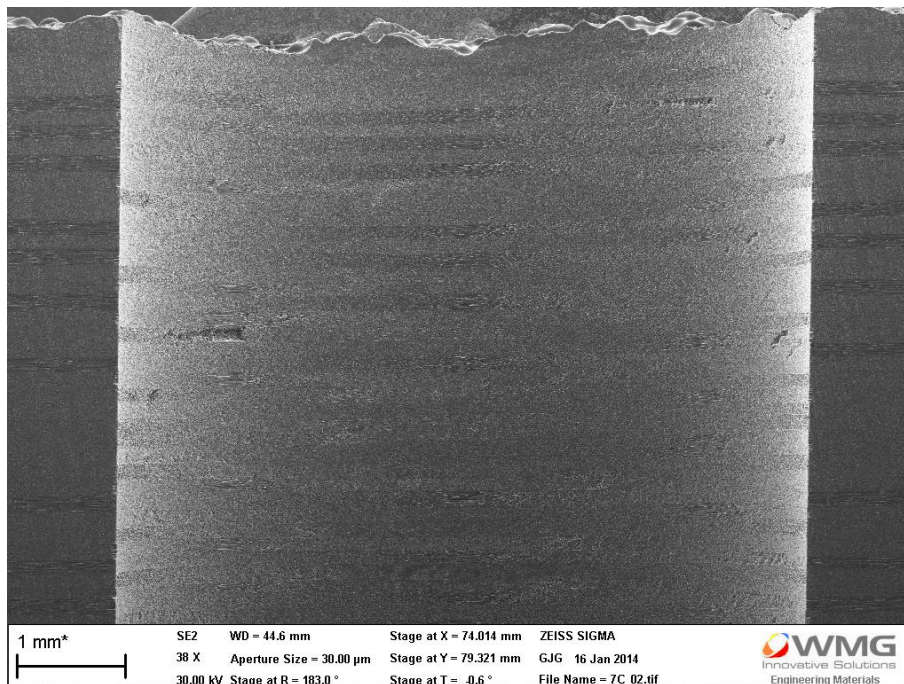


Figure 5-14: SEM image of the machined surface after sectioning the hole

To identify and quantify the damage on the machined surface, it was necessary to mount the section of material containing holes to support the damage inside the hole (created during drilling) with the mounting material, prior to sectioning and polishing. The machines for mounting, sectioning and polishing were standard metallurgical equipment provided by Buehler.

5.3.1.1 Mounting

For mounting the holes, castable resin system of EpoCure was used due to its better adhering with the samples and low curing temperature of 28°C and hence avoiding any thermal harm to the sample [189]. The resin mixture containing the sample was then further left for hardening.

5.3.1.2 Sectioning

The material containing the holes, in which the internal cylindrical machined surface was to be observed, were sectioned in the precision sectioning machine IsoMet® 5000 Linear precision saw. It was possible that additional damage could be introduced on the sectioning plane because of sectioning of the hole in this fast cutting machine. However, since the focus of this work was to observe internal cylindrical surface in SEM, any damage introduced on the sectioning plane because of sectioning would not affect the results.

The holes, where the internal damage was to be observed in SEM after polishing were sectioned in a slow cutting machine – IsoMet™ Low speed saw after mounting. Mounting of the hole in the epoxy resin system before sectioning was necessary to support the internal damage created during drilling.

5.3.1.3 Grinding and polishing

In the current research, the grinding and polishing of the mounted samples were performed in the polishing machines – Phoenix 4000 and EcoMet 300 provided by the Buehler. To polish the mounted samples, the four-step polishing procedure for polymer composite materials, recommended by Buehler, was followed, Table 5-5.

Table 5-5: Grinding and polishing steps followed for polishing the carbon fibre composite samples [189] (Comp. = complementary)

Surface	Abrasive/ Size	Load (N)	Base Speed (rpm)/ Direction	Time (min.)
Grinding by CarbiMet 2 abrasive discs (waterproof paper)	P400 grit SiC water cooled	18	150 -240 Comp.	Until plane
UltraPol or UltraPad cloth	6 µm MetaDi Supreme diamond suspension	18	120 - 150 Comp.	04:00
TexMet pad or TriDent or Nylon cloths	3 µm MetaDi supreme suspension	22	120-150 Comp.	04:00
ChemoMet or MicroCloth cloths	~0.05 µm MasterMet colloidal silica or MasterPrep alumina suspension	27	120-150 Comp.	02:00-04:00

5.3.2 Optical microscopy and scanning electron micrography (SEM)

In order to inspect the polished samples and to quantify the damage in some samples, optical microscopy (LEICA DM 4000 M microscope) and SEM were adapted. SEM was also adapted for analysing the damage near to the machined surface, chips formed during the drilling and the machined surface itself at the higher magnification and great depth of field. A **ZEISS Sigma** SEM was used for these purposes in the present research, Figure 5-15.

5: Experimental Methodology



Figure 5-15: ZEISS Sigma HV SEM

Since the mounted epoxy and CFRP are non-conducting materials, in order to examine them in the SEM, the top surface of the sample was coated with a thin film of gold using an Automatic Sputter Coater in order to make it conducting for electrons and to avoid charge accumulation. Further, silver paint was used to create a conducting path between the top surface and the stub attached at the bottom of the mounted sample. Samples prepared with this methodology were free from the water/alcohol/small particles trapped inside the cracks of the polished material as shown in Figure 5-16.

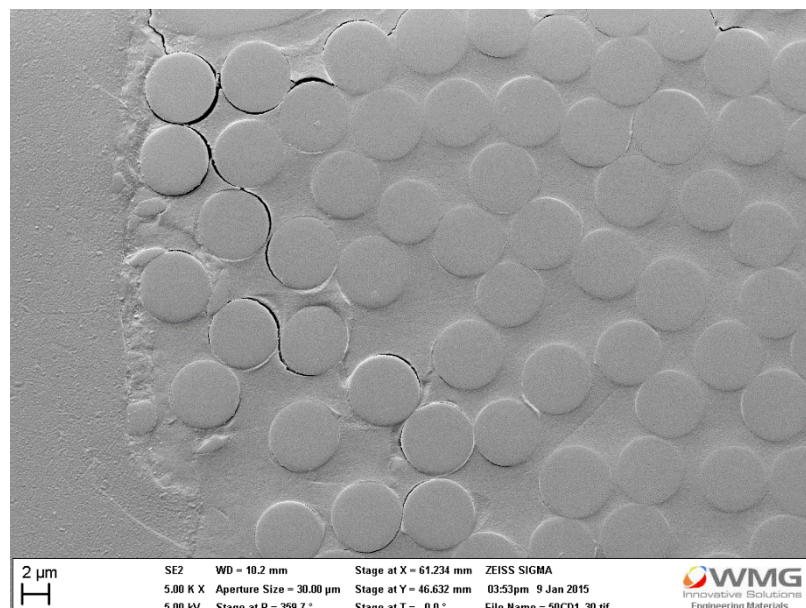


Figure 5-16: Polished and cleaned surface after polishing exhibiting damage propagation and fibre-matrix debonding

Since CFRP used in the present research is a low-density material, electron beam having low energy (low voltage in SEM) is sufficient to produce the secondary electrons from the surface of CFRP unlike in the case of heavy and dense metals [190]. Therefore, low voltages in the range of 5-10 kV were used in SEM in order to examine the surface characteristics of polished CFRP. In addition, a low voltage (and hence, low energy electron beam) between 5-10 kV was used in order to minimise any damage to the sample surface.

5.4 Damage analysis through X-ray CT scanning

To examine the extent of the damage accurately around the drilled holes, the non-destructive technique of X-Ray computed tomography (CT) was used in the present research and a methodology was developed in collaboration with another research group. Selected drilled holes were scanned separately by Nikon Metrology system X-TEK 320.

In order to examine and quantify the internal damage (fibre pull out) in a hole through this methodology, the location of the physical centre of the hole was required. Therefore, four straight marks were machined prior to drilling around where the hole was going to be produced, Figure 5-17(a). A 2 mm diameter, two flute, Q-coat tungsten carbide slot drill with flat end was used to machine the marks at the cutting speed of 113 m/min (18000 rpm), axial feed rate of 250 mm/min cross-feed and 100 mm/min axial feed with two passes – first 0.4 mm deep and then further 0.3 mm making the final depth of the machined marks to be 0.7 mm. After machining four marks with a marking tool, the tool was changed to drilling tool and then the hole was drilled keeping the workpiece fixed. The centre of the hole was identified by the point of intersection of the lines joining the midpoints of the

machined marks around the hole through image processing, (Figure 5-17(b)). However, there was a tolerance of $4\ \mu\text{m}$ (provided by the machine manufacturer-DMG SAUER) in the process of tool change from marking to drilling tool in Ultrasonic 65 machine.

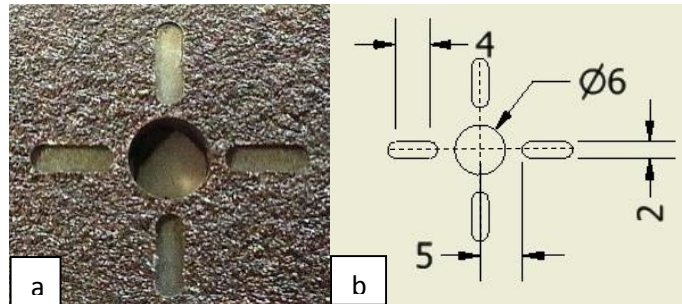


Figure 5-17: (a) Straight machined marks and the drilled hole, (b) centre identification and the dimensions of hole and marks in millimetres.

The drilled specimen were scanned with the X-rays having 215 kV voltage, 6 W power, 4 s exposure time and 18 dB gain. Data provided by CT scanning was reconstructed to a 3D representation of the hole with back-projection reconstruction algorithms in CT Pro software from Nikon Metrology as shown in Figure 5-18. As explained in Section 3.4.1.4, the 3D model is constituted by voxels. The reconstructed data is represented by different grey values. The samples were measured with an NEXIV VM2 – R6555 optical coordinate measuring machine (CMM) scanner just after being scanned to calculate the voxel size. The voxel size for the present 3D model of the specimen was $15\ \mu\text{m}$ [101].

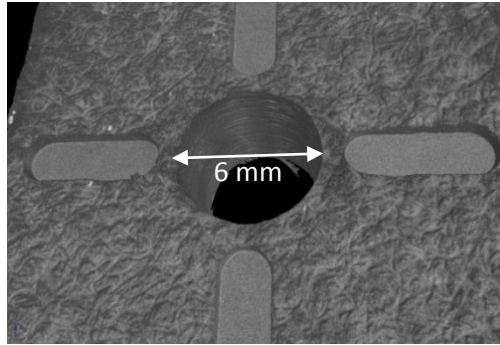


Figure 5-18: An image of 3D scan of the hole exhibiting the machined marks around the hole and damage on the internal walls of the hole (282.6 m/min, 0.05 mm/rev)

Since the reconstructed model is constituted of voxels, the model can be broken into horizontal or vertical layers of a specimen having a thickness of the voxel size as shown in the schematic in Figure 5-19. Analysing the entire layers in horizontal and vertical planes would provide the complete information of internal defects in a specimen.

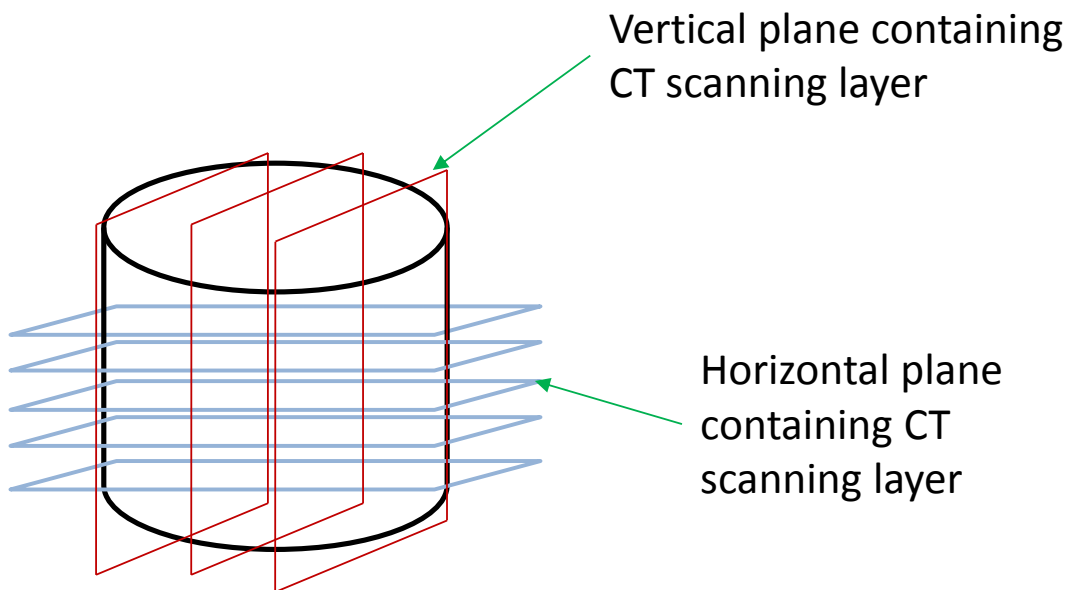


Figure 5-19: A schematic elaborating the horizontal and vertical CT scanning layers of a cylindrical specimen

In the present research, CT scanning layers in both horizontal and vertical planes were exported through VG Studio Max 2.2 software as two-dimensional images for further analysis of the internal damage. The images of horizontal CT scanning layers of the specimen were used for MATLAB image processing tool to acquire complete internal information of each drilled hole. While, the image in vertical planes were

used for visualization of the damage in a vertical plane. Figure 5-20 presents the image of a CT scanning layer in a vertical plane exhibiting the machined marks and exit delamination. It is clear from Figure 5-20 that the maximum extent of the exit delamination is inside the part a few laminates before the hole-exit. Therefore, the maximum extent of crack in a specimen cannot be seen from the outside with a visual inspection through human eye because it is located a few laminates earlier than the exit. This information also supports the argument stated in section 3.4.1.1 that the visual inspection techniques through optical microscopy [93, 96, 98-100] would not be able to identify the accurate extent of damage due to CFRP material being opaque. Figure 5-21 shows the exported image of a vertical CT scanning layer displaying the fibre pull out on the internal cylindrical surface of a hole. It is to note in Figure 5-21 that the vertical layer is not on the diametrical plane of the cylindrical hole.

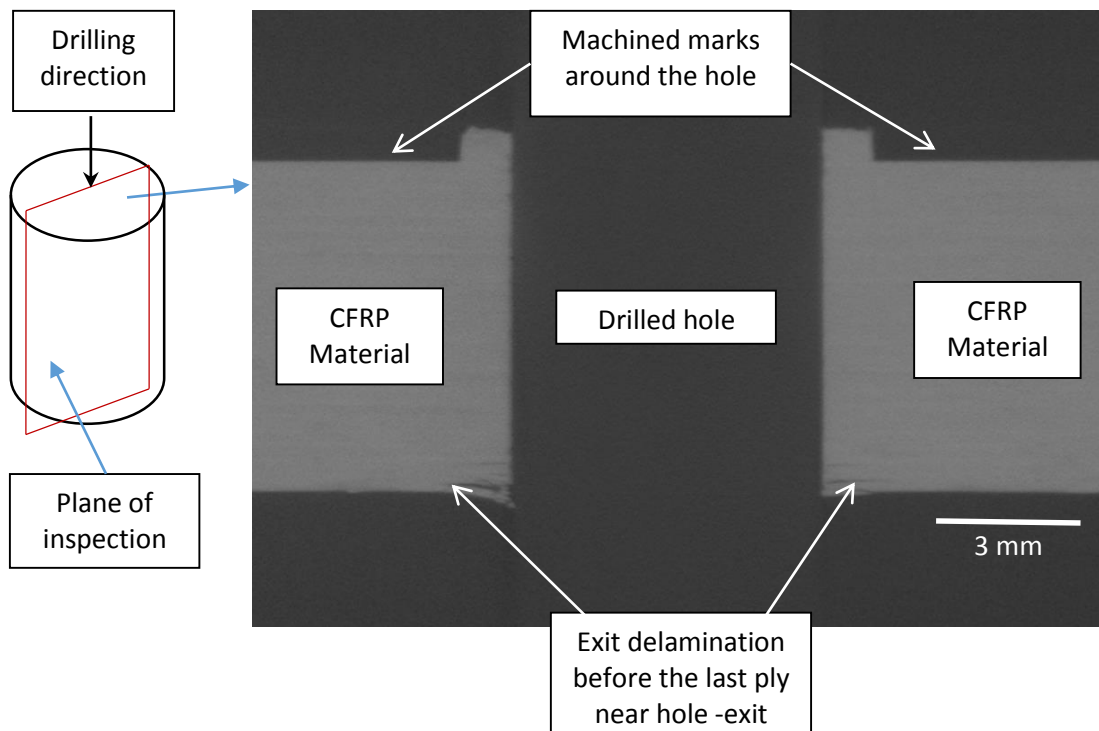


Figure 5-20: Image of Vertical CT scanning layer on a diametrical plane visualizing the exit delamination (282.6 m/min, 0.05 mm/rev). P.S. the blank space between the two grey coloured CFRP material is the drilled hole.

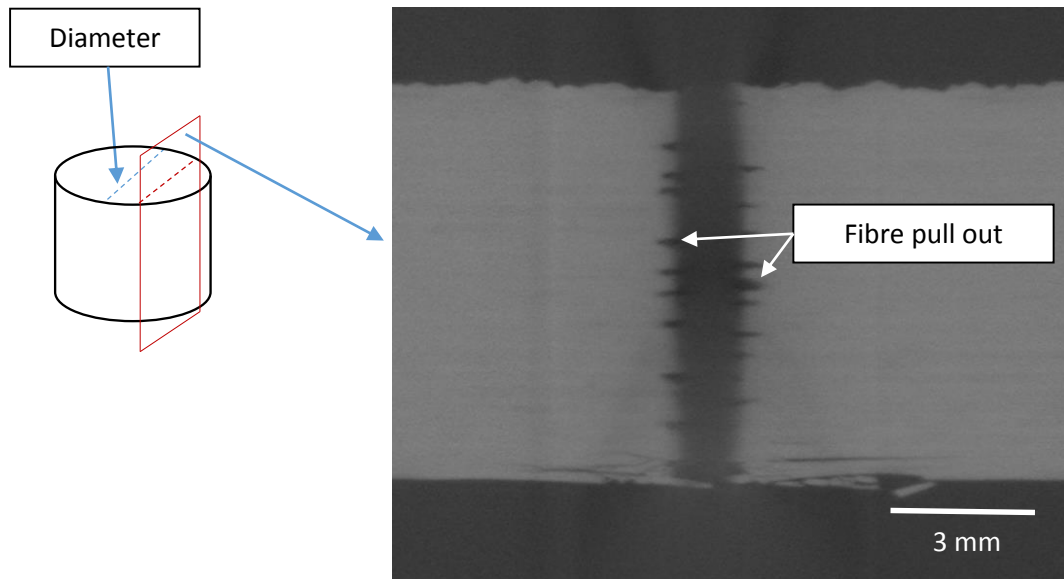


Figure 5-21: Fibre pull-out in side view of internal damage obtained from CT scanning in a vertical layer (P.S. the vertical layer is not on a diametrical plane)

With the help of image processing in two-dimensional images, the exit delamination and the dimensional metrological results on the deviation of the radius were calculated for each layer. The delamination at hole-entrance could not be measured by this method because the depth of the machined marks around the hole was 0.7 mm and the analysis of the image processing was started from the layer where the centre of the hole was determined at the depth of 0.7 mm from the entrance. Furthermore, the exit delamination and internal damage were quantified with the methodologies explained in Sections 5.4.1 and 5.4.2.

5.4.1 Exit delamination

Area delamination factor as explained by Faraz et al.[95] and Faraz and Biermann [76] was considered exit delamination criteria for CT scanning. In order to calculate the exit delamination factor, 30 CT scanning layers near hole-exit in horizontal planes were selected from CT scanning images of a hole (see, schematic in Figure 5-22). The delaminated area in the image of the CT scanning layer is highlighted in a loop in Figure 5-23. Such area in a loop was calculated in the images

of CT scanned layers near hole-exit (30 layers) using image processing. Further, the delaminated area variation was plotted with respect to depth in the direction of drilling.

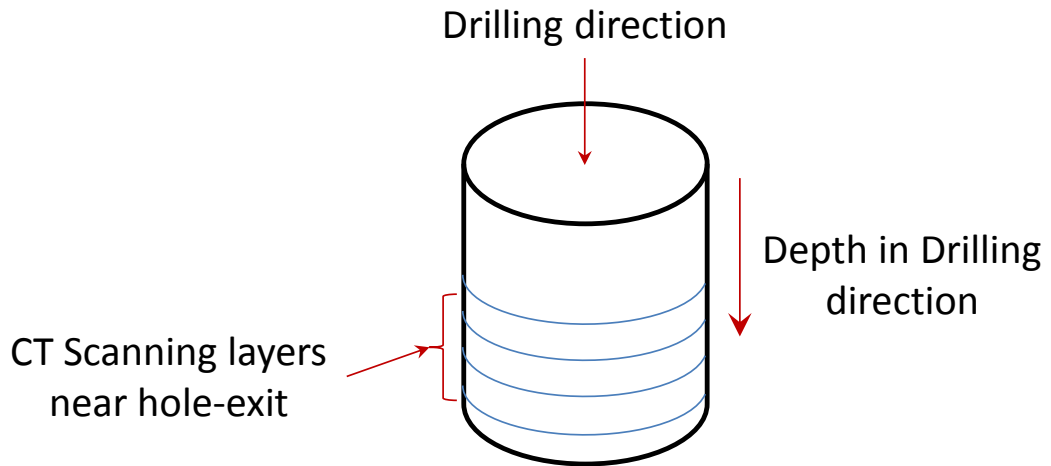


Figure 5-22: A schematic displaying the drilling direction, drilling depth and CT scanning layers for exit delamination calculations

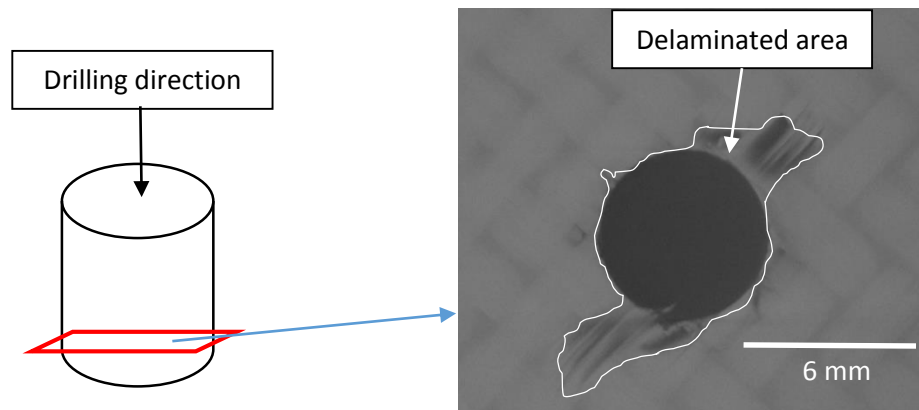


Figure 5-23: DICOM image of a horizontal CT scanning layer exhibiting the delaminated area in a loop near hole-exit for a 6 mm diameter hole (282.6 m/min, 0.05 mm/rev)

The area variation for one of the holes near hole-exit is plotted in Figure 5-24. The maximum area amongst all these areas of the layers near hole-exit was considered as the area for exit delamination of a particular hole. Such area was termed as 'maximum exit delamination area', e.g. the maximum exit delamination area for the variation shown in Figure 5-24 is 29.9 mm².

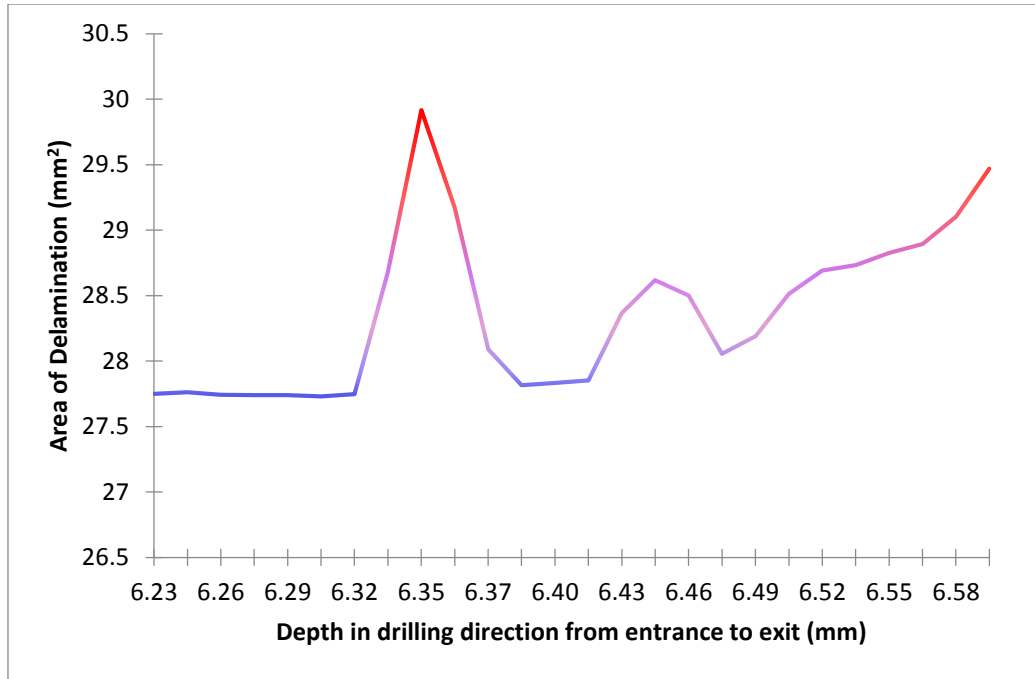


Figure 5-24: Delaminated area with respect to depth in drilling direction near hole-exit (282.6 mm/min, 0.05 mm/rev in CD)

Further, the area of originally intended hole was calculated by using formula πr^2 (r being the radius of originally intended hole). Area delamination factor was calculated by dividing the difference of maximum exit delamination area and area of originally intended hole by the area of originally intended hole. If A_{max} is the maximum exit delamination area and A_0 is the area of originally intended hole, then area delamination factor as mentioned by Faraz et al.[95] and Faraz and Biermann [76] would be –

$$\text{Area delamination factor} = \left(\frac{A_{max} - A_0}{A_0} \right) \times 100 \%$$

5.4.2 Internal damage

To measure the internal damage, the radius of every point on the circumference in a CT scanned layer of the hole was measured through image processing in MATLAB at first and then the maximum of these radii (R_{max} in Figure 5-25) was considered to be the radius of damage in that specific layer. The maximum radii in

all the CT scanning layers from the entrance to exit were thus calculated and were plotted against the drilled depth from the entrance to exit as shown in Figure 5-26.

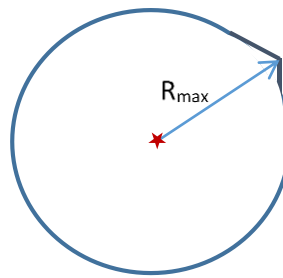


Figure 5-25: Schematic for Maximum radius of a CT scanned layer in horizontal direction

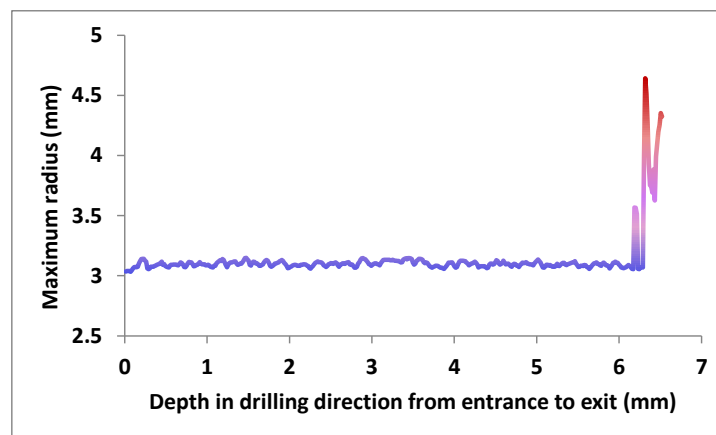


Figure 5-26: Maximum radius variation from entrance to exit in a hole (9.42 mm/min, 0.05 mm/rev)

In order to calculate the average depth of fibre pull out, the average was considered between the drilling depths from 2 mm to 5 mm. The drilling depth between 2 mm to 5 mm was considered in order to avoid the effects of entrance and exit, e.g. the average maximum radius of the variation shown in Figure 5-26 is 3.1 mm. Further, the radius of drilled hole was subtracted from this ‘average maximum radius’ to achieve the average fibre pull out depth in that hole, e.g. the average fibre pull out depth of hole shown in Figure 5-26 is $3.1 - 3 = 0.1$ mm (100 μ m). The average depth of fibre pull out thus obtained was considered as average internal damage in the CT scanning samples.

5.5 Damage analysis through sectioning, mounting and polishing

Drilled holes were sectioned off-centre (1.5 mm away from centre) using low speed cutting saw, Figure 5-27. The Larger part was mounted and polished. Polishing was performed such that the surface was ground to approximately the centre and damage at diametrically opposite points could be analysed.

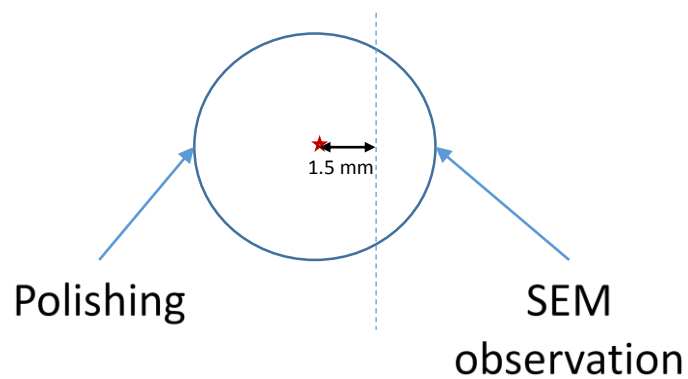


Figure 5-27: Schematic for representing off-centre sectioning of holes for mounting and SEM observation

The edges of the machined surface in the polished sample, Figure 5-28, were examined in the SEM further.

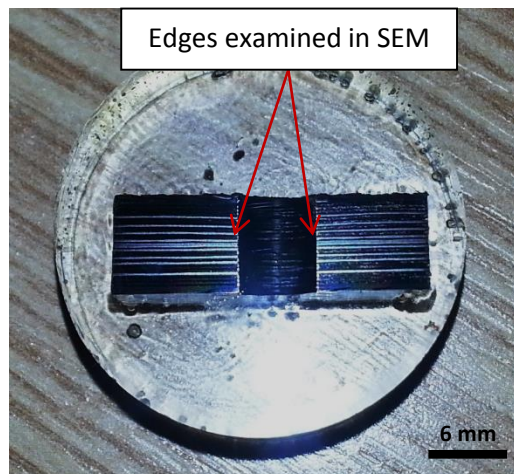


Figure 5-28: Sectioned hole mounted in EpoCure 2 resin system and polished

The information obtained from this analysis in the SEM was then segmented into three categories –

5.5.1 Crack propagation depth

Crack propagation depth data was measured in the samples similar to as shown in Figure 5-29 by examining both the edges of the sectioned hole from the entrance to exit in SEM. Average of all the values obtained from both edges was considered as ‘average crack propagation’ for a particular hole. Crack propagation found in SEM analysis, could not be detected in CT scanning because objects having lower dimension than the voxel size (15 μm) were not visible in CT scanning and the thickness of these cracks in Figure 5-29 are less than 15 μm .

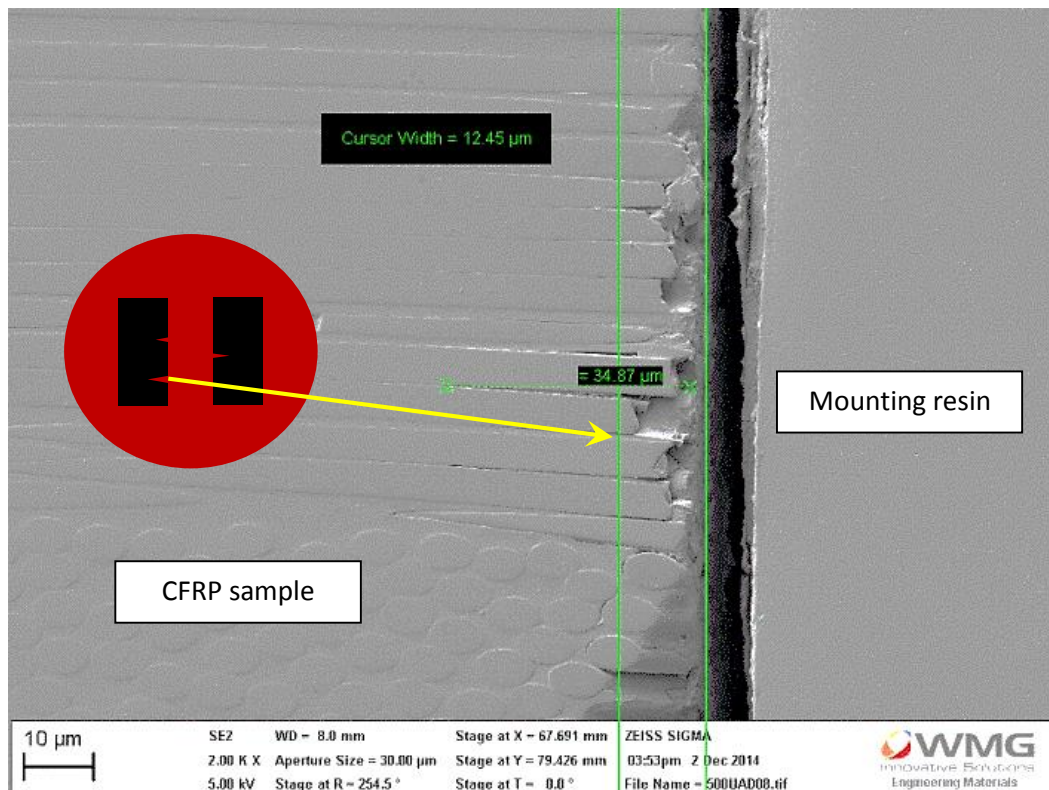


Figure 5-29: Crack propagation and fibre pull out (9.42 m/min UAD). The diagram in the inset shows the location of the specific damage in a mounted sample.

5.5.2 Fibre pull out and disorientation

Similar to crack propagation, depth of fibre pull-out and fibre-disorientation was also measured at both edges of a polished sample from the entrance to exit in the SEM and average of these values was considered as average fibre pull-out for a particular hole. The example of fibre pull out depth measurement is shown in Figure

5-30. Similar to fibre pull-out, there was another type of damage found in the edges of holes which is shown in Figure 5-31. In this type of damage, a cluster of fibres near to machined surface was found to be disoriented. It was examined further by mounting, sectioning and polishing a hole in the plane perpendicular to its axis as shown in Figure 5-32. This disorientation of fibres was found to be similar to that reported by the other authors during machining of fibres at 90° and 135° relative orientation, discussed in Section 3.1. Quantitatively, the depth of fibre orientation was found to be in similar order to that of fibre pull-out in a particular hole. Therefore, fibre pull-out and fibre disorientation were merged and analysed together and an average of these two together was considered as an average fibre pull-out and fibre disorientation (average internal damage) for a particular hole.

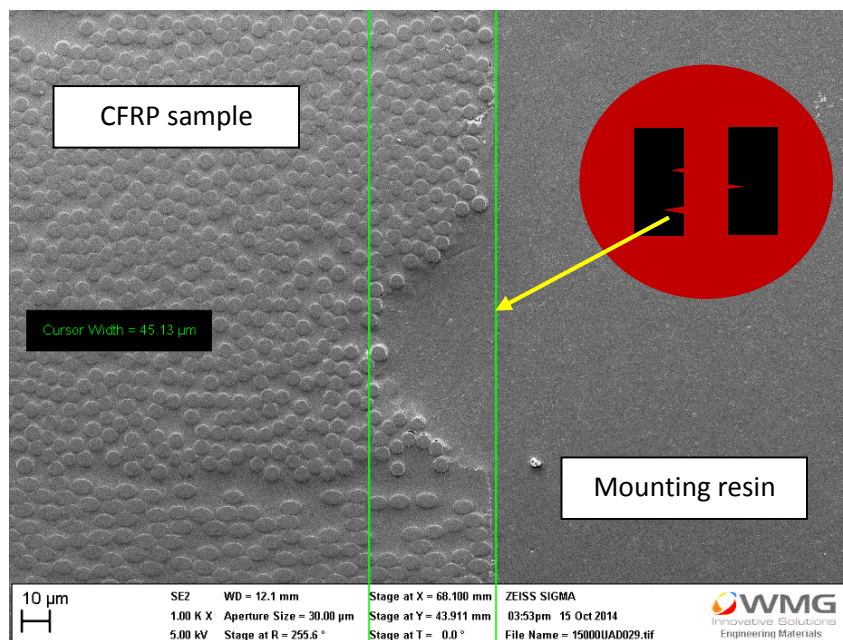


Figure 5-30: Fibre pull out depth measurement (282.6 m/min cutting speed, 0.05 mm/rev, CD). The diagram in the inset shows the location of the specific damage in a mounted sample.

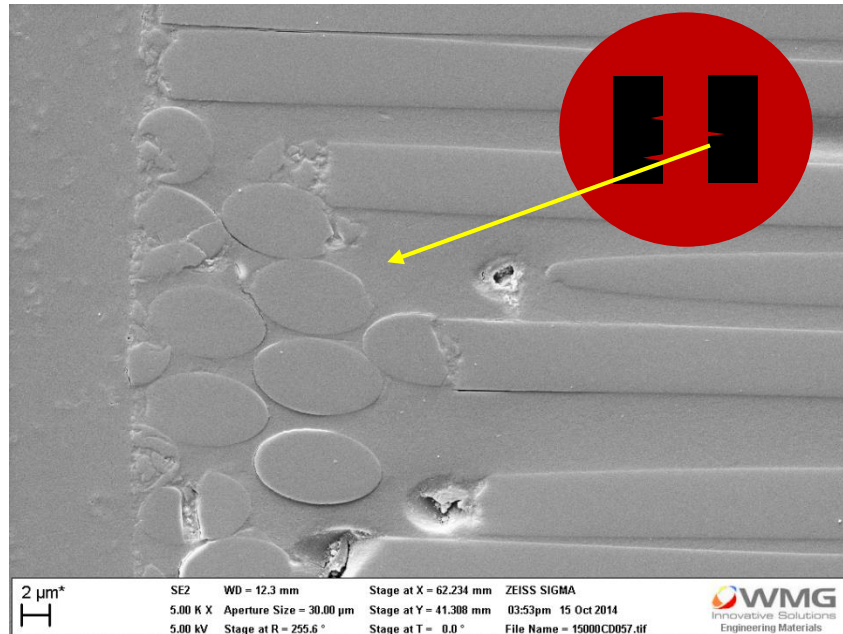


Figure 5-31: Fibre dis-orientation (282.6 m/min cutting speed, 0.05 mm/rev, CD). The diagram in the inset shows the location of the specific damage in a mounted sample.

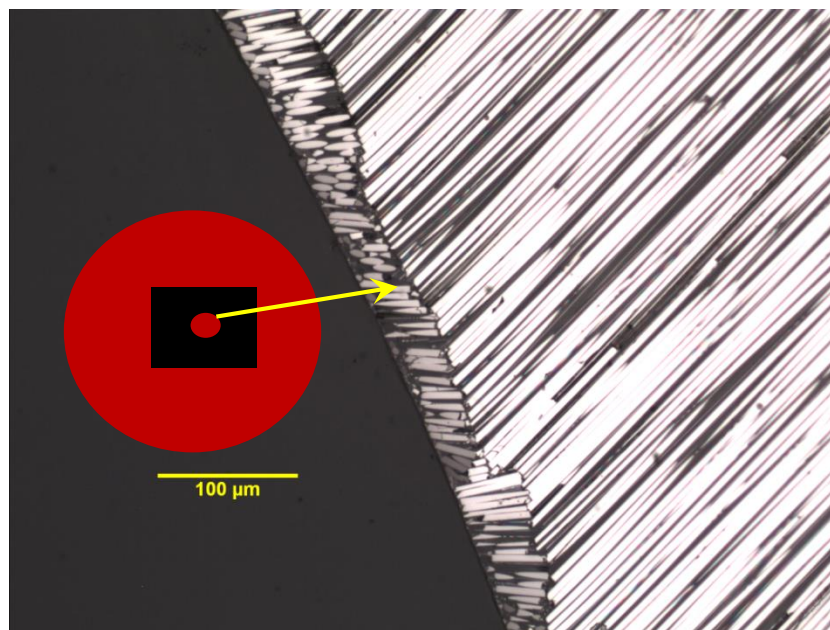


Figure 5-32: Disorientation of fibres during drilling of CFRP (282.6 m/min, 0.05 mm/rev, UAD). The diagram in the inset shows the location of the specific damage in a mounted sample.

5.5.3 Maximum delamination depth at entrance and exit

In order to measure the maximum delamination depth at the entrance and exit, the sectioned region near hole-exit and entrance, at both the edges of the hole, were examined in SEM and the crack propagation depth from the edge into the material was measured, Figure 5-33 and Figure 5-34. The maximum crack

5: Experimental Methodology

propagation depth out of these was considered to be the maximum delamination depth at the exit for that particular hole, e.g. the maximum delamination at the exit for the hole shown in Figure 5-33 and Figure 5-34 is 1.163 mm (1163 μm). Maximum delamination depth at the entrance was also measured in the same way. All the damage measurements were compared in micrometer (μm) units and rounded off to zero decimal places. In addition, as explained in section 5.3.2, the damage introduced by the electron beam in the material in Figure 5-33 and Figure 5-34 was minimised by restricting the beam voltage between 5 kV and 10 kV.

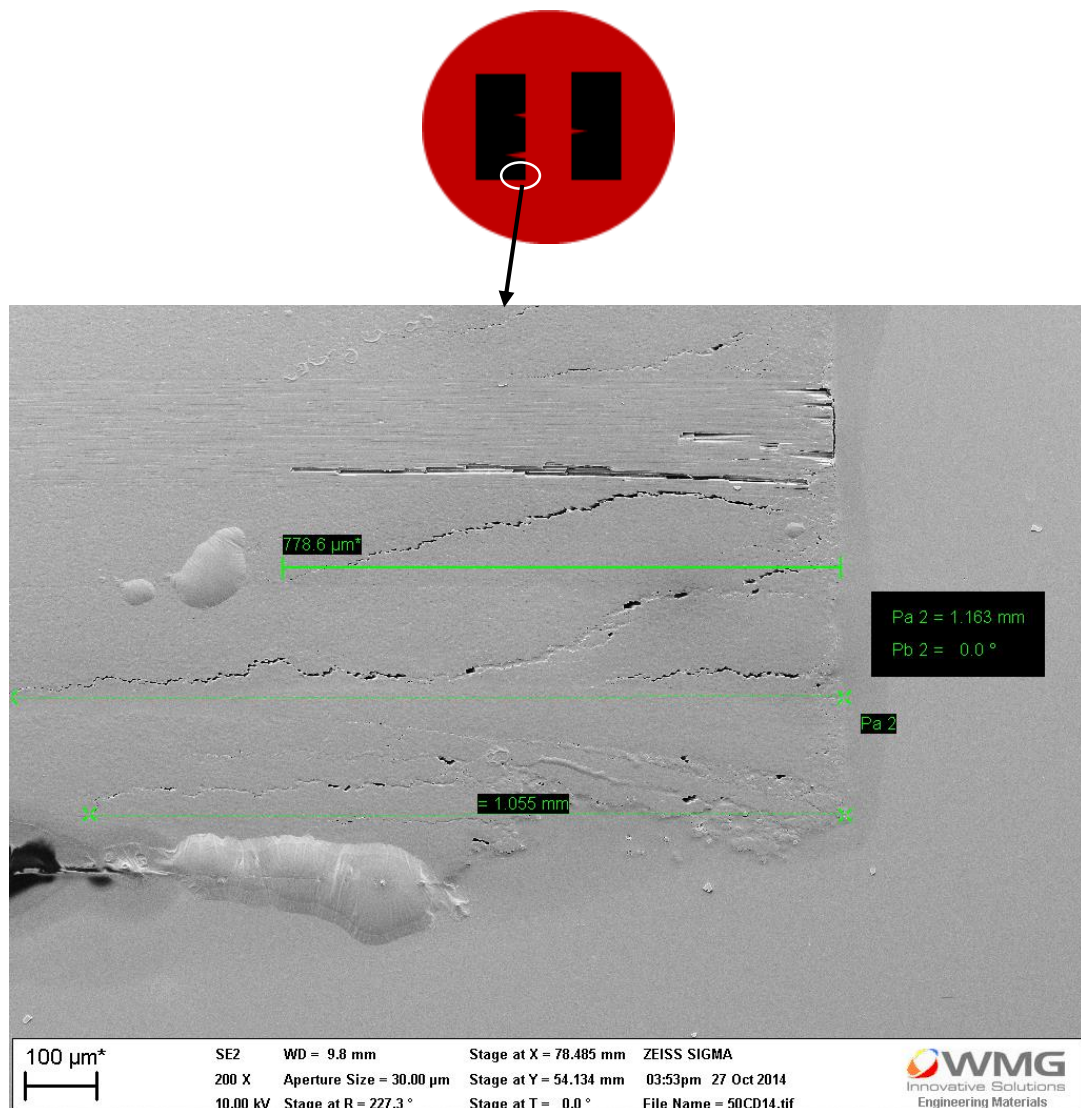


Figure 5-33: Exit delamination depth measurement on the first side of the hole (0.942 m/min, 0.05 mm/rev CD). The diagram in the inset shows the location of the specific damage in a mounted sample.

5: Experimental Methodology

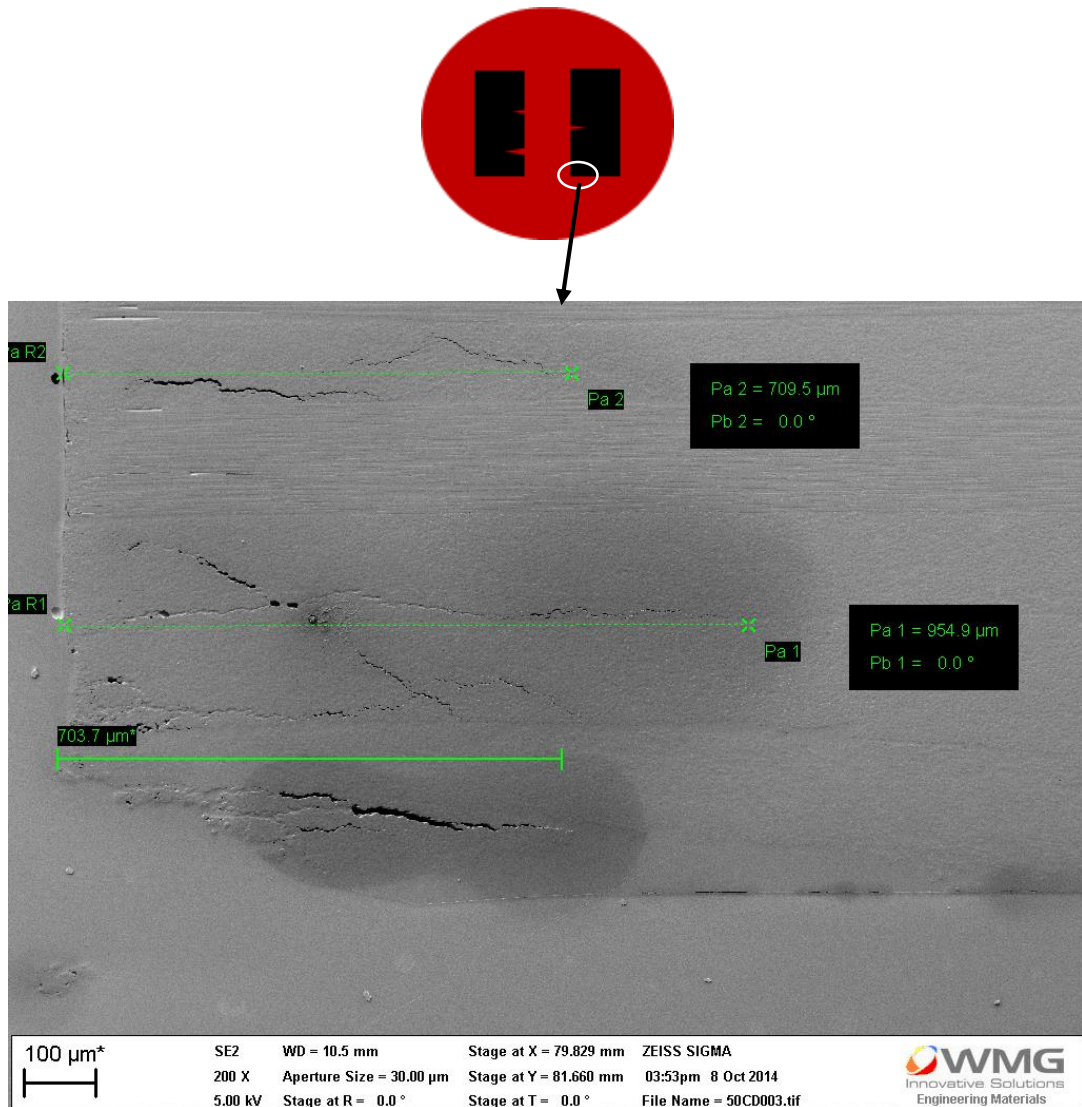


Figure 5-34: Exit delamination depth measurement on the second side of the hole (0.942 m/min, 0.05 mm/rev CD). The diagram in the inset shows the location of the specific damage in a mounted sample.

SEM measurement of sectioned samples was performed in only Phase-1 mentioned in Section 6.1. Subsequently, it was found that these measurements were also possible through optical microscopy and it was quicker as compared to the in SEM. Therefore, measurements of fibre pull disorientation, pull-out, maximum damage depth at entrance and exit were performed through optical microscopy in the subsequent studies explained in 6.2 and 6.3.

In addition, it can be observed from this methodology of sectioning, mounting and polishing that the data of damage depends on the plane of sectioning. As CFRP

is an anisotropic material, it is possible that the selection of the specific plane for sectioning could have an effect on damage depth measured. To examine the consistency of the damage around the hole, a hole was sectioned in two perpendicular planes of sectioning as shown in Figure 5-35 and the maximum damage depth at the entrance, exit and average fibre pull out and fibre disorientation were measured through optical microscopy. The damage data measured in the two respective planes is presented in Table 5-6. From Table 5-6 it can be seen that the variation in maximum damage depth at entrance data is only 9% and it is only 6% at exit. The variation in the internal damage (fibre pull out and disorientation) is only 7%. Therefore, it is inferred that the damage around the hole is consistent having a maximum variation of 9%.

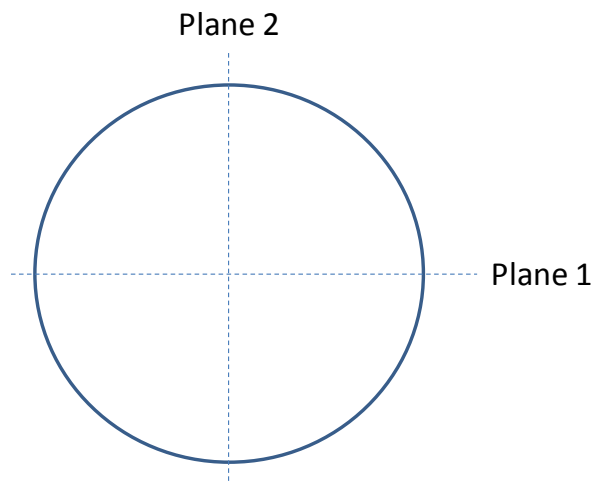


Figure 5-35: Schematic displaying two perpendicular planes of sectioning for assessment of damage variation in a hole in the two respective planes of sectioning

Table 5-6: Data table for maximum damage depth at entrance/exit and internal damage at two perpendicular planes in a hole

Damage location	Plane 1	Plane 2	Percentage difference
Maximum damage depth at entrance (μm)	1095.5	1202.096	9%
Maximum damage depth at exit (μm)	2958.2	3129.93	6%
Average internal damage (μm)	150.22	140.24	7%

5.6 Tool wear measurement

Tool wear is a parameter for identifying the condition of the tool to determine when it is not useful for further machining and hence, to estimate its overall life. The setup used for measuring tool wear in the present research is mentioned in Section 5.6.1.

5.6.1 Setup for tool wear measurement

The setup used for tool wear measurement is shown in Figure 5-36. The microscope used for tool wear measurement was '*Nikon SMZ 74 ST*'. In order to measure the tool wear, the flank surface of the tool was required to be horizontal with respect to the microscope. For this, a 3D rotating base was used to hold the tool holder. This rotating base could be fixed in any desired orientation in 3D. Thus, once it was made sure that the tool flank surface was horizontal with respect to the microscope, the rotating base was fixed in that orientation. The base of the tool holder was fixed on a micrometer cross-table for precise movements in X and Y directions of the tool during wear measurement in order to adjust the full cutting edge in a frame of ZEISS camera. '*ZEISS AxioCam ERc 5s*' microscope camera was used to record tool wear images. To record the pictures with the microscope, ZEISS camera was attached to the microscope, having a resolution of 5 megapixels which was further connected to a laptop. To control the recording from the laptop, ZEN software provided by ZEISS was used. The measurements from the microscope were calibrated using a graticule provided by Buehler. Further, the alignment of the flank surface was made horizontal with respect to the computer screen with the help of cross wires provided in Zen software. After making sure the flank surface being horizontal with respect to the microscope and with respect to the computer screen,

the frame containing flank surface was captured. The measurement error in this setup was found to be $0.5\ \mu\text{m}$.



Figure 5-36: Setup for recording tool flank wear. ZEISS camera was attached to the microscope in connection with a laptop for imaging.

5.6.2 Tool wear quantification

In Phase-1 (Section 6.1) and Phase-3 (Section 6.3) the wear on flank surfaces of tungsten carbide (WC) drills was found to be a regular uniform wear band on cutting edge due to an abrasive wear mechanism similar to that reported by other authors during conventional drilling of CFRP [3, 137, 138]. The width of flank wear was measured by determining the difference between the width of unworn and worn flank surfaces of the same tool. The width of the flank surface was measured at three locations in the flank surface as shown in Figure 5-37 and Figure 5-38 in a new and a worn tool respectively. The tool shown in Figure 5-37 and Figure 5-38 is a 3-flute twist drill (details of this particular tool is provided in Section 5.7.1.1). The measured lengths were deducted from those obtained with a new tool. Average of the worn lengths at three locations was considered as the average tool wear for that particular tool condition e.g. the average tool wear for the tool shown in Figure 5-38

is = $[(0.33-0.287) + (0.390 -0.317) + (0.465-0.371)] / 3 = (0.043+0.073+0.094)/3 = 0.07 \text{ mm (70 } \mu\text{m)}$.

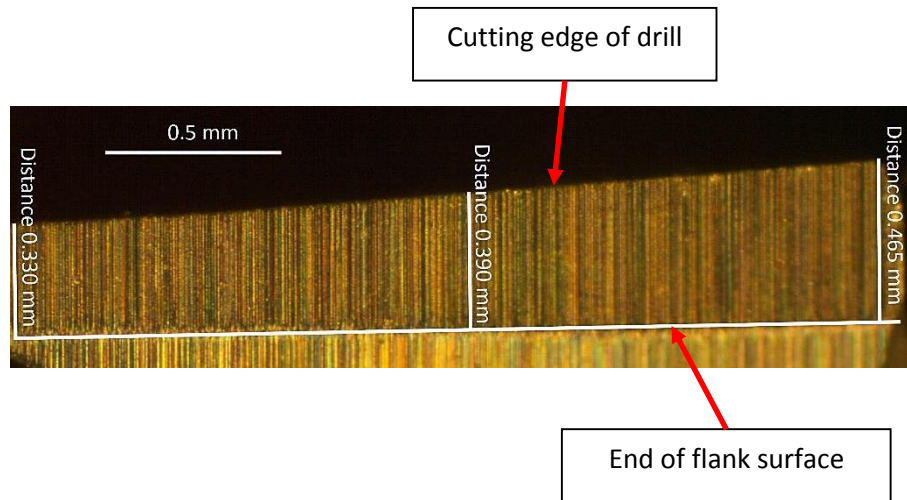


Figure 5-37: Flank surface width measurement at three locations in a new tool

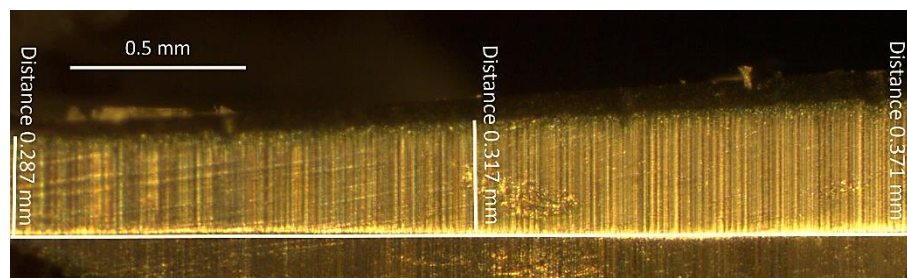


Figure 5-38: Flank surface width measurement at three locations in a worn tool

Unlike Phase-1 (Section 6.1) and Phase-3 (Section 6.3), the wear on high speed steel (HSS) drills in Phase-2 (Section 6.2) was excessive and irregular in shape. Selecting the worn width of the flank surface as tool wear criteria would not do justice for tool wear in this case as the entire width of the flank surface was already worn after drilling of the second hole. Upon continuing the drilling with the same tool after the second hole, the area of the unworn flank surface reduced having the maximum width of flank surface already worn. In this case, measurement of width of worn flank surface would not indicate the actual variation of tool wear with respect to number of drilled holes. Therefore, variation in tool flank surface wear area was considered as a tool wear criteria for this phase (Phase-2) [191]. In Phase-2, wear

area in the flank surface of cutting edges was recorded after drilling of every hole in each drilling set using the setup mentioned in Section 5.6.1. In order to quantify the worn area, the area of the flank surface in a new tool and the area of a unworn flank surface in a worn tool was measured and the difference of the two was considered as tool wear as shown in Figure 5-39 and Figure 5-40. The tool shown in Figure 5-39 and Figure 5-40 is a two flue twist drill (details are provided in Section 5.7.2.1). From Figure 5-39 and Figure 5-40, the worn area in flank surface = $1.183 - 1.005 = 0.178 \text{ mm}^2$.

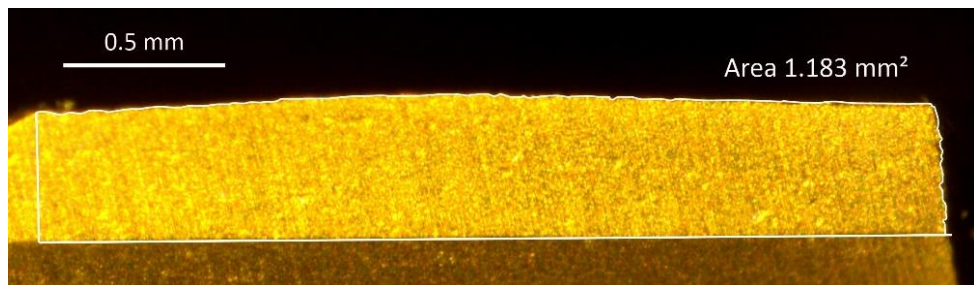


Figure 5-39: Flank area measurement in a new tool

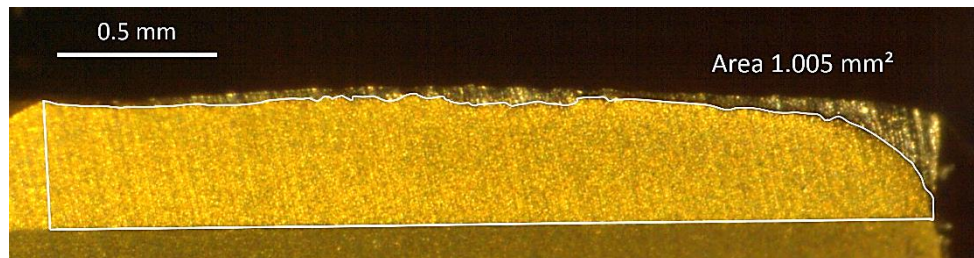


Figure 5-40: Unworn flank area measurement in a worn tool

5.7 Experimental Tooling and procedure

This section details the procedure followed in the experimental studies in order to achieve the objectives of the present research. The workpiece used in all the experiments was CFRP having bismaleimide matrix (HTM 552) as described in Section 5.2. The workpiece was kept consistent throughout the research so that the

results would not be affected due to variation in the workpiece in the subsequent experimental studies.

5.7.1 Phase 1: Preliminary experiment to investigate theoretical effective normal rake angles in CD and UAD and its effect on damage

5.7.1.1 Drills

The drill for this preliminary trial experiment was a flat rake and flat clearance angle, 6 mm diameter, tungsten carbide, uncoated, three-flute twist drill provided by SGS Tools Limited. The specifications of the drill provided by the tool manufacturer are presented in Table 5-7. The side and front views of drill used in the current experiment are shown in Figure 5-41.

Table 5-7: Data table for three-flute twist drill used in the current experimental study

Drill supplier	SGS Tools Ltd.
Model number	63010
Drill material	Tungsten carbide
Coating	Uncoated
Diameter (mm)	6
Point angle	150°
Helix angle	30°
Axial rake angle	4°
Axial relief (clearance) angle	11°

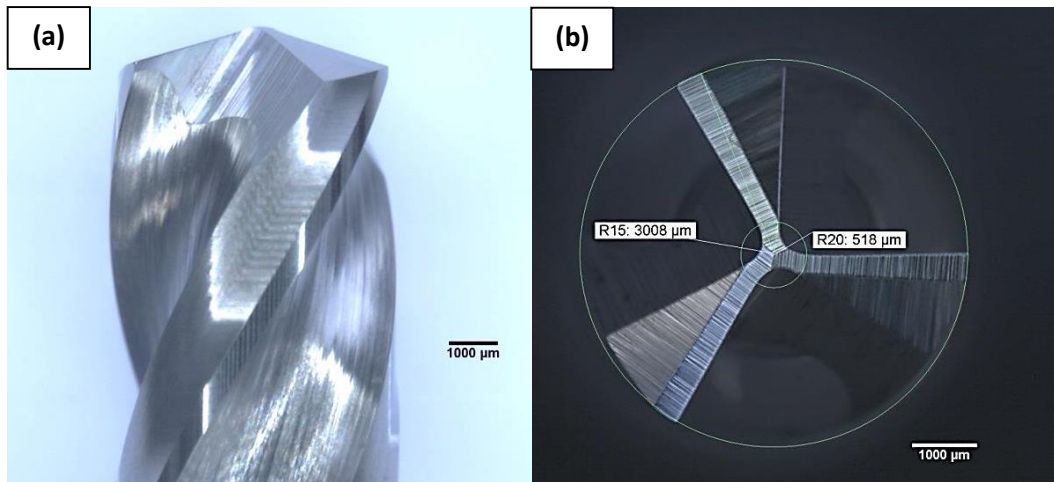


Figure 5-41: (a) Side and (b) front view of 3 flute twist drill used in current experimental study

5.7.1.2 Experimental setup and procedure

As explained in Section 5.1.1, the ultrasonic oscillation parameters depend on the tool and tool holder combination in Ultrasonic 65 machine. In this study, the frequency of the oscillation of the selected drilling tool was 37,220 Hz and the maximum peak-to-peak oscillation amplitude was 2.9 μm . Once the amplitude was measured on the particular tool and tool holder combination, the tool could not be detached from tool holder otherwise, the ultrasonic frequency and amplitude would not be the same even if the tool is reattached with the same length inside tool holder. In addition, the Keyence system was not available at the time of this study. Therefore, the *entire experimental study was performed with just one drill in this phase*. The drilling experiment was performed on 300 mm long, 25 mm wide and 7.4 mm thick CFRP strips attached to a Kistler dynamometer of ‘type 9257 B’ as shown in Figure 5-42. The centre-to-centre distance between two consecutive holes was kept as 25 mm. The image of overall experimental setup is shown in Figure 5-42.

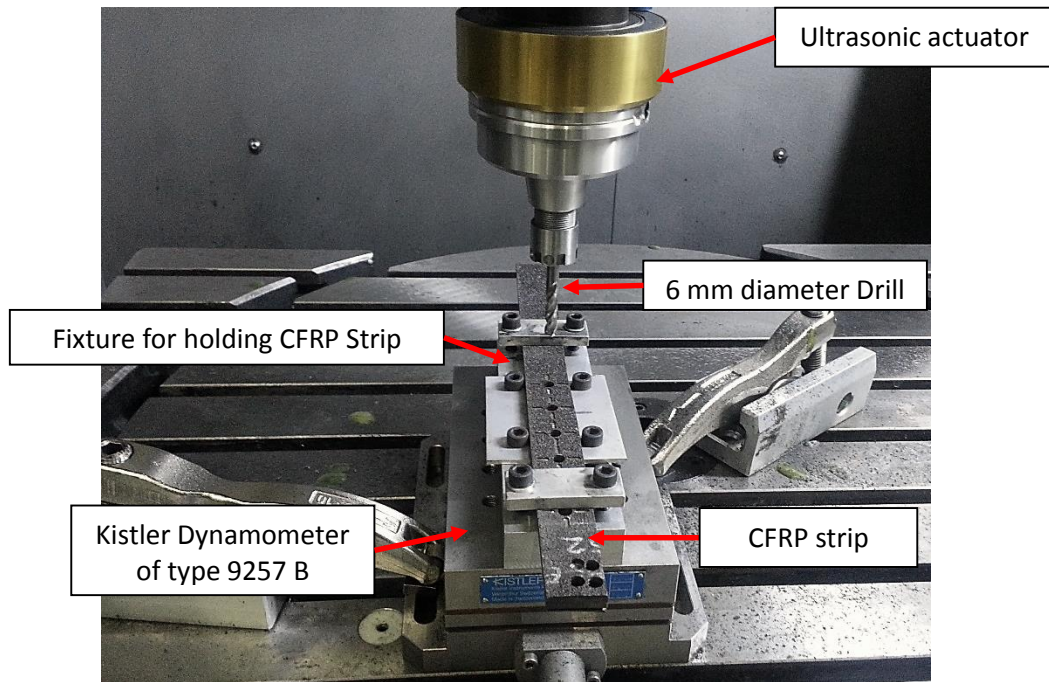


Figure 5-42: Experimental set-up having dynamometer, fixture holding carbon fibre strip, ultrasonic tool holder and the 6 mm diameter drilling tool

As per the effective rake calculation and discussion in Section 4.6, the effect on thrust force, torque, and damage in CFRP was to be examined with respect to variation in cutting speed in CD and UAD. Since cutting speed was the only factor for study in the present research, the approach of design of experiments was not followed. The approach of design of experiments is more helpful when there are multiple factors involved in a study. In addition, the approach of design of experiments would only be able to identify the variation of output (machining forces and damage) and it would not be helpful for identifying the mechanism at the cutting edge in UAD. Therefore, the approach of effective rake angles with respect to cutting speed was followed in the present research instead of design of experiments. Since the value of effective rake angles in UAD was found to be increasing with a reduction in the cutting speeds in Section 4.6, therefore, a set of cutting speeds would be required in order to examine the concept of effective rake angles in UAD. In Phase-1, four levels of cutting speeds of 0.942, 9.42, 94.2 and 282.6 m/min (50,

5: Experimental Methodology

500, 5000 and 15000 rpm respectively) were chosen for the experimentation. Feed rate was (recommended by the tool manufacturer) 0.05 mm/rev and was kept constant throughout the test. The feed rate was kept constant as 0.05 mm/rev so that the depth of cut (and hence, uncut chip thickness in drilling) across the various cutting speeds could be kept constant. The constant depth of cut would make sure that only effective normal rake angle would vary when varying the cutting speeds from 0.942 to 282.6 m/min when comparing CD and UAD. The machining parameters for the current experiment are summarised in Table 5-8.

Table 5-8: Machining parameters used in current experimental study

Cutting speeds (m/min)	0.942, 9.42, 94.2, 282.6
Feed rate (mm/rev)	0.05
Ultrasonic frequency (Hz)	37720
Ultrasonic peak-to-peak amplitude (μm)	2.9
Coolant	No coolant (dry machining)

Due to only one drill being used in this experiment, a specific order of drilling was followed in the drilling test. The holes were drilled in the order of 282.6, 94.2, 9.42 and 0.942 m/min cutting speeds. In addition, for each cutting speed, first CD and then UAD was performed and thus, first eight holes were drilled. Since, first eight holes were to be examined by X-ray CT scanning for damage assessment, therefore, four marks were machined around each hole for first eight holes as per the methodology explained in Section 5.4.

Since, the drill could not be detached from tool holder in this experiment, therefore, drilling experiment was continued further with the same worn drill three

times consecutively to see if there was a change in the results. The damage around these holes was to be examined by the methodology of sectioning, mounting and polishing explained in Section 5.5, so no machining of marks was required around a hole when drilling with a worn drill. Drilling order was kept as three holes with CD at 282.6 m/min cutting speed first, then three holes with 282.6 m/min UAD, then three holes with 94.2 m/min with CD and then three holes at 94.2 m/min cutting speed with UAD. The same order was continued further for cutting speeds 9.42 and 0.942 m/min. Thus, 24 holes were drilled. The results of this phase are summarised and discussed in detail in Section 6.1.

5.7.1.3 Cutting temperature measurement

The cutting temperature in CFRP machining is still a point of discussion amongst researchers. Some researchers have claimed the cutting temperature to be higher in UAD compared to that in CD [28]. In order to find out whether the matrix softening happened during the drilling with a new tool in UAD, the temperature during drilling was measured in the same experimental setup with a new tool and drilling was performed in the similar order as explained in Section 5.7.1.2 for a new tool so that similar experimental drilling conditions could be achieved. In the present study, cutting temperature was measured using a K-type “surface mount” thermocouple by sticking it between two CFRP plates as shown in a schematic in Figure 5-43. It was a CHROMEL-ALUMEL combination having 30 gage (0.25 mm) wire thickness supplied by Omega engineering limited company. It also means that while sandwiching the thermocouple in-between CFRP plates, there was a gap of 0.25 mm between the CFRP plates during the experiment for temperature measurement. The thermocouple was connected to a data logger which was in turn connected to a computer. The data logger used in the experiment was an 8-channel TC-08

thermocouple data logger having 0.025 °C temperature resolution over a –250 to +1370 °C range and 1000 Hz of data recording frequency. Therefore, sufficient temperature dataset could be recorded even in the case of fastest feed rate (750 mm/min in the case of 282.6 m/min cutting speed, i.e. 1.184 seconds for drilling of $7.4 \times 2 = 14.8$ mm thick CFRP material). PicoLog software was used for data acquisition and storage. To avoid damaging the welded joint of the thermocouple, drilling was performed within a distance of 0.1 mm from the welded joint of the thermocouple. The dimensions of the CFRP plates for temperature measurement were 70 mm x 25 mm x 7.4 mm. In addition, by the time of cutting temperature measurement, the Keyence device was obtained for amplitude measurement. This made sure the peak-to-peak amplitude to be 2.9 μm in order to recreate the similar experimental conditions as explained in Section 5.7.1.2 for a new tool for cutting temperature measurement.

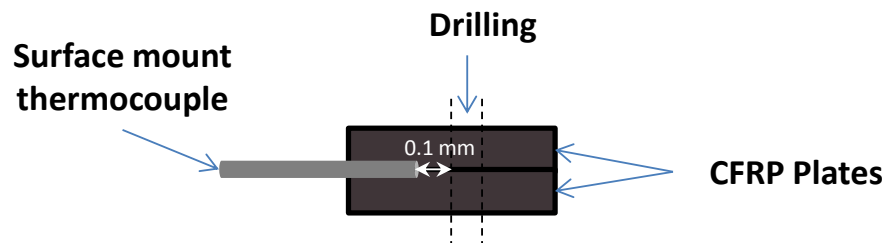


Figure 5-43: A schematic representation of thermocouple setup for cutting temperature measurement

5.7.2 Phase 2: Effect of cutting edge using pilot holes

5.7.2.1 Drills

The drills used in this work were two types of drills – Pilot-hole drill and main drill. The details of both types of drills are given in Table 5-9 and Table 5-10 respectively.

5: Experimental Methodology

Table 5-9: Details of pilot-hole drill used in the present experiment [192]

Drill supplier	Web Shop for Associated Production Tools Ltd
Model number	2MDD-030150-38-550
Drill material	Tungsten carbide
Coating	TiAlN
Diameter (mm)	1.5

Table 5-10: Details of the main drill used in the present experiment [193]

Drill supplier	Cutwel Limited
Model number	DJ544060
Drill material	High speed steel (HSS)
Coating	Titanium nitride (TiN)
Diameter (mm)	6
Point angle	120°
Helix angle	38°
Clearance angle	5°

The side and front views of and pilot-hole and main-hole drills are shown in Figure 5-44 and Figure 5-45 (a) and (b) respectively.

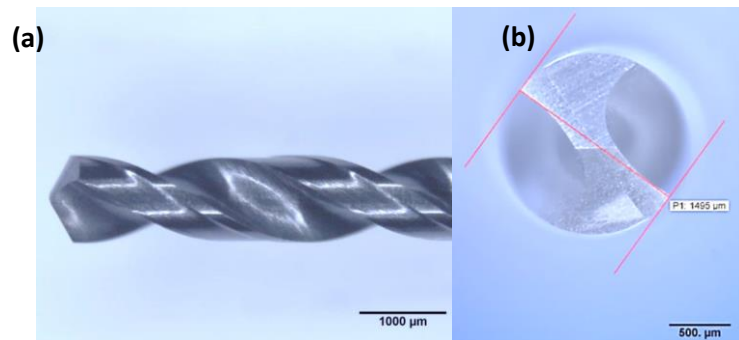


Figure 5-44: (a) Side and (b) front view of 1.5 mm diameter TiAlN coated Tungsten carbide 2-flute twist drill used in the current experiment for pilot-hole drilling

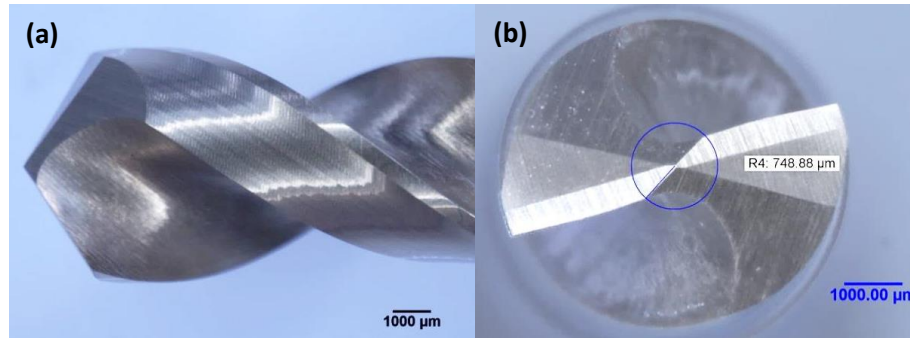


Figure 5-45: (a) Side and (b) front view of 6 mm diameter TiN coated HSS 2-flute twist drill used in the current experiment for drilling of main-hole and displaying chisel edge radius to be 748.88 μm

5.7.2.2 Experimental setup and procedure

The experimental setup for the study in Phase-2 is shown in Figure 5-46 displaying pilot hole drilling on a CFRP strip fixed with the Kistler dynamometer of ‘type 9271 A’. The holes were drilled at 100 m/min cutting speed and 0.05 mm/rev feed rate. The cutting speed was decided from the Phase-1 (Section 6.1) in which dynamic variation of effective normal rake angles was calculated theoretically. It was found that the effective rake angle in UAD at 94.2 m/min (Almost 100 m/min) cutting speed was still larger than those obtained in CD. Achievement of larger effective rake angle in UAD at 100 m/min cutting speed should result in a reduced machining forces. In order to examine this and its effect on damage in CFRP, the present experiment was performed in Phase-2. Every hole was drilled at the centre of Kistler dynamometer ‘Type 9271 A’ on a 150 mm long, 28 mm wide and 7.4 mm thick CFRP strip keeping 15 mm centre-to-centre distance between two consecutive holes. Similar to Phase-1, no cutting coolant was used in the experiment.

During drilling of every hole, the thrust force and torque were recorded on a dynamometer. Tool wear was recorded and measured by the setup shown in Section 5.6.1. With one HSS drill, maximum 10 holes could be drilled in each case of CD, UAD, with and without pilot-hole due to excessive tool wear and matrix burning in

the 10th hole. During drilling of the 10th hole, the smoke of matrix burning was visually observed and chip fragments, fibres along with burnt matrix were found to be attached to the tool. The experiment was repeated three times for reproducibility of results.

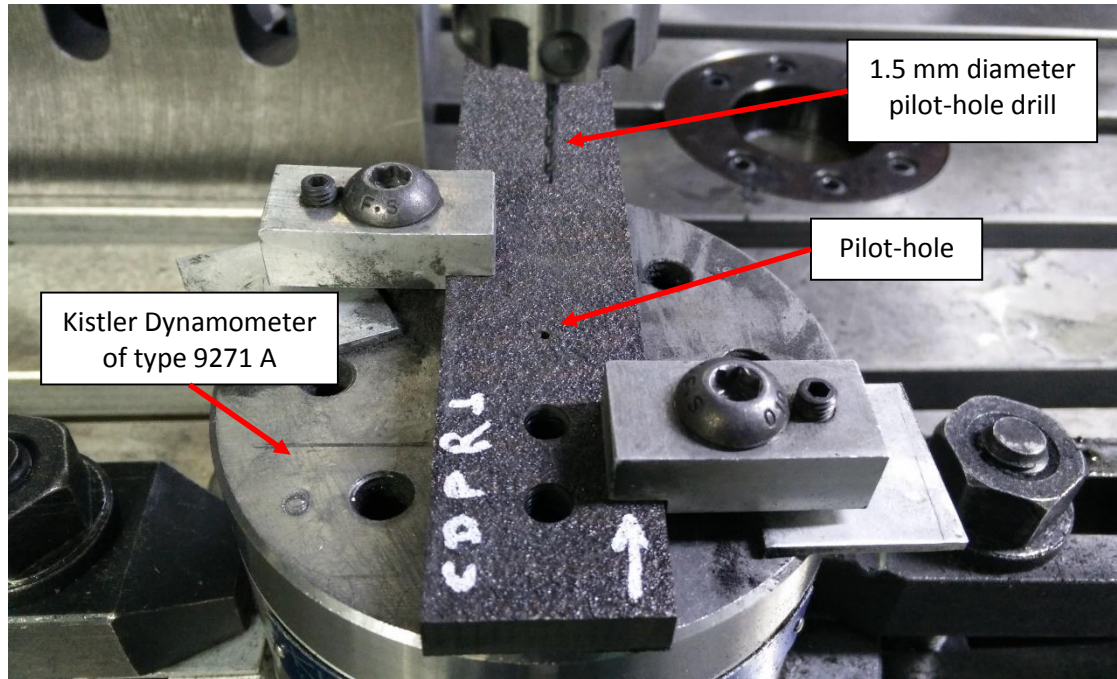


Figure 5-46: Drilling of a pilot hole with 1.5 mm diameter two-flute twist drill

Note - Although the experiment was repeated three times, there were two problems identified during the analysis of results of this study –

- It was found in a microhardness test later that the HSS drills used in the third repetition in each drilling case were harder than the drills used in the other two drilling sets.
- There was a localised disorientation of fibres found at drilling point in the case of the third repetition in Ultrasonic without pilot hole drilling, Figure 5-47. This localised disorientation was a defect in the CFRP plaque itself. Thus, the results were affected by the localised variation in CFRP material provided in this case.

Due to these reasons, the results obtained from the third repetition of each case had to be removed and the average of the two repetitions was considered for the analysis.

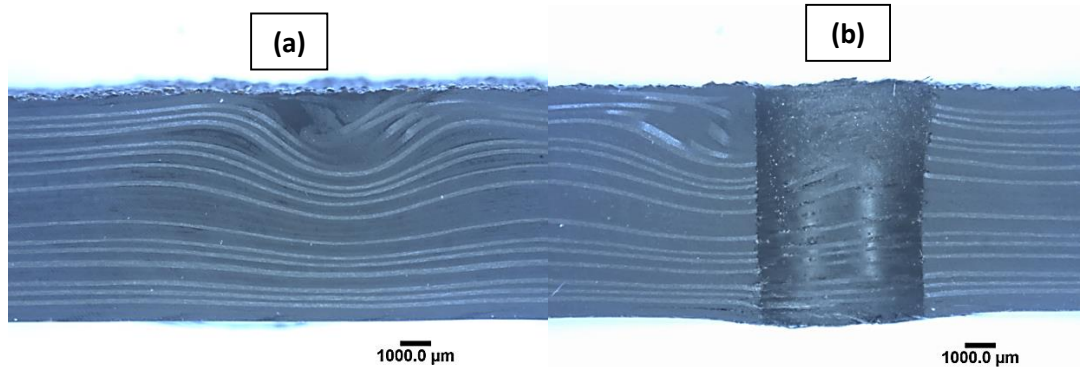


Figure 5-47: (a) Localised disorientation in carbon fibres (b) disorientation of carbon fibres at drilling site

The ultrasonic frequencies and amplitudes for the tool and tool holder combinations in the two repetitions of UAD with and without pilot hole cases are presented in Table 5-11. The results of this phase are summarised and discussed in Section 6.2. It is to be noted in Table 5-11 that although the repetitions were performed, the frequency and amplitude was not exactly the same in the repetition (different frequency and amplitude in 1 and 2 repetitions for both with and without pilot cases). The reason for this is that the amplitude and frequency were specific to a particular combination of a tool and tool holder in Ultrasonic 65 machine. As the tool was replaced with a new tool for a repetition, the frequency and amplitude varied. The tool was fixed with the tool holder in multiple attempts for repetitions in order to keep the amplitude and frequency “approximately” similar in the present research.

Table 5-11: Ultrasonic parameters used in the current experiment for UAD with and without pilot hole

Ultrasonic parameters	UAD 1	UAD 2	UAD with pilot 1	UAD with pilot 2
Frequency (Hz)	40350	40020	40120	39970
Peak-to-peak amplitude (μm)	5.3	4.7	5.2	4.3

5.7.3 Phase 3: Effect of cutting and chisel edges when drilling with Tungsten carbide drills

5.7.3.1 Drills

Two flute twist drills having diameter 6 mm and chisel edge diameter 2.5 mm respectively were used. The specification of twist drill for main-hole (actual test hole) drilling is presented in Table 5-12 and top and side views of twist drill for drilling main-holes are shown in Figure 5-48 (a) and (b) respectively. Figure 5-48 (a) also displays measurement of chisel edge radius of twist drill for main-hole drilling to be 1.249 mm (1249 μm). This is why the diameter of pilot-hole drills was chosen to be 2.5 mm so that the interaction between material and chisel edge could be avoided during main-hole drilling when drilling with a pilot-hole.

Table 5-12: Data of 2-flute twist drills used for main-hole drilling in the present study

Drill supplier	Cutwel Limited
Model number	D5432060
Drill material	Tungsten carbide
Coating	Uncoated
Diameter (mm)	6
Point angle	118°
Helix angle	30°

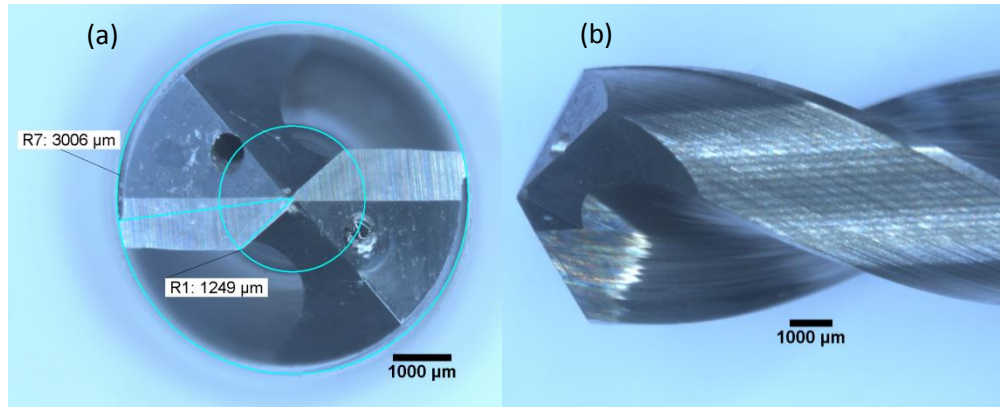


Figure 5-48: Top and side view of 2-flute twist drills used in the experiment

The clearance angle data of main-hole drill was not provided by the tool manufacturer. In order to calculate the clearance angle, margin angle of twist drill was measured in the lab through optical microscopy as shown in Figure 5-49. From Figure 5-49, the margin angle of the present twist drill is 49° .

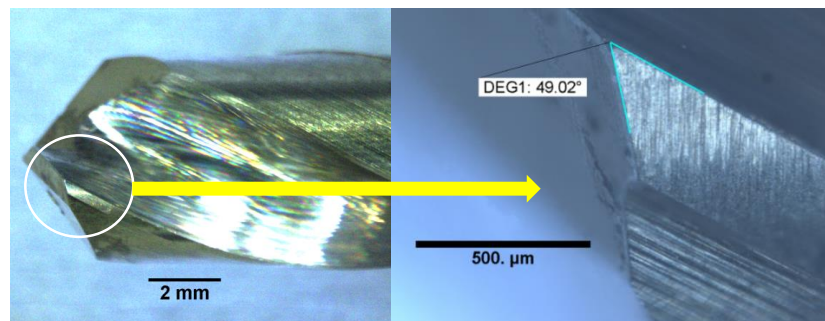


Figure 5-49: Margin angle measurement of twist drill through optical microscopy

The rake, margin and clearance angles of a twist drill are shown in a schematic in Figure 5-50 where it can be seen that –

$$\text{rake angle } (\gamma) + \text{margin angle} + \text{clearance angle } (\alpha) = 90^\circ$$

$$\text{Therefore, clearance angle} = 90 - (\text{margin angle} + \text{rake angle})$$

Since, the rake angle of twist drill at its edge is its helix angle which is 30° , provided by the tool manufacturer, therefore, the clearance angle at the edge = $90 - (49+30) = 11^\circ$.

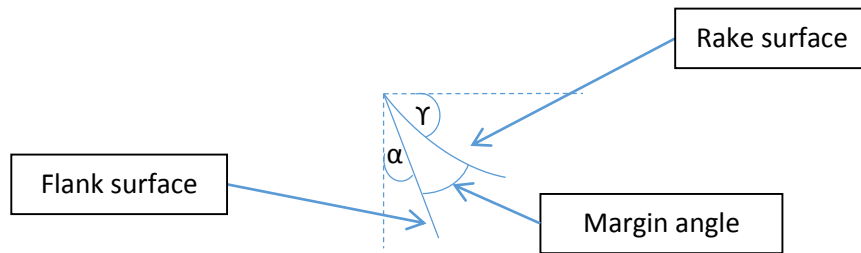


Figure 5-50: Schematic of rake, margin and clearance angles in side view of drill

Since the flank surface of the main-hole drill is a flat ground surface as shown in Figure 5-48 (a), therefore, the clearance angle for the entire cutting edge would be 11° for the current drill.

To drill the pilot holes, uncoated tungsten carbide two-flute twist drills having diameter 2.5 mm were used. The diameter of pilot hole drill was decided from the chisel edge diameter of the main-hole drill as shown in Figure 5-48 (1249 μm chisel edge radius i.e. 2498 μm diameter). The details of pilot-hole drills are presented in Table 5-13 and top and side views of pilot-hole drills are shown in Figure 5-51.

Table 5-13: Details of pilot-hole drills used in the current experimental study

Drill supplier	G T S S Engineers Supplies Ltd
Model number	SHR-158-5250K
Drill material	Tungsten carbide
Coating	Uncoated
Diameter	2.5 mm

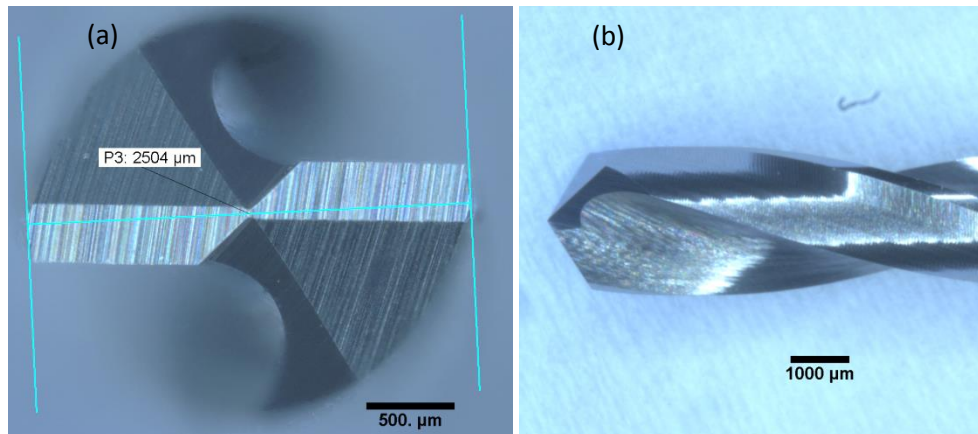


Figure 5-51: (a) top and (b) side views of two 2.5 mm diameter flute twist drills used for pilot holes

5.7.3.2 Experimental setup and procedure

The objective was to determine and compare the effect of cutting edges in CD and UAD at two cutting speeds in terms of thrust force, torque and damage in a drilled hole in CFRP. Therefore, the holes were drilled with and without pilot holes similar to those in Phase-2 (Section 5.7.2). Table 5-14 summarises the drilling tests performed in the present study. The ultrasonic frequencies and peak-to-peak amplitude (measured in air i.e. when the tool is not machining) utilised in the present study for all the cases are presented in Table 5-15.

Table 5-14: Summary of the drilling tests performed in Phase-3

Feed rate (mm/rev)	Cutting speed (m/min)	Drilling tests	Coolant
0.05	10	CD	No coolant (dry machining)
		UAD	
		CD with pilot	
		UAD with pilot	
	100	CD	
		UAD	
		CD with pilot	
		UAD with pilot	

Table 5-15: Ultrasonic experimental parameters (frequencies and peak-to-peak amplitude) for Phase-3

Ultrasonic parameters	Cutting speed			
	10 m/min		100 m/min	
	UAD	UAD with pilot	UAD	UAD with pilot
Frequency (Hz)	40160	39740	40220	40300
Peak-to-peak amplitude (μm)	7.3	7.6	7.4	6.8

During drilling tests, thrust force and torque were measured for the first five holes consecutively and after five holes, it was measured at every fifth hole till 60 holes. To achieve this, first five holes were drilled on a CFRP strip of dimensions 150 mm x 28 mm x 7.4 mm on a drilling dynamometer (type 9271 A) and tool condition was recorded using the setup shown in the section 5.6.1. Then, four holes were drilled consecutively on the A4 size CFRP plaque shown in Figure 5-52. The tenth hole was drilled on the CFRP strip on the dynamometer for thrust force and torque measurement and tool condition was recorded consequently. The same process was repeated at every fifth hole till 60 holes were drilled. The results of this phase are summarised and discussed in Section 6.3.

5: Experimental Methodology

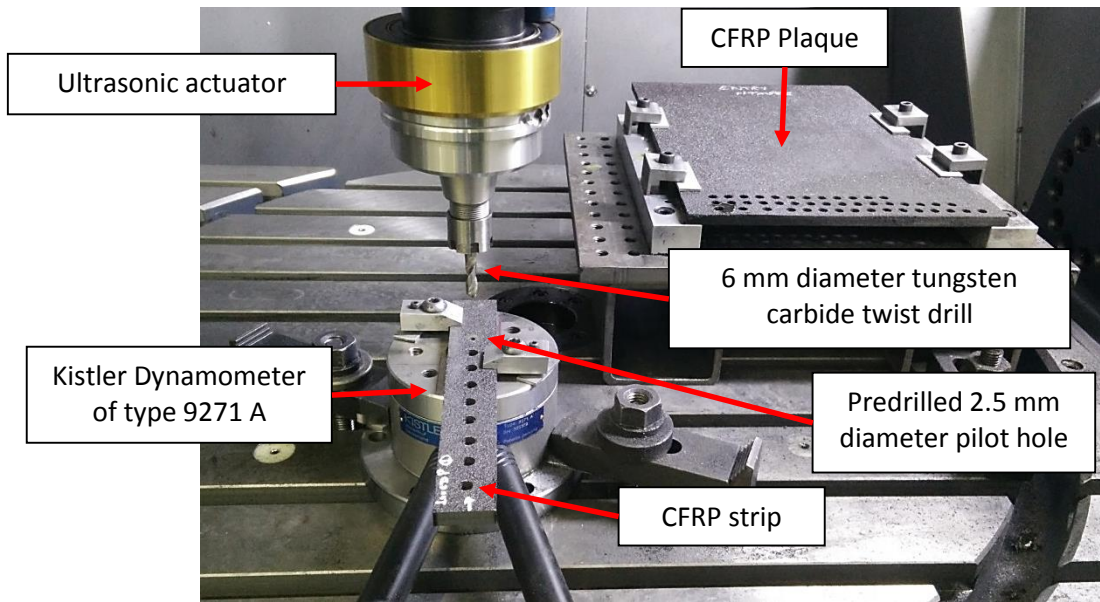


Figure 5-52: Experimental setup for pilot-hole drilling using tungsten carbide drill in Phase-3

6 Results and discussion

As explained in Section 4.6, larger effective rake angle is obtained in UAD as compared to that in CD. In order to examine the effect of higher and rapidly varying effective normal rake and axial clearance angles on thrust force, torque and damage during CD and UAD, the current research was performed. To do this, a preliminary experiment was performed in the first phase (Phase-1) of the present research in the preliminary experimental setup as explained in Section 5.7.1.

6.1 Phase 1: Preliminary experiment to investigate theoretical effective normal rake in CD and UAD and its effect on damage

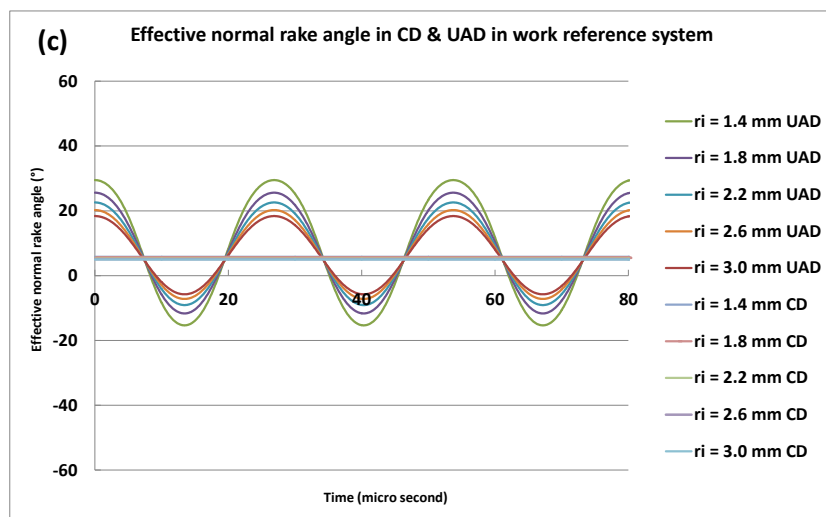
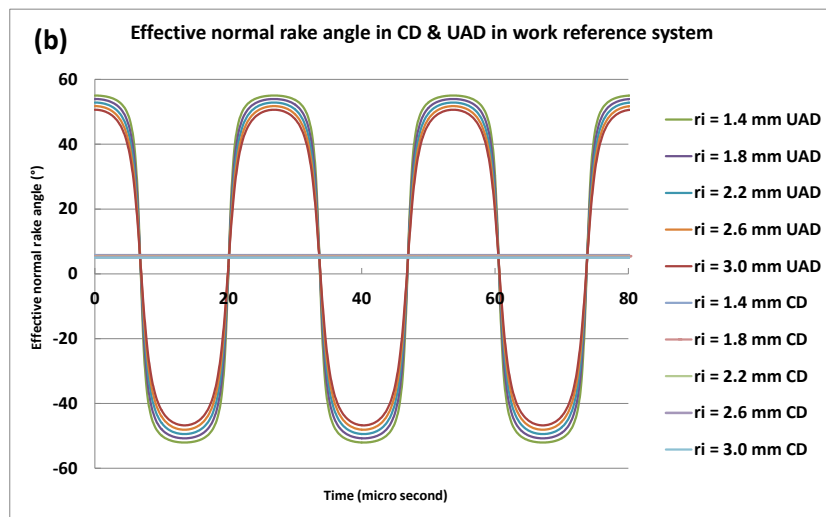
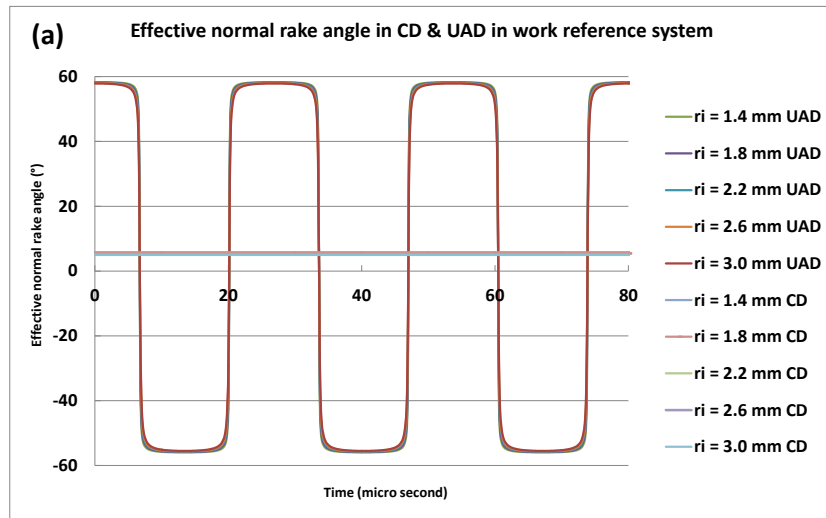
A single drill was used in this experiment due limitations in the experimental setup as explained in Section 5.7.1. This was a pilot experiment and the drills for this experiment were provided by SGS Tools Ltd. Company to examine. The effective rake angle was calculated for the experimental parameters (cutting speed, feed rates, ultrasonic frequency and ultrasonic oscillation amplitude) used in the present experiment for the tool geometry of the drills provided by SGS tool company presented in Section 5.7.1.1 so that the effects of theoretical effective normal rake angles could be correlated with the experimental observations.

6.1.1 Effective normal rake angle and clearance angle calculation for current drill geometry

Effective normal rake angles and axial clearance angles were calculated at each cutting speed from the method explained in Section 4.6 for drill geometry described in Section 5.7.1.1 during CD and UAD. The calculated effective normal rake and

6: Experimental studies, results and discussions

axial clearance angles for all the cutting speeds in CD and UAD are plotted in Figure 6-1 and Figure 6-2.



6: Experimental studies, results and discussions

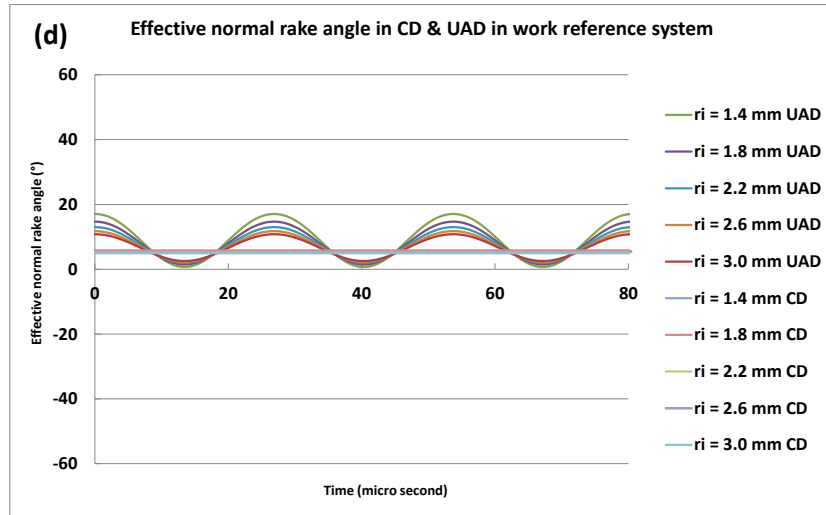
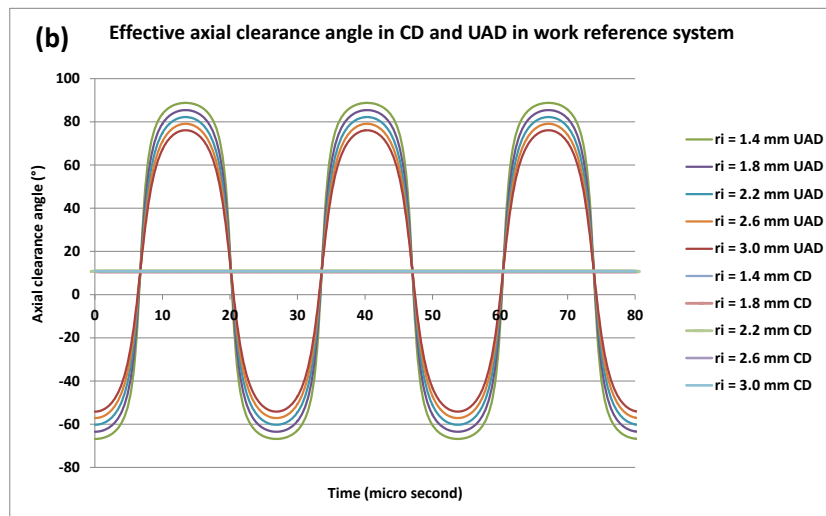
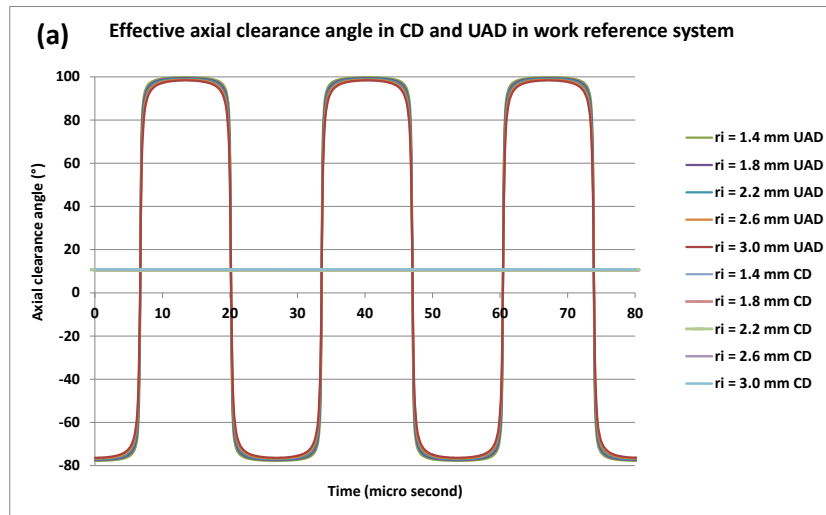


Figure 6-1: Plots of effective normal rake angles calculated at (a) 0.942, (b) 9.42 (c) 94.2 and (d) 282.6 m/min cutting speeds in CD and UAD



6: Experimental studies, results and discussions

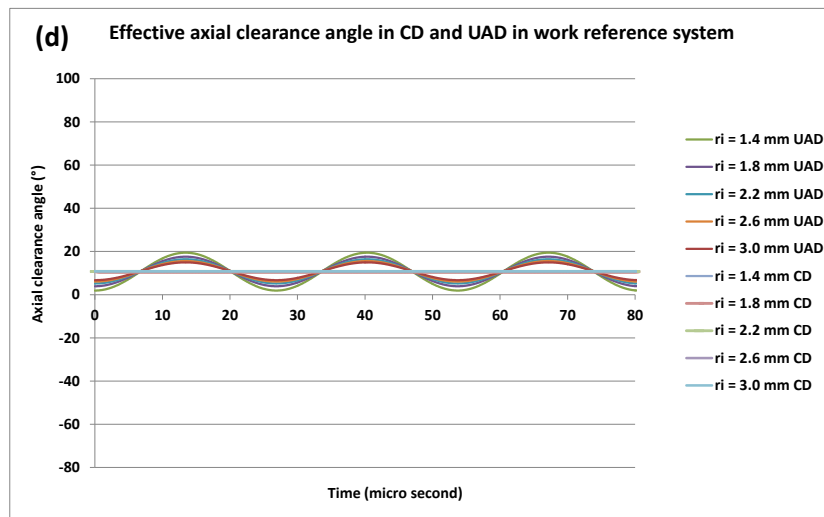
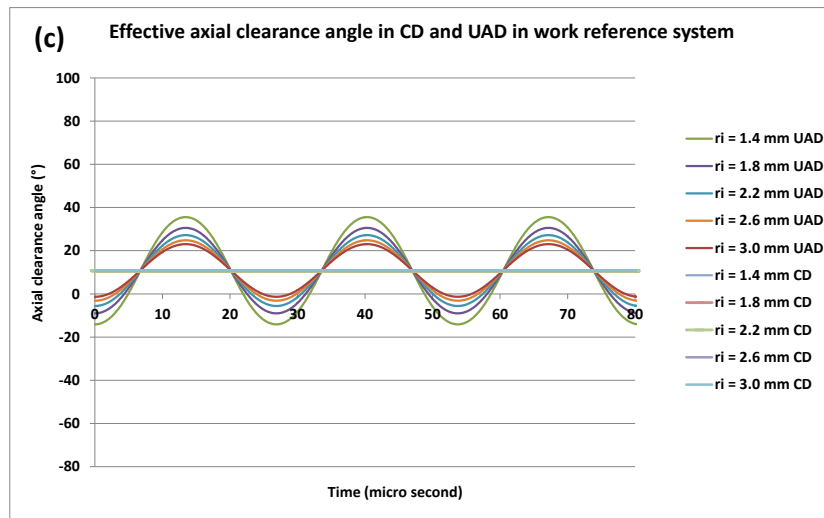


Figure 6-2: Plots of axial clearance angles calculated at (a) 0.942, (b) 9.42 (c) 94.2 and (d) 282.6 m/min cutting speeds in CD and UAD

It can be seen in Figure 6-1 that the effective normal rake angle attains the largest value at 0.942 m/min cutting speed (58°) in UAD as compared to 5° in CD. In addition, the maximum value of the effective normal rake angle reduces from 58° at 0.942 m/min to 17° at 282.6 m/min in UAD as compared to a constant effective rake angle (5°) at all the cutting speeds in CD. This indicates that larger effective rake angle is obtained in UAD at lowest cutting speed.

It is to be noted in Figure 6-2 that clearance angle achieves negative values alternatively at all the cutting speeds in UAD. Also, the most negative value of

clearance angle was found at lowest cutting speed of 0.942 m/min (-76.3°) and least negative clearance was found at 282.6 m/min cutting speed (-1.6°). In any machining process, negative clearance angles are not desirable because at negative clearance angles, the flank surface of tool rubs against machined surface resulting in deteriorated machined surface [168].

6.1.2 Results of thrust force and tool wear

Thrust force profiles at all the cutting speeds are shown in Figure 6-3 to Figure 6-10. In Figure 6-3, the thrust force profile during drilling at 280 m/min cutting speeds is shown which is annotated by four locations of (a), (b), (c) and (d). These locations are related to the thrust force drilling profiles mentioned in the literature [194]. The chisel edge of drill comes into contact with the material at location (a). The thrust force rapidly rises between the locations (a) and (b) due to drill being progressed inside the material and more area of cutting edges being involved in machining. At location (b) the entire cutting edge of twist drill comes into contact with the material and therefore, thrust force attains a nominally constant value between the locations (b) and (c). At location (c), the drill starts exiting the material and the chisel edge of twist drill is about to exit. Between locations (c) and (d) the value of thrust force falls rapidly because around 40 to 60% of thrust force comes from chisel edge. Therefore, as the chisel edge exits, the value of thrust force continues to fall because the drill continues towards the exit and the contact between cutting edges of drill and material continues to reduce [194].

When comparing the thrust force profiles across the cutting speeds, the thrust force profile between locations (b) and (c) was found to be constant at cutting speeds 282.6 and 94.2 m/min (Figure 6-3 to Figure 6-6) while it was found to be gradually reducing at cutting speeds 9.42 and 0.942 m/min (Figure 6-7 to Figure 6-10). It is

suggested that this happened because the time taken for drilling a hole at 282.6 m/min cutting speed (0.58 second) was relatively low compared to that at 9.42 and 0.942 m/min (17.76 seconds and 177.6 seconds respectively). Therefore, the heat accumulated during machining at cutting speeds of 9.42 and 0.942 m/min, made the material softer resulting in lower forces required for machining as compared to that at 282.6 m/min cutting speed. This is similar to the suggestion made by Wang et al. [38] who noted that the heat production associated with the chip formation causes concentrated heat build-up in the material adjacent to the tip of the drill due to the low conductivity of matrix. Therefore, the temperature increased due to concentrated heat build-up causes lowering of the mechanical strength of matrix and a consequent decrease of thrust force.

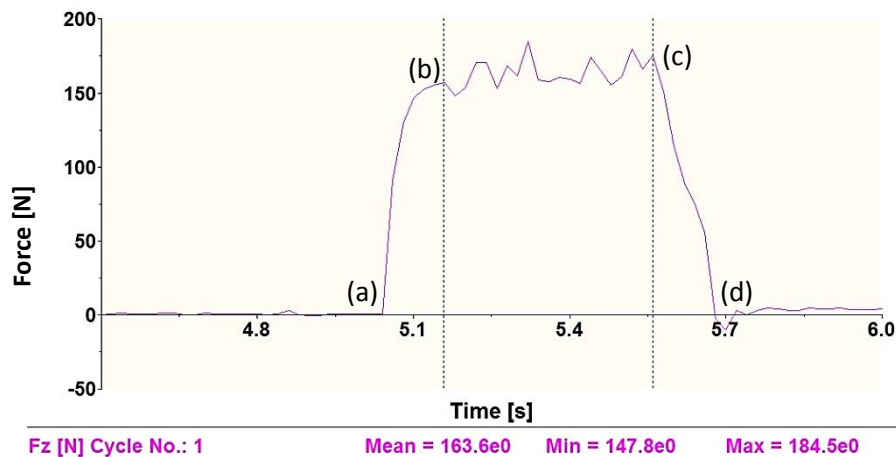


Figure 6-3: Thrust force profile at 282.6 m/min cutting speed in CD

6: Experimental studies, results and discussions

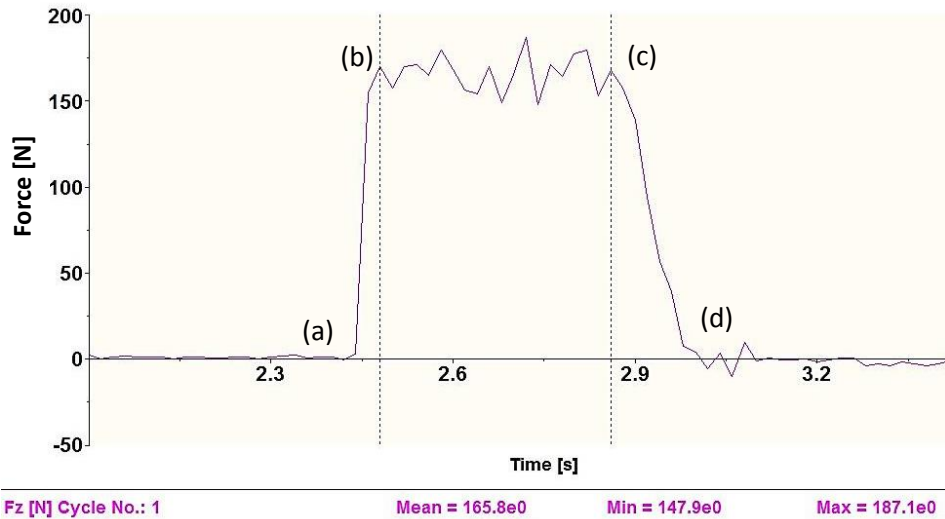


Figure 6-4: Thrust force profile at 282.6 m/min cutting speed in UAD

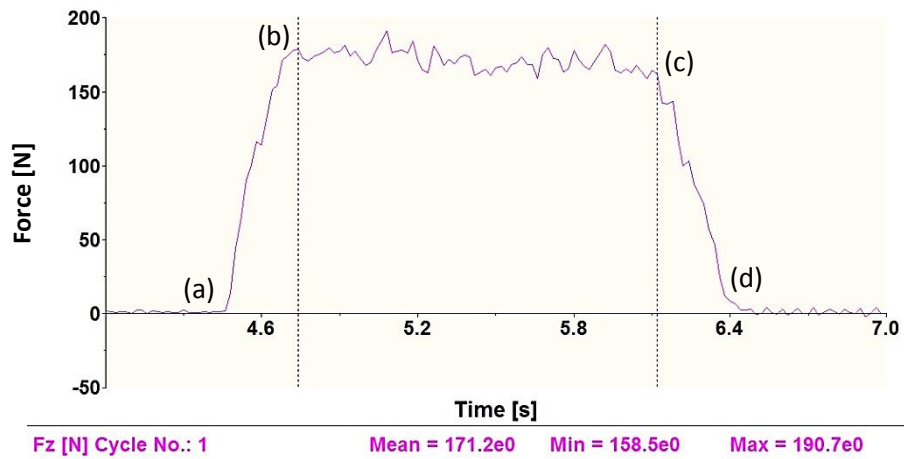


Figure 6-5: Thrust force profile at 94.2 m/min cutting speed in CD

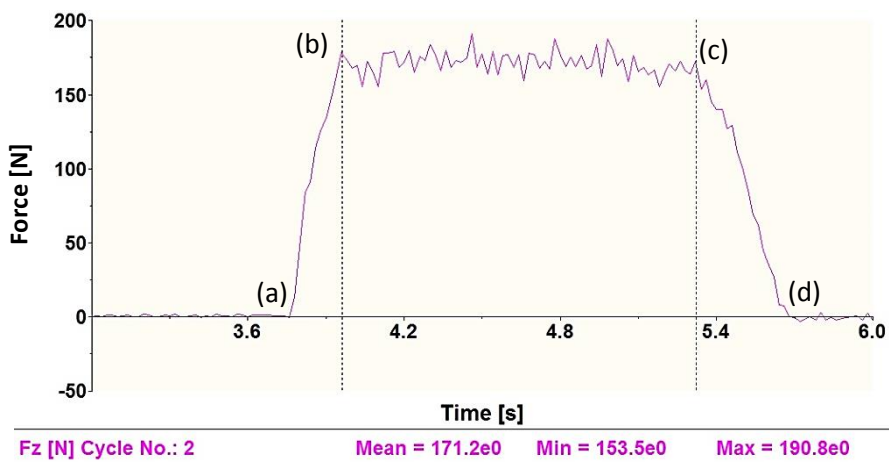


Figure 6-6: Thrust force profile at 94.2 m/min cutting speed in UAD

6: Experimental studies, results and discussions

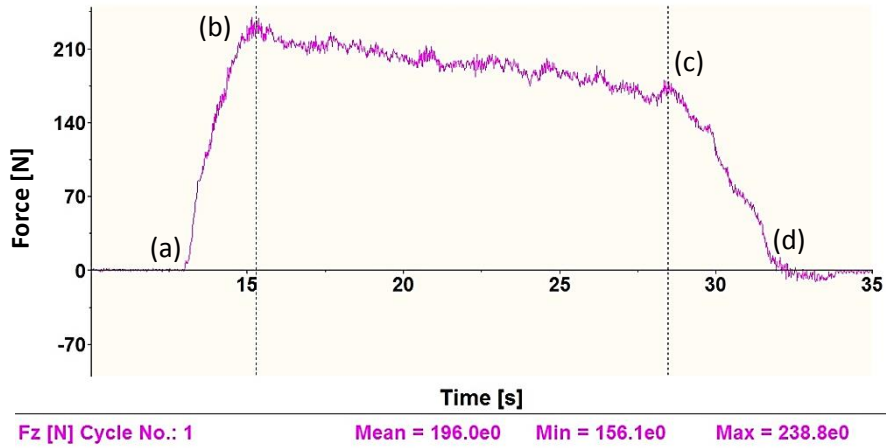


Figure 6-7: Thrust force profile at 9.42 m/min cutting speed in CD

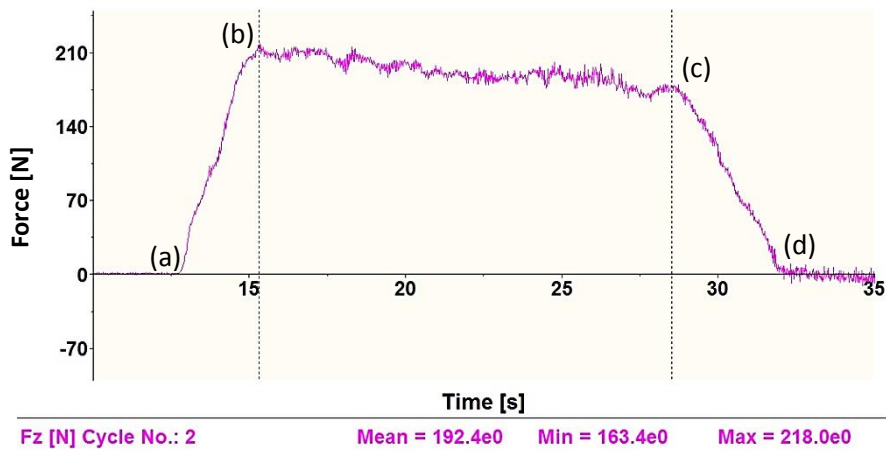


Figure 6-8: Thrust force profile at 9.42 m/min cutting speed in UAD

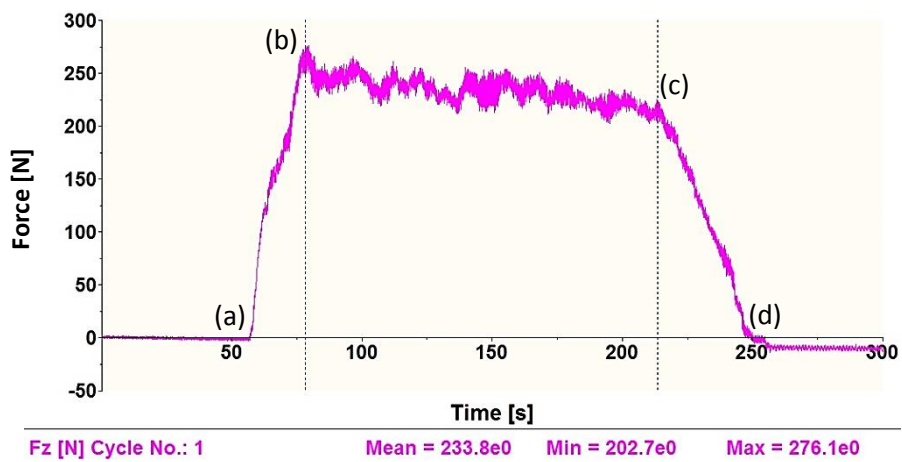


Figure 6-9: Thrust force profile at 0.942 m/min cutting speed in CD

6: Experimental studies, results and discussions

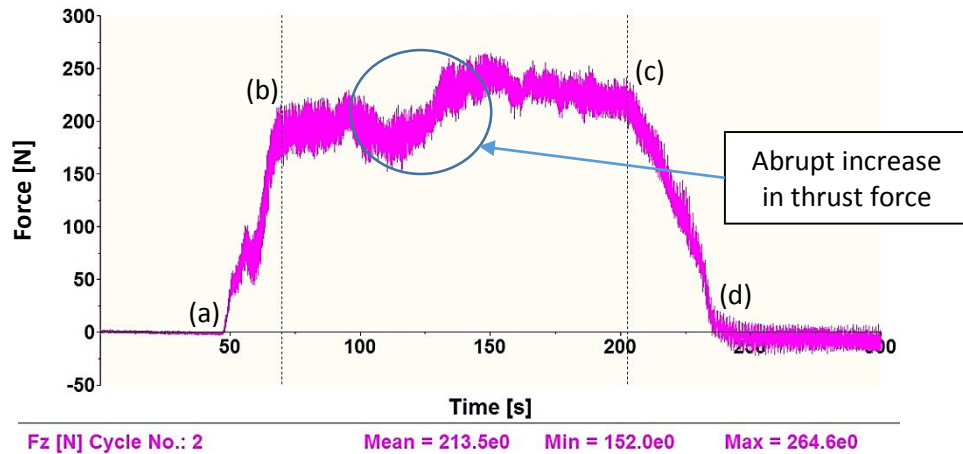


Figure 6-10: Thrust force profile at 0.942 m/min cutting speed in UAD

During ultrasonic assisted drilling at 0.942 m/min cutting speed, the thrust force profile was found to be abruptly increasing between drilling locations (b) and (c) as shown in Figure 6-10. Upon verification of tool conditions after this hole, it was found that during this particular drilling, there was a chip-out near chisel edge as shown in Figure 6-11. It was suspected that this broken chip in the tool near chisel edge affected thrust force variation displayed in Figure 6-10. The average tool wear after drilling of eight holes was 0.07 mm which was measured using the methodology explained in Section 5.6.2.

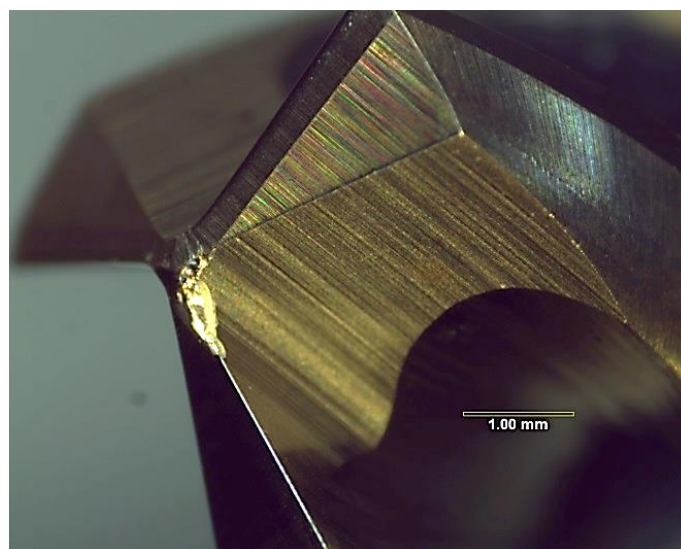


Figure 6-11: Image of tool displaying chip-out near chisel edge after drilling at 0.942 m/min cutting speed in UAD

The average thrust force data for obtained from the new tool is presented in Table 6-1 and plotted in Figure 6-12.

Table 6-1: Thrust force data for drilling with fresh tool

Cutting speed (m/min)	Average thrust force (N)		Thrust force reduction (N) (CD - UAD)
	CD	UAD	
0.942	234	214	20
9.42	196	192	4
94.2	171	171	0
282.6	164	166	-2

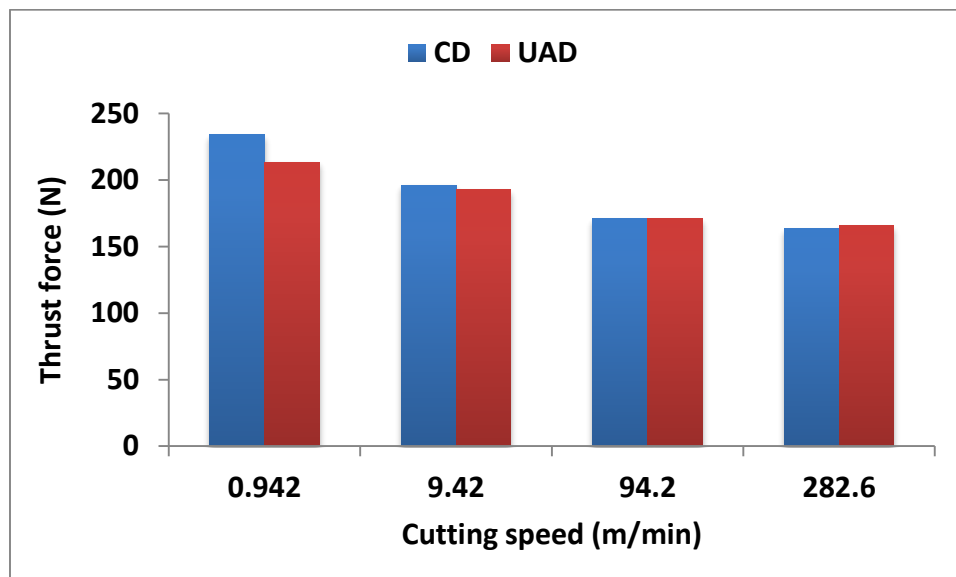


Figure 6-12: Average thrust force variation in CD and UAD at all the cutting speeds with new tool

Similar to as reported by other authors [14, 15], thrust force was found to reduce with respect to increasing cutting speed in CD. Also in UAD, thrust force was found to reduce with respect to increasing cutting speed. From thrust force data in Table 6-1 and Figure 6-12, it can be seen that thrust force continued to reduce from 234 N at 0.942 m/min to 164 N at 282.6 m/min cutting speed in CD. Similarly in UAD, it reduced from 214 N at 0.942 m/min to 166 N at 282.6 m/min cutting speed.

Further, when comparing CD and UAD, the maximum reduction in thrust force due to ultrasonic assistance was found to be 20.3 N at the lowest cutting speed of 0.942 m/min. This can be correlated with the largest effective normal rake angle being obtained at lowest cutting speed of 0.942 m/min as shown in Figure 6-1. However, rake angle calculation was performed for only the cutting edges and in this experiment, both chisel and cutting edges of twist drill were involved in machining. Therefore, more evidence was required in order to verify the rake angle concept. It is attempted in further experimental studies in Sections 6.2 and 6.3.

At the end of the 24th hole, average tool wear was 0.11 mm. Thrust force data for CD and UAD with the worn tool is presented in Table 6-2 and Table 6-3 respectively and are plotted in Figure 6-13. The reduction in average thrust force in UAD in comparison to that in CD at all the cutting speeds is presented in Table 6-4.

Table 6-2: Thrust force (N) data for CD with worn tool

<i>Cutting speed (m/min)</i>	<i>Thrust force in CD (N)</i>			
	<i>Thrust force 1</i>	<i>Thrust force 2</i>	<i>Thrust force 3</i>	<i>Average</i>
0.942	480	480	479	480
9.42	391	391	388	390
94.2	339	340	344	341
282.6	377	375	376	376

Table 6-3: Thrust force (N) data for UAD with worn tool

<i>Cutting speed (m/min)</i>	<i>Thrust force in UAD (N)</i>			
	<i>Thrust force 1</i>	<i>Thrust force 2</i>	<i>Thrust force 3</i>	<i>Average</i>
0.942	474	475	481	477
9.42	381	368	360	370
94.2	339	339	340	340
282.6	385	380	390	385

Table 6-4: Reduction in thrust force due to UAD in comparison to that in CD with worn tool

Cutting speed (m/min)	Average force in CD (N)	Average force in UAD (N)	Thrust force reduction (N) (CD - UAD)
0.942	480	477	3
9.42	390	370	20
94.2	341	340	2
282.6	376	385	-9

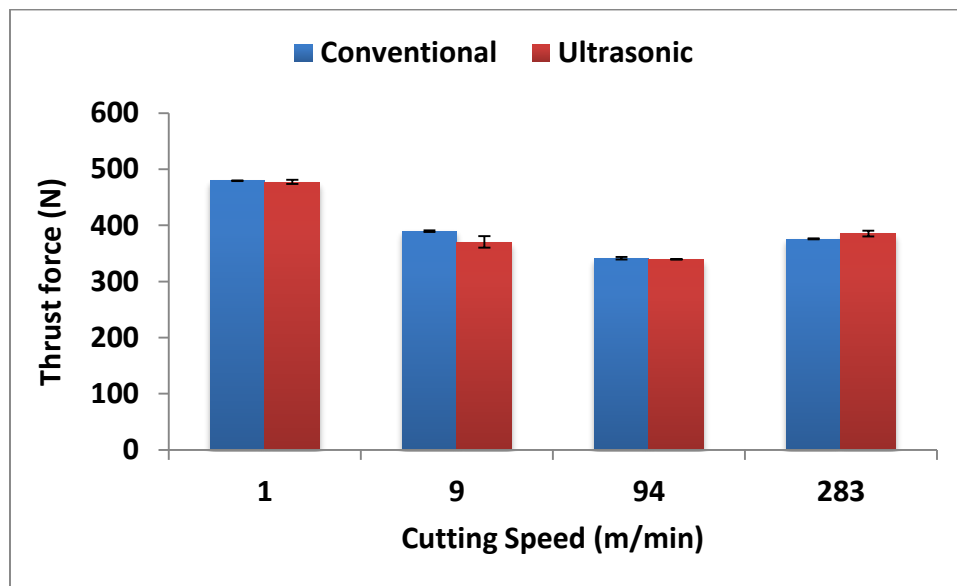


Figure 6-13: Thrust force plot for conventional drilling and UAD, obtained from worn tool (error bars indicate maximum and minimum values of forces during three times repetitions)

Similar to thrust force data from the new tool in Figure 6-12, average thrust force data obtained from the worn tool presented in Table 6-2, Table 6-3 and Figure 6-13 also indicates a reduction in thrust force with respect to cutting speed. Thrust force was found to be reduced from 480 N to 341 N in CD and from 477 N to 340 N in UAD as cutting speed increased from 0.942 to 94.2 m/min. Although, interestingly, upon further increasing cutting speed from 94.2 to 282.6 m/min, thrust force was found to increase from 341 N to 376 N in CD and from 340 N to 385 N in UAD. This particular observation of increasing thrust force with increasing cutting speed in CD has also been reported by other authors in the literature [96, 100, 128],

Section 3.5.1. However, no explanation was provided by the authors in support of an increase in the thrust force with increasing cutting speed. When comparing CD and UAD, maximum reduction due to ultrasonic assistance was found to be at 9.42 m/min cutting speed. Thrust forces at all other cutting speeds were found to be similar in CD and UAD.

6.1.3 Results of damage analysis

Damage in the holes was segmented into two major categories:

- Entrance and exit delamination
- Damage on the internal cylindrical machined surface termed as ‘Internal damage’ in the present research.

In the present work, two methodologies were adopted for analysing and quantifying the damage in a hole –

- X-ray computed tomography (CT)
- Sectioning, mounting and polishing

6.1.3.1 X-ray CT Scanning

X-ray CT scanning was used for analysing the holes drilled with a new tool (first eight holes). The damage in a hole was assessed through X-ray CT scanning data as per the methodology explained in Section 5.3. The damage was referred to as exit delamination and internal damage or fibre pull-out in a hole.

The exit delamination data was quantified with the method explained in Section 5.4.1. Maximum delamination area, delaminated area and delamination factor for each hole in CD and UAD are presented in Table 6-5 and delamination factors for CD and UAD at all the cutting speeds are plotted in Figure 6-14.

Table 6-5: Area delamination factor values obtained from CT scanning

Cutting speed (m/min)	Maximum exit delamination area A_{max} (mm ²)		Original area of the hole A_0 (mm ²)	Delaminated area in CD ($A_{max} - A_0$) (mm ²)	Delaminated area in UAD ($A_{max} - A_0$) (mm ²)	Delamination factor ($(A_{max} - A_0) \times 100 / A_0$)	
	CD	UAD				CD	UAD
0.942	32.24	34.65	28.26	3.98	6.39	14%	23%
9.42	37.67	33.43		9.41	5.17	33%	18%
94.2	31.99	29.91		3.73	1.65	13%	6%
282.6	29.92	31.2		1.66	2.94	6%	10%

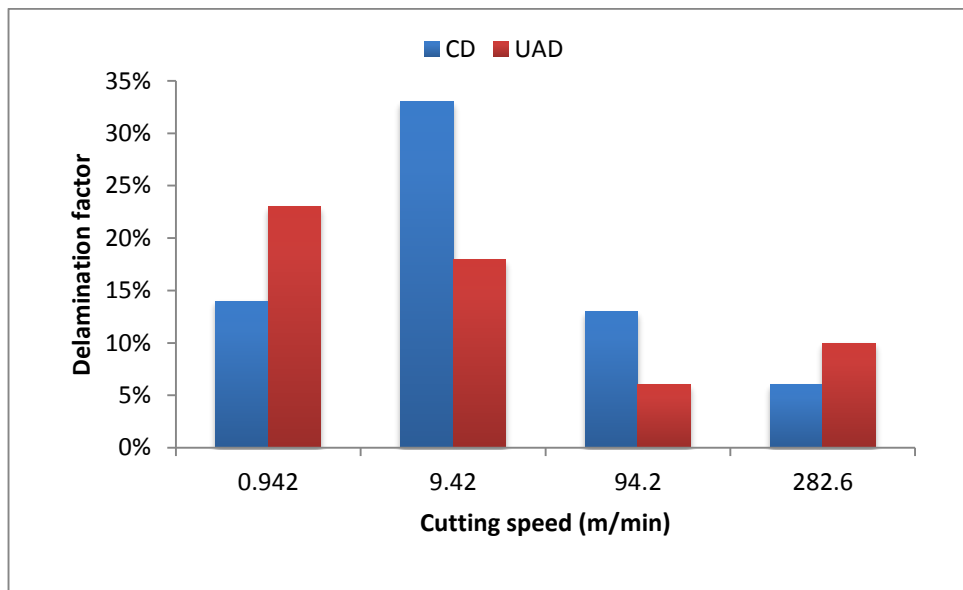


Figure 6-14: Area delamination factor for the CT scanning samples

The variation of exit delamination data in Table 6-5 and in Figure 6-14 with respect to cutting speed indicates that it increased in conventional drilling from 14% to 33% as the cutting speed was increased from 0.942 to 9.42 m/min. Exit delamination was found to decrease from 33% to 6% when increasing the cutting speed from 9.42 to 282.6 m/min. In UAD, exit delamination was found to decrease from 23% to 6% when cutting speed was increased from 0.942 m/min to 94.2 m/min. Exit delamination in UAD was found to increase from 6% to 10% when cutting speed was increased from 94.2 to 282.6 m/min.

When comparing conventional and ultrasonic assisted drilling, the maximum reduction due to ultrasonic assistance was found at 9.42 m/min cutting speed. It is discussed further in ‘exit delamination’ subsection of Section 6.1.7.2.

The internal damage from CT scanning data was quantified with the method explained in 5.4.2. Average fibre pull-out depth values for each hole for all the cutting speeds CD and UAD and percentage of fibre pull out reduced due to ultrasonic assistance as compared to that in CD is presented in Table 6-6 and is plotted in Figure 6-15.

Table 6-6: Average maximum radius values obtained from CT scanning

Cutting speed (m/min)	CD (μm)	UAD (μm)	% reduction in UAD
0.942	62	56	9.7%
9.42	72	71	1.3%
94.2	108	88	18.5%
282.6	108	101	6.4%

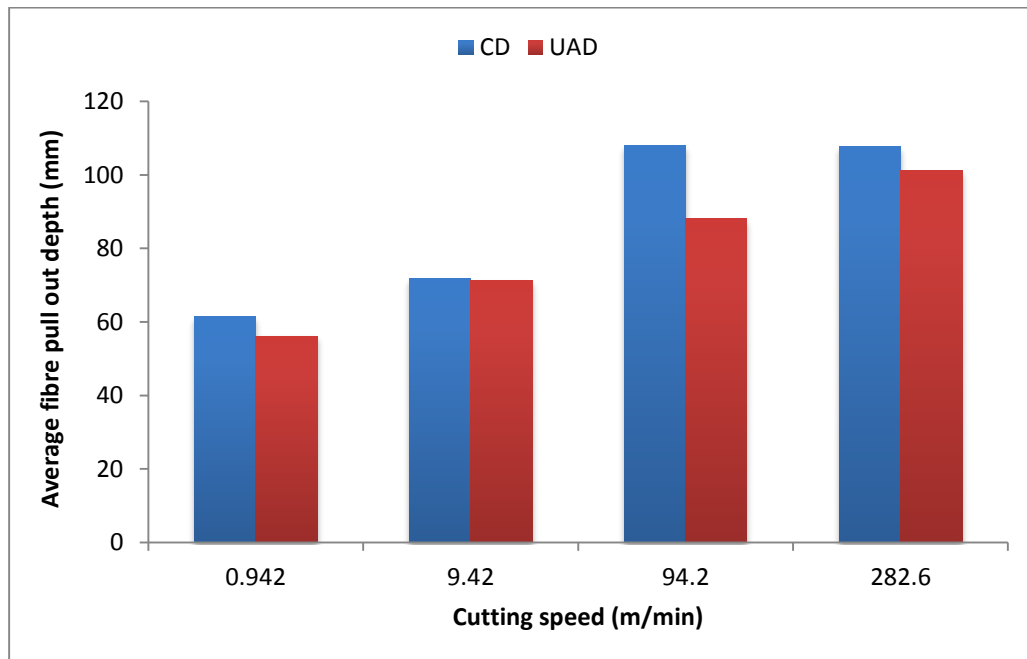


Figure 6-15: Variation of average fibre pull out obtained from CT scanning at all the cutting speeds

With the average fibre pull out depth values from Table 6-6 and Figure 6-15, it can be seen that the average fibre pull out depth increased with increasing cutting speed in both CD and UAD. Also, comparing CD and UAD, the maximum reduction in fibre pull-out due to ultrasonic assistance was found at 94.2 m/min cutting speed. It is discussed further in ‘internal damage’ subsection of section 6.1.7.2.

6.1.3.2 Damage analysis through Sectioning, mounting and polishing

In order to determine the damage in a hole in greater detail, sectioning of the holes was performed. The drilled holes were sectioned, mounted and polished with the methodology explained in Section 5.5.

When examining the holes drilled by a new tool (i.e. first eight holes), it was found that there was no damage at the entrance with both CD and UAD. SEM images showed no evidence of damage near the hole-entrance, See Appendix A.

Unlike the holes drilled with a new tool, damage at the entrance was found to be present in the holes drilled with the worn tool. Maximum damage depth at the entrance was quantified in every hole drilled with a worn tool with the methodology explained in Section 5.5.3. An example of maximum damage depth at entrance measurement is shown in Appendix A (Figure A-5) for the hole drilled with 0.942 m/min cutting speed in UAD. The maximum damage depth at entrance thus measured in each hole in CD and UAD for all the cutting speeds is mentioned in Table 6-7 and Table 6-8 for CD and UAD respectively and is plotted in Figure 6-16 with respect to cutting speed. Error bars in Figure 6-16 denote maximum and minimum values of maximum damage at entrance out of three repetitions.

6: Experimental studies, results and discussions

Table 6-7: Maximum damage depth data at entrance in CD for three times repetitions with worn tool

Cutting speed (m/min)	Damage depth 1 (μm)	Damage depth 2 (μm)	Damage depth 3 (μm)	Average (μm)
0.942	1352	1476	2040	1620
9.42	1272	1421	1780	1490
94.2	847	735	552	710
282.6	405	119	0	170

Table 6-8: Maximum damage depth data at entrance in UAD for three times repetitions with worn tool

Cutting speed (m/min)	Damage depth 1 (μm)	Damage depth 2 (μm)	Damage depth 3 (μm)	Average (μm)
0.942	1551	1699	2088	1780
9.42	1255	847	317	810
94.2	1112	565	704	790
282.6	641	172	444	420

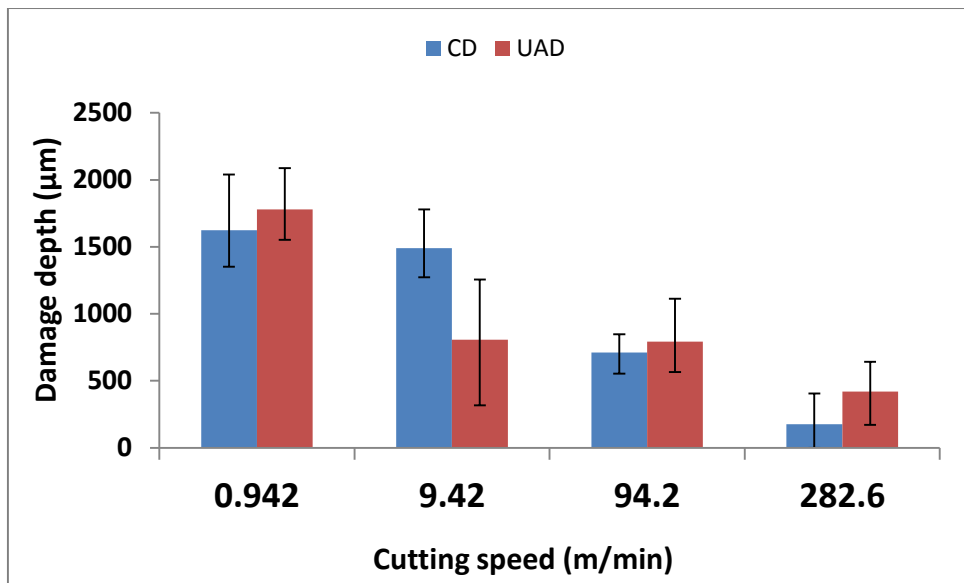


Figure 6-16: Maximum damage at the entrance of the holes obtained from worn tool at all the cutting speeds in CD and UAD

From the plot of maximum damage at the entrance in Figure 6-16, it can be seen that the maximum damage at the entrance was reduced with increasing cutting speed in both CD and UAD. A similar finding for entrance delamination in CD has also

been reported by other researchers [16]. The reason behind this reduction of entrance delamination with increasing cutting speed has been suggested to be that increasing cutting speed increases the cutting temperature which softens the matrix. Therefore, it requires lower cutting forces to for machining and hence it diminishes the delamination (due to reduction in machining forces) [16]. Further, when comparing CD and UAD, the variation in data does not indicate any clear difference between CD and UAD at any cutting speed in terms of maximum damage at entrance.

The internal damage in a hole drilled with the new tool was analysed with the method explained in Sections 5.5.1 and 5.5.2. Both crack propagation and fibre pull out were quantified for holes drilled with a new tool. The average values of crack propagation and fibre pull out for each hole produced with CD and UAD with a new tool are mentioned in Table 6-9 and are plotted in Figure 6-17 and Figure 6-18 respectively. In addition, although the crack propagation depth into the material is more than 15 μm in Table 6-9, it was not detected in CT scanning because one of the dimensions of the crack was less than the resolution of X-ray CT scanning.

Table 6-9: Data table for average crack propagation and fibre-pull out data in the holes drilled by fresh tools

Cutting speed (m/min)	Average fibre pull out (μm)		Average crack propagation (μm)	
	CD	UAD	CD	UAD
0.942	30	24	30	24
9.42	22	17	20	18
94.2	66	47	22	15
282.6	106	105	14	16

6: Experimental studies, results and discussions

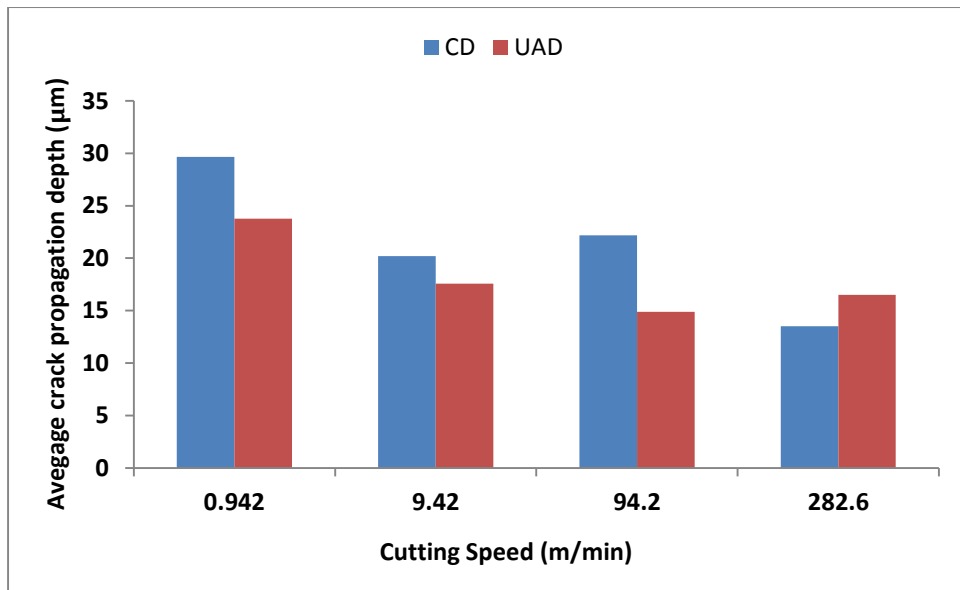


Figure 6-17: Average crack propagation at all the cutting speeds in CD and UAD with a new tool

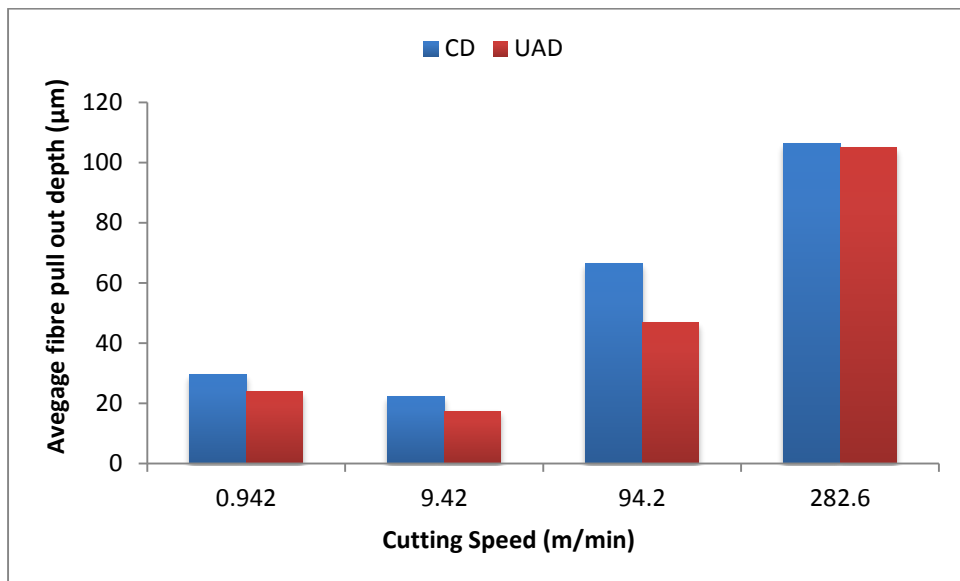


Figure 6-18: Average fibre pull out in all the samples with a new tool

Average crack propagation data plotted in Figure 6-17, indicates reduction in crack propagation depth with respect to increasing cutting speed in both CD and UAD. Also, when comparing CD and UAD, the maximum reduction in crack propagation depth due to ultrasonic assistance was found to be at 94.2 m/min cutting speed.

Average fibre pull out variation with respect to cutting speed in Figure 6-18 indicates fibre pull out to be increasing with respect to cutting speed in both CD and UAD. Also, when comparing CD and UAD, the maximum reduction due to ultrasonic assistance was found to be 19 μm at 94.2 m/min cutting speed. The similar indication was also found in the CT scanning data analysis in Figure 6-15 where the maximum reduction in fibre pull out depth due to ultrasonic assistance was found to be at 94.2 m/min. However, this data is obtained from a single hole per cutting speed. Therefore, no firm conclusion can be drawn with it.

Crack propagation damage was found to be absent in the holes drilled by the worn tool. Therefore, only fibre pull-out and disorientation were analysed in the holes drilled with the worn tool. The value of internal damage for each cutting speed in CD and UAD is presented in Table 6-10 and Table 6-11 and are plotted in Figure 6-19. Error bars in Figure 6-19 denote maximum and minimum values of ‘maximum damage at entrance’ out of three repetitions.

Table 6-10: Data table for internal damage in CD from the holes drilled with a worn tool

Cutting speed (m/min)	Damage depth 1 (μm)	Damage depth 2 (μm)	Damage depth 3 (μm)	Average (μm)
0.942	66	69	83	73
9.42	124	148	146	139
94.2	121	115	118	118
282.6	223	160	252	212

Table 6-11: Data table for internal damage in UAD from the holes drilled with a worn tool

Cutting speed (m/min)	Damage depth 1 (μm)	Damage depth 2 (μm)	Damage depth 3 (μm)	Average (μm)
0.942	89	65	68	74
9.42	112	130	123	122
94.2	170	139	146	152
282.6	273	120	164	186

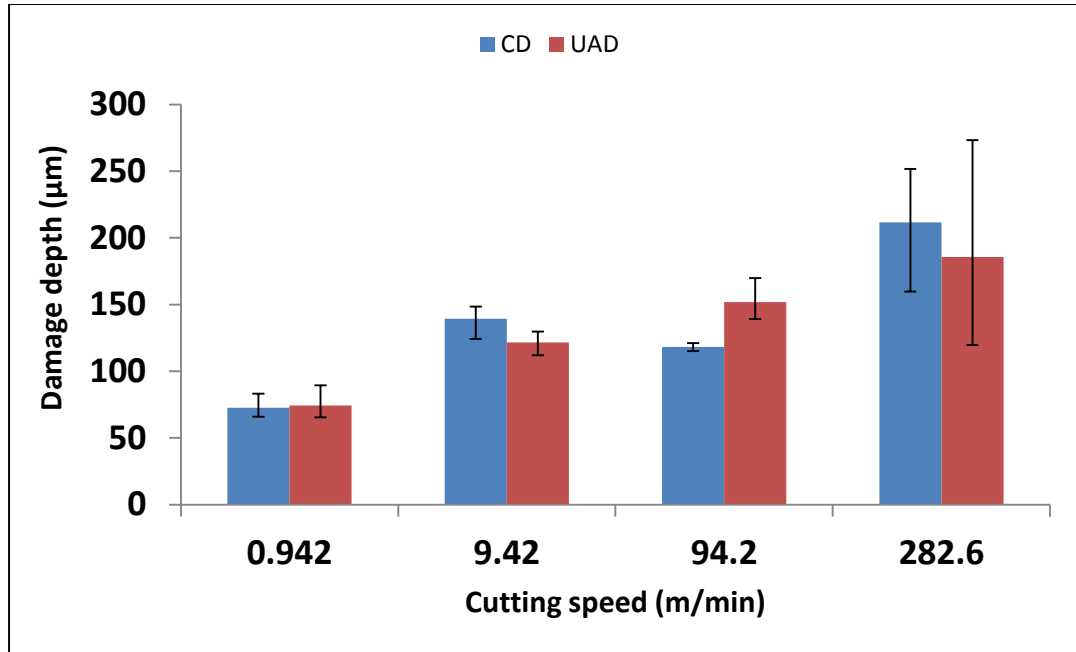


Figure 6-19: Variation of average damage depth at the internal cylindrical machined surface (internal damage) obtained from worn tool in CD and UAD at all the cutting speeds

From internal damage data from the worn tool in Figure 6-19, it can be seen that similar to holes drilled by a new tool, the average fibre disorientation and pull out increased with increasing cutting speed in both CD and UAD. When comparing CD and UAD, there was no clear difference found between average fibre pull out in CD and UAD at all cutting speeds.

Maximum damage at exit data was collected with the methodology explained in Section 5.5.3. Maximum damage depth at the exit in the hole obtained from the new tool is presented in Table 6-12 and plotted in Figure 6-20.

Table 6-12: Data table for maximum damage at exit in the holes drilled by a new tool

Cutting speed	Exit delamination (µm)	
	CD	UAD
0.942	1163	1091
9.42	1500	740
94.2	708	999
282.6	735	545

6: Experimental studies, results and discussions

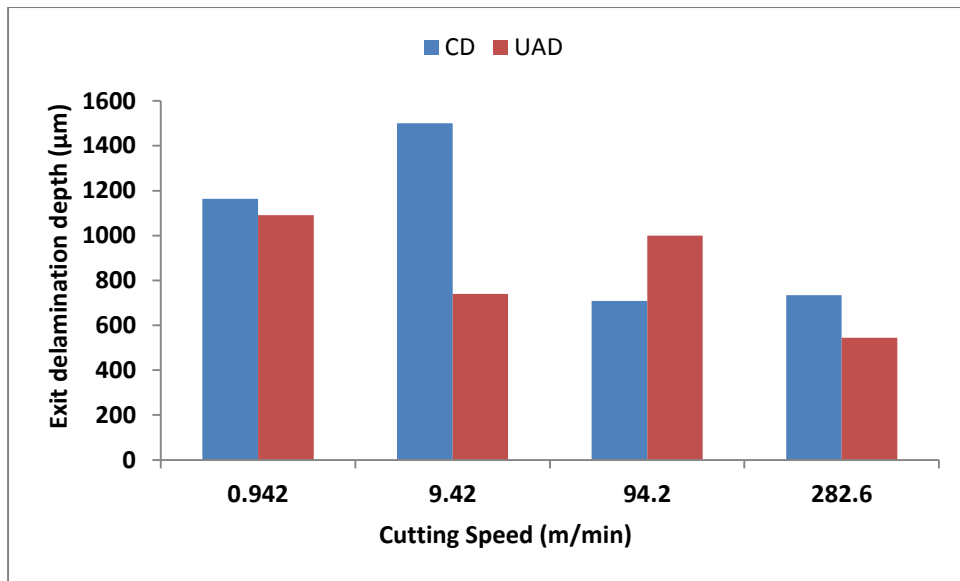


Figure 6-20: Exit delamination at all the cutting speeds in CD and UAD with a new tool

The maximum damage depth at exit data collected from the holes drilled by a worn tool with CD and UAD is presented in Table 6-13 and Table 6-14 respectively and is plotted in Figure 6-21. Error bars in Figure 6-21 denote maximum and minimum values of ‘maximum damage at exit’ out of three repetitions.

Table 6-13: Maximum damage depth at exit data obtained from the holes drilled by worn tool in CD

Cutting speed (m/min)	Damage depth 1 (µm)	Damage depth 2 (µm)	Damage depth 3 (µm)	Average (µm)
0.942	2950	3971	4003	3640
9.42	2350	2325	2390	2360
94.2	1950	1627	2368	1980
282.6	2163	2157	2274	2200

Table 6-14: Maximum damage depth at exit data obtained from the holes drilled by worn tool in UAD

Cutting speed (m/min)	Damage depth 1 (µm)	Damage depth 2 (µm)	Damage depth 3 (µm)	Average (µm)
0.942	3916	2286	3986	3400
9.42	3117	2627	2700	2810
94.2	2222	1724	1900	1950
282.6	2765	1846	2294	2300

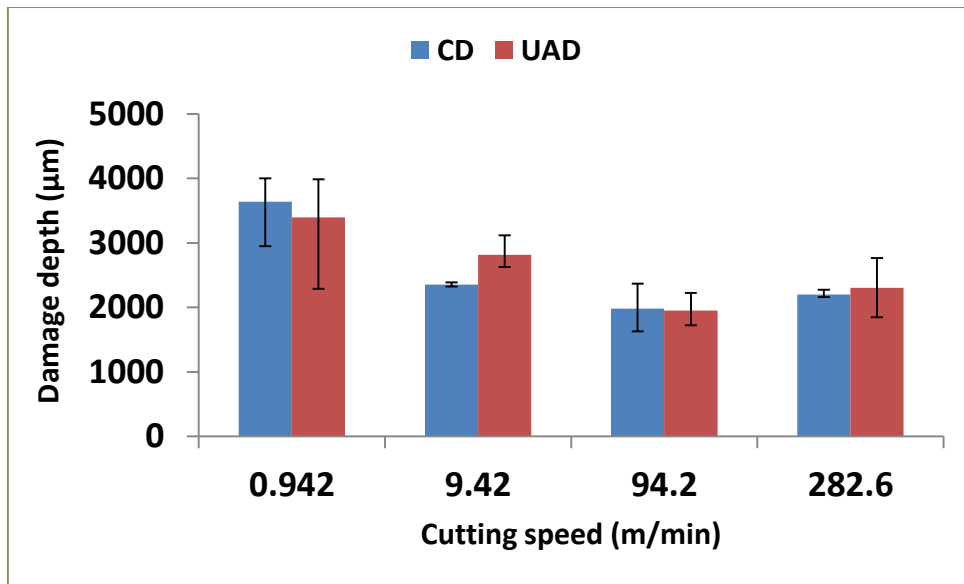


Figure 6-21: Maximum damage depth at exit obtained from worn tool in CD and UAD at all the cutting speeds

In addition to the damage quantification, it was also found that the propagation of damage resulted from fibre-matrix debonding and it also occurred across the laminates as shown in Figure 6-22.

6: Experimental studies, results and discussions

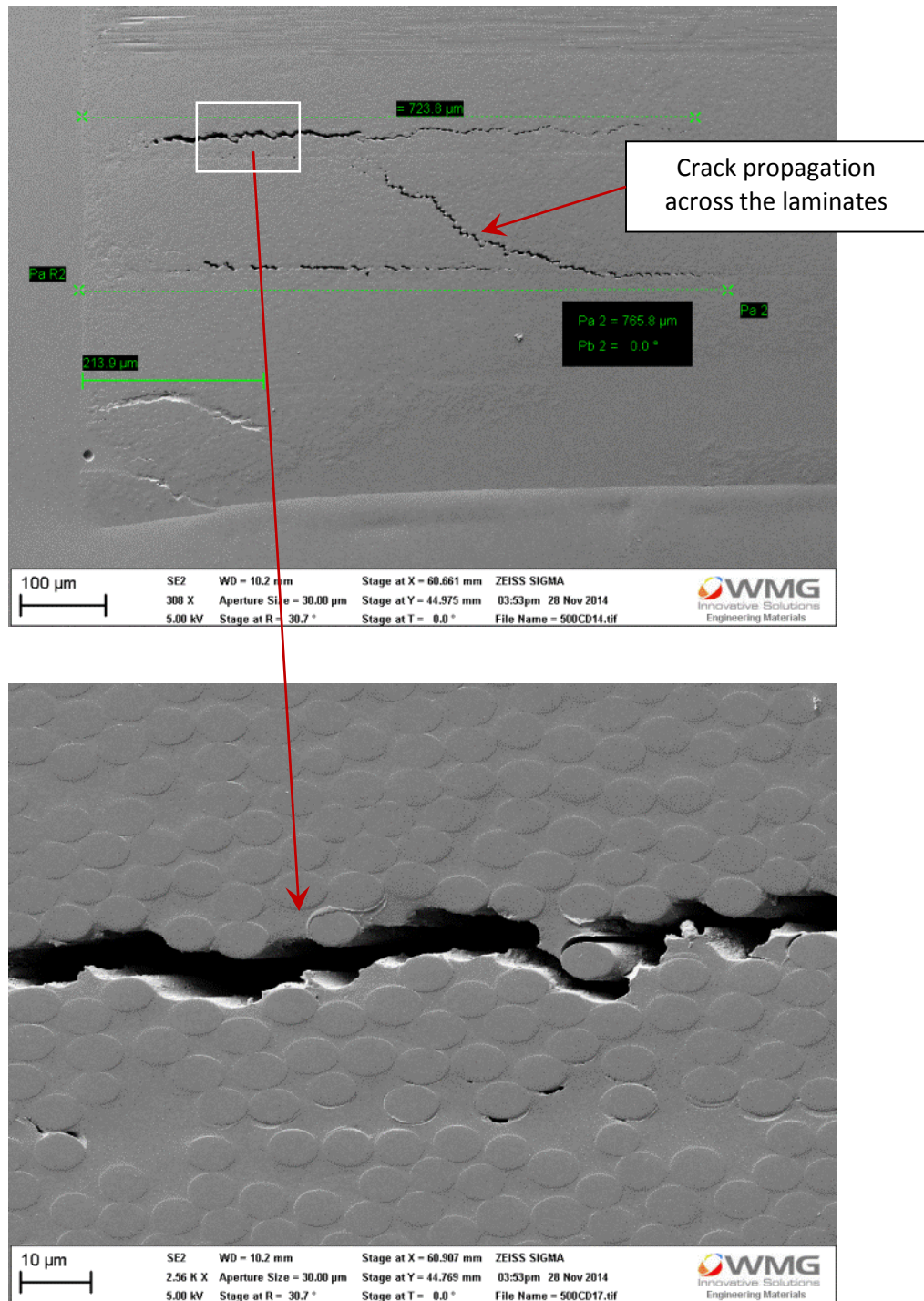


Figure 6-22: Visualisation of fibre-matrix debonding and crack propagation across the laminates near exit around the hole drilled at 9.42 m/min cutting speed and 0.05 mm/rev feed rate in CD

6.1.4 Machined surface

It becomes necessary to mention here that during the methodology of sectioning mounting and polishing explained in Section 5.3.1, the holes were first sectioned and then mounted in EpoCure resin system. This process was followed for the holes

drilled with a new tool. The holes drilled with worn tool were first mounted in EpoCure resin system and then sectioned. Because of this process, the machined surface due to worn tool could not be examined as it was covered with the EpoCure resin system. Thus, the machined surface could be examined only in the holes drilled by the new tool in this particular study.

The internal cylindrical surface of the holes was analysed in the scanning electron microscope (SEM). The machined surfaces provided by CD and UAD “look” similar at all the parameters when observed at a low magnification of 40x, Figure 6-23 & Figure 6-24 (except for near hole-exit). Although the internal damage of fibre pull-out was seen to be higher at 282.6 m/min CD and UAD, Figure 6-25 and Figure 6-26, in comparison to those at 0.942 m/min cutting speeds, Figure 6-23 and Figure 6-24.

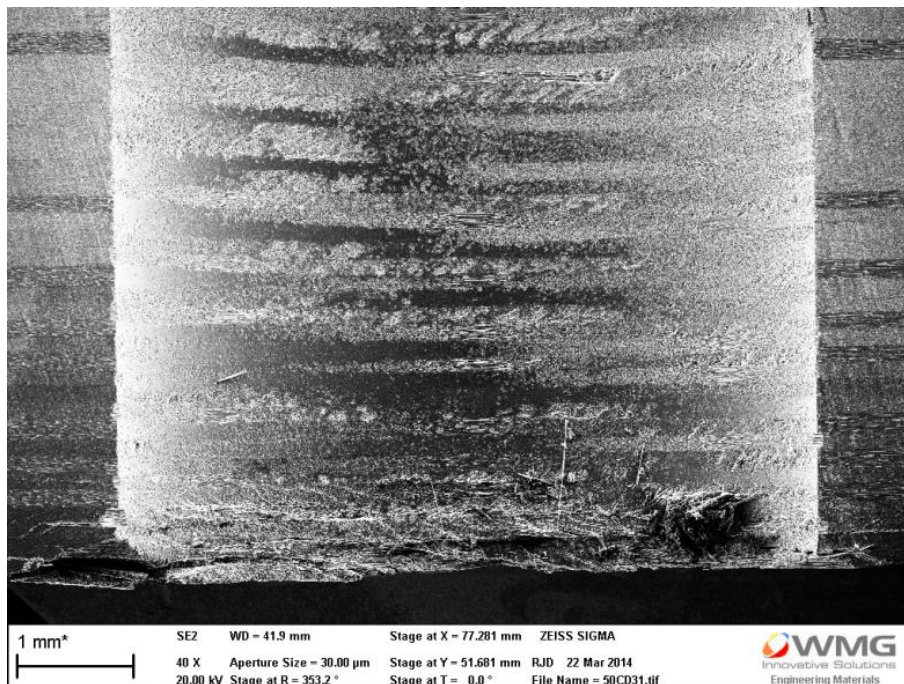


Figure 6-23: Machined surface, CD (0.942 m/min, 0.05 mm/rev)

6: Experimental studies, results and discussions

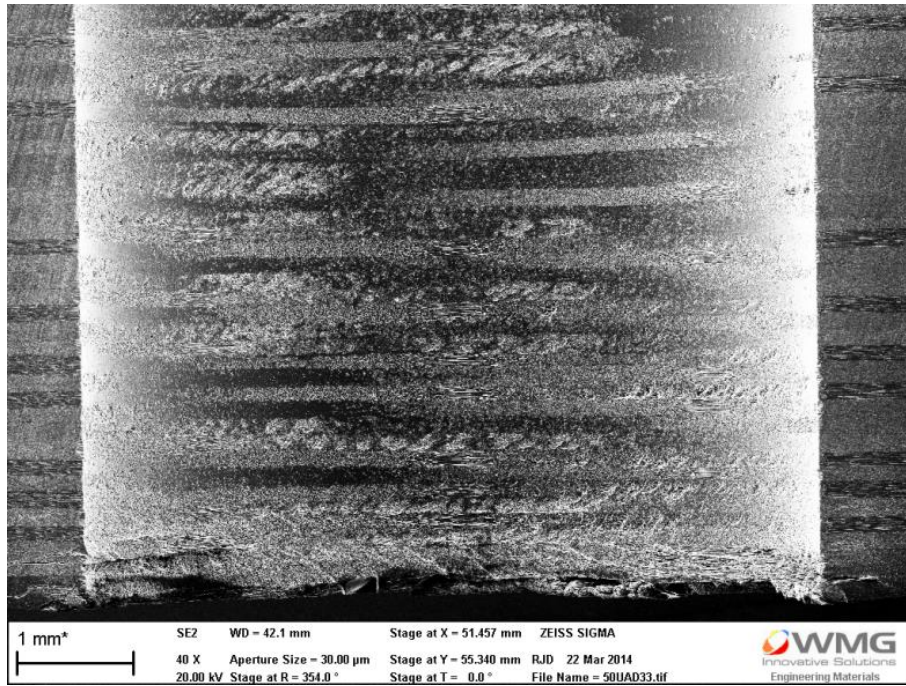


Figure 6-24: Machined surface, UAD (0.942 m/min, 0.05 mm/rev)

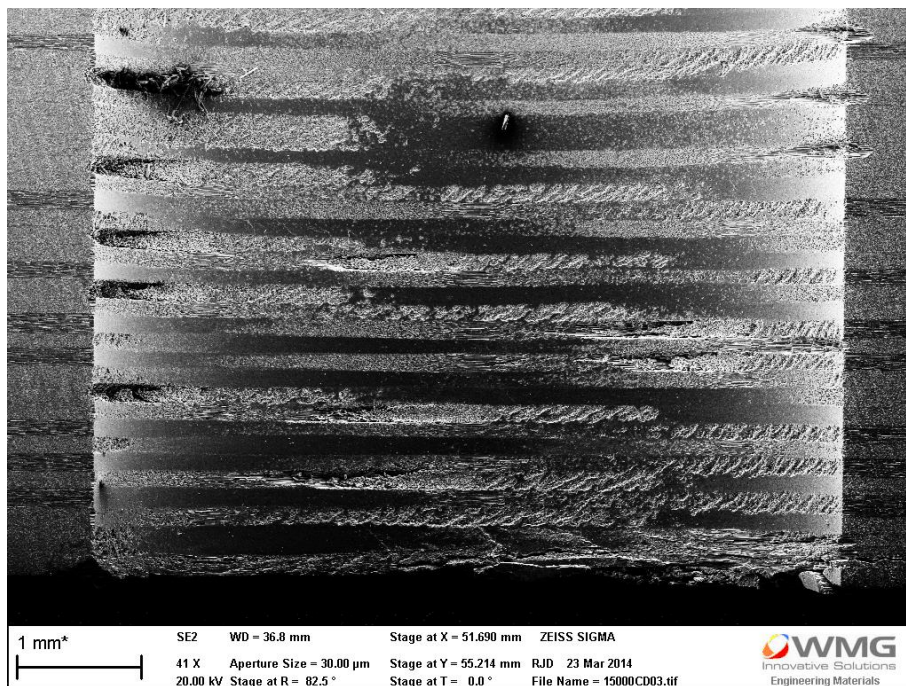


Figure 6-25: Machined surface, CD (282.6 m/min, 0.05 mm/rev)

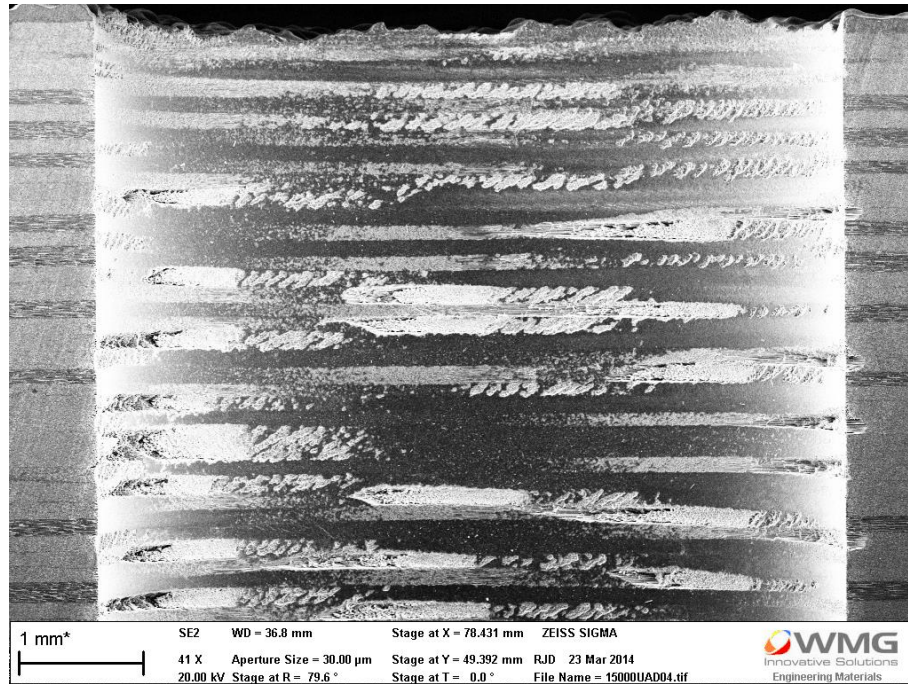


Figure 6-26: Machined surface, UAD (282.6 m/min, 0.05 mm/rev)

Also, when observed at a higher magnification (60,000 x), plastically deformed matrix was found in CD and UAD at 0.942 m/min cutting speed as shown in Figure 6-27 and Figure 6-28. No clear visible difference between the machined surfaces after machining through the CD and UAD was found at 0.942 m/min cutting speed. Similar matrix smearing has also been reported by other authors during orthogonal machining of CFRP [81].

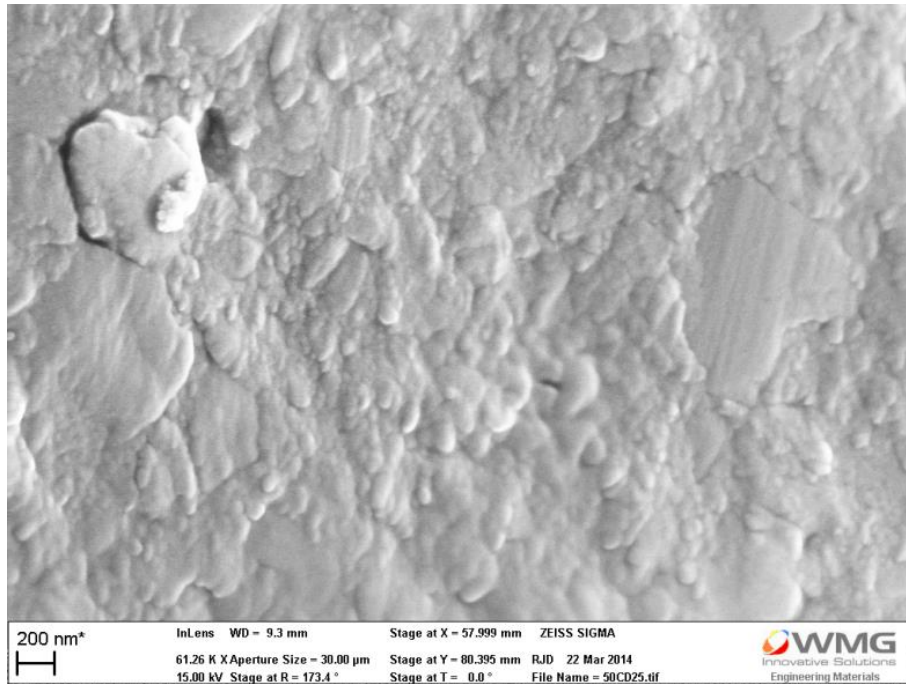


Figure 6-27: Plastic deformation of the smeared matrix on the machined surface after CD at higher magnification (0.942 m/min, 0.05 mm/rev)

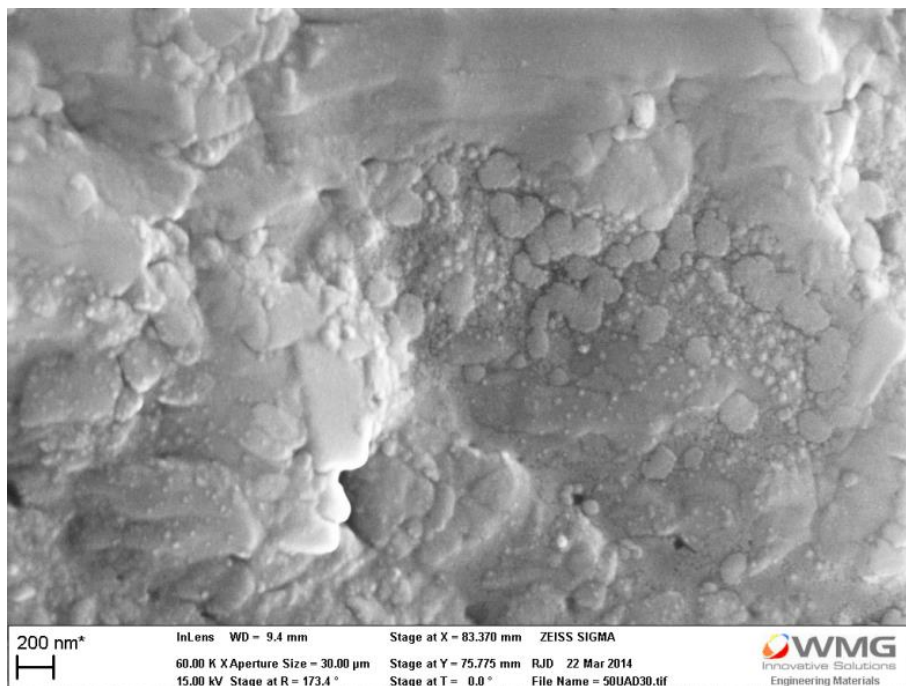


Figure 6-28: Plastic deformation of the smeared matrix on the machined surface after UAD at higher magnification (0.942 m/min, 0.05 mm/rev)

At 9.42 m/min cutting speed, regular, sharp cracks were found on the smeared matrix in the conventionally drilled hole, Figure 6-29, while the smeared matrix in the UAD was found to have edge-rounding and round crack ends at the cracked

edges in the smeared matrix of the machined surface in UAD, Figure 6-30. This edge rounding in UAD gave an indication of matrix softening in UAD. In a recent study, Makhdum et al. [40] and Phadnis et al. [165] reported matrix being softened in UAD due to brittle to ductile transition of matrix in UAD. Larger lengths of the chips of CFRP material in UAD as compared to those in CD were presented as evidence to support the argument of matrix softening. To verify whether this edge rounding happened because of thermal softening or smearing of matrix, the cutting temperature measurement was attempted further as discussed in the section 6.1.5.

At 94.2 m/min, Figure 6-31 and Figure 6-32, the machined surface in conventional drilling was found to have debris on the machined surface while in UAD, the surface was machined cleaner.

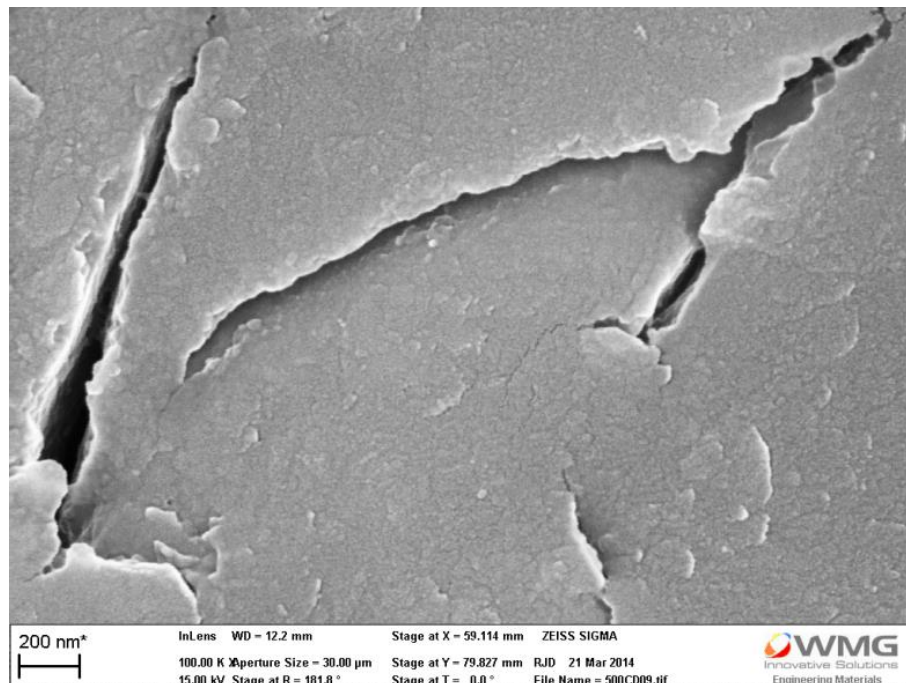


Figure 6-29: Sharp cracks in CD (9.42 m/min, 0.05 mm/rev)

6: Experimental studies, results and discussions

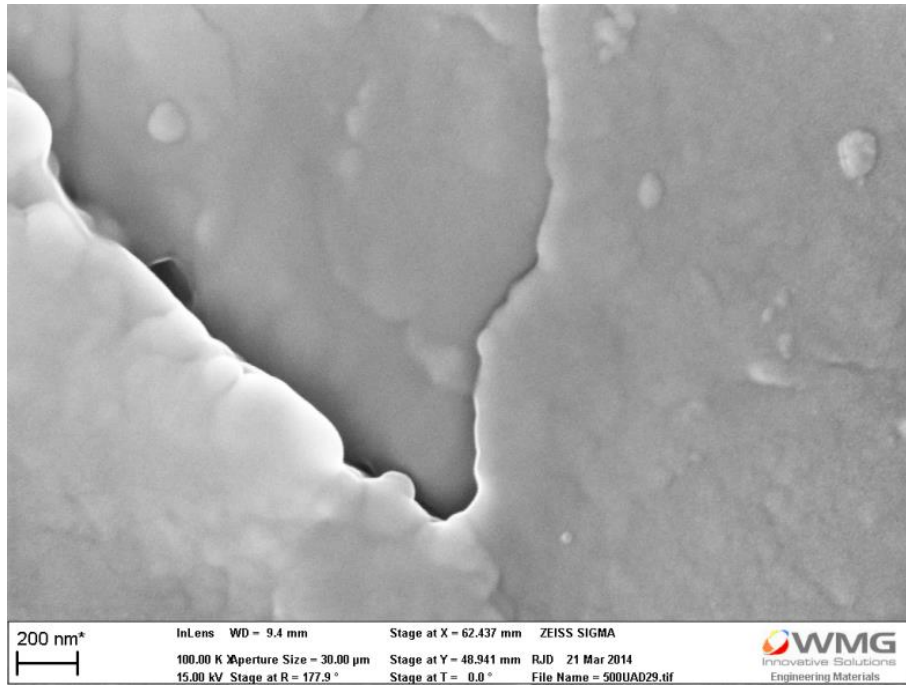


Figure 6-30: Machined Matrix in UAD (9.42 m/min, 0.05 mm/rev)



Figure 6-31: Machined matrix surface in CD (94.2 m/min, 0.05 mm/rev)

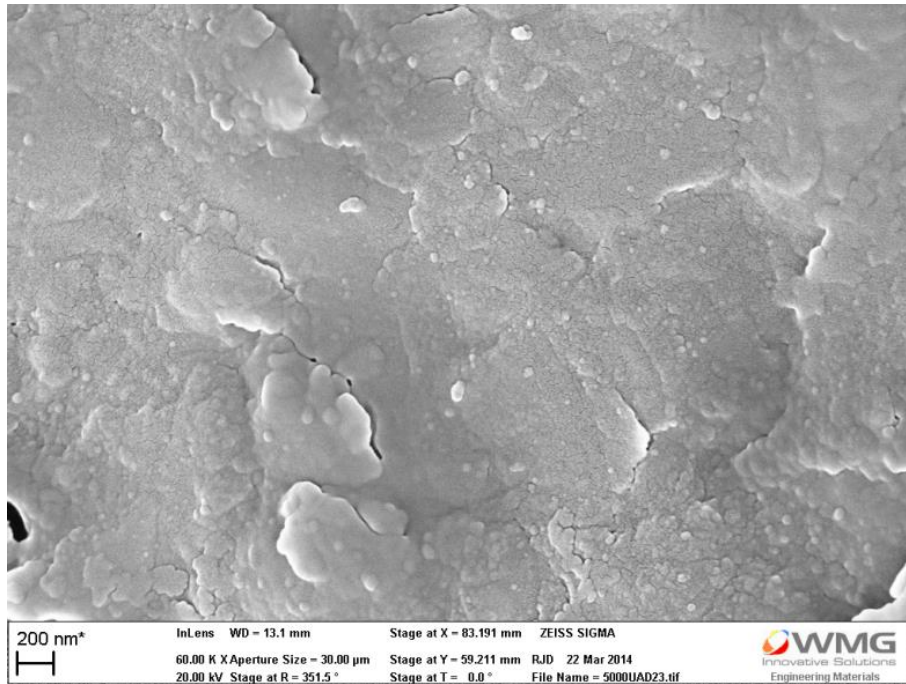


Figure 6-32: Machined matrix surface in UAD (94.2 m/min, 0.05 mm/rev)

6.1.5 Cutting temperature variation

The cutting temperature variation in CD and UAD is plotted in Figure 6-33. The cutting temperature was found to increase with increasing cutting speed; however, it decreased down to 57.56°C and 56.73°C at 282.6 m/min from 143.81°C and 152.1°C at 94.2 m/min cutting speed in CD and UAD respectively.

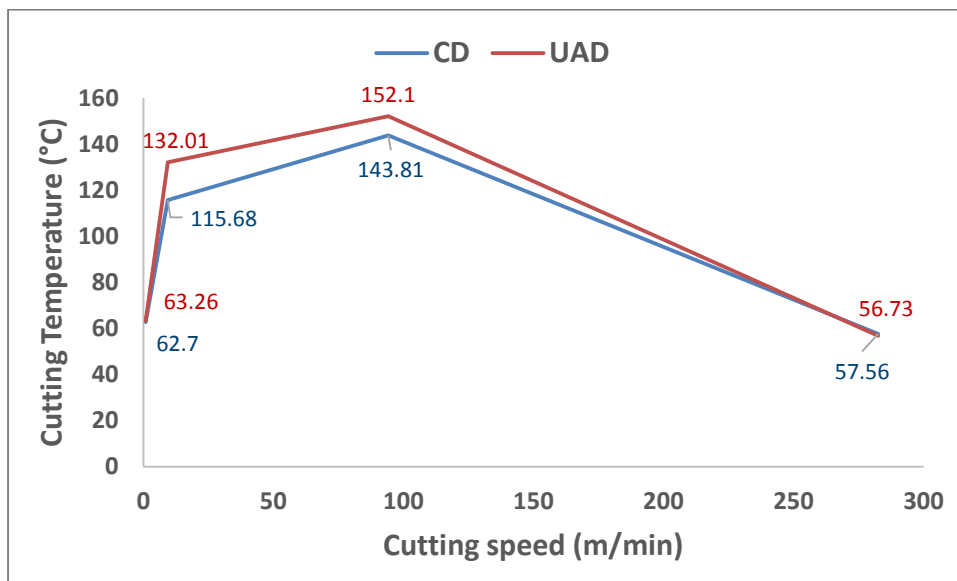


Figure 6-33: Cutting temperature measurement at various cutting speeds in CD and UAD

Weinert and Kempmann [136] have also attempted measuring the cutting temperature during drilling of carbon/epoxy composite material with respect to cutting speed at a constant feed rate. In their work, the temperature was measured by mounting the thermocouple on flank face of the drill. The cutting speed was varied from 100 to 260 m/min at a constant feed rate of 0.1 mm/rev and cutting temperature was found to rise from 200°C to 275°C. Therefore, the cutting temperature was found to be increasing with increasing cutting speed in their work. The results in the work of Klaus et al [136] suggest that the cutting temperature in the present research should have been increased further while increasing the cutting speed from 94.2 to 282.6 m/min instead of reducing. It is suspected that the reason behind the drop in the cutting temperature at 282.6 m/min cutting speed is “very high” feed rate of 750 mm/min at 282.6 m/min. It took 1.2 s to drill 15 mm of material at 750 mm/min feed rate (considering the top and bottom 7.4 mm thick CFRP plates into account as shown in Figure 5-43) and hence, the heat generated during drilling could not be conducted to the thermocouple in this short duration of 1.2 s and was taken away by the chip fragments generated during drilling.

The cutting temperature was found to be 16°C higher in UAD than that in CD at 9.42 m/min cutting speed while it was 8°C higher in UAD than that in CD at 94.2 m/min. At cutting speeds of 0.942 and 282.6 m/min, the cutting temperature did not show a difference between CD and UAD (1°C difference only). Since, the cutting temperature was measured only once per hole, therefore, no clear difference between cutting temperatures during CD and UAD could be stated from the cutting temperature data in the present research.

When the polymer matrix is heated, the minimum temperature at which the matrix ceases to be brittle and glassy in character and becomes less rigid and more

rubbery, is defined as glass transition temperature [195]. The glass transition temperature of Bismaleimide matrix lies between 210°C to 288°C based on the composition [196]. Maximum cutting temperature with a new tool was found to be 152°C in the present research which is lower than glass transition temperature of Bismaleimide matrix. However, the temperature could not be measured at cutting edges in the present setup because of impracticality in fitting the thermocouple at cutting edge of twist drill. In a recent study, Makhdum et al. [40] reported cutting temperature during UAD to be 265°C and maximum cutting temperature in CD to be 90°C. They used a thermal camera to record the cutting temperature at the drill entrance. The reason behind higher temperature in UAD was reported to be repetitive ultrasonic impacts during UAD leading to a rise in temperature at tool material interface. Also, the glass transition temperature (T_g) was found to be 360°C through thermogravimetric analysis (TGA) in their work and thus it was concluded that the matrix softening happened due to brittle-to-ductile transition of matrix in UAD. The matrix was epoxy in their work.

Nevertheless, it is also to be noted at this point that the actual cutting temperature at tool and material interface during machining has not been recorded by any methodology in the literature. Although Weinert and Kempmann [136] attempted to measure the cutting temperature, the thermocouple was mounted at the flank surface of the drill which provided an approximate value of cutting temperature in their work. Thus, it is possible that the actual temperature at tool-material interface during machining is higher than that measured by the methodologies of thermocouple at the flank surface and thermal camera. Therefore, it cannot be concluded that the actual cutting temperature during drilling did not exceed the glass transition temperature of

matrix of CFRP. Further advanced techniques are required to assess the actual cutting temperature at tool-material interface during machining.

6.1.6 Chip analysis

The chips were collected after drilling each hole on a double-sided carbon tape. Further analysis was performed in SEM after applying the gold coating. In order to have overall information of the average chip formation, 3 random samples were analysed out of every drilled hole. The chips obtained in both the processes of CD and UAD were found to be similar. At every cutting speed, a mixture of three types of chip-fragments were found in both the processes–

- Large (1.4 mm) fragments of chip, Figure 6-34
- Small (100 μm to 300 μm length) fragments of chip, Figure 6-36
- Small broken fibres (10 to 200 μm length)

The large fragments of the chips were found at 0.942 m/min and 282.6 m/min cutting speeds in CD, Figure 6-34 and Figure 6-35. Short broken chip-fragments with length between 100 μm to 300 μm were the most common fragments type obtained at all the cutting speeds in both the processes of CD and UAD, Figure 6-36. Because of the fibre-matrix debonding, the broken loose fibres were also obtained at every cutting speed in both the processes of CD and UAD. At every cutting speed, there was a portion of chips having a plastic deformation in the matrix. These types of chips were obtained in a large portion at the cutting speeds of 94.2 m/min and 282.6 m/min in both CD and UAD. Though a small portion of chips having plastic deformation were also found at the cutting speed of 0.942 m/min in CD and UAD. Hence, there was a mixture of chips found at every cutting speed in CD and UAD and in particular, no clear visible difference could be found in the chips formed in CD and UAD at the current machining parameters. The respective SEM images of the chips obtained are presented in Appendix B.

6: Experimental studies, results and discussions



Figure 6-34: Large fragment of the chip obtained in CD (0.942 m/min, 0.05 mm/rev)



Figure 6-35: Large chip fragment found in UAD (282.6 m/min, 0.05 mm/rev)



Figure 6-36: Long and short, broken chip-fragments in UAD (0.942 m/min, 0.05 mm/rev)

Makhdum et al. [40, 163] reported generation of larger chips in UAD in comparison to that in CD unlike the case in present research where no difference could be found in the chips between CD and UAD. A possible explanation for this is the matrix used in their work was epoxy matrix having glass transition temperature of 132°C. In the current case, the matrix used was Bismaleimide which is brittle in nature [48, 197], however, more evidence is required to confirm this.

6.1.7 Discussion

6.1.7.1 Thrust force

Effective normal rake angle calculations in Figure 6-1 indicated achievement of highest values of effective normal rake angles at the lowest cutting speed of 0.942 m/min in UAD. This indicated that maximum reduction in thrust force due to ultrasonic assistance in UAD should happen at lowest cutting speed of 0.942 m/min as. Comparing CD and UAD, thrust force variation obtained from a new tool, Figure 6-12 suggests the maximum reduction in thrust force due to ultrasonic assistance at lowest cutting speed of 0.942 m/min. However, thrust force data obtained from the

worn tool in Figure 6-13 suggests that the maximum reduction in thrust force due to ultrasonic assistance happened at 9.42 m/min cutting speed instead of the lowest cutting speed of 0.942 m/min. Although during drilling with a new tool in the last hole, there was a broken chip observed near chisel edge of the drill, Figure 6-11. This raises a concern about thrust force obtained from worn tool being affected by variation in tool geometry near chisel edge due to the chip. Also, the effective normal rake angle calculation was performed for cutting edges in Section 4.5. Therefore, in order to investigate effects of effective normal rake angles during CD and UAD, separate examination of effects of chisel and cutting edges is required.

When analysing the thrust force obtained from worn tool in Figure 6-13, there was no clear difference between thrust forces at any cutting speed when comparing CD and UAD. Also, both in CD and UAD, thrust force was found to be reducing with cutting speed 0.942 m/min to 94.2 m/min and increasing from 94.2 m/min to 282.6 mm/min. In the literature, other authors have reported thrust force being reduced with respect to increasing cutting speed at a constant feed rate. The reason suggested for this is that as the cutting speed is increased, the friction forces between the tool-flank surface and material increases which generates a more heat. Evidence of cutting temperature measurement in the present research in section 6.1.5 and that reported by Weinert and Kempmann [136] verify this statement. Authors [16] have suggested that due to a higher cutting temperature at higher cutting speeds, the matrix in the vicinity of cutting edges softens which requires lower force for machining resulting in lower thrust force at higher cutting speed. Also, the thrust force has been found to be increasing when feed rate is increased [13]. In the present case, when the feed rate in mm/min is used, the feed rate has also been increasing from 2.5 to 750 mm/min when the cutting speed is increased from 0.942 to

282.6 m/min. This suggests that increasing cutting temperature and increasing feed rate in mm/min with respect to increasing cutting speed in the present case have become contradictory deciding factors for thrust force and therefore rise in the thrust force at 282.6 m/min cutting speed. In addition, since there was a chip broken near chisel edge in the drill, this could also affect the thrust force values. This needs to be investigated further.

6.1.7.2 *Damage*

In the present research, damage was segmented in three categories – entrance delamination, exit delamination and internal damage (Average crack propagation and fibre pull out) which are discussed as follows:

The holes drilled with a new tool were free from **entrance delamination**. The entrance delamination in the holes drilled by the worn tool in Figure 6-16 indicates a reduction in entrance delamination with respect to increasing cutting speed in both CD and UAD. This happened because increasing cutting speed caused an increment in cutting temperature which further softened the matrix and hence requiring lower force for machining. Lower machining force caused lower entrance delamination. This behaviour of reduction in entrance delamination with respect to increasing cutting speed in CD has already been reported by other authors in the literature [16].

From CT scanning data in Figure 6-14 and sectioning, mounting and polishing data in Figure 6-20, it is indicated that for the holes drilled by new tool, **exit delamination** was found to be increased when increasing cutting speed from 0.942 to 9.42 m/min in CD. Upon further increasing the cutting speed, the exit delamination continued to reduce. However, this data was obtained from only one hole. Further, with three times repetition with a worn tool, the exit delamination

from worn tool, Figure 6-21, reduced as the cutting speed was increased from 0.942 to 94.2 m/min and an increase of 0.35 mm was found when cutting speed was increased from 94.2 to 282.6 m/min in both CD and UAD. This happened because exit delamination is dependent on thrust force and similar behaviour of thrust force was found in the case of the worn tool as discussed in Section 6.1.7.1.

Average crack propagation in the holes drilled with a new tool in Figure 6-17 suggests that average crack propagation into the material during drilling reduces as the cutting speed is increased in both CD and UAD. This can be justified from the fact that average thrust force for the holes drilled with a new tool decreased with increasing cutting speed in CD and UAD, Figure 6-12. Due to reducing thrust force with respect to increasing cutting speed, the axial force on the plies during drilling reduced and hence the extent of crack propagation into the material reduced as the cutting speed was increased, although, this data is obtained from just one hole per cutting speed. More evidence is required to support this and due to the same reason, no clear difference between CD and UAD can be stated in terms of average crack propagation into the material.

Fibre pull out data obtained from X-ray CT scanning for the holes drilled by a new tool in Figure 6-15 indicates fibre pull-out to be increasing with respect to increasing cutting speed. Further, the fibre pull-out and fibre disorientation depth data obtained through sectioning, mounting and polishing method for holes drilled by a new tool in Figure 6-18 and that for the holes drilled by a worn tool in Figure 6-19 also indicate that average fibre pull out depth increased with increasing cutting speed in both CD and UAD. As it has already been established by other authors that cutting temperature increases with respect to increasing cutting speed due to higher friction forces between cutting tool and material being machined [136]. The authors

have reported that when cutting speed is increased, due to rise in cutting temperature, the matrix is softened requiring lower forces to be machined and hence lower thrust force and lower exit delamination during drilling [38, 109, 198]. Alauddin et al. [199] mentioned that elevated temperatures cause softening of plastics “considerably”. It was reported that thrust force reduced from 80 N to 10 N during drilling of thermosetting plastic when its temperature was increased from room temperature to 125°C. Morioka et al. [200] reported the bending fracture stress of CFRP having epoxy matrix being reduced from 82 to 38 MPa when its temperature was increased from 300 to 500 K. In addition, it has also been found that upon reducing the temperature of CFRP material, the matrix dominant properties of CFRP such as in-plane shear strength and bending fracture strength increase [201, 202]. Kinloch et al. [203] reported true compressive modulus of epoxy to be reducing from 4.25 to 2.75 GPa and true compressive yield stress from 150 to 60 MPa when its temperature was increased from -60 to 60°C.

Keeping the findings reported by the authors in mind, it can be stated that when the cutting temperature is increased due to increasing cutting speed, strength of matrix for holding the fibres in-place gets diminished. This caused greater depth of fibre disorientation and fibre pull-out when cutting speed was increased in the current research. This is why the internal damage was found to be increasing with respect to increasing cutting speed in the present study. Also, this is why the chip fragments having larger dimensions between 100 µm to 300 µm were mostly obtained at 282.6 m/min cutting speed in CD and UAD. The respective SEM images of chips are presented in Appendix B.

When comparing the internal damage generated in CD and UAD, data obtained from the holes drilled with a new tool, through X-ray CT scanning in Figure 6-15

and sectioning, mounting & polishing in Figure 6-18 indicate that the maximum reduction in internal damage of fibre pull-out was obtained at the cutting speed of 94.2 m/min. Since the data obtained from the new tool is from only one hole, no clear conclusion could be drawn. However, the fibre pull-out data obtained from worn tools indicates that internal damage in UAD was higher than that in CD at the same cutting speed of 94.2 m/min. Since, in this repetition of experiment with worn tool, three holes were first drilled with CD and then three holes with UAD, at any cutting speed, therefore, it is also possible that the increment in fibre pull out at 94.2 m/min cutting speed in UAD with respect to that in CD happened due to incremental tool wear after drilling three holes with CD which needs to be investigated further.

As explained in Section 3.4.3, many authors have used stylus-based surface roughness measurement as a parameter for damage quantification on the internal cylindrical machined surface of a hole [7, 75, 83, 121-126]. However, using the stylus for surface roughness has limitations on the stylus size itself. If the depth of damage is more than the dimensions of the stylus, the stylus would provide inaccurate results. Also, using a stylus method, the fibre disorientation could not be detected as the stylus can only detect the absence of material. In contrast to the findings of the current research, Davim et al. [122] reported fibre pull out to be reducing with respect to increasing cutting speed. Similarly, Tsao [126] also reported surface roughness to be reducing at high cutting speed. However, no argument was provided by the authors in support of reducing fibre pull out with respect to increasing cutting speed. Wang et al. [8] compared the methodologies of stylus-based profilometers and confocal microscopy for damage quantification and found that more accurate values of fibre pull-out were achieved with the help of

confocal microscopy than that in stylus-based profilometer. Also, Wang et al. [8] reported fibre pull out to be increasing with increasing cutting speed which is also found in the current research. However, Wang et al. [8] did not explain the reason behind the increment of fibre pull out with respect to increasing cutting speed which current research explains in detail. In the present research fibre pull-out and fibre disorientation was found to increase with increasing cutting speed due to increasing cutting temperature.

6.1.8 Conclusions from Phase-1

With this study, various types of damage during drilling of CFRP have been explored and compared in CD and UAD through techniques of CT scanning and sectioning, mounting and polishing. The difference between thrust forces was indicated at lower cutting speeds when comparing CD and UAD. However, thrust force could not be assessed properly due to a chip broken near chisel edge of drill. Also, the whole experiment was performed with just one drill due to the limitation on detachment of drilling tool from tool-holder. Since almost 40% of thrust force comes from chisel edge during conventional drilling [131], it was suspected that due to chip breaking near chisel edge, the results could have been affected by deteriorated chisel edge in the present experiment. Also, the effective rake angle calculation was performed for cutting edge. Therefore, the effect of cutting edge on thrust force and damage needs to be examined in such a way that during drilling, chisel edge should not be involved in machining process i.e. pilot holes need to be used [18-21] so that the effect of with and without a chisel edge could be analysed during CD and UAD.

Regarding damage assessment and quantification, CT scanning was found to be accurate for overall damage measurement but it is a slow process which made it

useful for examining only a few holes. In a private communication [204], it was confirmed by Ms. Nadia Kourra and Prof. Mark Williams that it took 10 hours for scanning each hole and at least four hours per hole for damage quantification analysis through image processing. In addition, since the X-ray CT scanning detects the absence of material, the fibre disorientation could not be assessed through X-ray CT scanning because the material is not “Absent” at fibre disorientation damage.

In contrast, sectioning, mounting and polishing methodology provided information of damage only in the plane of sectioning and it provided similar variation in damage as that in CD and it is quicker than X-ray CT scanning. Thus, it was decided to use sectioning, mounting and polishing methodology in the remaining research for damage analysis and quantification.

6.2 Phase 2 – Effect of cutting edge using pilot holes

In Phase-1 (Section 6.1), cutting speed of 9.42 m/min was found to be indicating for thrust force reduction in both the cases of a new and worn tool in UAD compared to CD, however, it was not clear what was causing the reduction in thrust force. Even though effective normal rake and clearance angle calculations were performed in Section 6.1.1 but the calculations were valid only for cutting edges of the twist drill and not for chisel edge. During drilling of CFRP material, both chisel and cutting edges are involved in machining. Therefore, in order to find out the actual effect of effective normal rake angle at cutting edges on thrust force, torque and damage in a hole during drilling, the hole would have to be drilled in such a way that the fraction of cutting and thrust forces coming from chisel edge would not affect the results. Thus, before drilling an actual test hole, a pilot hole with an equivalent diameter of chisel edge (of the actual main-hole drill) was to be drilled in order to avoid any effect coming from chisel edge during drilling of the actual test hole (main-hole drilling). To test this philosophy, the present study was performed in Phase-2 of the research in which the effect of cutting edge was studied using a pilot-hole before CD and UAD.

In addition, the objective was to examine the effect of effective rake angles with increasing tool wear. Due to the workpiece material being unavailable in excess, it was necessary to examine the effect of cutting edges with new and worn drill within less number of drilled holes. Since, high speed steel (HSS) tool material drills wear rapidly as compared to other tool materials [72, 100, 139-141], the effect of a new and worn tool could be examined with HSS drills within less number of drilled holes. Therefore, drills made of HSS tool material were used for this experiment.

It can be noted that the geometry of drills in the experiments described in Phases 1 and 2 (Sections 5.7.1.1 and 5.7.2.1) are different. Since the objective was to understand the effects of variation in effective normal rake angles in CD and UAD, therefore, the variation in the drill geometry would not affect the results as long as the same geometry is used in CD and UAD for a particular experimental study. Thus, even though the geometry of twist drill is different in Phase-2 as compared to that in Phase-1, the effective rake angles effect could still be studied by examining the theoretical effective rake and clearance angles for a particular drill geometry and performing the experiments for the same in a particular phase.

6.2.1 Effective normal rake angle and clearance angle calculation for the current drill geometry

The effective normal rake angle and axial clearance angle for the given tool geometry described for the main drill in Section 5.7.2.1, UAD parameters in Section 5.7.2.2 and machining parameters of 100 m/min cutting speed, 0.05 mm/rev feed rate was calculated by the method explained previously in Section 4.6 and are plotted in Figure 6-37 and Figure 6-38. As it can be seen in Figure 6-37 that the effective normal rake angle at 100 m/min cutting speed is still higher in UAD than that in CD which should results in lower thrust force in torque in UAD than that in CD. This was the reason for selecting 100 m/min cutting speed in the present experimental study.

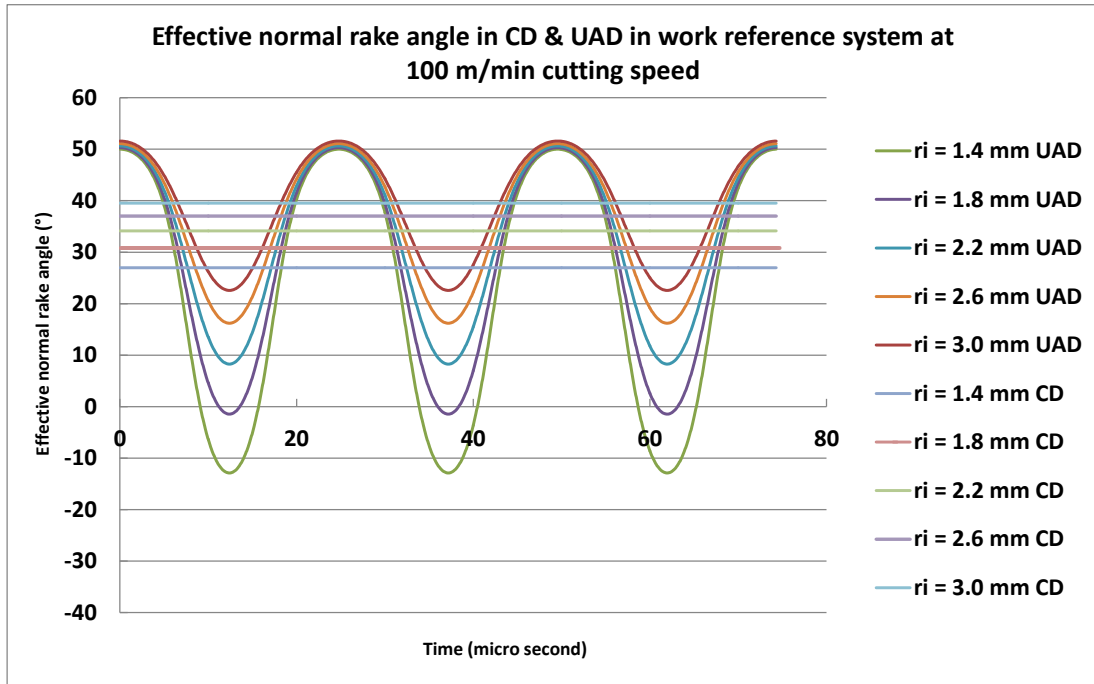


Figure 6-37: Effective normal rake angle in CD and UAD at 100 m/min cutting speeds for the given tool geometry and UAD parameters

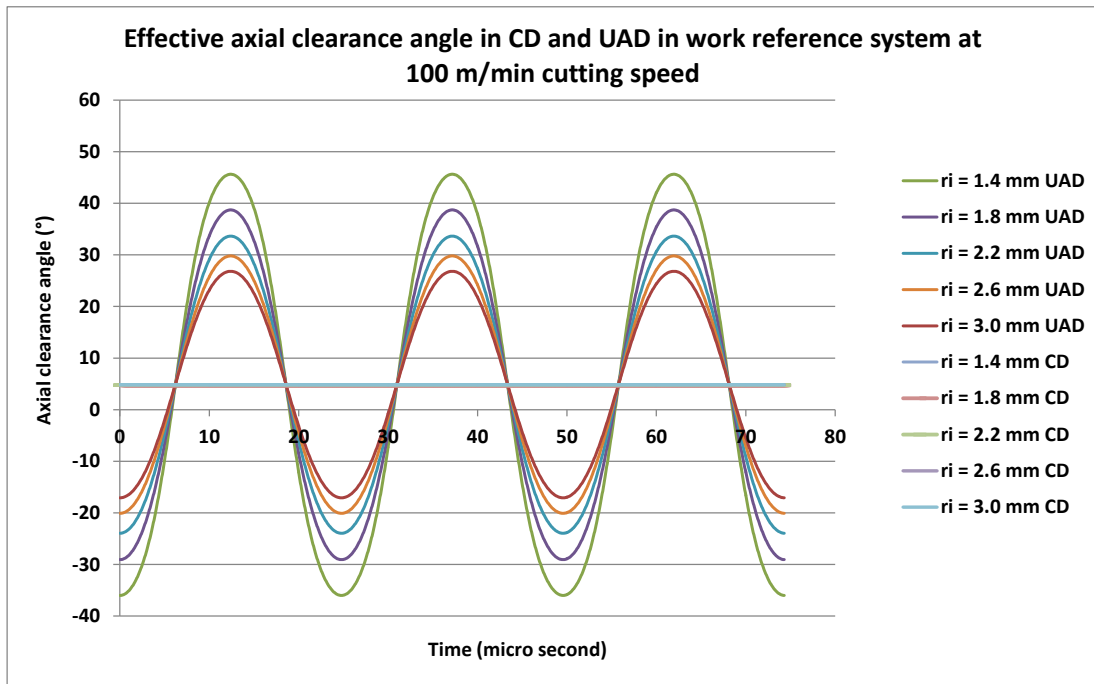


Figure 6-38: Effective axial clearance angle in CD and UAD at 100 m/min cutting speeds for the given tool geometry and UAD parameters

In the effective rake and clearance angle plots, Figure 6-37 and Figure 6-38, it can be seen that the effective normal rake angle at 100 m/min cutting speed in UAD attains maximum value of 51° and it is dynamically varying as compared to constant

(with respect to time) maximum 39° in CD. In addition, clearance angle is being negative in alternate time intervals in UAD.

6.2.2 Results of thrust force, torque and tool wear

6.2.2.1 Thrust force profile variation and measurement

Thrust force profiles during drilling of 1st hole in the cases of CD with and without pilot holes are shown in Figure 6-39 and Figure 6-40. The thrust force and profile in the case of 1st hole with CD without pilot-hole is shown in Figure 6-39. Point A in Figure 6-39 denotes the time instant when the chisel edge of twist drill comes into the contact of material. After point A, the drill starts propagating inside the CFRP material and the thrust force rises quickly to point B when the entire cutting edges of twist drill come in the contact of material. After this point, the drill progresses into the material and thrust force increases at a slower rate as compared to the thrust force increasing rate between points A and B. *This particular behaviour of twist drills, in this case, is discussed and explained further in section 6.2.4.1, later in this chapter.* At point C, the chisel edge of twist drill reaches towards the exit of hole, and the moment it crosses point C, the chisel edge exits from the hole and cutting edges start to progress further and exit the hole which produces the rapid reduction in thrust force and at last at point D, the cutting edges of twist also exit completely from the hole. The similar behaviour of thrust force was also observed in the case of UAD without pilot hole.

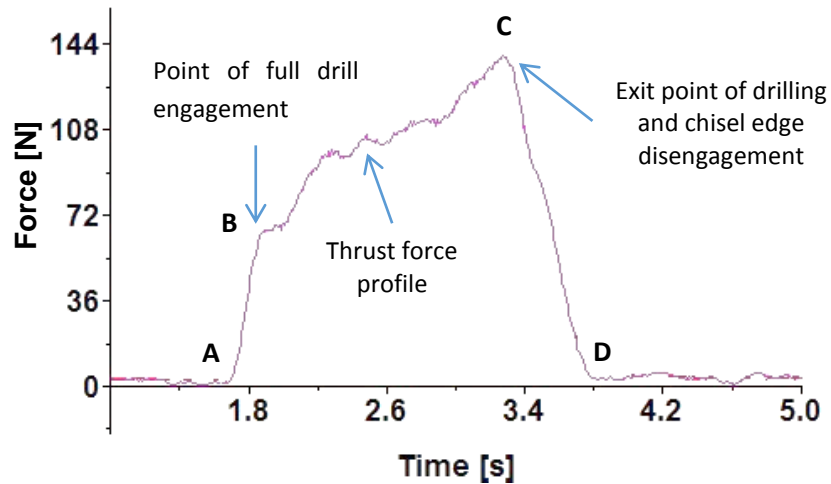


Figure 6-39: Thrust force profile in the case of CD without pilot-hole

In the case of previously drilled pilot-hole drilling, the thrust force profile was found in CD and UAD to be similar to as shown in Figure 6-40. It can be seen in Figure 6-40 that the point of chisel edge disengagement is apparent to be seen, however, the point of full drill engagement cannot be clearly seen the way it can be identified in Figure 6-39.

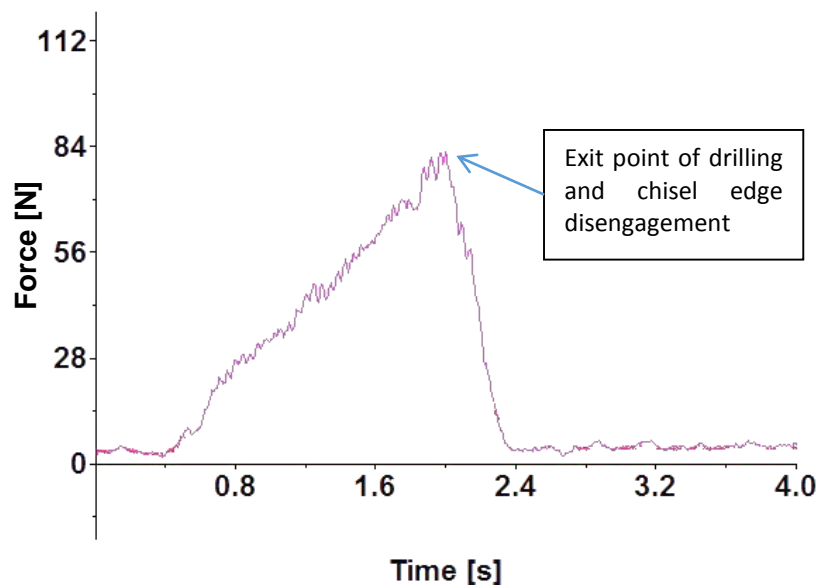


Figure 6-40: Thrust force profile in the case of CD with pilot-hole

Thus, in order to find out the point of full drill engagement, a small calculation was performed in the case of with and without pilot holes. Figure 6-41 shows a side

view of twist drill having measurements of chisel edge depth and full cutting edge depth along its axis (0.324 mm and 1.647 mm respectively).

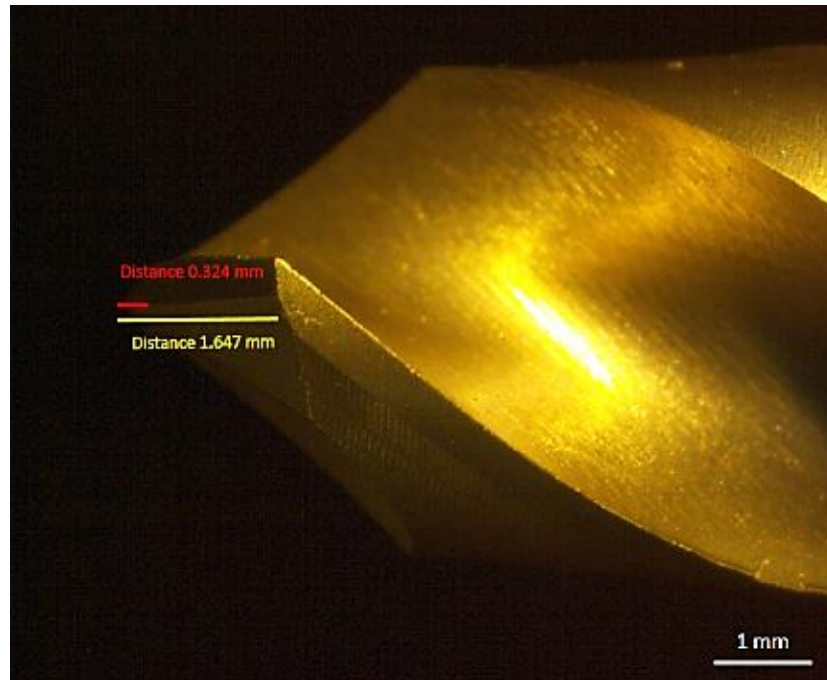


Figure 6-41: Side view of twist drill used in the present experiment

The cases of with and without pilot-hole drilling have been seen in Figure 6-42 in which length of the full cutting edge can be visualised in each case. In the case of without pilot-hole drilling, Figure 6-42 (a), the drill has to travel 1.647 mm at the entrance before entire cutting edges of drill could be in contact with the material. However, in the case of with pilot-hole drilling, Figure 6-42 (b), the drill travels $1.647 - 0.324 = 1.323$ mm distance at the entrance before entire cutting edge of drill could come in contact with the material.

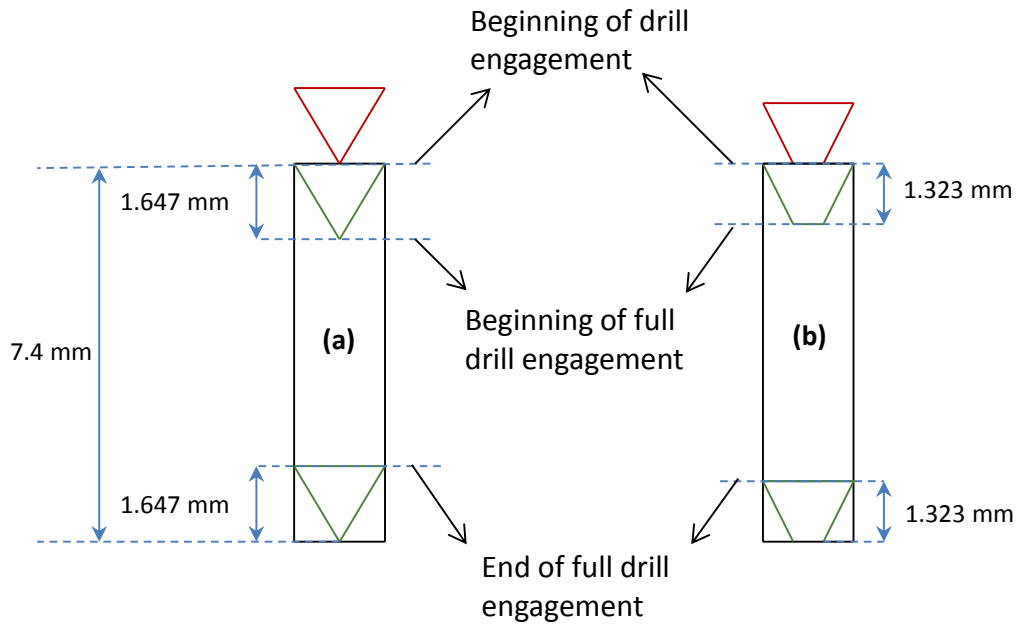


Figure 6-42: Schematic of full drill engagement in (a) without and (b) with pilot-hole drilling

The feed rate during drilling was 0.05 mm/rev i.e. 265.25 mm/min at the cutting speed of 100 m/min (5305 rpm) for 6 mm diameter drill. The thickness of work piece was 7.4 mm. Therefore, without a pilot hole, the distance travelled by twist drill during full drill engagement was $= 7.4 - (2 \times 1.647) = 4.106$ mm

While, with pilot hole, the distance travelled by drill during full drill engagement was =

$$7.4 - (2 \times 1.323) = 4.754 \text{ mm}$$

The time taken when drilling without a pilot hole was therefore $= (4.106 \times 60) / 262.5 = 0.929$ seconds and the time for drilling with a pilot hole was $(4.754 \times 60) / 262.5 = 1.087$ seconds.

Thus, due to thrust force gradually rising during the full drill engagement, the thrust force for analysis was considered to be the average between the time interval of 0.929 sec for the case of drilling without a pilot-hole and 1.087 sec for with pilot-

6: Experimental studies, results and discussions

Table 6-15: Thrust force data for CD

Hole number	CD without pilot			CD with pilot		
	Thrust Force 1 (N)	Thrust Force 2 (N)	Average (N)	Thrust Force 1 (N)	Thrust Force 2 (N)	Average (N)
1	113	121	117	54	55	55
2	261	283	272	159	185	172
3	452	445	448	319	323	321
4	543	541	542	437	424	431
5	626	636	631	528	500	514
6	685	683	684	590	569	580
7	745	735	740	630	620	625
8	795	776	785	663	666	664
9	838	815	826	722	693	708
10	884	860	872	747	731	739

Table 6-16: Thrust force data for UAD

Hole number	UAD without pilot			UAD with pilot		
	Thrust Force 1 (N)	Thrust Force 2 (N)	Average (N)	Thrust Force 1 (N)	Thrust Force 2 (N)	Average (N)
1	92	93	92	68	55	61
2	144	141	142	238	169	204
3	212	200	206	377	323	350
4	279	259	269	492	424	458
5	345	327	336	563	503	533
6	394	384	389	617	569	593
7	436	430	433	661	621	641
8	473	469	471	708	662	685
9	510	512	511	740	693	716
10	554	557	556	782	734	758

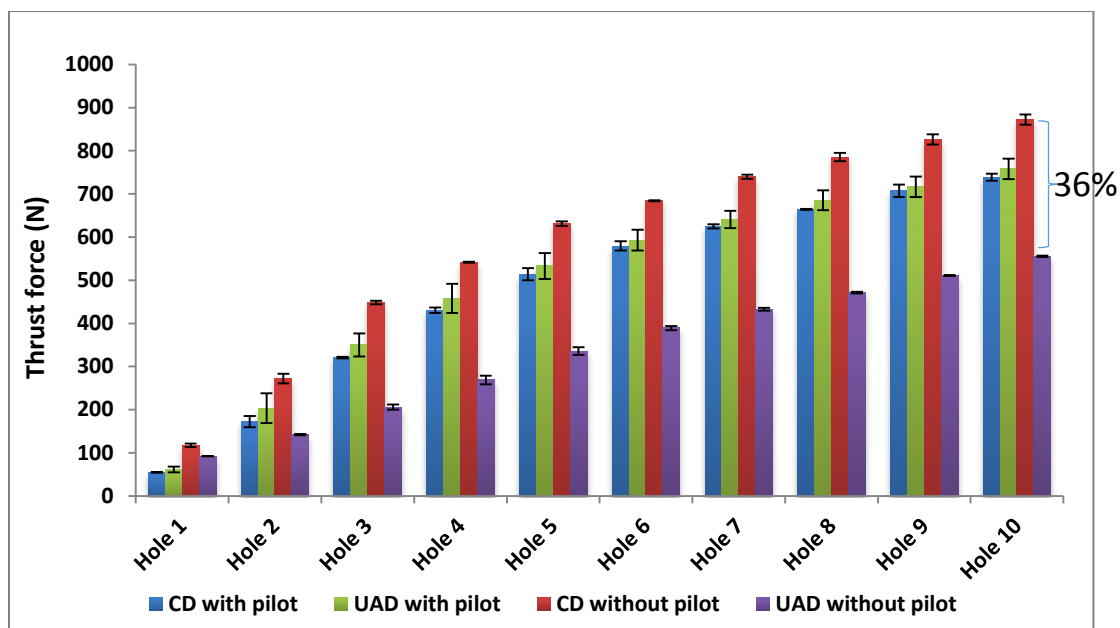


Figure 6-44: Thrust force variation obtained in the cases of CD, UAD, with and without pilot hole

Thrust force data in Figure 6-44, shows that average thrust force increases after drilling of each hole in every case of drilling. In a particular hole, average thrust force in CD without pilot was found to be more than that in CD with pilot. This is an expected result which has already been found and reported by other authors [18-21]. This happens because 40-60% of thrust force comes from chisel edge [131]. Therefore, in the case of previously drilled pilot-hole having an equivalent diameter of chisel edge, the force coming from chisel edge is avoided while drilling main hole and hence, it results in a lower thrust force than that in the case of without pilot-hole. Further, thrust force data reveals that in any particular hole, thrust forces in ‘CD with pilot’ and ‘UAD with pilot’ cases are similar and ‘UAD without pilot’ is lowest of the four drilling cases. This finding is further explained in Section 6.2.4.1.

6.2.2.2 Torque

Similar to thrust force, the average value of torque in one cycle was considered as the torque value for a particular drilled hole in all the drilling cases. The average

6: Experimental studies, results and discussions

value of drilling torque per drilling cycle in all the drilling sets is presented in Table 6-17 and Table 6-18 for CD and UAD respectively and is plotted in Figure 6-45. Error bars in Figure 6-44 display maximum and minimum values of average thrust forces in two repetitions.

Table 6-17: Torque data for CD

Hole number	CD without pilot			CD with pilot		
	Torque 1 (N-cm)	Torque 2 (N-cm)	Average (N-cm)	Torque 1 (N-cm)	Torque 2 (N-cm)	Average (N-cm)
1	37	35	36	32	30	31
2	35	39	37	35	33	34
3	36	35	36	36	34	35
4	40	34	37	37	35	36
5	37	35	36	38	38	38
6	39	35	37	40	36	38
7	39	37	38	40	35	38
8	39	36	38	41	36	38
9	39	37	38	39	36	37
10	40	42	41	40	42	41

Table 6-18: Torque data for UAD

Hole number	UAD without pilot			UAD with pilot		
	Torque 1 (N-cm)	Torque 2 (N-cm)	Average (N-cm)	Torque 1 (N-cm)	Torque 2 (N-cm)	Average (N-cm)
1	32	26	29	34	32	33
2	36	27	31	36	32	34
3	36	34	35	38	33	36
4	36	33	35	41	37	39
5	39	38	39	37	44	40
6	39	35	37	41	34	38
7	37	37	37	39	38	39
8	40	34	37	39	36	37
9	40	37	39	41	37	39
10	40	34	37	40	37	39

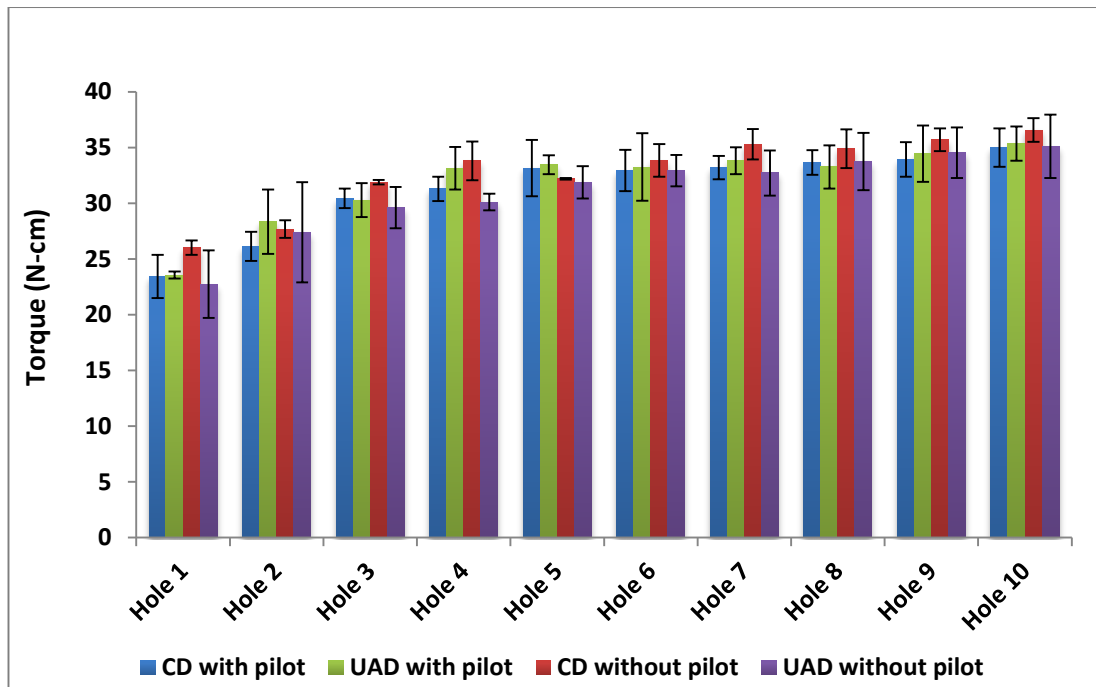


Figure 6-45: Average torque variation obtained in the cases of CD, UAD, with and without pilot hole

Average torque values plotted in Figure 6-45 indicates a gradual increase in torque with respect to number of holes in each drilling case. However, no clear difference could be observed amongst various cases of drilling in a particular hole. As the majority of torque comes from cutting edge, therefore, this indicates that average cutting forces during drilling are similar in each drilling case of conventional, ultrasonic, with and without pilot-holes.

6.2.2.3 Tool condition monitoring and wear measurement

The tool wear was monitored and quantified using the methodology explained in Section 5.6. Wear area in the flank surface of cutting edges was recorded after drilling of every hole in each drilling set using the methodology explained in Section 5.6.2. The images of tool flank surface for a new tool and tool wear after drilling of first hole in all the cases for CD and UAD along with SEM images of flank surfaces after drilling of 10 holes in CD, UAD with and without pilot hole drilling cases are presented in Appendix C.

The data of worn area in the flank surface of drilling tool in each drilling set is presented in Table 6-19 and Table 6-20 for the cases of CD and UAD respectively and is plotted further in Figure 6-46.

Table 6-19: Flank wear data for CD

Hole number	CD without pilot			CD with pilot		
	Tool wear area 1 (mm ²)	Tool wear area 2 (mm ²)	Average (mm ²)	Tool wear area 1 (mm ²)	Tool wear area 2 (mm ²)	Average (mm ²)
1	0.198	0.209	0.204	0.121	0.178	0.15
2	0.482	0.463	0.473	0.342	0.415	0.379
3	0.715	0.694	0.705	0.59	0.636	0.613
4	0.926	0.921	0.924	0.826	0.856	0.841
5	1.121	1.08	1.101	0.998	1.041	1.02
6	1.268	1.19	1.229	1.169	1.194	1.182
7	1.338	1.332	1.335	1.263	1.32	1.292
8	1.519	1.46	1.49	1.323	1.379	1.351
9	1.55	1.586	1.568	1.457	1.532	1.495
10	1.593	1.656	1.625	1.589	1.62	1.605

Table 6-20: Flank wear data for UAD

Hole number	UAD without pilot			UAD with pilot		
	Tool wear area 1 (mm ²)	Tool wear area 2 (mm ²)	Average (mm ²)	Tool wear area 1 (mm ²)	Tool wear area 2 (mm ²)	Average (mm ²)
1	0.134	0.12	0.127	0.213	0.194	0.204
2	0.233	0.214	0.224	0.519	0.438	0.479
3	0.373	0.318	0.346	0.764	0.694	0.729
4	0.502	0.451	0.477	0.949	0.86	0.905
5	0.612	0.597	0.605	1.174	1.042	1.108
6	0.716	0.717	0.717	1.258	1.219	1.239
7	0.847	0.825	0.836	1.304	1.317	1.311
8	0.914	0.93	0.922	1.422	1.43	1.426
9	1.026	1.043	1.035	1.448	1.593	1.521
10	1.111	1.098	1.105	1.633	1.677	1.655

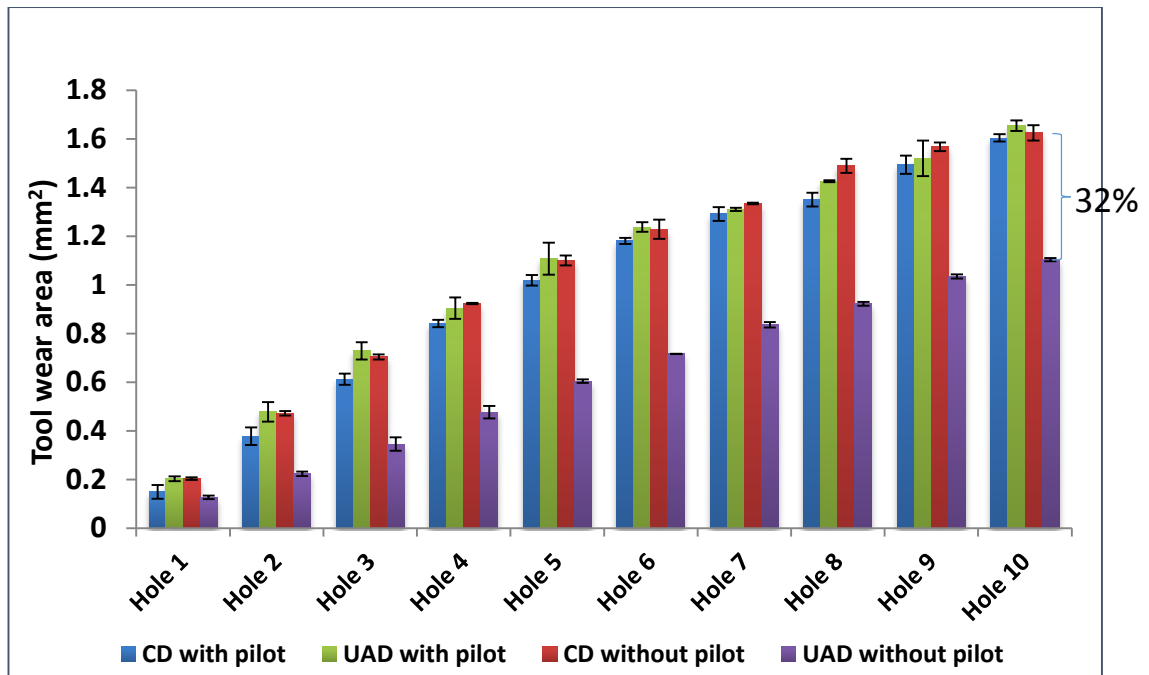


Figure 6-46: Variation of tool flank wear in the cases of CD, UAD with and without pilot holes

The lowest tool wear was found to be in the case of UAD without pilot. When comparing the cases of CD without pilot and UAD without pilot, the average tool wear was found to be 32% lower in UAD without pilot than that in CD without pilot after drilling of 10 holes. However, when comparing the cases of CD with pilot, UAD with pilot and CD without pilot, no clear difference could be observed in flank surface wear area values. This finding is further explained along with tool wear and thrust force in Section 6.2.4.1.

6.2.2.4 Chisel edge wear

Similar to flank wear area on cutting edges, wear on the chisel edge was also recorded in the cases of CD and UAD without pilot-hole. The Chisel edge wear is presented in Table 6-21 and is plotted in Figure 6-47. In addition, SEM images displaying the condition of chisel edge after drilling of 10 holes in CD and UAD is shown in Figure 6-48 and Figure 6-49 respectively.

6: Experimental studies, results and discussions

Table 6-21: Data table for wear area in chisel edge in CD and UAD without pilot hole tests

Hole Number	CD without pilot (mm ²)			UAD without pilot (mm ²)		
	CD 1	CD 2	Average	UAD 1	UAD 2	Average
1	0.014	0.014	0.014	0.010	0.009	0.009
2	0.021	0.021	0.021	0.018	0.011	0.015
3	0.023	0.028	0.026	0.025	0.015	0.020
4	0.036	0.032	0.034	0.027	0.017	0.022
5	0.039	0.034	0.037	0.032	0.018	0.025
6	0.044	0.036	0.040	0.034	0.018	0.026
7	0.046	0.039	0.043	0.036	0.019	0.028
8	0.049	0.042	0.046	0.037	0.019	0.028
9	0.054	0.048	0.051	0.039	0.020	0.030
10	0.063	0.051	0.057	0.041	0.021	0.031

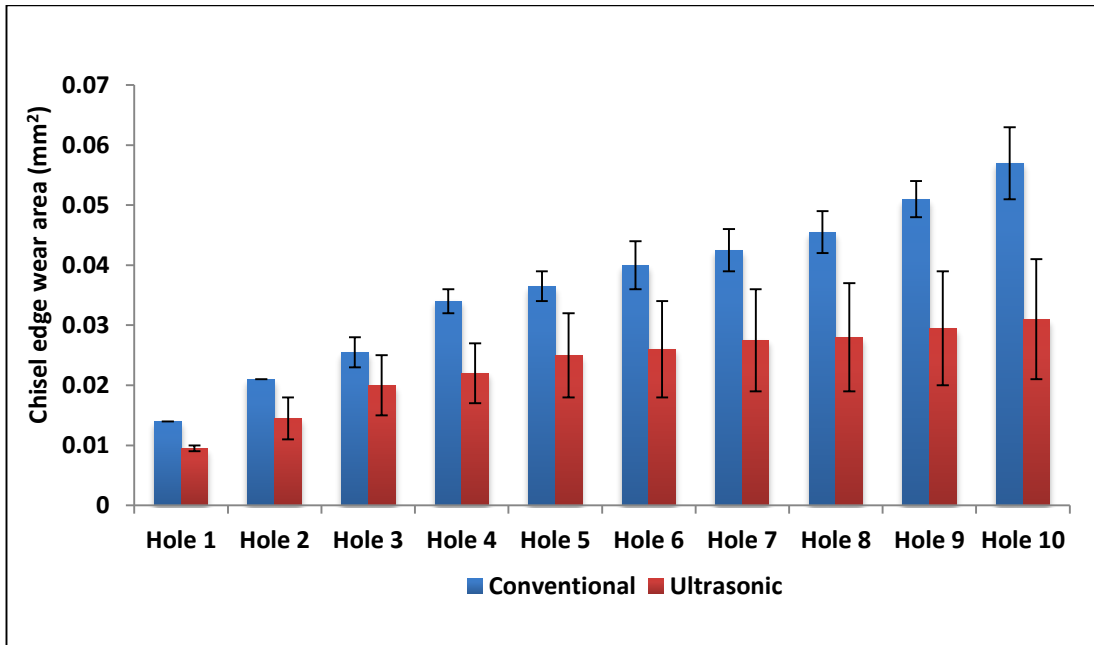


Figure 6-47: Chisel edge wear area after drilling of every hole in the cases of conventional and ultrasonic without pilot-hole drilling.

6: Experimental studies, results and discussions

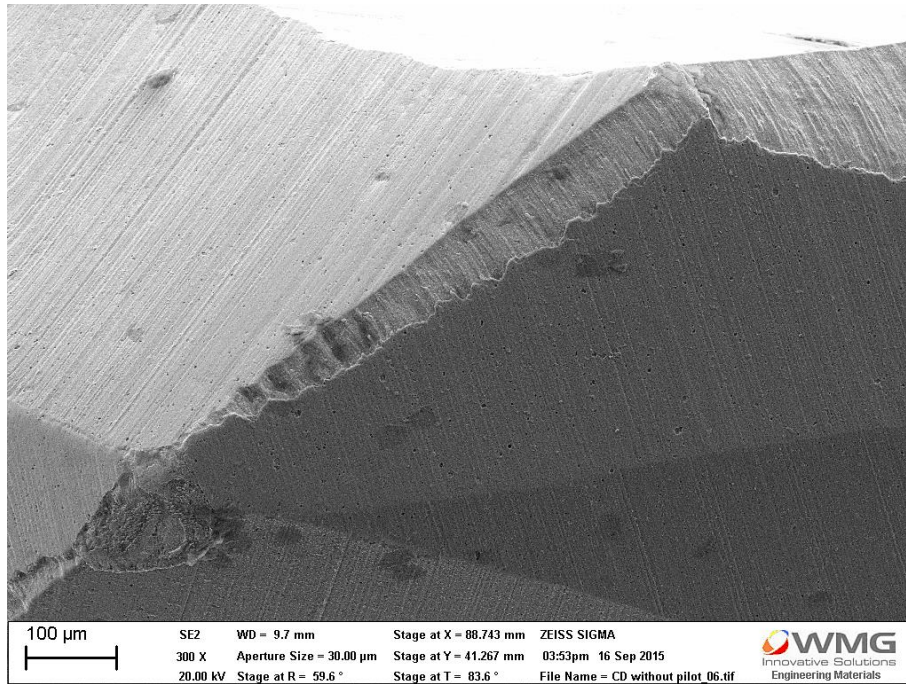


Figure 6-48: SEM image of chisel edge displaying chisel edge condition in the case of CD without pilot hole drilling after drilling of 10 holes

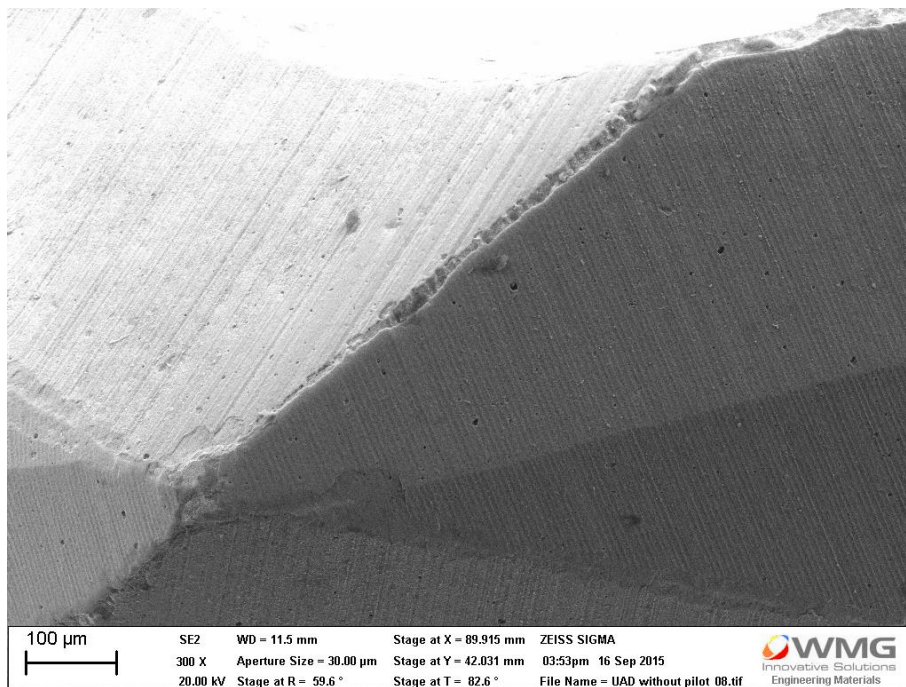


Figure 6-49: SEM image of chisel edge displaying chisel edge condition in the case of UAD without pilot hole drilling after drilling of 10 holes

With the chisel edge wear area data plotted in Figure 6-47 and the SEM images of chisel edges in Figure 6-48 and Figure 6-49 in CD and UAD respectively it becomes evident that chisel-edge wear after 10 holes in UAD is lower than that in CD.

6.2.3 Results of damage analysis

Damage quantification analysis was performed by sectioning the holes away from central diametrically opposite points and then mounting and polished them back to the centre as using the methodology discussed in Section 5.5. Due to a large number of drilled holes, it was impractical to section, mount, polish and analyse every hole. Therefore, 1st, 5th and 10th holes were selected for damage analysis. Optical stereo microscopy was performed on the polished samples to visualize the damage at the entrance, exit and internal damage in a hole in two sides of the hole. Similar to Phase-1, the damage in a drilled hole has been segmented into three categories:

- Maximum damage at entrance
- Maximum damage at exit
- Internal damage

6.2.3.1 *Maximum damage at entrance and exit*

In order to measure damage at the entrance, the entrance of the both sides of hole was analysed using an optical microscope and the damage was quantified with the methodology explained in Section 5.5.3 using the optical microscope. The same method was repeated for all the test repetitions and the average of those repetitions was considered for analysis. The example for maximum damage depth measurement at the entrance is shown in Figure 6-50 and the maximum damage depth at 1st. 5th

and 10th hole is plotted further in Figure 6-51 for all the cases of CD, UAD, with and without pilot-hole drilling.

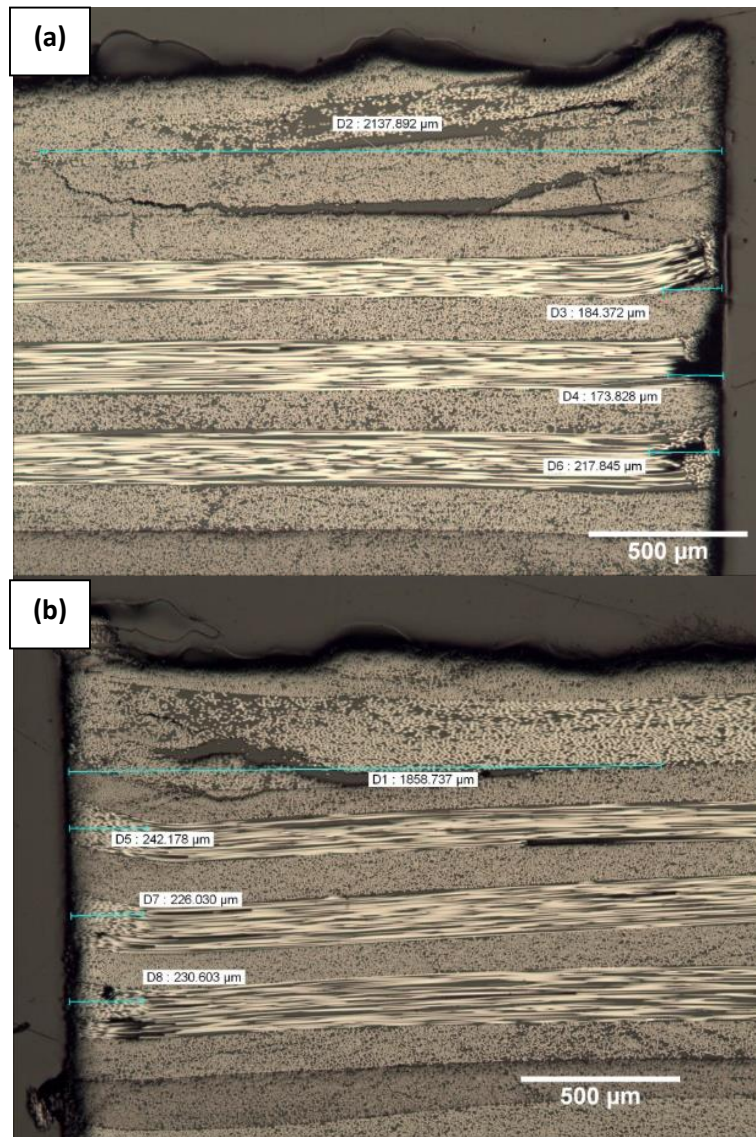


Figure 6-50: Maximum damage depth measurement in (a) side 1 and (b) side 2 of 5th hole in the case of CD with pilot. The overall maximum depth at entrance for this hole would be 2137.892 μm which is the maximum of the two measurements.

Table 6-22: Data table for maximum damage at entrance in the cases of with and without pilot-holes in CD

Hole number	CD without pilot (μm)			CD with pilot (μm)		
	Damage depth 1	Damage depth 2	Average	Damage depth 1	Damage depth 2	Average
1	0	0	0	0	0	0
5	2330	1860	2100	2140	1480	1810
10	2040	1670	1850	1910	1890	1900

Table 6-23: Data table for maximum damage at entrance in the cases of with and without pilot-holes in UAD

Hole number	UAD without pilot (μm)			UAD with pilot (μm)		
	Damage depth 1	Damage depth 2	Average	Damage depth 1	Damage depth 2	Average
1	0	0	0	0	0	0
5	1210	1420	1310	1980	1680	1830
10	980	1730	1350	1590	2150	1870

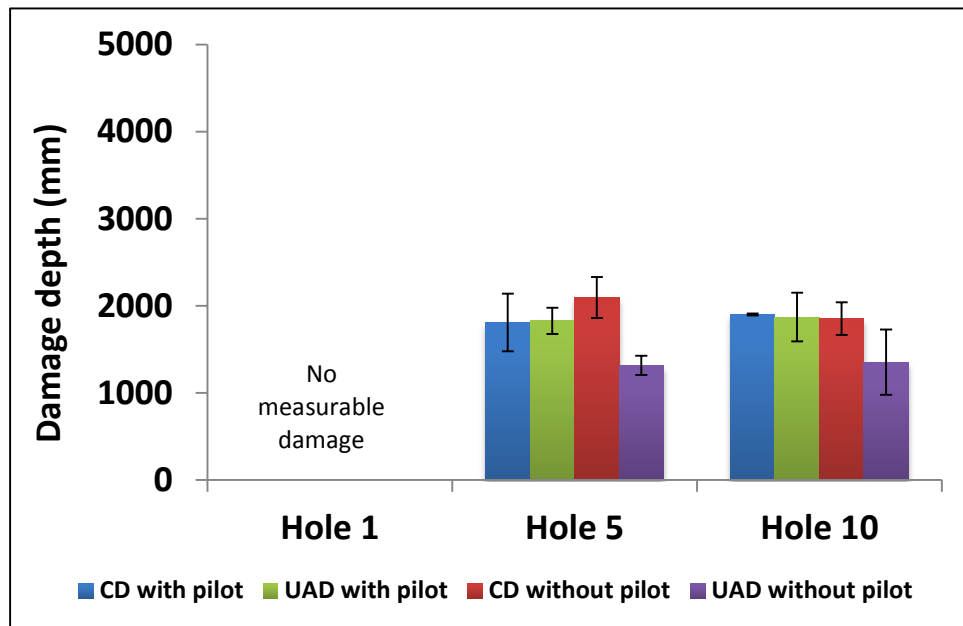


Figure 6-51: Maximum damage depth at entrance for 1st, 5th and 10th hole in all the cases of conventional, ultrasonic, with and without pilot-hole drilling

From Figure 6-51, it can be seen that there was no damage at entrance of the 1st hole in any case of drilling. The 5th and 10th hole show similar level of maximum damage depth at entrance. The lowest average value of damage at entrance is found

in the case of UAD without pilot in 5th and 10th holes. Damage at rest of the drilling cases seems to be at similar level at entrance of holes.

Similar to maximum damage depth at entrance, the damage depth at exit was also measured and analysed. The individual values of maximum damage at exit in 1st, 5th and 10th holes in conventional drilling (with and without pilot-holes) is presented in Table 6-24 and that for UAD (with and without pilot-holes) is presented in Table 6-25. Further, the maximum damage at exit is plotted in Figure 6-52 for all the cases of conventional, ultrasonic, with and without pilot-hole drilling.

Table 6-24: Data table for maximum damage at exit in the cases of conventional without and with pilot holes drilling

Hole number	CD without pilot (μm)			CD with pilot (μm)		
	Damage depth 1	Damage depth 2	Average	Damage depth 1	Damage depth 2	Average
Hole 1	1377	1977	1680	1159	1642	1400
Hole 5	3736	3832	3780	2566	2606	2590
Hole 10	3820	4192	4010	4201	3890	4050

Table 6-25: Data table for maximum damage at exit in the cases of ultrasonic assisted without and with pilot holes drilling

Hole number	UAD without pilot (μm)			UAD with pilot (μm)		
	Damage depth 1	Damage depth 2	Average	Damage depth 1	Damage depth 2	Average
Hole 1	934	1343	1140	1934	2177	2060
Hole 5	2876	2308	2590	2850	3479	3160
Hole 10	3384	2794	3090	3727	3991	3860

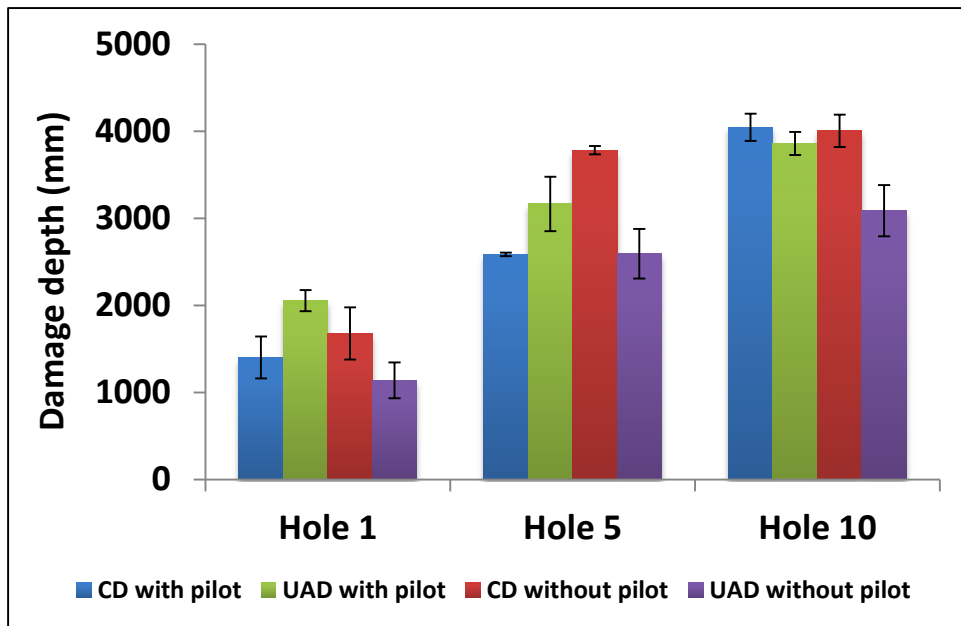


Figure 6-52: Plot of Maximum damage depth at exit for 1st, 5th and 10th hole in all the cases of conventional, ultrasonic, with and without pilot-hole drilling

From the data of maximum damage at the exit, it can be observed that the damage increase with respect to number of holes in all the cases. This happened because as the number of drilled holes increased, tool wear increased which caused a further increase in thrust force. Therefore, due to increase in thrust force damage at the exit is increased. The fact of increasing exit delamination due to increase in thrust force has been established and presented by the other authors [13]. This variation in damage data is further explained and discussed in section 6.2.4.2.

6.2.3.2 Internal damage from the polished samples

Internal damage consists of fibre pull out and fibre disorientation. Optical microscopy was performed to quantify the depth of fibre pull out and fibre disorientation in both sides of a polished sample as shown in Figure 6-53 and Figure 6-54.

6: Experimental studies, results and discussions

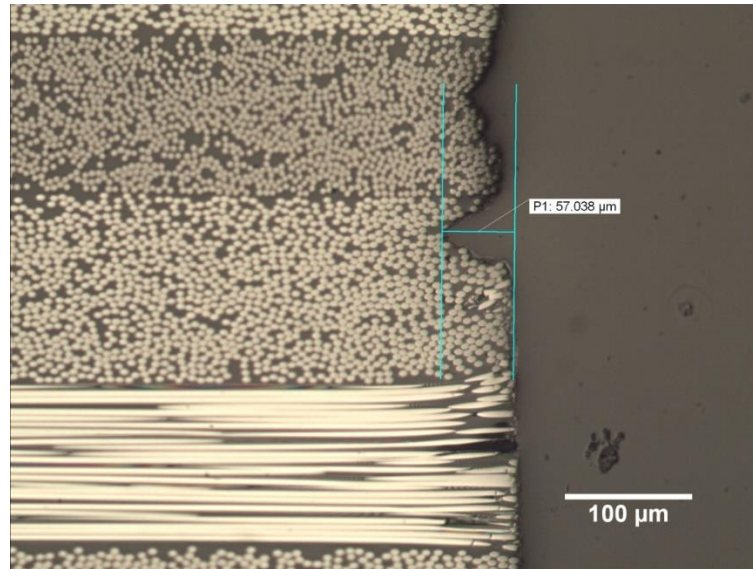


Figure 6-53: Depth of Fibre pull out measurement in the 1st hole in the case of conventional drilling with pilot hole

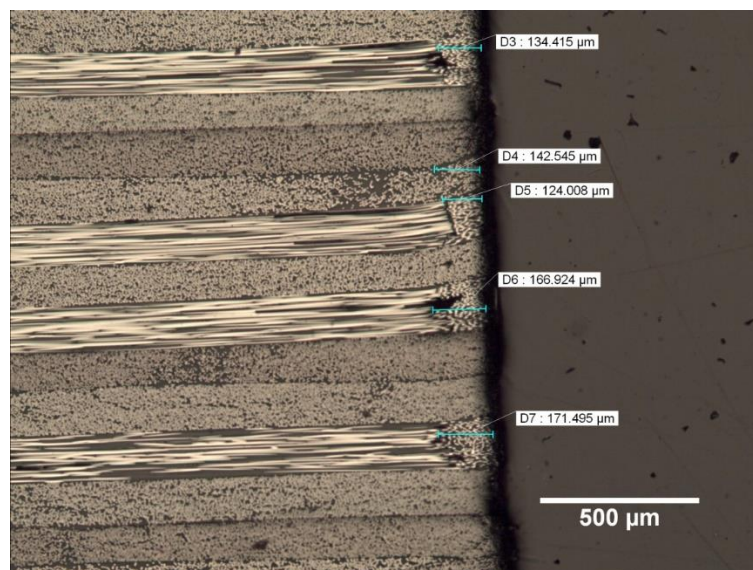


Figure 6-54: Depth of Fibre disorientation measurement in the 5th hole in the case of conventional drilling with pilot hole

In addition, it was observed that in the first hole, the depth of damage at the starting of hole i.e., near the entrance of hole was lower than that near exit as shown the images Figure 6-55 and Figure 6-56.

6: Experimental studies, results and discussions

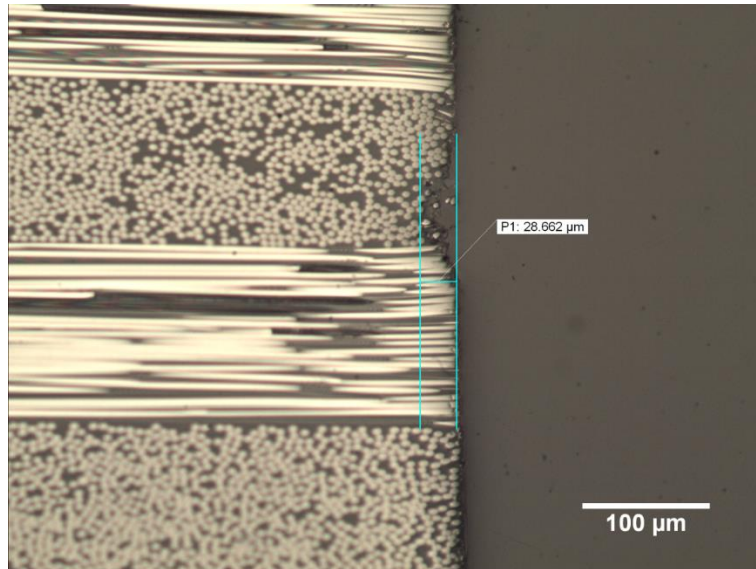


Figure 6-55: Damage depth near entrance in the 1st hole in the case of conventional with pilot-hole drilling

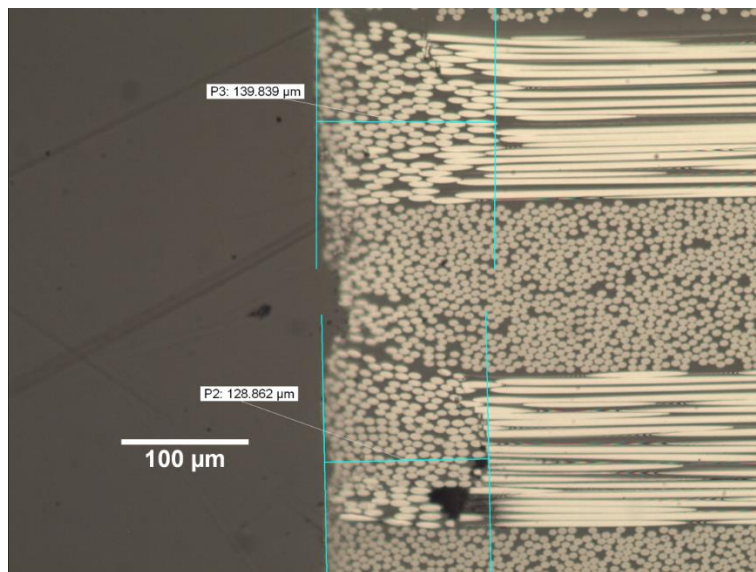


Figure 6-56: Damage depth near exit in the 1st hole in the case of conventional with pilot-hole drilling

Figure 6-55 is an image of fibre pull out damage near hole-entrance having 28.662 μm and Figure 6-56 is an image of fibre disorientation near hole-exit having 139.839 μm depth of damage. Thus, Figure 6-55 and Figure 6-56 indicate that the damage depth near hole-entrance is lower than that near hole-exit. The average of damage thus measured in the both sides in a sectioned hole was considered as the

average internal damage in a hole. Data for average internal damage in CD and UAD is presented in Table 6-26 and Table 6-27 and further plotted in Figure 6-57.

Table 6-26: Data table for average internal damage in the cases of CD with and without pilot-holes

Hole number	CD without pilot (μm)			CD with pilot (μm)		
	Damage depth 1	Damage depth 2	Average	Damage depth 1	Damage depth 2	Average
Hole 1	74	79	76	69	79	74
Hole 5	134	163	148	165	149	157
Hole 10	162	130	146	194	159	177

Table 6-27: Data table for average internal damage in the cases of UAD with and without pilot-holes

Hole number	UAD without pilot (μm)			UAD with pilot (μm)		
	Damage depth 1	Damage depth 2	Average	Damage depth 1	Damage depth 2	Average
Hole 1	60	67	63	73	71	72
Hole 5	113	138	125	164	138	151
Hole 10	124	147	136	156	155	155

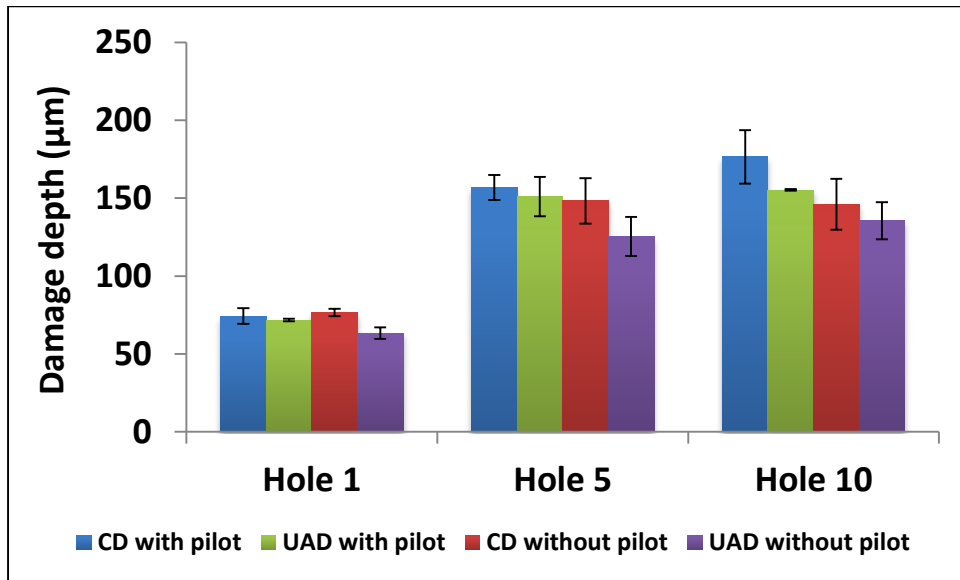


Figure 6-57: Plot of internal damage in 1st, 5th and 10th holes in all the cases of conventional, ultrasonic, with and without pilot-hole drilling

Variation in internal damage in Figure 6-57 shows that internal damage increases as the number of drilled holes increases in all the cases of CD, UAD, with and without pilot-holes. Also, it can be seen in Figure 6-57 that average internal damage

in 1st hole is lowest in UAD without pilot case. In the other cases there is a similar internal damage level in 1st, 5th and 10th holes and there is no clear difference between the damage levels across various cases of CD with and without pilot and UAD with and without pilot-hole cases. This result is explained further in Section 6.2.4.2.

6.2.3.3 *Machined surface and burnt matrix*

Machined surfaces in 1st, 5th and 10th holes of every set were examined in the SEM. When comparing the images of the matrix in the phase with those discussed in Section 6.1.4 of Phase-1, it suggests that the matrix has been thermally affected to a greater extent in this phase. As the smoke was visually observed during this experiment unlike that in Phase-1, it suggests that the matrix was burnt in this experiment in both conventional and ultrasonic samples in 5th and 10th holes. SEM images of burnt matrix in the 5th hole of CD without pilot and UAD without pilot-hole drilling are shown in Figure 6-58 and Figure 6-59 respectively. Also, images of burnt matrix in the machined surfaces of conventional with pilot-hole and ultrasonic without pilot-hole drilling are shown in Figure 6-60 and Figure 6-61.

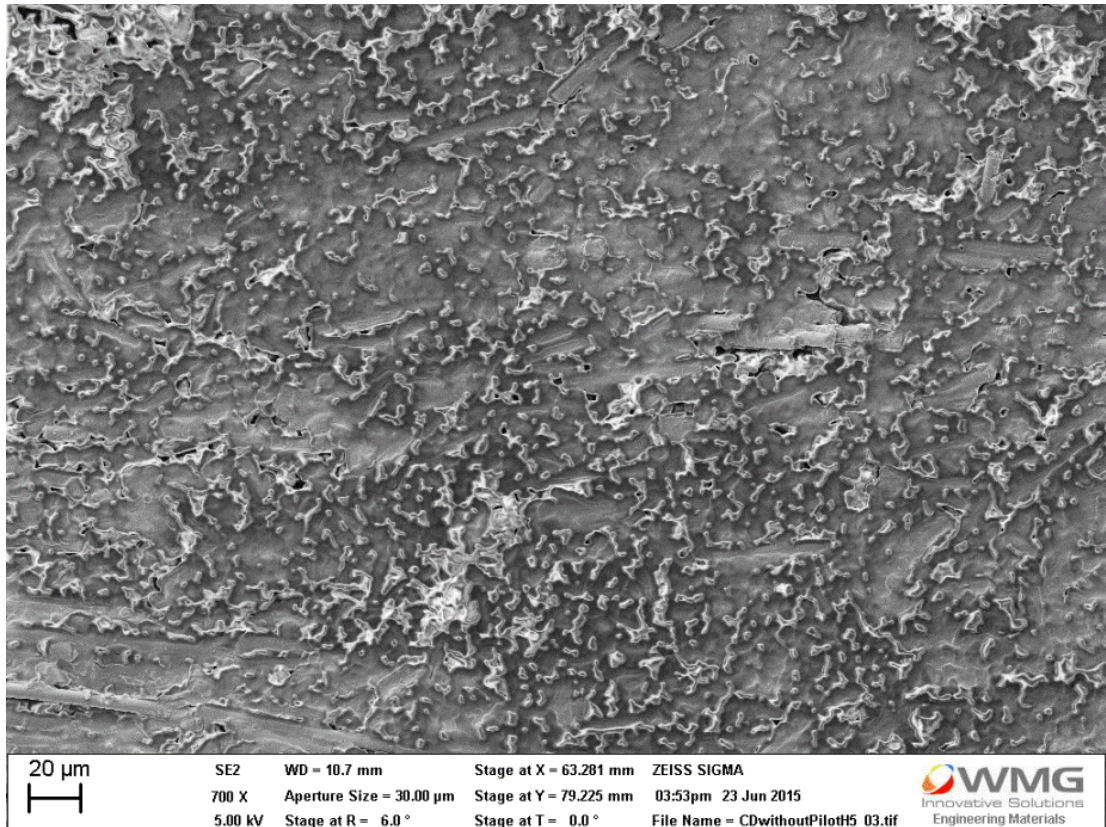


Figure 6-58: Burnt matrix in 5th hole of conventional without pilot-hole drilling

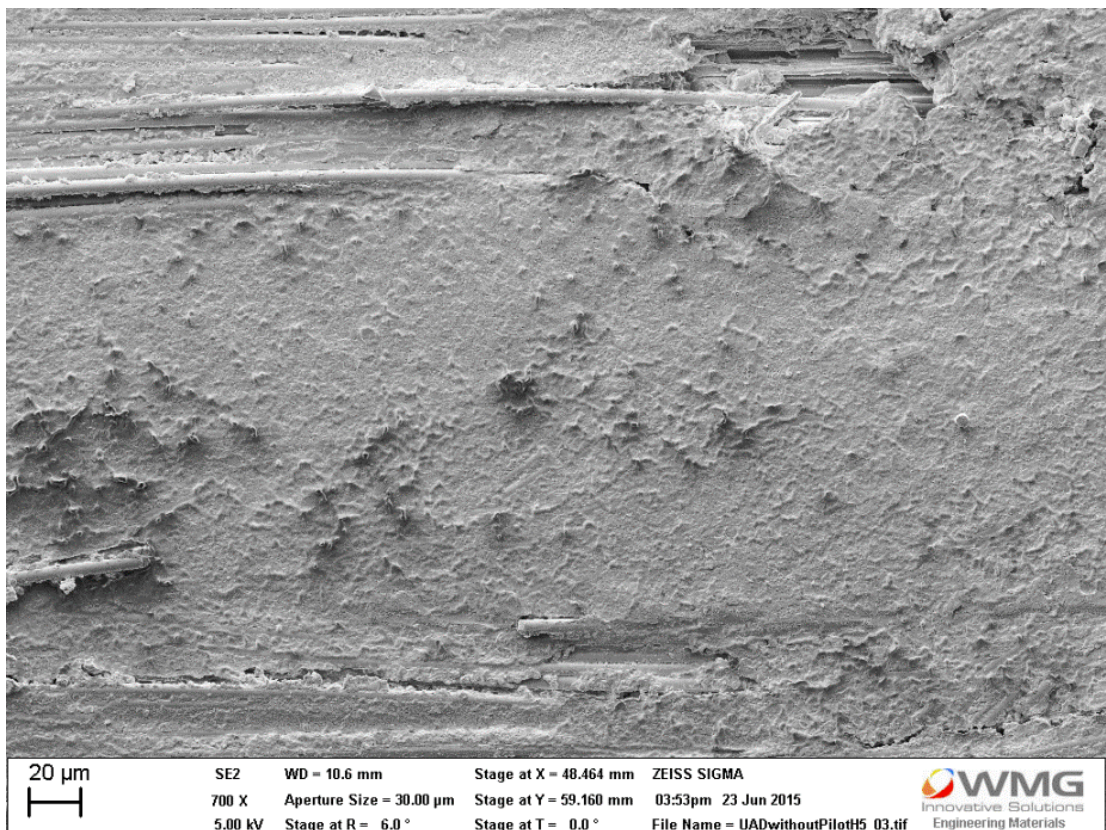


Figure 6-59: Traces of burnt matrix in 5th hole of Ultrasonic without pilot-hole drilling

6: Experimental studies, results and discussions

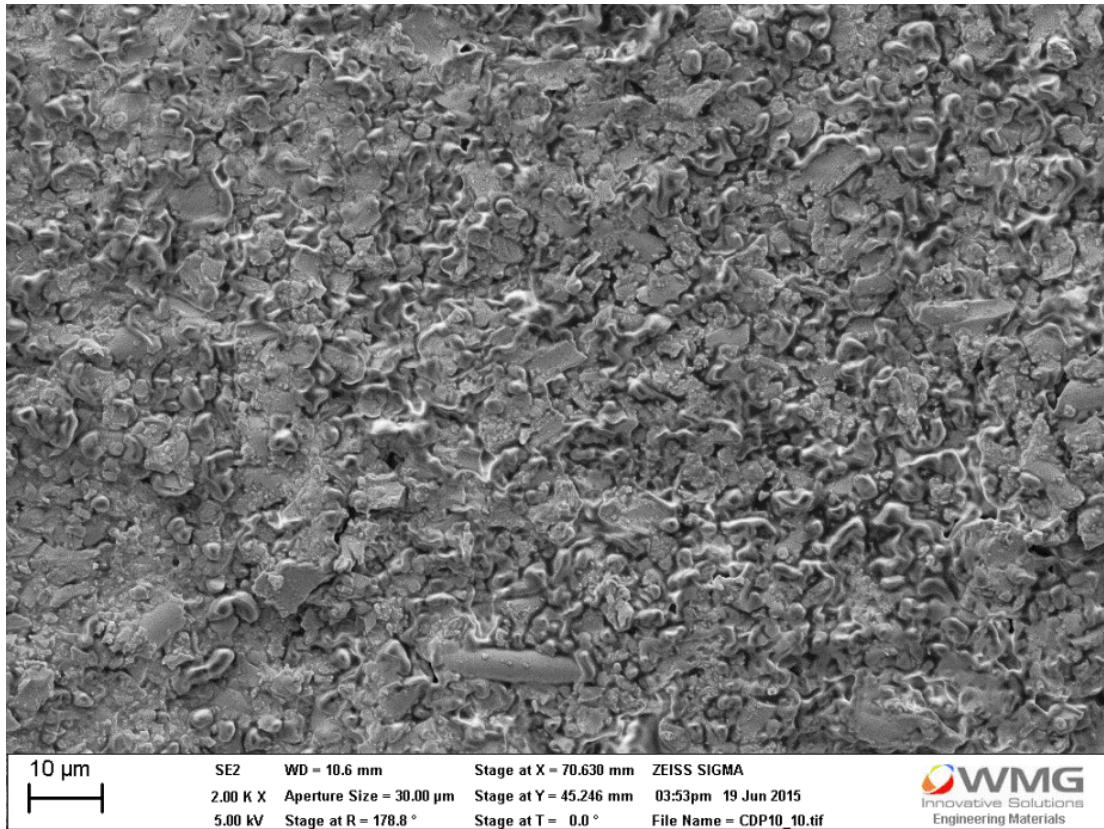


Figure 6-60: Burnt matrix in 10th hole of conventional with pilot-hole drilling

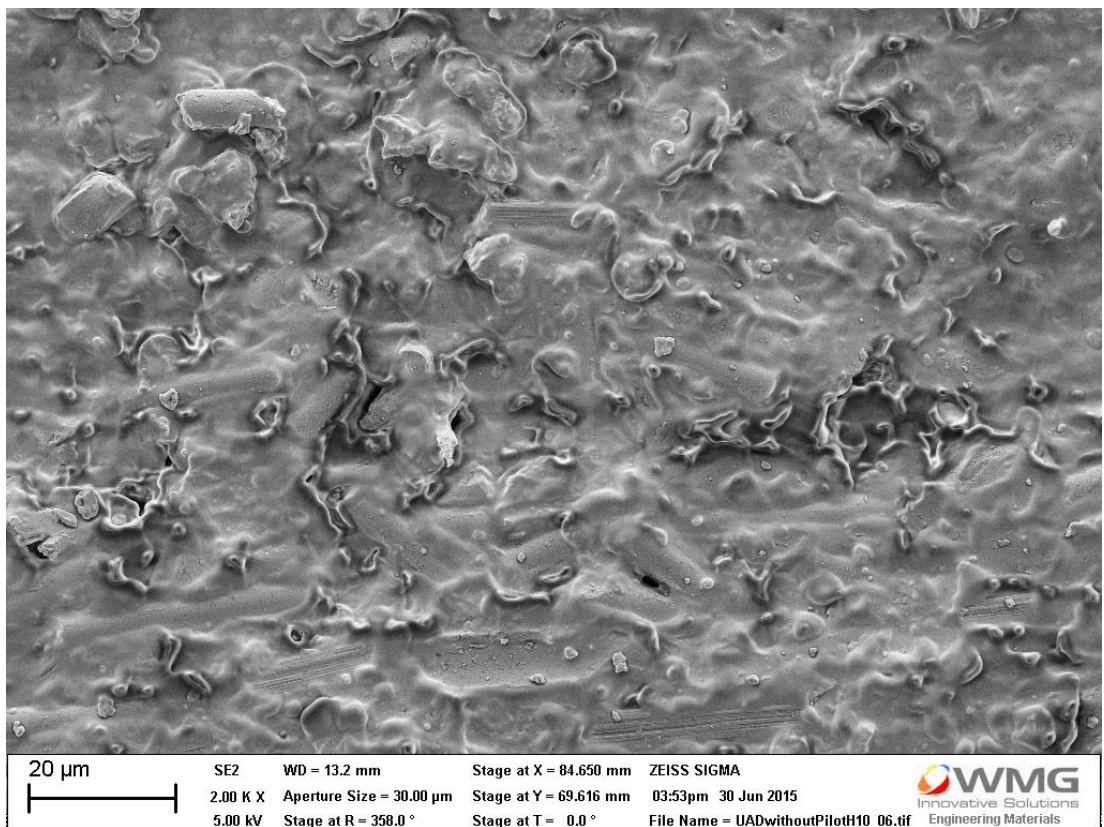


Figure 6-61: Burnt matrix in 10th hole of Ultrasonic without pilot-hole drilling

The burning of the matrix happened because of excessive tool wear. Since the tool was excessively worn out, more contact area of the flank surface of the drill was exposed to workpiece surface which resulted in high friction between the flank surface and workpiece resulting in excessive heat. Since CFRP material is a poor conductor of heat, the heat could not be conducted away and hence this generated heat resulted in a temperature at which matrix phase started burning. The burning of the matrix was also visually observed during the experiment as white smoke was observed coming out of the CFRP material during drilling experiment. Thus burning of the matrix can be related to tool wear. As mentioned previously, the tool wear and thrust force were lowest in the case of UAD without pilot-hole drilling, therefore, it can be concluded that the amount of matrix burning would have been lowest in UAD without pilot-hole drilling experiment. The visual inspection of SEM images also suggests the same. When comparing Figure 6-58 and Figure 6-59, it can be seen that the incidences of burnt matrix appeared more in CD without pilot-hole, Figure 6-58, as compared to those in UAD without pilot-hole, Figure 6-59. Similarly, upon comparing Figure 6-60 and Figure 6-61, it can be seen that incidences of burnt matrix in conventional with pilot-hole is more than those in ultrasonic without pilot-hole. However, more quantitative direct evidence through cutting temperature measurement techniques is required to prove this observation. Nevertheless, tool wear and thrust force data indicate towards low matrix burning in the case of UAD without pilot-hole indirectly.

6.2.3.4 Chip fragments analysis

The chip fragments were analysed in SEM after mounting them with double sided carbon tape followed by gold coating. Chip fragments obtained from first, fifth and tenth holes were analysed in SEM from all the cases. There was not any clear

6: Experimental studies, results and discussions

difference between CD and UAD, Figure 6-62 and Figure 6-63. However, evidence of burnt matrix was found in the chip fragments obtained from fifth and tenth holes in all the cases, Figure 6-64 and Figure 6-65.

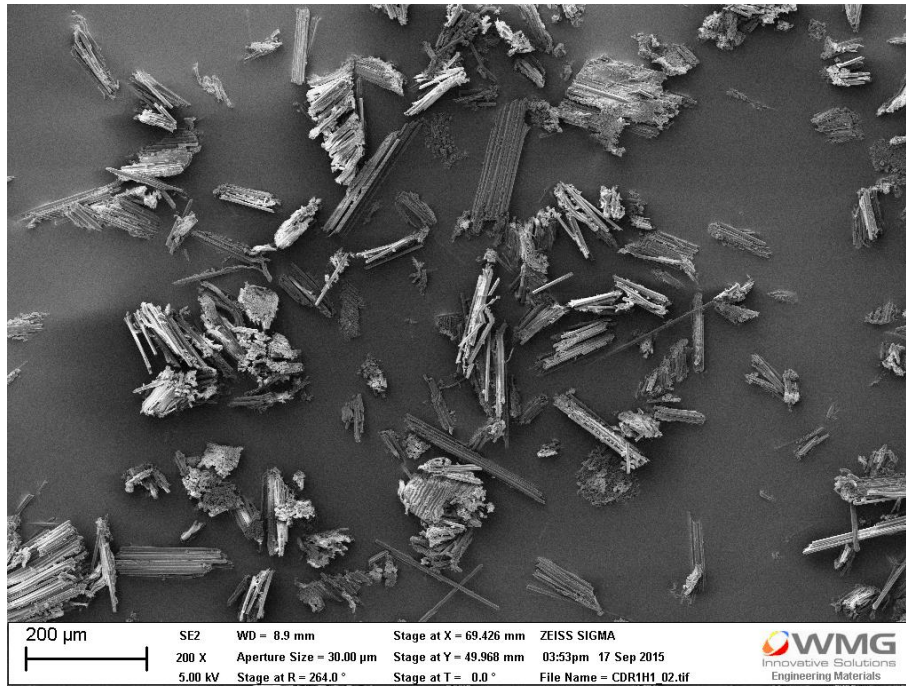


Figure 6-62: Chip fragments obtained at 100 m/min cutting speed in CD without pilot from 1st hole

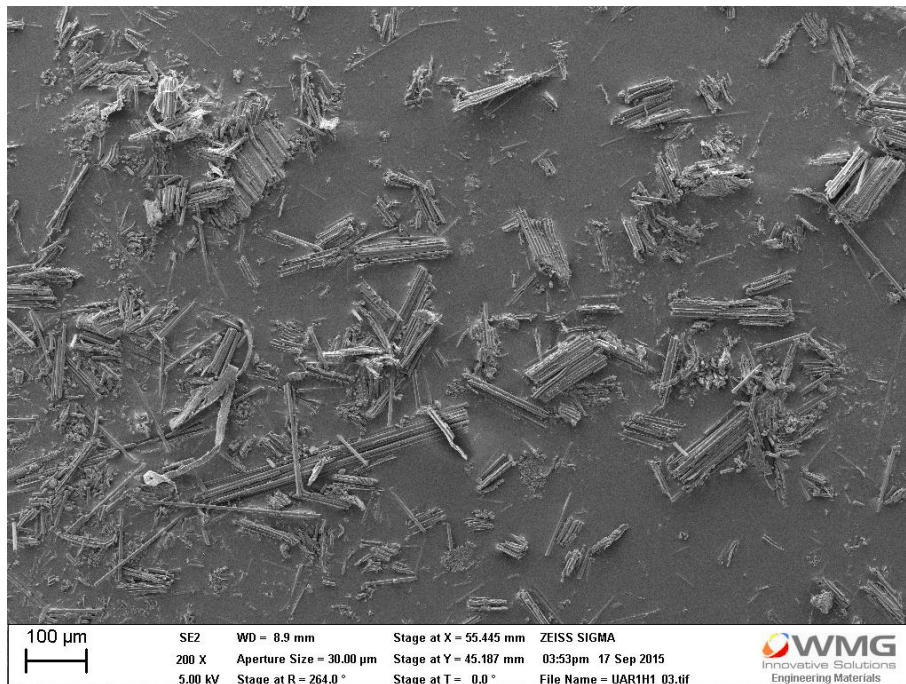


Figure 6-63: Chip fragments obtained at 100 m/min cutting speed in UAD without pilot from 1st hole

6: Experimental studies, results and discussions

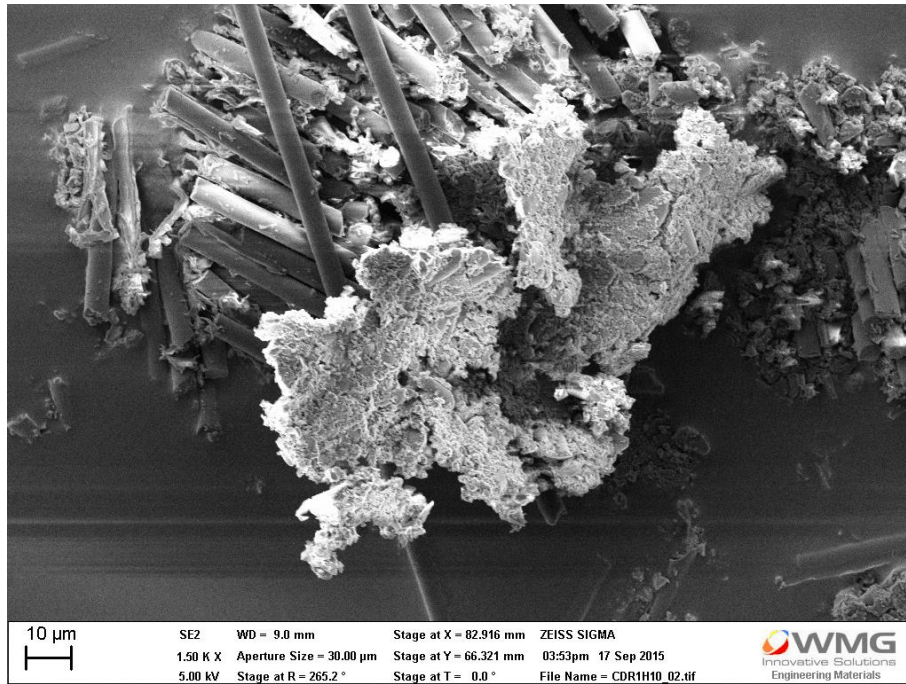


Figure 6-64: Burnt matrix in the chip fragments at 100 m/min cutting speed in CD without pilot from 10th hole

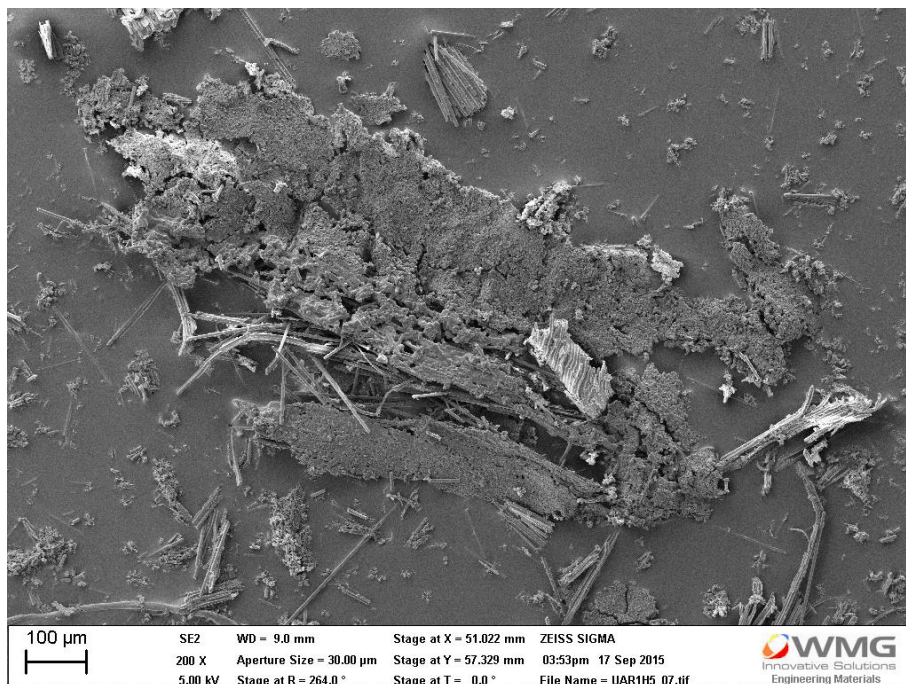


Figure 6-65: Burnt matrix in the chip fragments obtained at 100 m/min cutting speed and 0.05 mm/rev feed rate in UAD without pilot from 5th hole

6.2.4 Discussion

6.2.4.1 Thrust force, tool wear and torque

Thrust force variation in Figure 6-44 and tool-wear in Figure 6-46 show that thrust force and tool wear increase with respect to number of drilled holes in each drilling case. This can be explained from the fact that after drilling of every hole, tool-wear increases in every case of drilling which is evident from Figure 6-39 and Figure 6-40. The increase in tool-wear causes an increase in cutting and thrust forces during machining. Thus, tool wear and thrust force kept on increasing after drilling of every hole. A similar finding has been reported by Chen [10].

As mentioned previously in Section 6.2.2.1, thrust force data plotted in Figure 6-44 reveals that in any particular hole, thrust force in ‘CD with pilot’ and ‘UAD with pilot’ cases are similar and that in UAD without pilot test is lowest of the four drilling tests. In order to understand and explain this result, thrust force, tool flank surface wear and torque shown in Figure 6-44, Figure 6-46 and Figure 6-45 respectively, would have to be considered simultaneously. Since chisel edge is not involved in the cases of CD and UAD with pilot, for these cases, thrust force and torque are generated by cutting edges. Tool flank surface wear data is similar in a particular hole for the cases of CD and UAD with pilot in a particular hole. Therefore, a similar level of tool flank surface wear caused a similar level of cutting and thrust forces leading to similar values of torque and thrust forces in a particular hole. This is also evident from torque data plotted in Figure 6-45. Torque values for the cases of ‘CD with pilot’ and ‘UAD with pilot’ are similar in a particular hole in Figure 6-45 implying similar cutting forces in both the cases. Thus, this evidence suggests that ultrasonic oscillations were not effective in ‘UAD with pilot’ case and it behaved similar to ‘CD with pilot’ as far as thrust force, torque and tool flank

surface wear are concerned. One of the reasons for this behaviour could be excessive tool flank surface wear, however; more evidence is required to support this suggestion.

When comparing ‘CD without pilot’ and ‘UAD without pilot’ cases, thrust force and tool wear were found to be lower in ‘UAD without pilot’ in every hole as compared to those in ‘CD without pilot’. Also, chisel edge wear, shown in Figure 6-47, indicates lower chisel edge wear in the case of UAD without pilot. This evidence indicates that forces on chisel edge were lower in ‘UAD without pilot’ as compared to those in CD without pilot. Thus, lower forces on chisel edge in UAD without pilot, led to lower overall thrust force required for drilling. Lower overall thrust further caused lower flank wear leading to lower overall tool flank surface wear in the case of UAD without pilot as compared to that in CD without pilot. 40% – 60% of thrust force comes from chisel edge during conventional drilling [168] and forces coming from chisel edge during drilling were found to be reduced in UAD as compared to those in CD in this study, therefore, based upon this evidence it can be concluded that chisel edge plays an important role for thrust force reduction in UAD in comparison to that in CD. However, when comparing the thrust forces in the cases of UAD with and without pilot hole drilling cases, the thrust force in the case of UAD with pilot is larger than that in UAD without pilot. This is an unexpected and unconventional result. When a pilot hole is drilled, the material in front of the chisel edge for main-hole drilling is removed. Therefore, the forces required to drill the main-hole in the case of ‘with pilot’ should be lower than those in the case of without pilot because of machining less material relatively. However, implementation of ultrasonic assistance at chisel edge in the case of UAD without

pilot caused such unexpected result. The exact mechanism taking place at chisel edge causing such result is required to be investigated in future.

6.2.4.2 *Damage*

The 1st, 5th and 10th hole in each case of drilling were considered for damage analysis. In the first hole in every case, the entrance delamination was found to be zero. The reason behind this is the fact that at the starting of drilling of the first hole in each set, the cutting edge of the tool was sharp. Therefore it required lower force for machining near hole-entrance resulting in zero entrance delamination.

Further, as the tool progressed from entrance to exit in the 1st hole, it started to wear due to less wear resistant tool material (HSS) against the abrasive nature of CFRP material [100]. Increasing wear also exposed more flank face for friction between workpiece and tool flank face which increased friction force, heat and thrust force. This is why the increasing thrust force between entrance and exit was observed during drilling of first hole mentioned in Section 6.2.2.1 and shown in the image in Figure 6-39. As found in Phase-1, increasing cutting temperature reduces matrix strength to hold the fibres together. In the current Phase-2, tool wear near exit was more than that near entrance, which led to more frictional forces near exit than that near entrance. Due to increased frictional forces, more heat was generated which caused greater depth of fibre disorientation and pull out near exit as compared to that near entrance as shown in Figure 6-55 and Figure 6-56 in the first hole of each case.

Internal damage, Figure 6-57, was found to increase with respect to number of holes in every drilling case. This happened because, as the number of drilled hole increased, tool wear increased. Due to increasing tool wear, more flank surface was exposed to friction between the flank surface and the workpiece. This caused greater

thrust and cutting forces during drilling. Also, due to higher friction, higher heat generated. As found in Phase-1, higher cutting temperature causes the greater depth of matrix softening. Thus, fibre-pull out and fibre disorientation occurred to a greater depth leading to higher internal damage with respect to increasing number of drilled holes.

Comparing the individual drilling cases for internal damage in the hole in Figure 6-57, the internal damage data suggests that the average internal damage is lowest in 1st hole in the case of UAD without pilot. This is because of lowest tool flank wear in UAD without pilot hole in 1st hole. Lowest tool wear caused lowest frictional forces leading to lowest thrust and cutting forces and hence lowest damage [78, 95, 134, 135]. The rest of the drilling cases achieved similar tool wear therefore similar cutting and thrust forces which led to similar internal damage. In 5th and 10th holes, even though the tool wear is lowest in UAD without pilot case as compared to other cases, the outer cutting edge was completely worn out in all the drills. Since, machined surface is finalised by outer cutting edge, which is completely worn out in all the drills, therefore, generating similar cutting forces (torque, Figure 6-45) and hence, similar internal damage. The respective images of flank surfaces of the drill through optical microscopy and SEM are presented in Appendix C.

Maximum damage depth at exit is a parameter similar to exit delamination considered by other authors [86]. Exit delamination increases with increasing thrust force [13]. In the Phase-2, as thrust force increased with respect to number of holes in all the cases, Figure 6-44 due to increasing tool wear, Figure 6-46 which caused an increase in exit delamination.

6.2.5 Conclusions from Phase-2

- With this study, it was proven that forces coming from chisel edge during machining are reduced in UAD in comparison to those in CD (36% reduction by 10th hole in the present case). This reduction in thrust force from chisel edge also led to an overall reduction in thrust force during drilling which further caused a reduction in tool wear (both chisel and flank surfaces) and minimum damage at the exit in UAD than that in CD.
- Lower forces in UAD also resulted in lower thermal damage to machined surface in UAD than that in CD.
- Due to less wear resistant drills and excessive tool-wear, the effect of cutting edges and effective normal rake angles could not be demonstrated in this study. Therefore, more wear resistant drills than HSS, e.g. tungsten carbide drills [100], were required for demonstrating the effect of effective normal rake angles and cutting edge in UAD which will be performed in the next experimental study.

6.3 Phase 3 - Effect of cutting and chisel edges when drilling with Tungsten carbide drills

In Phase-2 (Section 6.2), the effective normal rake angle effect on cutting edges of twist drill could not be examined due to excessive tool wear in HSS twist drills and the results being affected by severe tool wear. Therefore, the same concept was to be examined with more wear resistant drills in this phase. Tungsten carbide drills have been proven to be more wear resistant as compared to HSS drills [100]. Thus, tungsten carbide drills were used so that the results could not be affected by severe tool wear. In addition, it can be seen in Section 5.7.3.1 that the geometry of twist drill used in the present experiment is different to those used in experiments in Phases 1 and 2 (Sections 5.7.1.1 and 5.7.2.1). Similar to as explained in Section 6.2, as the objective was to examine the larger effective rake angles in UAD than those in CD, the variation in the drill geometry would not affect the results as long as the same geometry is used in CD and UAD for a particular experimental study. Thus, even though the geometry of twist drill is different in Phase-3 as compared to those in Phases 1 and 2, the effective rake angles effect could still be studied by examining the theoretical effective rake and clearance angles for a particular drill geometry and performing the experiments for the same in a particular phase of the study. In addition, since the value of effective rake angles in UAD was found to be increasing with a reduction in the cutting speeds in Section 4.6, therefore, a high and a low cutting speed would be required in order to examine the concept of effective rake angles in UAD. Thus, in the present study, 10 m/min (low cutting speed) and 100 m/min (high cutting speed) were used for examining the theoretical effective rake angles in CD and UAD and conducting the experiments for the same rather than having a design of experiments approach. The cutting speed selection in this phase

was also inspired from the effective rake angles at 9.42 m/min and 94.2 m/min cutting speeds for CD and UAD in Phase-1. The feed rate was kept constant at 0.05 mm/rev across the cutting speeds so that the uncut chip thickness could be kept constant. This would make sure effects across the two cutting speeds would be because of the variation in the effective rake angles. The ultrasonic parameters (frequency and amplitude) in the present phase were used as described previously in Section 5.7.3.2.

6.3.1 Effective normal rake angle at 10 and 100 m/min cutting speeds at current drill geometries

The value of effective normal rake and effective axial clearance angles has been calculated using the method discussed in Section 4.6 for the geometry of drill used in the present experiment (Section 5.7.3.1). The values of effective normal rake and axial clearance angles at cutting speeds of 10 and 100 m/min are plotted in figures from Figure 6-66 to Figure 6-69 for the ultrasonic parameters described in Section 5.7.3.2 for 'UAD with pilot' drilling case.

6: Experimental studies, results and discussions

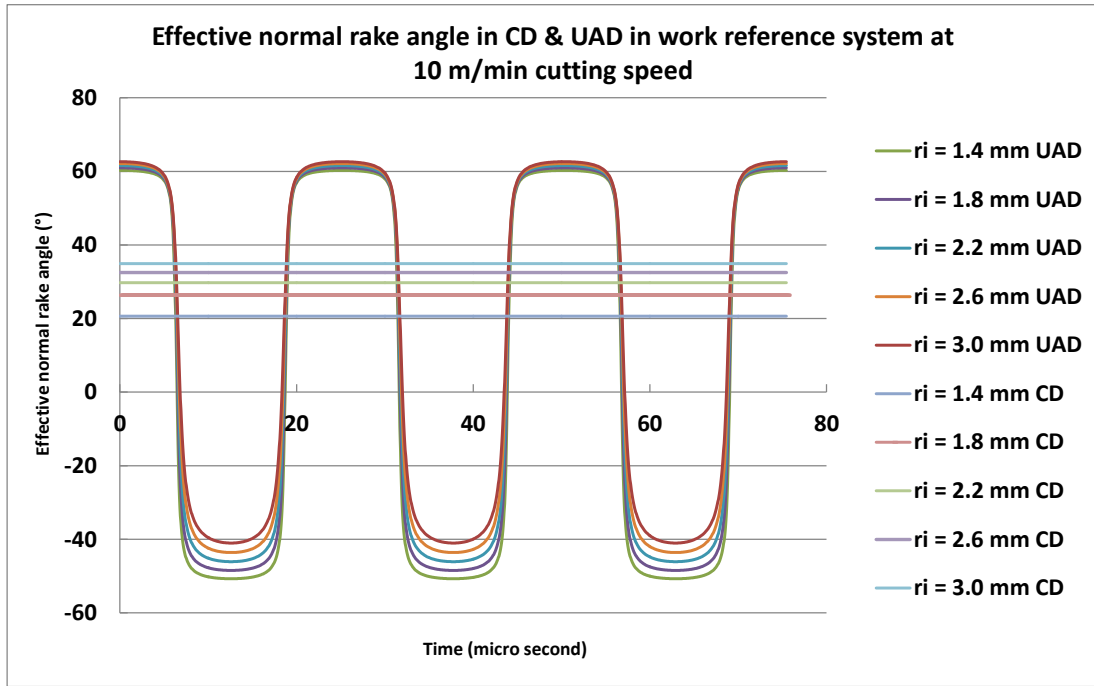


Figure 6-66: Effective normal rake angles obtained at 10 m/min cutting speed and 0.05 m/rev feed rate in CD and UAD (39740 Hz frequency and 7.6 μm amplitude)

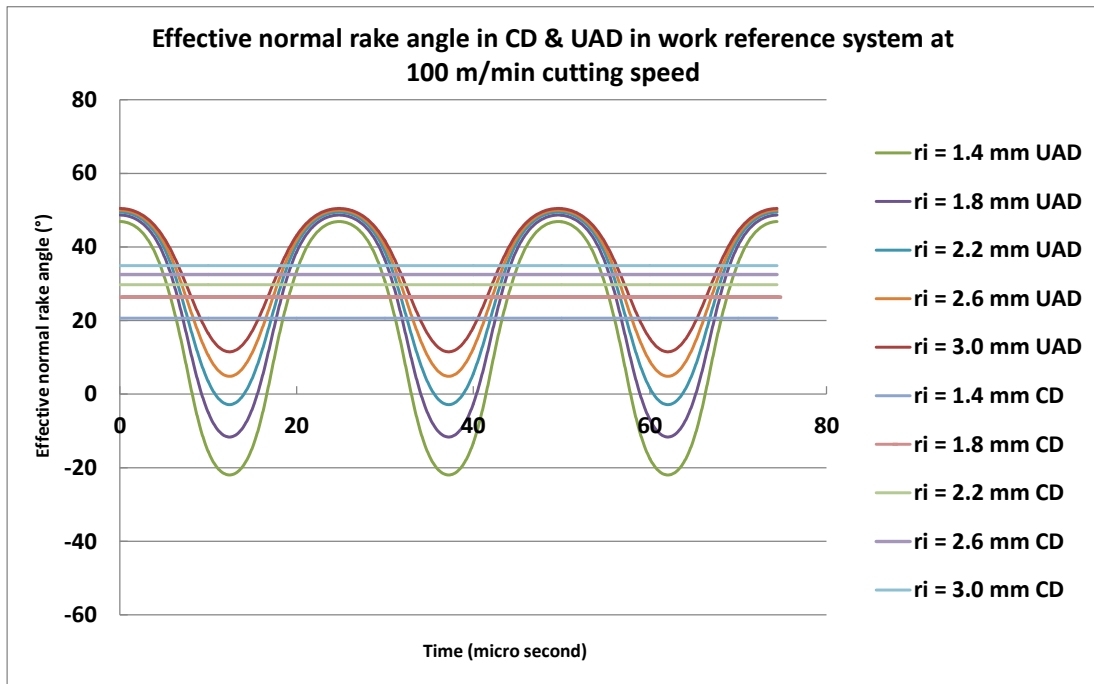


Figure 6-67: Effective normal rake angles obtained at 100 m/min cutting speed and 0.05 m/rev feed rate in CD and UAD (40300 Hz frequency and 6.8 μm amplitude)

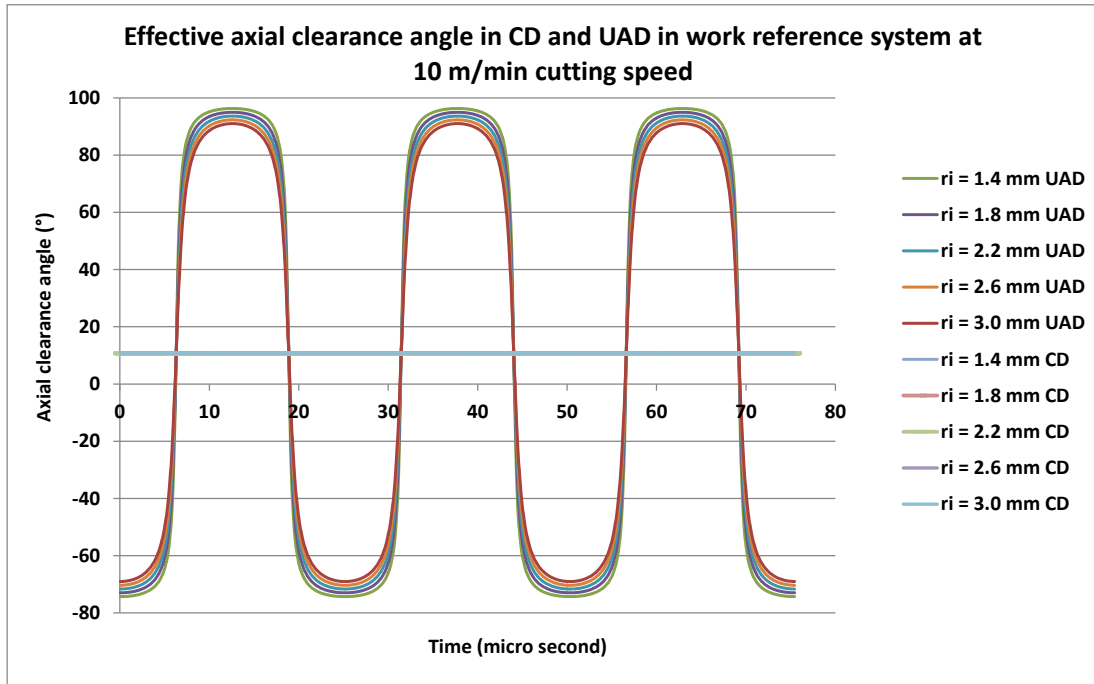


Figure 6-68: Effective axial clearance angles obtained at 10 m/min cutting speed and 0.05 m/rev feed rate in CD and UAD (39740 Hz frequency and 7.6 μm amplitude)

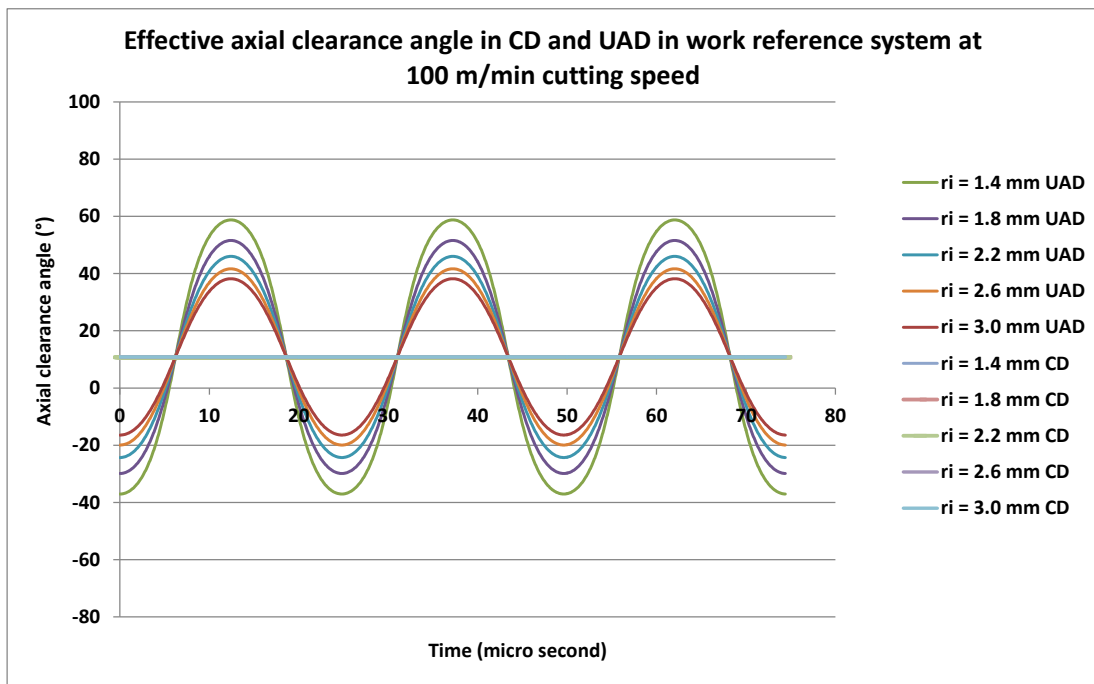


Figure 6-69: Effective axial clearance angles obtained at 100 m/min cutting speed and 0.05 m/rev feed rate in CD and UAD (40300 Hz frequency and 6.8 μm amplitude)

From Figure 6-66 and Figure 6-67, it can be seen that the maximum value of effective normal rake angle at 10 m/min is 62° while that at 100 m/min is 49° . Also, the minimum axial clearance angle at 10 m/min is -74° and that at 100 m/min cutting

speed is -37° . Thus, a larger value of effective rake angle and larger negative value of axial clearance angle have been obtained at 10 m/min cutting speed than that at 100 m/min cutting speed. The rake and clearance angle have been calculated for cutting edges only. Therefore, to examine the effect of these variations in effective rake and axial clearance angles, the experiment would have to be performed in such a way that only cutting edges of a drill could be involved during drilling. Thus pilot holes having equivalent diameters of chisel edge of twist drill were decided to be drilled such that the effect of only cutting edges could be identified during drilling of final holes.

6.3.2 Results of thrust force, torque and tool wear

6.3.2.1 Thrust force

The thrust force profiles during CD and UAD at both cutting speeds which are shown in the figures Figure 6-70 and Figure 6-71. Thrust force profile at 10 m/min cutting speed in UAD was found to have more oscillations as compare to those in CD, Figure 6-70 (55 and 22 N average thrust forces in CD and UAD for the profiles in Figure 6-70). However, at 100 m/min cutting speed, the thrust force profiles were found to be similar in CD and UAD (e.g. 44 and 38 N average thrust forces in CD and UAD respectively for the profiles shown in Figure 6-71).

In the literature, authors have reported this type of higher oscillations during UAD [164]. However, thrust force profiles being similar in CD and UAD at higher cutting speeds e.g. 100 m/min has not been previously reported in the literature.

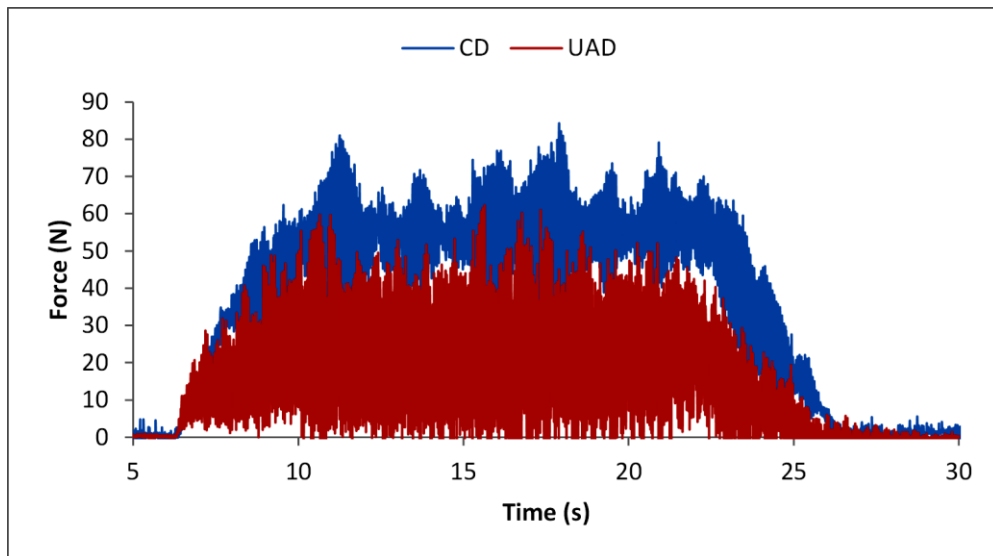


Figure 6-70: Thrust force profiles in CD and UAD (10 m/min, 0.05 mm/rev)

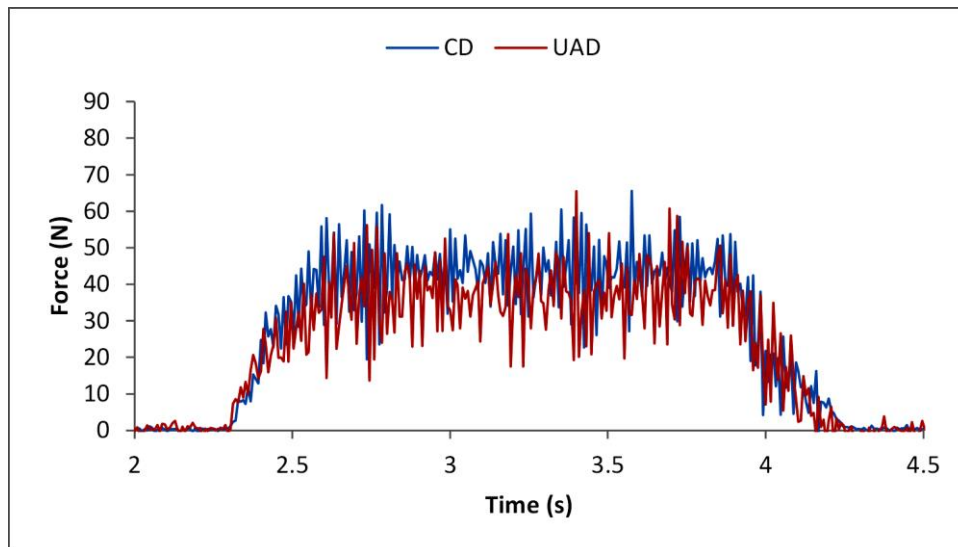


Figure 6-71: Thrust force profiles in CD and UAD (100 m/min, 0.05 mm/rev)

The average thrust forces data for 10 and 100 m/min cutting speeds are presented in Table 6-28 and Table 6-29 and are plotted in Figure 6-72 and Figure 6-73 respectively. In addition, to evaluate the effectiveness of ultrasonic oscillations on thrust force with respect to increasing number of drilled holes, the percentage reduction in thrust force in UAD (with and without pilot) with respect to CD (with and without pilot) is also calculated with the help of Equation 6.1 in Table 6-28 and Table 6-29.

6: Experimental studies, results and discussions

$$\% \text{ reduction in thrust force} = \frac{(\text{Thrust force in CD} - \text{Thrust force in UAD})}{\text{Thrust force in CD}} \times 100\%$$

- Equation (6.1)

Table 6-28: Data for average thrust force at 10 m/min cutting speed and 0.05 mm/rev feed rate in all the drilling sets of CD, UAD, with and without pilot holes

Hole Number	Average thrust force at 10 m/min (N)					
	CD	UAD	Percentage reduction of thrust force in UAD with respect to CD (%)	CD with pilot	UAD with pilot	Percentage reduction of thrust force in 'UAD with pilot' with respect to 'CD with pilot' (%)
1	37	16	56	18	8	55
2	49	19	61	22	14	37
3	55	22	59	26	16	37
4	60	27	55	34	19	42
5	64	30	54	32	22	31
10	82	42	49	45	33	26
15	95	55	42	54	41	25
20	108	67	38	62	42	32
25	115	77	33	69	45	34
30	123	74	40	74	60	20
35	132	86	35	80	64	19
40	137	92	33	87	63	27
45	143	100	30	90	62	31
50	149	107	28	95	68	29
55	155	111	29	99	71	28
60	160	117	27	104	75	27

6: Experimental studies, results and discussions

Table 6-29: Data for average thrust force at 100 m/min cutting speed and 0.05 mm/rev feed rate in all the drilling sets of CD, UAD, with and without pilot holes

Hole Number	Average thrust force at 100 m/min (N)					
	CD	UAD	Percentage reduction of thrust force in UAD with respect to CD (%)	CD with pilot	UAD with pilot	Percentage reduction of thrust force in 'UAD with pilot' with respect to 'CD with pilot' (%)
1	32	27	16	14	11	20
2	39	33	14	18	15	18
3	44	37	14	22	18	15
4	48	40	17	23	20	14
5	51	43	15	25	23	11
10	66	55	16	33	30	9
15	75	65	14	39	35	11
20	83	74	11	45	41	10
25	88	79	11	50	46	9
30	99	87	12	54	50	9
35	104	93	10	59	51	12
40	108	98	9	62	58	7
45	112	105	7	67	61	9
50	118	108	9	71	66	7
55	122	115	6	75	69	8
60	125	118	6	77	73	6

6: Experimental studies, results and discussions

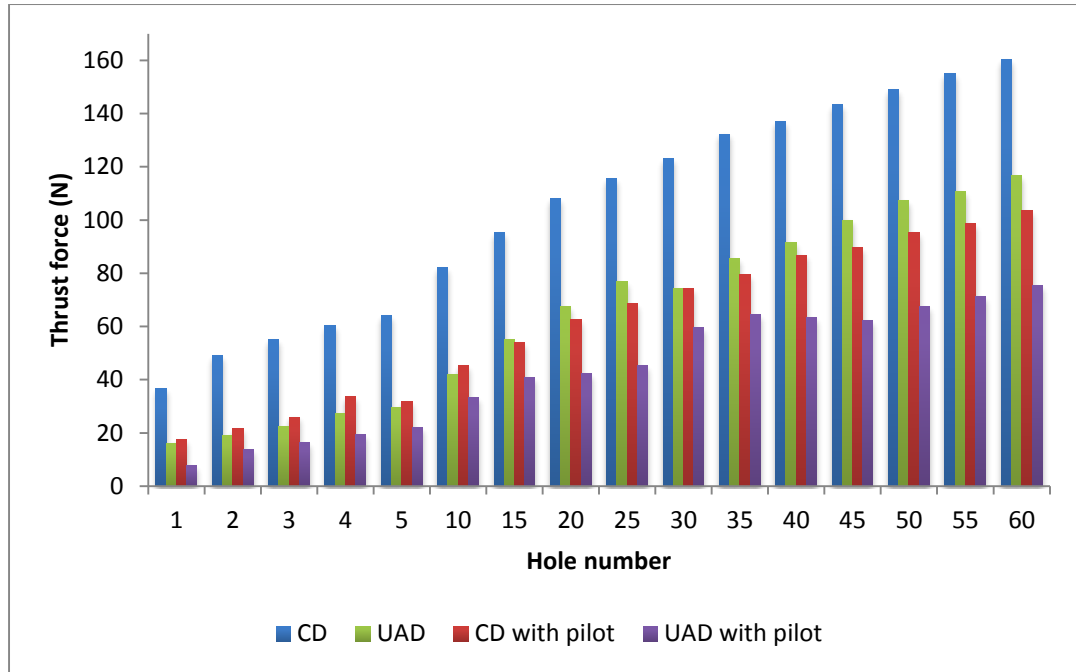


Figure 6-72: Thrust force variation at 10 m/min cutting speed and 0.05 mm/rev feed rate in all the cases of CD, UAD, with and without pilot holes

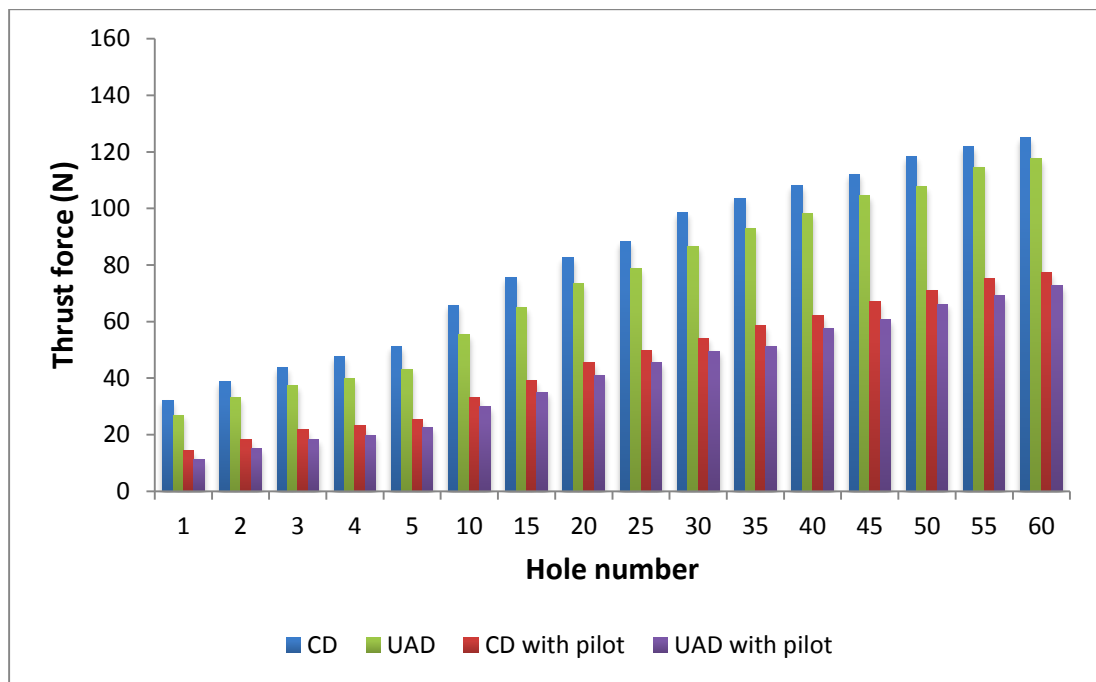


Figure 6-73: Thrust force variation at 100 m/min cutting speed and 0.05 mm/rev in all the cases of CD, UAD, with and without pilot holes

When comparing the thrust forces with and without pilot holes, the plots of thrust forces in Figure 6-72 and Figure 6-73 display the reduction in thrust force in the case of 'with pilot' as compared to that in the case of 'without pilot'

in both CD and UAD. Similar results were also reported and explained by other authors [18-21] for CD. It is mentioned by Jain and Yang [131] that 40 to 60% of the overall thrust force comes from chisel edge. The material normally machined by the chisel edge is taken away by drilling a pilot hole. Thus, forces coming from chisel edge are avoided during drilling of the main-hole resulting in lower thrust force in comparison to the thrust force obtained in 'without pilot-hole' case.

Percentage reduction of thrust force in UAD with respect to CD data in Table 6-28 indicates that it decreased from 56 to 27% from hole 1 to hole 60 in the case of without pilot hole and from 55 to 27% in the case of with-pilot hole at 10 m/min. Similarly, Percentage reduction of thrust force data in Table 6-29 indicates that it decreased from 16 to 6% from hole 1 to hole 60 in the case of without pilot hole and from 20 to 6% in the case of with-pilot hole at 100 m/min cutting speed.

Thus, the thrust force data in Table 6-28 and Table 6-29 suggests that the thrust force reduction due to ultrasonic assistance was reduced as the number of drilled holes increased at both 10 and 100 m/min cutting speeds. In addition, higher reduction in thrust force due to ultrasonic assistance was obtained at lower cutting speed i.e. 10 m/min.

6.3.2.2 *Thrust force from chisel edge*

In addition, the thrust force from chisel edge in CD and UAD was also calculated from the data presented in Table 6-28 and Table 6-29 for 10 and 100 m/min with the help of Equations (6.2) and (6.3) and is plotted in Figure 6-74.

Thrust force from chisel edge in CD = Thrust force in CD – Thrust force in ‘CD with pilot’
- Equation (6.2)

Thrust force from chisel edge in UAD = Thrust force in UAD – Thrust force in ‘UAD with pilot’
- Equation (6.3)

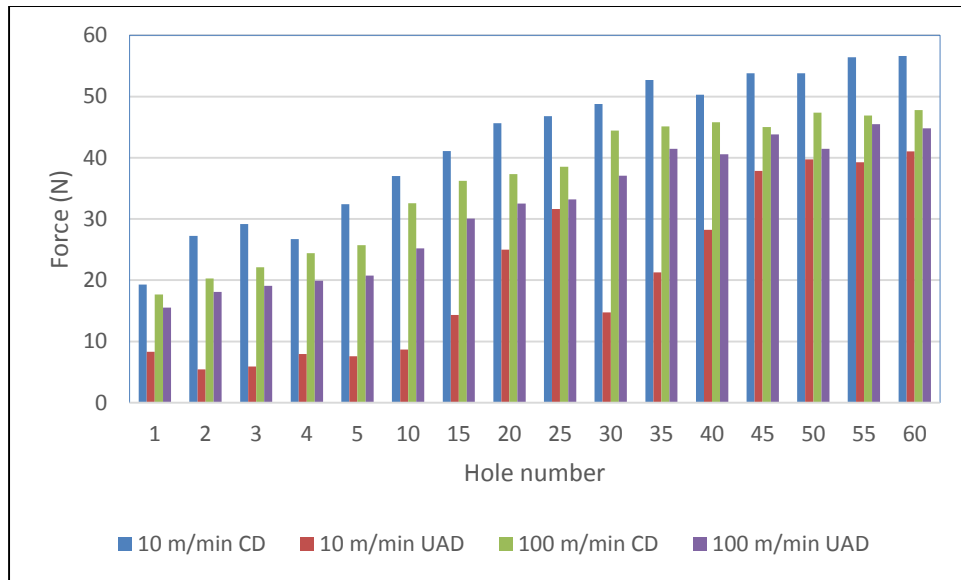


Figure 6-74: Thrust force from chisel edge in CD and UAD at 10 and 100 m/min and 0.05 mm/rev

From Figure 6-74, the fraction of the thrust force from chisel edge ranges from 52% to 35% At 10 m/min in CD and UAD while that at 100 m/min ranges between 55% to 38% in CD and 46% to 29% in UAD. It can also be noted that the fraction of thrust force from chisel edge in UAD has been reduced in comparison to that in CD. Similar evidence of reduction in forces at chisel edge due to ultrasonic assistance were also found in Section 6.2.2.4 in Phase-2. The evidence of Phase-2 and Phase-3 indicates that the machining mechanism at chisel edge is different in CD and UAD.

In conventional drilling, extrusion at chisel edge has been suggested by Watson [205] at the central portion of chisel edge. At the outer portion of chisel edge, authors argue about orthogonal and oblique machining [174, 205]. Therefore,

it is suggested to investigate the mechanism of machining at chisel edge further which causes a reduction in forces during drilling in UAD.

6.3.2.3 Torque

Similar to Phase-2 the average torque values during drilling were analysed. Average torque values at 10 and 100 m/min cutting speeds are presented in Table 6-30 and Table 6-31 and are plotted in Figure 6-75 and Figure 6-76 respectively. Similar to thrust force, the percentage reduction in torque in UAD with respect to CD was also calculated with the help of Equation 6.1 by replacing thrust force with torque.

Table 6-30: Data for average torque values in CD and UAD at 10 m/min cutting speed and 0.05 mm/rev feed rate

Hole Number	Average torque at 10 m/min (N-cm)					
	CD	UAD	Percentage reduction of thrust force in UAD with respect to CD (%)	CD with pilot	UAD with pilot	Percentage reduction of thrust force in 'UAD with pilot' with respect to 'CD with pilot' (%)
1	8	4	49	8	4	45
2	10	5	54	11	7	39
3	11	6	50	12	9	29
4	12	7	45	13	10	24
5	13	7	42	15	11	28
10	17	9	47	19	14	26
15	20	12	39	22	16	24
20	22	15	33	22	18	19
25	25	16	35	25	16	35
30	25	14	46	25	22	14
35	27	16	40	26	22	15
40	28	17	38	26	18	31
45	30	21	28	28	16	43
50	31	20	36	29	16	44
55	32	22	33	29	18	38
60	33	22	33	30	18	39

6: Experimental studies, results and discussions

Table 6-31: Data table for average torque values in CD and UAD at 100 m/min cutting speed and 0.05 mm/rev feed rate

Hole Number	Average torque at 100 m/min (N-cm)					
	CD	UAD	Percentage reduction of thrust force in UAD with respect to CD (%)	CD with pilot	UAD with pilot	Percentage reduction of thrust force in 'UAD with pilot' with respect to 'CD with pilot' (%)
1	9	8	14	7	7	10
2	11	10	9	12	9	31
3	12	11	8	13	10	20
4	12	12	1	12	10	14
5	13	12	11	12	12	0
10	16	15	7	16	13	16
15	18	16	11	18	15	16
20	18	17	4	18	15	18
25	19	17	14	19	16	17
30	21	19	10	20	17	12
35	20	19	6	20	18	13
40	21	19	11	22	18	16
45	21	19	11	22	18	16
50	22	20	7	22	19	12
55	22	21	5	22	19	12
60	22	21	6	22	19	14

6: Experimental studies, results and discussions

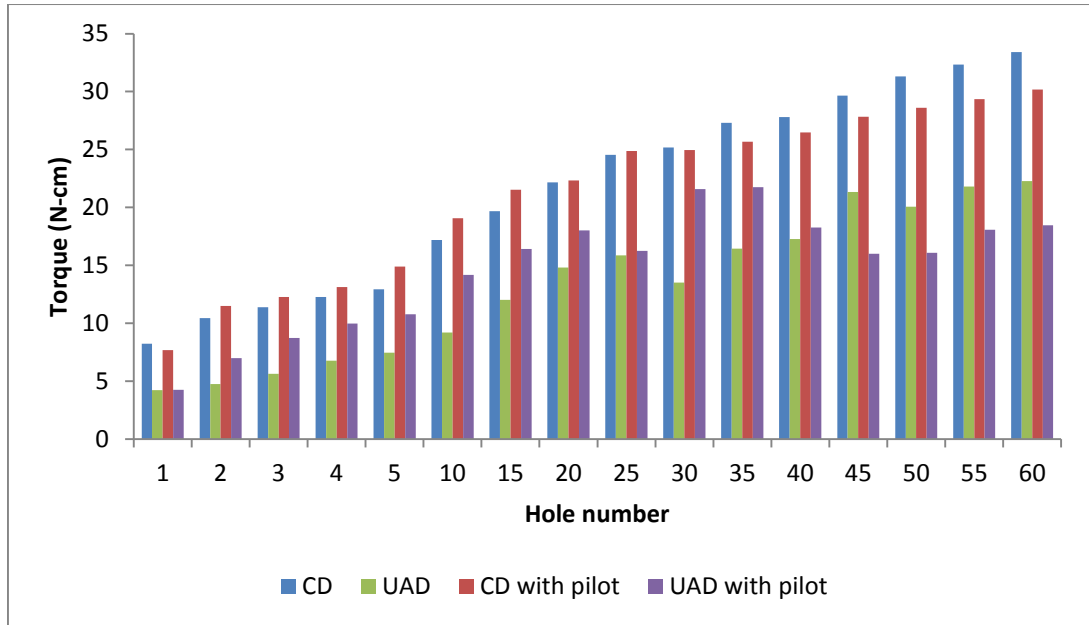


Figure 6-75: Torque variation at 10 m/min cutting speed and 0.05 mm/rev feed rate in all the cases of CD, UAD, with and without pilot holes

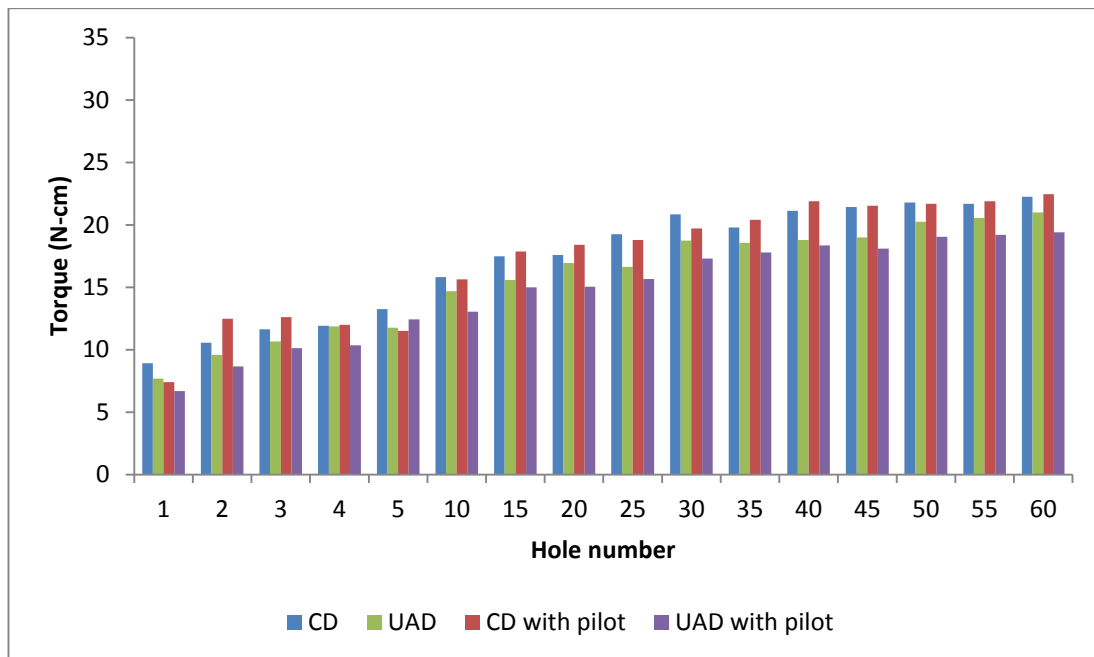


Figure 6-76: Torque variation at 100 m/min cutting speed and 0.05 mm/rev feed rate in all the cases of CD, UAD, with and without pilot holes

Percentage reduction of torque in UAD with respect to CD data in Table 6-30 indicates that it decreased from 49 to 33% from hole 1 to hole 60 in the case of without pilot hole and from 45 to 39% in the case of with-pilot hole at 10 m/min. Similarly, percentage reduction of torque data in Table 6-31 indicates that it

decreased from 14 to 6% from hole 1 to hole 60 in the case of without pilot hole and from 31 to 14% from hole 2 to hole 60 in the case of with-pilot hole at 100 m/min cutting speed.

Thus, similar to thrust force data, torque data also indicates that reduction in torque due to ultrasonic assistance reduced with increasing number of holes at both 10 and 100 m/min cutting speeds. Also, the reduction in torque due to ultrasonic assistance was found to be higher at lower cutting speed i.e. 10 m/min.

6.3.2.4 Tool wear

The tool wear was monitored and quantified using the methodology explained in Section 5.6. The tool wear was monitored after drilling of every fifth hole up to 60 holes. The average values of tool wear at 10 and 100 m/min in all the cases of CD, UAD, with and without pilot hole drilling is presented in Table 6-32 and Table 6-33 respectively and are plotted in Figure 6-77 and Figure 6-78.

Table 6-32: Tool wear data at 10 m/min cutting speed and 0.05 mm/rev feed rate for all the cases

Hole number	Average tool wear at 10 m/min cutting speed (μm)			
	CD	UAD	CD with pilot	UAD with pilot
5	24	28	22	25
10	28	32	33	29
15	37	39	39	33
20	41	46	42	38
25	45	48	44	41
30	50	52	47	45
35	53	54	50	46
40	56	56	50	49
45	58	59	53	50
50	59	61	56	52
55	62	66	57	53
60	67	66	58	55

6: Experimental studies, results and discussions

Table 6-33: Tool wear data at 100 m/min cutting speed and 0.05 mm/rev feed rate for all the cases

Hole number	Average tool wear at 100 m/min cutting speed (μm)			
	CD	UAD	CD with pilot	UAD with pilot
5	23	12	20	11
10	30	19	24	17
15	33	24	28	21
20	35	26	32	25
25	44	34	36	29
30	44	38	43	34
35	45	41	48	36
40	47	44	52	38
45	52	46	54	43
50	57	50	57	44
55	61	53	57	46
60	68	55	61	49

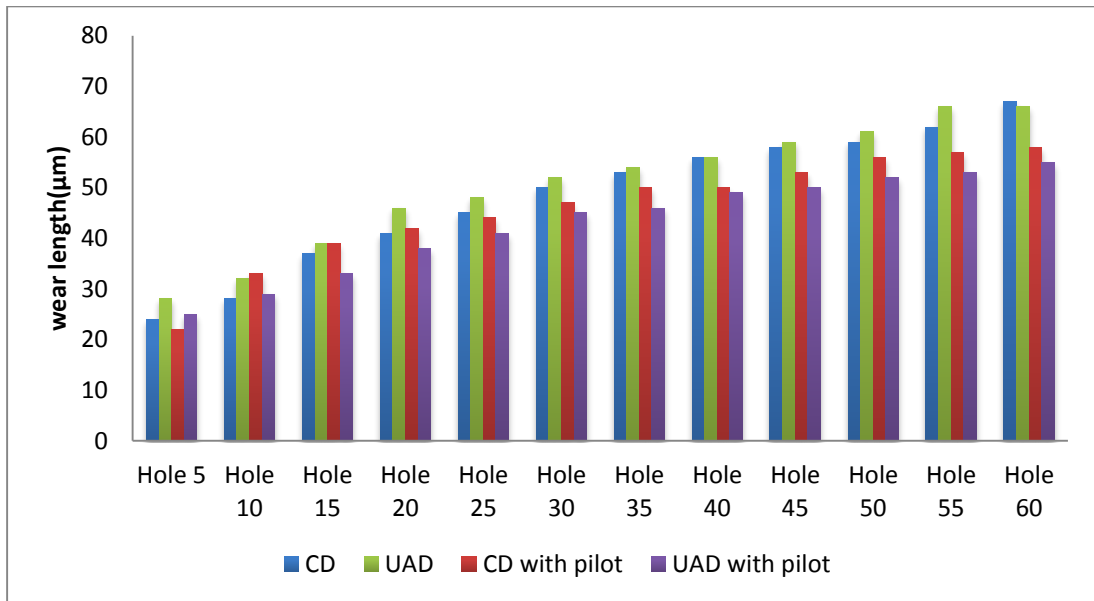


Figure 6-77: Variation of average tool wear at 10 m/min cutting speed and 0.05 mm/rev feed rate for all the cases with respect to number of drilled holes

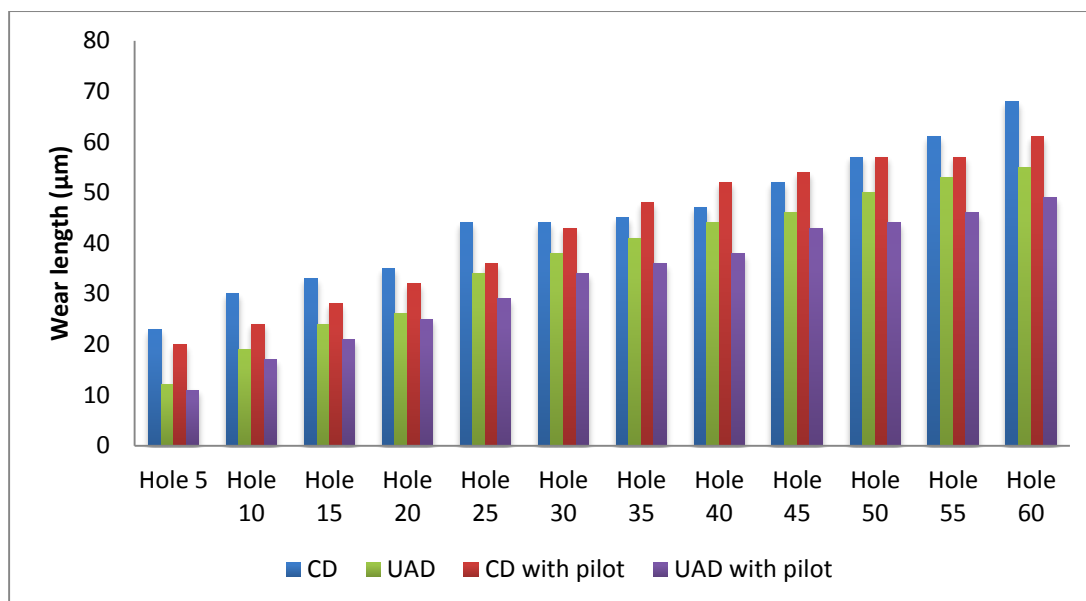


Figure 6-78: Variation of average tool wear at 100 m/min cutting speed and 0.05 mm/rev feed rate for all the cases with respect to number of drilled holes

From the plot of tool wear for 10 and 100 m/min, it can be seen that tool wear increases with an increasing number of holes in all the cases at both cutting speeds of 10 and 100 m/min as expected [10]. When comparing CD and UAD, the tool wear was found to be similar (maximum difference of 6 μm only) in CD and UAD at 10 m/min in both the cases of without and with pilot hole. After 60 holes a difference of 1 μm and 3 μm respectively was recorded when comparing CD and UAD in without and with pilot-hole drilling cases respectively as reported in Table 6-32.

When comparing CD and UAD, the tool wear at 100 m/min was found to be lower in UAD than that in CD in cases of without and with pilot-hole drilling in all the 60 holes, Figure 6-78. The reduction in tool wear due to ultrasonic assistance was found to be 48% after hole-1 and 19% after 60th hole in UAD in comparison to that in CD in the case of without pilot-hole drilling. In the case of with-pilot hole drilling, tool wear was found to be 45% less after hole-1 and 20% less after hole-60 in the case of UAD than that in CD.

When comparing CD and UAD, with the tool wear data, it is concluded that the larger reduction in tool wear due to ultrasonic assistance was obtained at a higher cutting speed of 100 m/min as compared to that in the case of 10 m/min for both with and without pilot-hole drilling cases. This observation is justified by the effective axial clearance angle calculation shown in Figure 6-68 and Figure 6-69 respectively. As mentioned by the authors [168, 173], negative clearance angle is not desired in any machining process. Negative clearance angle leads to rubbing of the flank surface against the workpiece being machined during machining. At 10 m/min, the minimum effective clearance angle was -74° while that at 100 m/min was -39° . Higher effective axial clearance angles led to lower rubbing of the flank surface against the workpiece and hence the tool wear was found to be reduced. At 10 m/min, larger negative clearance angles of -74° led to higher rubbing of the flank surface which did not result in a reduction in tool wear (in fact tool wear is higher in UAD on holes 1 and 20 by 4 and 5 μm respectively).

SEM images of drilling tools were recorded in order to visualise the flank surfaces after drilling 60 holes. However, the SEM images of flank surfaces did not reveal significant information other than cutting edges having some tool wear.

6.3.2.5 *Effect of tool wear on ultrasonic assistance*

Through the results of thrust force, torque and tool wear, it has been found that the effectiveness of ultrasonic assistance is diminished with increasing number of drilled holes i.e. increasing tool wear.

In the case of micromachining, where the depth of cut is comparable to the radius of curvature of cutting edge of the machining tool, the effective rake angle becomes negative [206, 207]. To visualize this and examine the effectiveness of ultrasonic

assistance with increasing tool wear, the rake angle of a new and worn tool has been visualized in the schematic shown in Figure 6-79. In Figure 6-79 (b), ‘r’ is the radius of curvature at cutting edge, ‘d’ is the uncut chip thickness, ‘ γ ’ is the rake angle. It can be seen in Figure 6-79 (a) and (b) that unlike a new tool, the rake angle becomes negative in case the uncut chip thickness is lower than the radius of curvature of cutting edge in a worn tool.

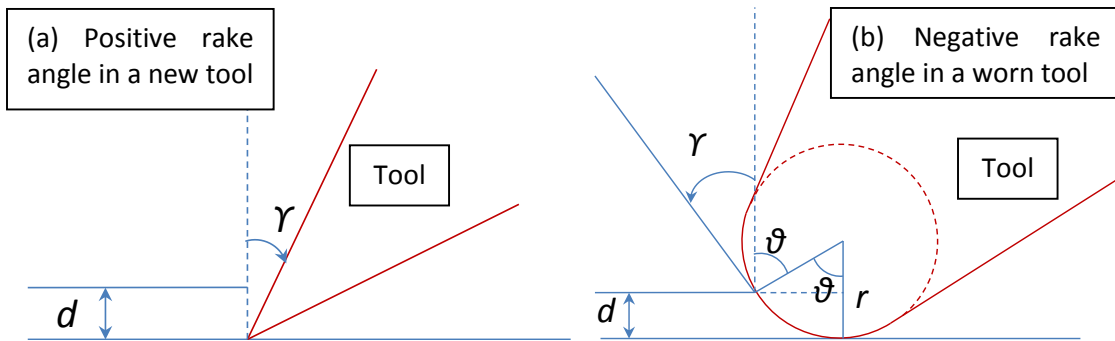


Figure 6-79: Schematic showing rake angles in a (a) new and a (b) worn tool. It can be seen that the rake angle in a worn tool becomes negative if the uncut chip thickness becomes lower than the radius of curvature of cutting edge.

$$\text{From Figure 6-79 (b),} \quad \gamma = 90 - \theta \quad \text{- Equation (6.4)}$$

$$\cos \theta = \frac{r-d}{r} \quad \text{- Equation (6.5)}$$

$$\Rightarrow \gamma = 90 - \cos^{-1} \left(\frac{r-d}{r} \right) \quad \text{- Equation (6.6)}$$

The value of ‘ γ ’ can be determined from the Equations (6.5) and (6.6). In addition, the value of ‘ γ ’ will be negative.

Using this concept, the radius of curvature of worn drills (after drilling of 60 holes) used in ‘UAD without and with pilot’ at 10 and 100 m/min were measured at the outer corner of margin through optical microscopy as shown in Figure 6-80. The respective values are presented in Table 6-34. Similar kind of cutting edge rounding

during drilling of CFRP has also been reported and considered as a wear criteria in the work of Faraz et al. [95].

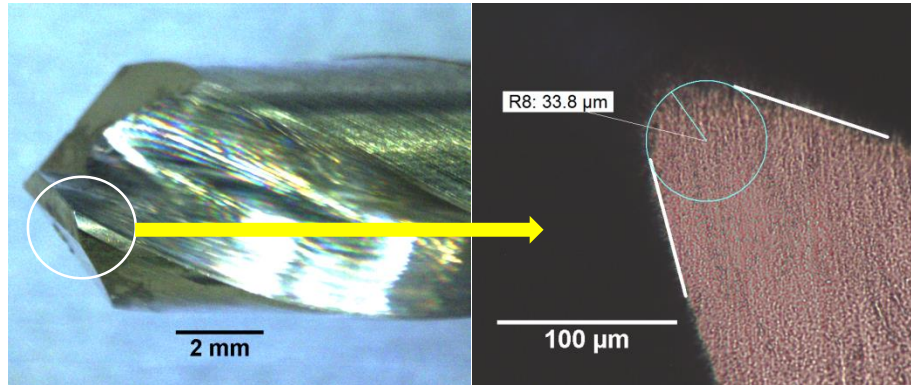


Figure 6-80: Measurement of radius of curvature at the outer margin of cutting edge of tool through optical microscopy after drilling of 60 holes in 'UAD with pilot' at 10 m/min

Table 6-34: Data of radius of curvature in the case of UAD with and without pilot hole drilling

Cutting speed (m/min)	Drilling condition	Radius of curvature (μm)
10	UAD	37.8
	UAD with pilot	33.8
100	UAD	47
	UAD with pilot	40

The uncut chip thickness for a twist drill has been calculated in the present research using the formula presented by Astakhov [173] in Equation (6.7). 'S₀' is feed rate of twist drill in mm/rev and 'ρ' is half cone angle of a twist drill in Equation (6.7)

$$d = \frac{S_0}{2} \frac{1}{\sqrt{1 + \left(\frac{\cot \rho}{\cos \beta_i}\right)^2}} \quad \text{- Equation (6.7)}$$

The value of β_i in Equation (6.7) can be determined from Equation (4.18) and ρ is the half cone angle of the drill. The cone angle of drill used in the current experiment is presented in Section 5.7.3.1 (118°).

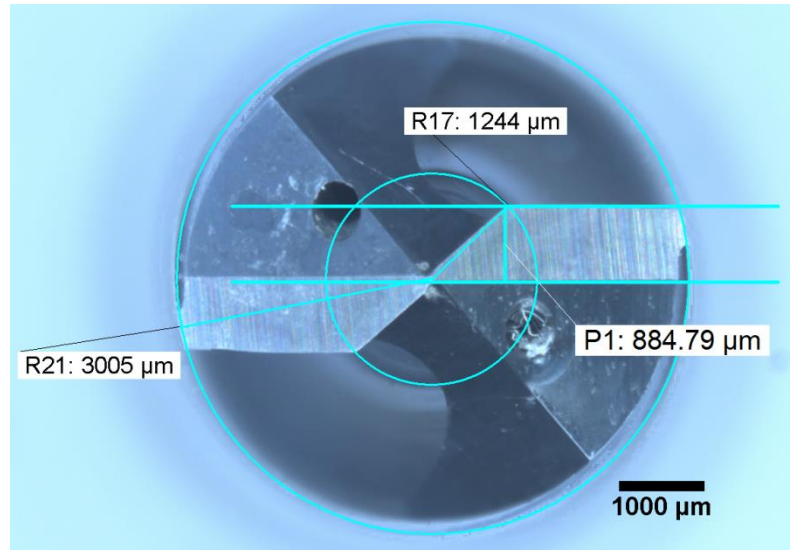


Figure 6-81: Measurement of chisel edge thickness for the drill used in present experiment

From Equation (4.18), $\beta_i = \sin^{-1} \left(\frac{w}{r_i} \right)$;

Where the value of 'w' is 884.79 μm from Figure 6-81 and value of 'r_i' will be 3005 μm for the outermost point of cutting edge (at the margin). At the same point of cutting edge, the radius of curvature was measured in Figure 6-80.

Therefore value of $\beta_i = \sin^{-1} \left(\frac{884.79}{3005} \right) = 17.1^\circ$

Using value of β_i (17.1°), ρ (59° for the present drill) and S_0 (0.05 mm/rev for the present experiment) the value of uncut chip thickness has been calculated from Equation (6.7).

Its value comes out to be = 0.021 mm (21 μm).

The axial rake angles were calculated using the data of Table 6-34 and Equation (6.6). The value of negative axial rake angles of twist drills at 10 and 100 m/min is presented in Table 6-35.

Table 6-35: Negative axial rake angles of twist drills at the outermost corner of cutting edge

Cutting speed (m/min)	Drilling condition	Axial rake angle
10	UAD	-26.4°
	UAD with pilot	-22.3°
100	UAD	-33.6°
	UAD with pilot	-28.4°

The maximum effective normal rake angle in an ultrasonic cycle corresponding the negative axial rake angles from Table 6-35 and for a new tool are calculated using Equations (4.5), (4.14) and (4.15) for the outermost point of twist drill (at which the radius of curvature was measured in Figure 6-80). The ultrasonic parameters for calculating effective normal rake angles were used from Table 5-15 in Section 5.7.3.2. The respective values are presented in Table 6-36.

Table 6-36: Effective normal rake angle in UAD for hole 1 and hole 60 in the case of UAD with pilot

Cutting speed (m/min)	Drilling condition	Effective normal rake angle at hole 1 (New tool)	Effective normal rake angle at hole 60 (worn tool)
10	UAD	64°	9.2°
	UAD with pilot	64°	14°
100	UAD	54°	1.7°
	UAD with pilot	54°	5.5°

From, the data in Table 6-36 it becomes evident that due to axial rake angles being negative at the worn tool, the effective normal rake angles in UAD were reduced in worn tool in comparison to those in a new tool. This justifies the diminishing behaviour of ultrasonic assistance with increasing tool wear.

6.3.3 Results of damage quantification and analysis

Maximum damage at the entrance, fibre pull-out, disorientation and maximum damage depth at exit were selected to analyse the damage in Phase-3. The damage analysis was performed by using the methodology of sectioning, mounting and polishing of holes mentioned in Sections 5.5.2 and 5.5.3. Optical microscopy was used to quantify the damage. Hole numbers 1, 2, 3, 28, 29, 30, 58, 59 and 60 were sectioned and the damage in them was quantified.

6.3.3.1 *Maximum delamination damage at entrance*

Maximum damage at the entrance was analysed using the methodology explained in Section 5.5.3. Zero damage at the entrance was found in the initial holes i.e. when the cutting edge of the tool was sharp as shown in Figure 6-82. The data for maximum delamination damage depth at the entrance for the holes examined in CD and UAD is presented in Table 6-37 and Table 6-38 for cutting speeds 10 and 100 m/min respectively.

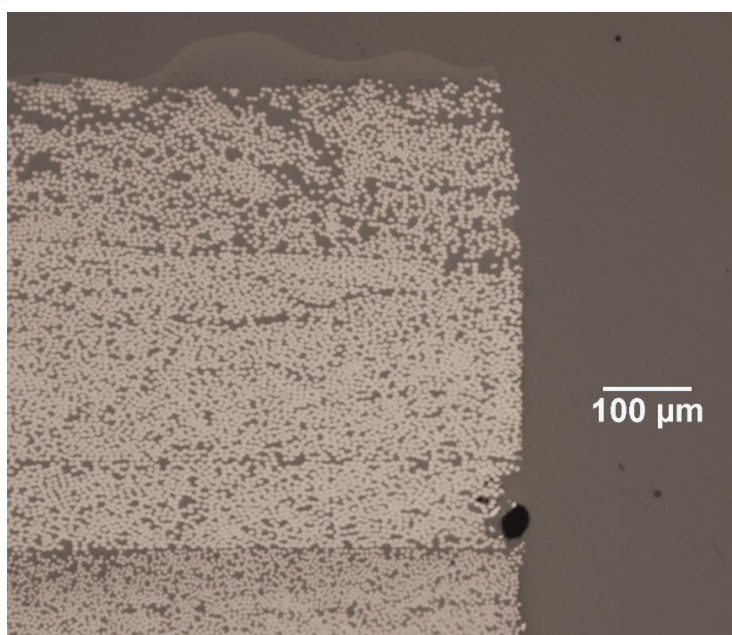


Figure 6-82: Zero delamination damage at entrance at 10 m/min cutting speed in CD with pilot hole drilling in the first hole

Table 6-37: Data for maximum delamination damage depth at entrance at 10 m/min cutting speed

Hole number	Maximum damage at entrance at 10 m/min			
	CD (μm)	CD with pilot (μm)	UAD (μm)	UAD with pilot (μm)
1	367	0	0	0
2	163	0	0	112
3	0	407	438	119
28	760	824	399	469
29	597	879	412	568
30	457	931	358	525
58	817	1089	739	1068
59	874	762	666	1928
60	711	1273	630	1021

Table 6-38: Data for maximum delamination damage depth at entrance at 100 m/min cutting speed

Hole number	Maximum damage at entrance at 100 m/min			
	CD (μm)	CD with pilot (μm)	UAD (μm)	UAD with pilot (μm)
1	0	230	0	0
2	0	0	0	146
3	0	410	292	0
28	718	604	457	589
29	168	715	0	329
30	115	549	242	477
58	245	570	629	919
59	399	549	726	2191
60	549	1062	191	1291

To analyse the damage, three consecutive holes were considered by considering average, minimum and maximum in each case. The averages of a set of holes, i.e. holes 1-3, holes 28-30 and holes 59-60 at cutting speeds 10 and 100 m/min were plotted as shown in Figure 6-83 and Figure 6-84. The error bars in these figures indicate the maximum and minimum values of damage out of the three consecutive drilled holes.

6: Experimental studies, results and discussions

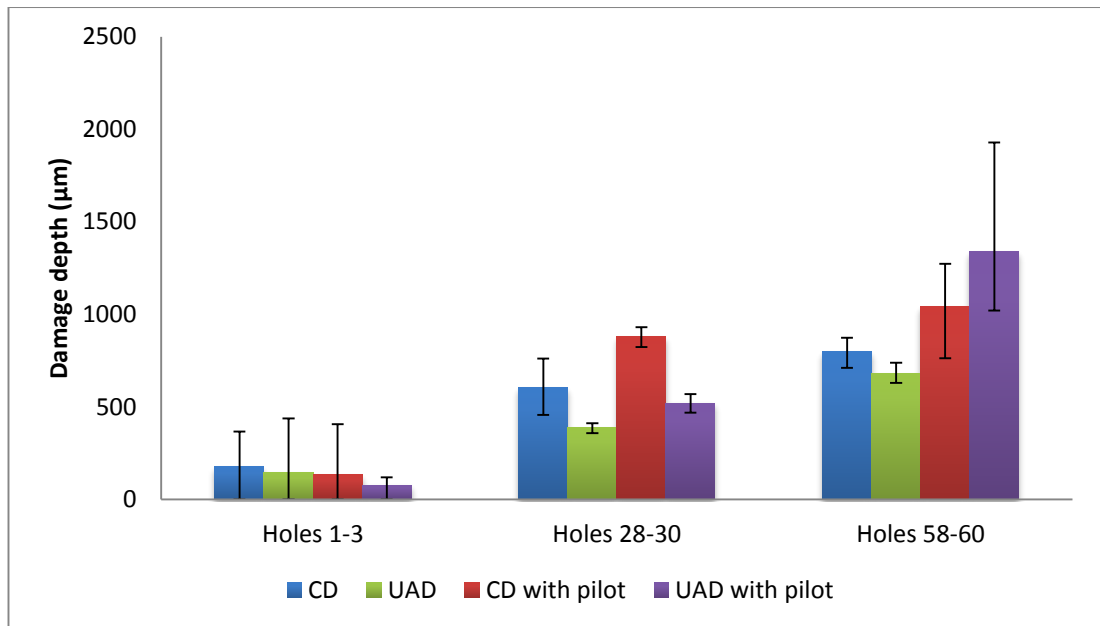


Figure 6-83: Variation in maximum damage at entrance at 10 m/min cutting speed and 0.05 mm/rev feed rate in CD and UAD

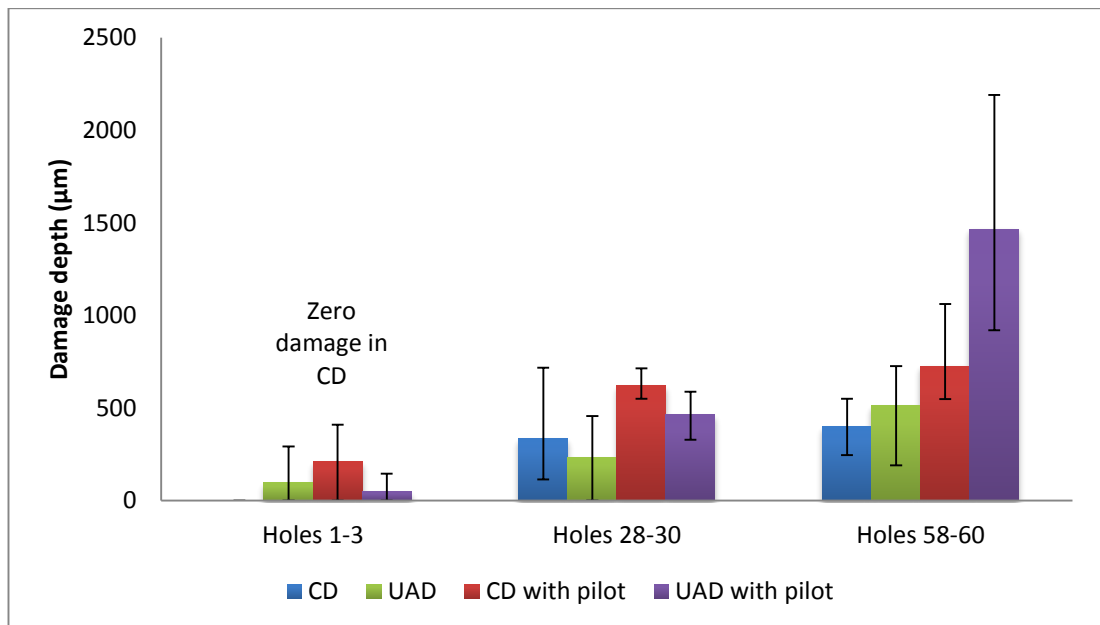


Figure 6-84: Variation in maximum damage at entrance at 100 m/min cutting speed and 0.05 mm/rev feed rate in CD and UAD

From Figure 6-83 and Figure 6-84, it can be observed that the variation in the data in the holes 1-3 does not indicate any clear difference between the cases of CD, UAD, with and without pilot holes at both cutting speeds of 10 and 100 m/min.

In the set of holes 28-30, the variation in the data for 10 m/min in Figure 6-83 and 100 m/min in Figure 6-84 suggests that the maximum damage at the entrance in UAD has been reduced in both with and without pilot holes in comparison to those in CD respectively. When comparing CD and UAD, a reduction of 36% was found at 10 m/min in 'without pilot case' and 41% in 'with-pilot' case through the average of maximum damage depth at entrance.

In the set of holes 58-60, the variation in the data at both cutting speeds of 10 and 100 m/min in Figure 6-83 and Figure 6-84 suggests no clear difference between the respective cases of CD, UAD, with and without pilot-holes except for UAD with pilot case at 100 m/min. The average damage depth is highest in UAD with pilot at 100 m/min cutting speed.

It can also be seen in Figure 6-83 and Figure 6-84 that the average values of damage in the case of 'with pilot' was found to be larger than that in 'without pilot' at both cutting speeds of 10 and 100 m/min in the set of holes 28-30 holes 58-60. This is further discussed in section 6.3.6.3.

In addition to the maximum depth of damage, maximum depth of crack initiation from the entrance was also measured. The maximum depth of crack initiation signifies the drilling depth at entrance up to which the delamination at entrance affected the hole during drilling. An example of measurement of crack initiation depth is shown in Figure 6-85.

6: Experimental studies, results and discussions

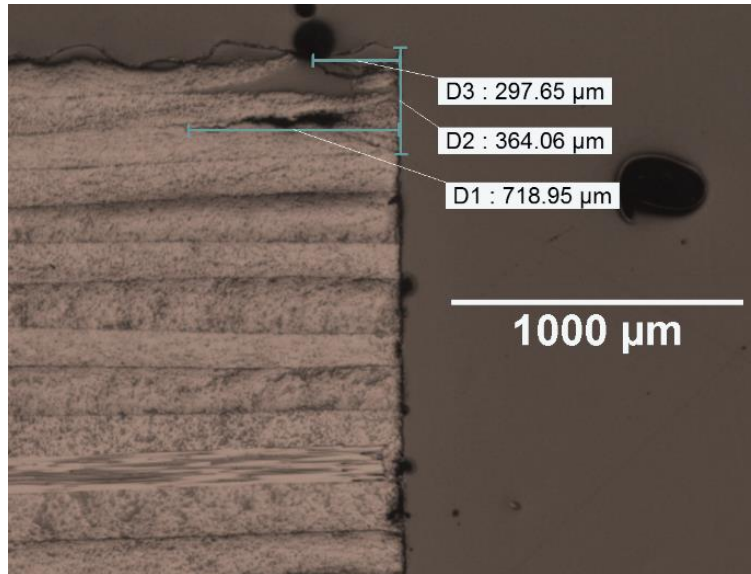


Figure 6-85: Measurement of maximum depth of crack initiation and maximum damage depth in the case of conventional drilling without pilot at 10 m/min at 59th hole (maximum depth of crack initiation = 364.06 μm and maximum damage depth = 718.95 μm)

Similar to maximum damage depth at the entrance, maximum depth of crack initiation at the entrance was plotted against the number of holes. The variation of maximum depth of crack initiation of damage with respect to hole-number is plotted in Figure 6-86 and Figure 6-87 for cutting speeds 10 and 100 m/min respectively.

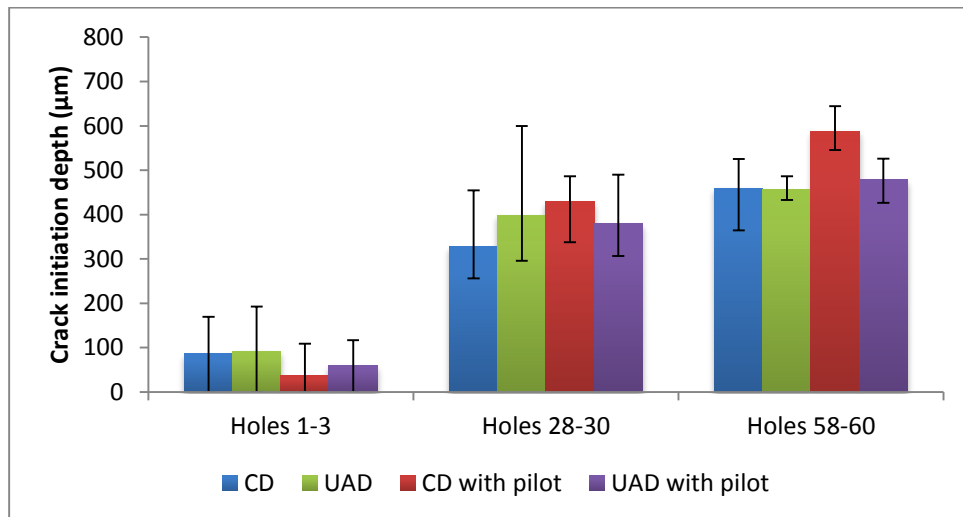


Figure 6-86: Plot of maximum depth of crack initiation at entrance at 10 m/min cutting speed and 0.05 mm/rev feed rate

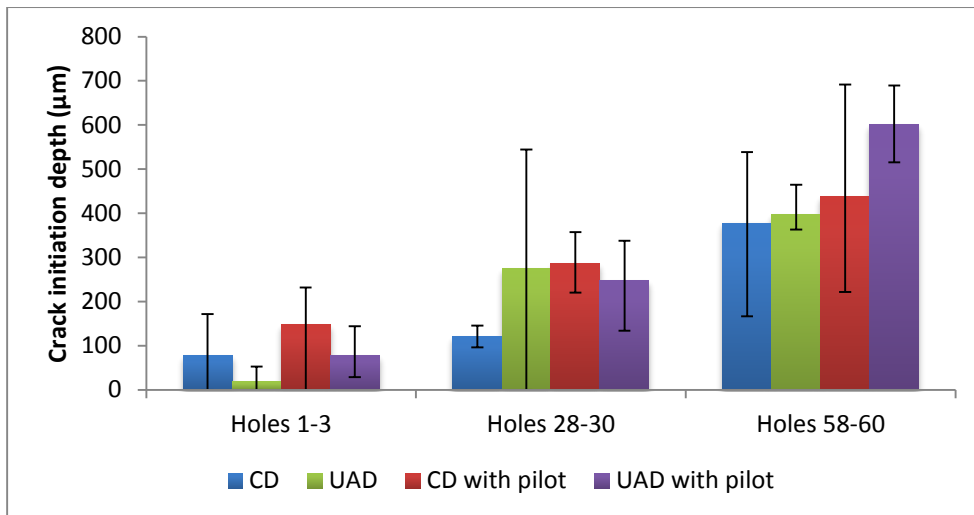


Figure 6-87: Plot of maximum depth of crack initiation at entrance at 100 m/min cutting speed and 0.05 mm/rev feed rate

The variation in the maximum depth of crack initiation at entrance data indicates an increase in maximum depth of crack initiation with respect to increasing number of holes. This indicates that the damage affects the hole up to the larger drilling depth at the entrance during drilling as the number of holes is increased at both cutting speeds of 10 and 100 m/min. This took place because with an increasing number of holes, the tool wear increases as shown in Figure 6-77 and Figure 6-78. The increase in tool wear caused an increase in thrust force and torque discussed in Sections 6.3.4.1 and 6.3.4.2. According to Ho-Cheng and Dharan [87], delamination at the entrance is governed by peeling force which in turn is controlled by cutting forces i.e. torque. In addition, in their work, it was shown that increasing thrust force and torque causes an increase in critical depth for delamination at the entrance. Thus, the depth of delamination at the entrance increases with increasing tool wear i.e. with increasing number of drilled holes.

When comparing CD and UAD, no difference between at any set of holes could be identified in both cutting speeds of 10 and 100 m/min. This implies that the damage affects up to a similar level of heights at the entrance in both CD and UAD.

However, comparing CD and UAD for 10 m/min cutting speed, in terms of the results of maximum damage depth in Figure 6-84 and maximum depth of crack initiation at entrance in Figure 6-86 together for the set of holes 28-30, it can be concluded that although the maximum depth of crack initiation of damage at entrance is similar in CD and UAD however, the maximum extent of damage at entrance is lower in UAD than that in CD in both the cases of with and without pilot hole drilling. This happened because of lower thrust force and torque in UAD than that in CD at 10 m/min.

6.3.3.2 Maximum delamination damage at exit

Similar to maximum damage at the entrance, maximum damage at the exit was also analysed using the same methodology. As shown in Figure 6-88, zero delamination damage at exit was obtained at the exit in the initial holes in some cases. The data for maximum delamination damage depth at the exit for the selected holes in CD and UAD is presented in Table 6-39 and Table 6-40 for cutting speeds 10 and 100 m/min respectively.

6: Experimental studies, results and discussions

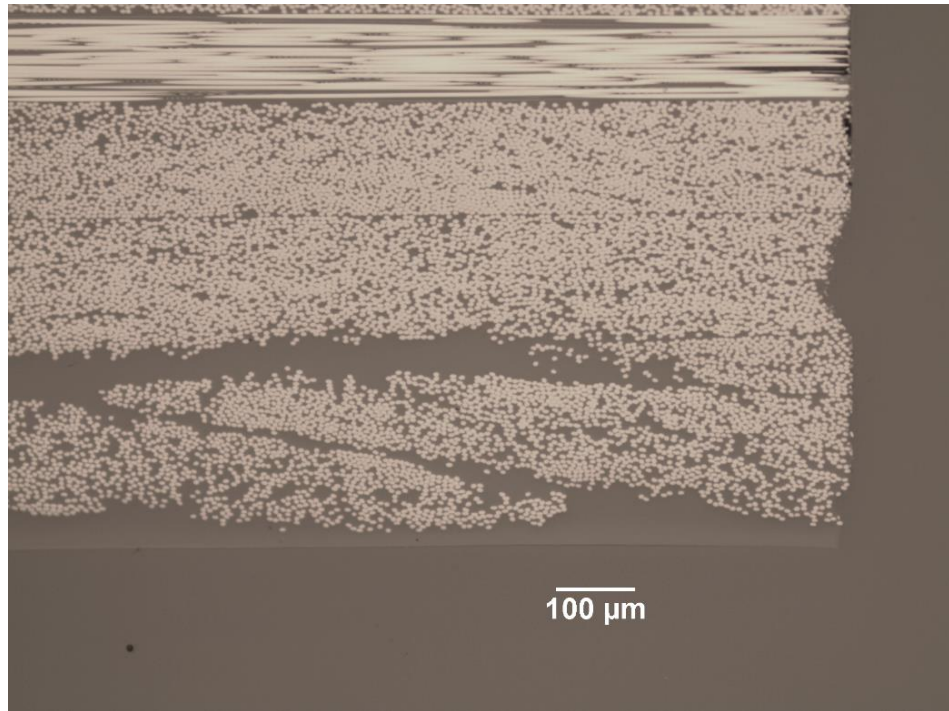


Figure 6-88: Zero delamination damage at exit at 100 m/min cutting speed in UAD with pilot hole drilling in the first hole

Table 6-39: Data for maximum damage depth at exit at 10 m/min cutting speed and 0.05 mm/rev feed rate

Hole number	Maximum damage at exit at 10 m/min			
	CD (μm)	CD with pilot (μm)	UAD (μm)	UAD with pilot (μm)
1	176	0	199	143
2	0	0	88	688
3	264	264	190	156
28	1595	1333	1136	1109
29	1431	1539	1198	1335
30	1309	1478	1039	1258
58	1461	1860	2140	1514
59	1348	1905	2039	1640
60	1687	1949	1394	1826

Table 6-40: Data for maximum damage depth at exit at 100 m/min cutting speed and 0.05 mm/rev feed rate

Hole number	Maximum damage at exit at 100 m/min			
	CD (μm)	CD with pilot (μm)	UAD (μm)	UAD with pilot (μm)
1	170	255	170	0
2	0	218	234	0
3	193	197	208	0
28	492	1187	673	1087
29	735	1257	735	1052
30	536	1070	726	866
58	960	1098	1405	1287
59	1306	1326	1043	1377
60	1070	1018	1114	1063

Similar to maximum damage at the entrance, the averages of set of holes 1-3, holes 28-30 and holes 58-60 at cutting speeds 10 and 100 m/min were considered for analysis for maximum damage depth at the exit. The respective variation in the data is plotted Figure 6-89 and Figure 6-90. The error bars in these figures indicate the maximum and minimum values of damage out of the three consecutive drilled holes.

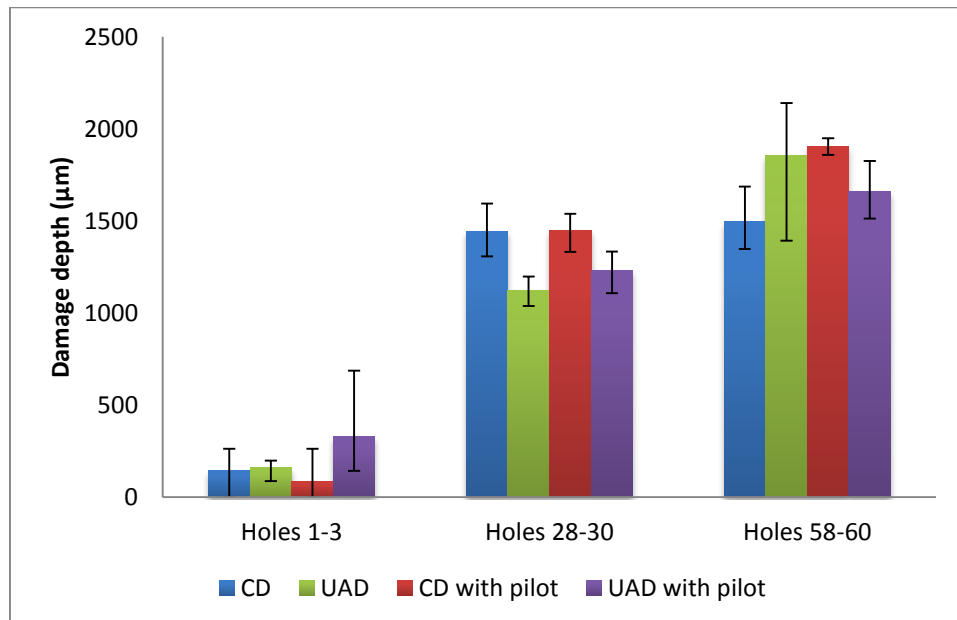


Figure 6-89: Variation in maximum damage at the exit at 10 m/min cutting speed and 0.05 mm/rev feed rate in CD and UAD

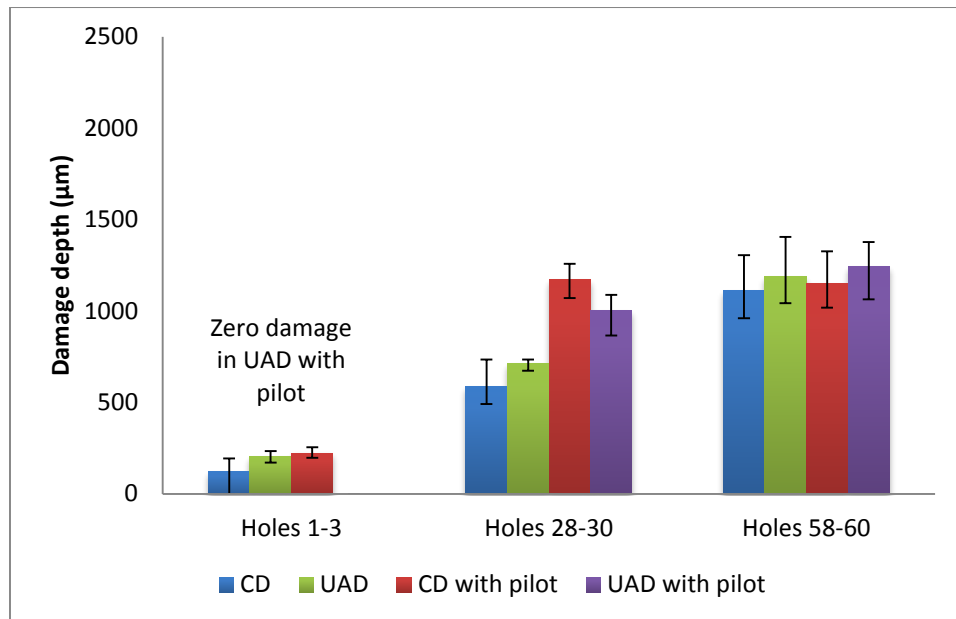


Figure 6-90: Variation in maximum damage at the exit at 100 m/min cutting speed and 0.05 mm/rev feed rate in CD and UAD

At 10 m/min in Figure 6-89, it can be observed that the variation of data in the first three holes does not indicate towards any clear difference between the cases of CD, UAD, with and without pilot holes. When comparing CD and UAD, the reduction in thrust force due to ultrasonic assistance at 10 m/min was found to be 56, 61 and 59% respectively in the first three holes in Table 6-28. However, the variation in maximum damage at exit data suggests no clear difference between CD and UAD. In the set of holes 28-30 at 10 m/min in Figure 6-90, a reduction of 22% in ‘without pilot’ and a reduction of 15% in the case of ‘with-pilot’ holes was obtained due to ultrasonic assistance in UAD in comparison to those in CD. In the set of holes 58-60, the variation in the data does not indicate any clear difference between CD, UAD, with and without pilot hole cases.

At 100 m/min cutting speed in Figure 6-90, it can be observed that the average damage near the exit in the case of ‘with-pilot’ holes is larger than that in the case of ‘without pilot’ holes in the sets of holes 1-3 and holes 28-30. In the literature, Faraz

and Biermann [99] have also reported for achieving higher damage at exit in the case of pilot hole drilling than that in the case of without pilot. Due to drilling a pilot hole, the critical thrust force required for delamination is reduced [21]. It was suggested in the work of Faraz and Biermann [99] that the critical thrust force for the onset of exit delamination was reduced “much significantly” after drilling pilot holes. Also, across the periphery at the exit, the fibres were more prone to bend instead of cutting under the action of cutting edges of twist drill propagating at the exit. Therefore, the exit delamination was not reduced even if a large reduction in the thrust force was observed in their work. The same incidence is suspected to cause higher damage at the exit in the present cases of 100 m/min cutting speed in the set of holes 1-3 and holes 28-30. In the holes 58-60, the variation in the data suggests no clear difference between the damage in the cases of CD, UAD, with and without pilot holes at 100 m/min.

Similar to maximum damage depth at the entrance, maximum depth of crack initiation at exit was also measured. An example of measurement of the maximum depth of crack initiation at the exit is shown in Figure 6-91.

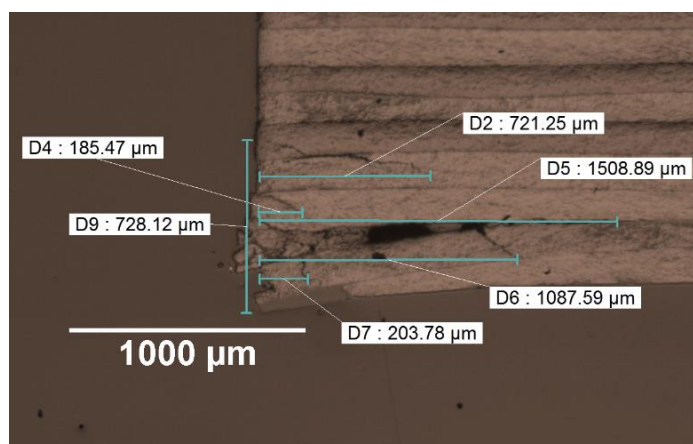


Figure 6-91: Measurement of damage height and depth in the case of conventional drilling without pilot at 10 m/min at 60th hole (maximum depth of crack initiation = 728.12 μm and maximum damage depth = 1058.89 μm)

6: Experimental studies, results and discussions

The variation of maximum depth of crack initiation at the exit with respect to hole-number is plotted in Figure 6-92 and Figure 6-93 for cutting speeds 10 and 100 m/min respectively. It is to be noted in Figure 6-92 and Figure 6-93 that there was a significant difference between the maximum crack initiation depths at 10 and 100 m/min (maximum of 985 μm at 10 m/min and 524 μm at 100 m/min respectively).

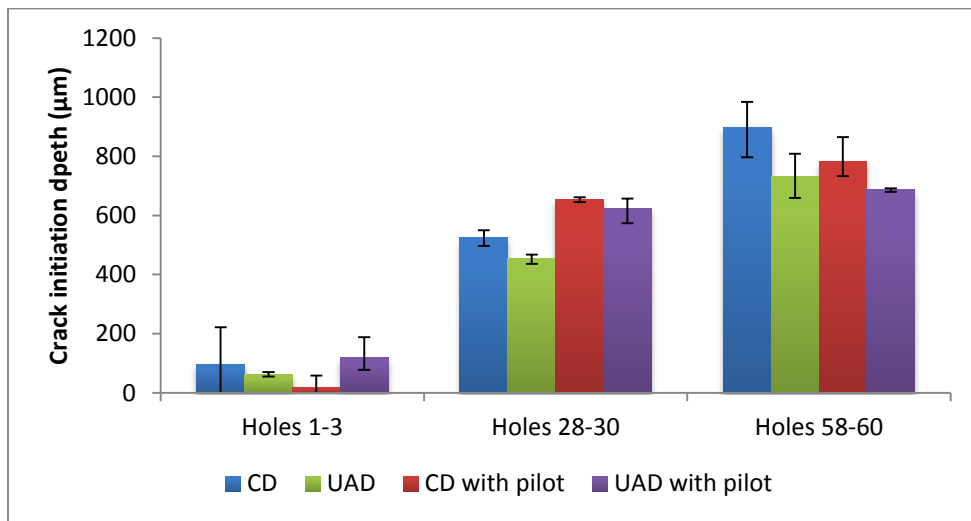


Figure 6-92: Plot of maximum crack initiation depth at exit at 10 m/min cutting speed and 0.05 mm/rev feed rate

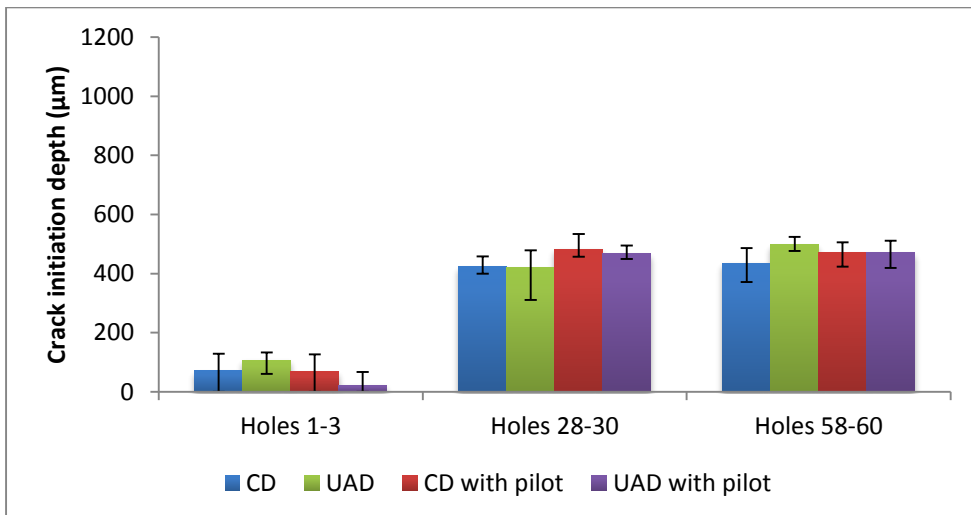


Figure 6-93: Plot of maximum crack initiation depth at exit at 100 m/min cutting speed and 0.05 mm/rev feed rate

The variation in maximum crack initiation depth at exit suggests it increases with increasing number of holes at both cutting speeds of 10 and 100 m/min. Similar findings were also discussed in Section 6.2.3.1 for maximum delamination depth at entrance. The damage at exit increased with increasing number of holes because thrust force increased with increasing number of holes due to increase in tool wear. As discussed by Ho-Cheng and Dharan [87], increasing thrust force increases the critical depth of delamination. Therefore, the delamination started at an earlier drilling depth at the exit with respect to increasing number of drilled holes due to increasing thrust force.

When comparing CD and UAD, at 10 m/min in Figure 6-92, the maximum crack initiation depth at the exit is found to be reduced by 13% in without pilot hole drilling case than that in CD in the hole sets 28-30. There was no obvious difference observed between CD and UAD in the hole sets 1-3 and hole set 58-60 in terms of maximum crack initiation depth at the exit. Also, considering the maximum delamination damage depth at exit and maximum crack initiation depth at exit for 10 m/min cutting speed in hole sets 28-30 together from Figure 6-90 and Figure 6-92, it can be concluded that the maximum delamination extent and crack initiation depth at exit have been reduced by 22 and 13% respectively in UAD as compared to that in CD due to reduction in thrust forces. At 100 m/min cutting speed, there could not be any difference found at any hole set between CD and UAD in maximum damage height.

6.3.3.3 *Internal damage*

Fibre pull-out and disorientation was examined for internal damage quantification with the methodology explained in Section 5.5.2. Holes number 1, 2, 3, 28, 29, 30, 58, 59, and 60 were chosen to analyse the internal damage during

machining. The data for the respective holes is presented in Table 6-41 for 10 m/min and in Table 6-42 for 100 m/min cutting speed respectively.

Table 6-41: Average internal damage data for selected holes at 10 m/min and 0.05 mm/rev feed rate in CD and UAD

Hole number	Internal damage at 10 m/min			
	CD (μm)	CD with pilot (μm)	UAD (μm)	UAD with pilot (μm)
1	38	31	31	24
2	44	33	27	25
3	40	32	27	30
28	63	55	59	66
29	51	62	61	68
30	61	53	56	59
58	93	92	76	81
59	84	82	74	80
60	84	77	70	83

Table 6-42: Average internal damage data for selected holes at 100 m/min and 0.05 mm/rev feed rate in CD and UAD

Hole number	Internal damage at 100 m/min			
	CD (μm)	CD with pilot (μm)	UAD (μm)	UAD with pilot (μm)
1	48	60	24	28
2	48	61	24	21
3	52	42	27	25
28	69	70	47	52
29	67	70	42	55
30	71	74	60	56
58	64	71	66	70
59	75	77	62	77
60	74	78	77	71

Similar to maximum damage at entrance and exit, the averages of each set of holes at cutting speeds 10 and 100 m/min were considered for analysis of the internal damage. The respective variation in the data is plotted Figure 6-94 and Figure 6-95 for cutting speeds 10 and 100 m/min respectively. The error bars in these figures

indicate the maximum and minimum values of damage out of the three consecutive drilled holes.

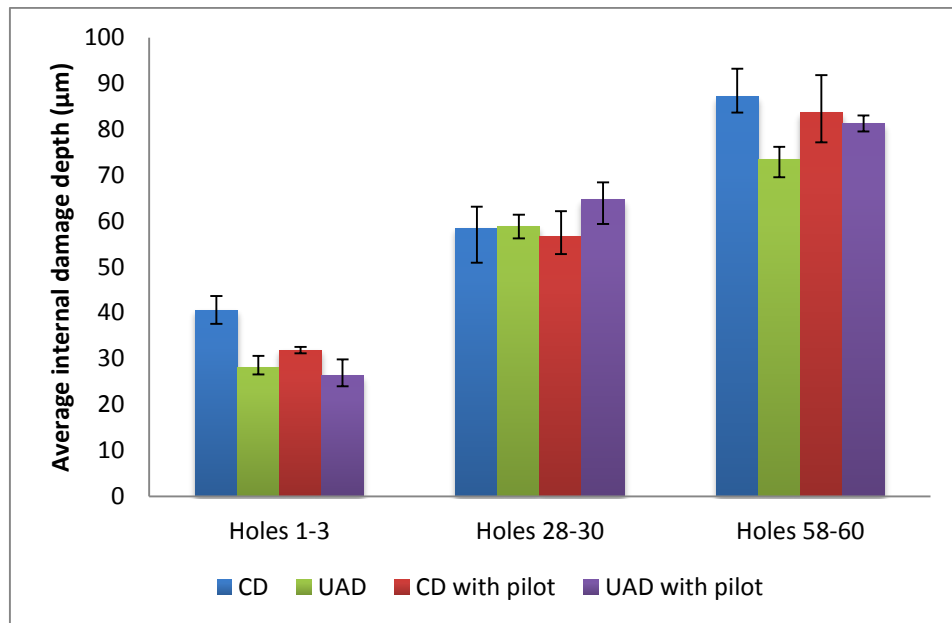


Figure 6-94: Variation of internal damage at 10 m/min and 0.05 mm/rev feed rate in all the cases of CD, UAD, with and without pilot holes

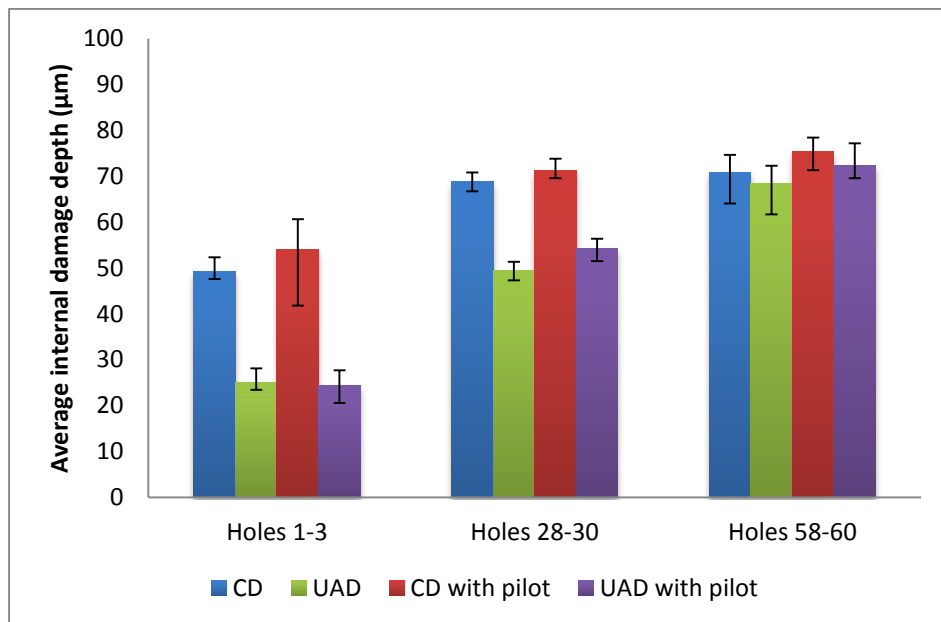


Figure 6-95: Variation of internal damage at 100 m/min and 0.05 mm/rev feed rate in all the cases of CD, UAD, with and without pilot holes

At 10 m/min, internal damage data in Figure 6-94 suggests that the internal damage in CD was highest in the first three holes. For the set of holes 28-30, the

variation in internal damage data did not show a clear difference between any cases. For the set of holes 58-60, a reduction of 16% was found in the case of ‘without pilot’ due to ultrasonic assistance in comparison to that in CD while no clear difference could be observed between CD and UAD in the case of ‘with pilot’ holes.

The internal damage data at 100 m/min in Figure 6-95 displays a reduction of 49% in the case of ‘without pilot’ and 55% in ‘with pilot’ was obtained due to ultrasonic assistance as compared to those from CD in the holes 1-3. For the set of holes 28-30 a reduction of 28% in the case of ‘without pilot’ and 24% in the case of ‘with pilot’ holes was obtained due to ultrasonic assistance as compared to that from CD. For the set of holes 58-60 the variation in the data does not indicate any difference between CD, UAD, with and without pilot-holes. Thus, when comparing CD and UAD, a considerable amount of internal damage reduction was obtained in UAD at 100 m/min cutting speed in the first three holes and holes 28-30. However, the internal damage at 10 m/min cutting speed was found to be similar in CD and UAD.

6.3.4 Machined surface

The SEM images of machined surfaces were considered to assess the damage in CD and UAD in various holes. However, no visual difference could be observed between the machined surfaces of CD and UAD at 10 m/min cutting speed. SEM images of hole numbers 1 and 60 at 10 m/min display that the damage on the machined surface in hole number 60 is more than that in the hole number 1. At 100 m/min cutting speed, the internal damage seemed to be less severe in UAD than that in CD. Also, hole number 60 contained higher internal damage than that in hole number 1. In general, comparing the machined surfaces at 10 m/min cutting speed that at 100 m/min, it became visually clear that machined surface at 100 m/min had

more severe internal damage than that in 10 m/min cutting speed. The respective SEM images are shown in Appendix D.

6.3.5 Analysis of chip fragments

The chip fragments were analysed in SEM after sticking them to double sided carbon tape onto stubs and by gold coating. Chip fragments obtained from the first three holes were analysed in SEM. No clear difference identified between the chip fragments obtained from CD and UAD at both the cutting speeds of 10 Figure 6-96 and 100 m/min Figure 6-97. However, comparing the chip fragments obtained at 10 m/min cutting speed with those obtained at 100 m/min, it becomes clear that larger fragments of chip were obtained at cutting speed of 100 m/min than that from 10 m/min cutting speed in both CD and UAD.

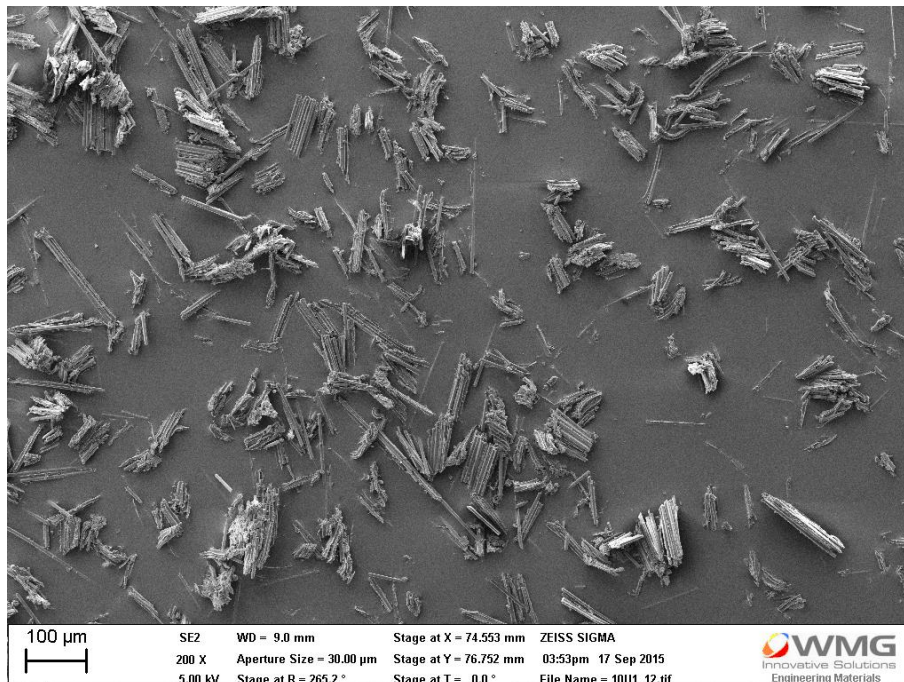


Figure 6-96: Chip fragments obtained in the hole number 1 at 10 m/min cutting speed in UAD



Figure 6-97: Chip fragments obtained in the hole number 1 at 100 m/min cutting speed in UAD

6.3.6 Discussion

6.3.6.1 Thrust force and torque

When comparing CD and UAD, the effective normal rake angles calculated for a new tool in section 6.3.1 at cutting speeds of 10 and 100 m/min indicated higher values of effective normal rake angles at the lower cutting speed of 10 m/min. The thrust force data mentioned in Table 6-29 and Table 6-28 makes it evident that larger percentage of thrust force reduction due to ultrasonic assistance in comparison to that in CD was obtained at a lower cutting speed of 10 m/min as compared to that in 100 m/min cutting speed. The reduction in the thrust force due to ultrasonic assistance varied between 61 to 54% at 10 m/min in the first five holes while that was 17 to 15% at 100 m/min in the cases of without pilot holes. In the case of with pilot holes the percentage reductions were 55 to 30% at 10 m/min while those were 20 to 11% at 100 m/min. Thus, higher thrust force reduction at lower cutting speed with constant feed rate becomes evident. This is further discussed in Section 6.3.6.2.

When comparing the worn tool data at the 60th hole, the reduction in thrust force due to ultrasonic assistance was 27% at 10 m/min and 6% at 100 m/min for with and without-pilot holes in with and without pilot holes. Thus, thrust force data suggests that with respect to increasing number of holes, as the tool wear increases, the reduction in thrust force diminishes due to reduction in effective normal rake angle with increasing tool wear.

Similar to thrust force data, it becomes clear from the average torque data presented in Table 6-30 and Table 6-31 that larger reduction in torque due to ultrasonic assistance was found to be in the case of 10 m/min cutting speed as compared to that at 100 m/min cutting speed. Torque data signifies cutting forces coming from cutting edge. Therefore, it can be concluded from torque data that lower cutting speed produces a larger reduction in cutting forces through ultrasonic assistance as compared to higher cutting speeds.

6.3.6.2 Discussion for thrust force reduction and intermittent cutting action

Some authors have argued for intermittent cutting action during ultrasonic assisted turning (UAT) process [47]. It has been explained that increasing the tool-material separation in every ultrasonic oscillation cycle in UAT causes lower mean stresses per ultrasonic oscillation cycle resulting in lower cutting forces. The same reason for thrust force reduction due to intermittent cutting action has been surmised by the authors during UAD [25, 40]. Since the oscillations are imposed in the axial direction during drilling, the relative tool-material separation will be higher at a low feed rate in UAD. The feed rate in the Phase-3 was 0.05 mm/rev. Larger effective normal rake angle at 10 m/min indicates to be the reason behind the larger reduction in thrust force at 10 m/min in comparison to 100 m/min. However, if the feed rate is counted in mm/min dimensions, it was 26.5 mm/min at 10 m/min and 265.5 mm/min

at 100 m/min cutting speed. Therefore, based on the literature [25, 40, 47], an argument could be made that due to the lower feed rate of 26.5 mm/min at 10 m/min cutting speed, the reduction in thrust force was larger when comparing CD and UAD.

In order to compare the feed rate and maximum velocity due to ultrasonic assistance, recalling Equation (4.11), the velocity due to ultrasonic assistance,

$$V_{f_{iUAD}} = a\omega \cos(\omega t)$$

Where 'a' is ultrasonic oscillation amplitude and $\omega = 2\pi f$ (f= ultrasonic oscillation frequency). The maximum value of $\cos(\omega t) = 1$.

Therefore, the maximum velocity due to ultrasonic assistance = $a\omega = a*2\pi f$. The respective values of feed rate and maximum velocity due to ultrasonic assistance have been calculated for the experimental study in Phase-3 from the ultrasonic parameters presented in Table 5-15 in Section 5.7.3.2 and are presented in Table 6-43 for 10 and 100 m/min cutting speeds.

Table 6-43: Comparison of feed rate and maximum velocity due to ultrasonic assistance at 10 and 100 m/min

Cutting speed (m/min)	Drilling condition	Feed rate (mm/rev)	Feed rate (mm/min)	Maximum speed due to ultrasonic assistance ($a\omega$) (mm/min)
10	UAD	0.05	26.5	55233
	UAD with pilot			56901
100	UAD		265.5	56073
	UAD with pilot			51629

From the feed rate and maximum velocity due to ultrasonic assistance data in Table 6-43, it is clear that the feed rates of 26.5 and 265.5 mm/min would not make a difference in comparison to the maximum velocity due to ultrasonic assistance

(56901 to 51629 mm/min) for intermittent cutting action. Nevertheless, for comparison of equivalence, the relative reduction of thrust force in UAD at 10 and 100 m/min with a common feed rate in mm/min units was investigated in a test which is explained in Section 6.4.

6.3.6.3 Discussion of damage

Unlike the clear effects on cutting and thrust forces, the effect of UAD on damage was not found to be utmost clear in the present study. For the set of holes 1-3 at 10 m/min cutting speed, there was no difference between damage depth and height was found even though the thrust force was reduced by 55% in the first hole during drilling. This particular result is in contrast with what is reported by other authors [40] and the reason behind this particular result is not yet explained. Although the damage depth at the exit is lower than 250 μm except the second hole in UAD with pilot hole drilling.

The reduction in thrust force and torque at 10 m/min cutting speed in the holes 28-30 did result in the reduction in the delamination depth at entrance and exit. At the average tool wear length of 52 μm (Table 6-32), a reduction of 36% in damage at the entrance and 22% reduction in damage at exit was found corresponding to 40% reduction in thrust force (Table 6-28) and 46% reduction in torque (Table 6-31). Holes 58-60 do not show a clear difference between CD and UAD in damage at entrance and exit which indicates that the effect of ultrasonic assistance was diminished as the tool wear increased from hole 1 to hole 60.

When comparing CD and UAD in terms of internal damage, the internal damage data plotted in Figure 6-94 and Figure 6-95 indicated that higher reduction in internal damage was found in UAD in comparison to that in CD for the set of holes 1-3 and

holes 28-30 at 100 m/min as compared to that at 10 m/min. At this point, if the CT scanning results of exit delamination from a new tool in Figure 6-15 in Section 6.1.3.1 are recalled, an indication of a reduction in internal damage due to ultrasonic assistance at 94.2 m/min cutting speed was found. At 9.42 m/min, the internal damage was similar in CD and UAD. However, since the data was from a single hole per cutting speed, therefore, no decisive conclusion could be drawn with CT scanning result at that point. However, internal damage in three consecutive holes in the Phase-3 gives a clear indication towards a larger reduction in internal damage at 100 m/min than that at 10 m/min when comparing CD and UAD.

This can be explained by tool wear at 10 and 100 m/min in Figure 6-77 and Figure 6-78. When comparing CD and UAD, the tool wear was found to be similar in CD and UAD at 10 m/min. At 100 m/min, it reduced in UAD in comparison to CD in both the cases of with and without pilot holes.

As reported by other authors, lower tool wear produces lower cutting temperature during machining [208, 209]. As found in Phase-1, lower the cutting temperature, lower the extent of matrix softening. Therefore, due to a lower cutting temperature in UAD, the matrix softened up to lower extent resulting in lower fibre pull-out and disorientation i.e. lower internal damage in comparison to that in CD at 100 m/min. At 10 m/min, the internal damage was similar in CD and UAD due to similar tool wear resulting in similar cutting temperature.

At 100 m/min cutting speed, when comparing CD and UAD, the internal damage was found to be reduced by 55% in the first three holes and 28% in the holes 28-30 due to ultrasonic assistance in comparison to that in CD, Figure 6-94. In the holes 58-60 there was no difference between CD and UAD in terms of internal damage.

This behaviour in internal damage indicates that the effect of ultrasonic assistance reduced with increasing number of drilled holes. The percentage reduction in thrust force data in Table 6-29 and percentage reduction in torque data in Table 6-30 for 100 m/min cutting speed also indicate a similar conclusion. The percentage reductions in thrust force and torque were reduced as the number of drilled holes increased, i.e. as the tool wear increased with increasing number of drilled holes, Table 6-33. Thus, the variation in all the parameters i.e. thrust force, torque, tool wear and internal damage data at 100 m/min cutting speed indicate towards one common conclusion that the effect of ultrasonic assistance was reduced with increasing tool wear. The reason behind this phenomenon has been explained in Section 6.3.2.5. It took place because the axial rake angle at the cutting edge was reduced due to increasing tool wear. This caused a reduction in effective normal rake angle in UAD in a worn tool as compared to a new tool. Thus, the diminishing effect of ultrasonic assistance was caused by decreasing effective normal rake angles with increasing tool wear.

In addition, the machined surfaces and chip fragments in CD and UAD discussed in Sections 6.3.4 and 6.3.5 do not show a clear difference between the material failure modes in CD and UAD which also negates the possibility of excessive effects of strain rates during machining in UAD. The effects of such strain rates during UAD has not been examined by any author in the literature and it is a subject of future research.

6.3.7 Conclusions from Phase-3

- With this study, it was evident that the extent of reduction in cutting and thrust forces due to ultrasonic assistance in UAD with respect to those in CD is higher at the lower cutting speed (10 m/min) at a constant feed rate of 0.05 mm/rev. Higher effective normal rake angles at 10 m/min in UAD indicate to be the reason behind larger thrust force reduction. However, the respective feed rates at 10 and 100 m/min cutting speeds were 26.5 and 265.5 mm/min. Although, 26.5 and 265.5 mm/min do not make a difference in comparison to the maximum velocity of 60620 mm/min from ultrasonic assistance. Nevertheless, for equivalence comparison, this has been tested and confirmed in Section 6.4.
- At lower cutting speed (10 m/min) the damage at entrance and exit, there was no reduction in exit delamination found with a new tool. Although At the average tool wear length of 52 μm (Table 6-32), a reduction of 36% in damage at the entrance and 22% reduction in damage at exit was found corresponding to 40% reduction in thrust force (Table 6-28) and 46% reduction in torque (Table 6-31).
- When comparing CD and UAD, the tool wear was found to be lower in UAD at 100 m/min. At 10 m/min, the tool wear was “similar” in CD and UAD (the maximum difference was 6 μm). This was justified by the larger negative clearance angles being obtained at 10 m/min of -74° which led to higher rubbing of flank surface and did not result in a reduction in tool wear (in fact tool wear is higher in UAD on holes 1 and 20 by 4 and 5 μm respectively).
- Due to reduction in tool wear at 100 m/min, larger reduction in internal damage was obtained at 100 m/min as compared to that at 10 m/min when

comparing CD and UAD. The reason behind this was found to be a reduction of tool wear at 100 m/min in UAD. Lower tool wear causes lower cutting temperature and hence lower internal damage. At 10 m/min, larger negative clearance angles of -74° led to higher rubbing of the flank surface which did not result in a reduction in tool wear and hence no clear reduction in internal damage was found.

- Thrust force, torque, tool wear and damage data together indicate that ultrasonic assistance is more effective with a new tool and it is diminished as the tool wear increases during machining. The fundamental reason behind diminishing the effect of ultrasonic assistance with increasing tool wear is due to a reduction in effective rake angle with increasing cutting edge radius with due to increasing tool wear, as discussed in Section 6.3.2.5.
- It has been found in the current study, the fraction of thrust force from chisel edge has been reduced in UAD as compared to CD. This indicates towards different machining mechanism at chisel edge in UAD with respect to CD which requires to be investigated further.
- No clear difference between the machined surfaces and chip fragments generated in CD and UAD process could be found.

6.4 Confirmation of effect of larger 'effective' normal rake angles at same intermittent cutting action

As discussed in Section 6.3.6.2, ultrasonic assistance has also been applied to the turning process of metals in the direction of cutting speed [43, 47]. Through a UAT process, authors found a higher reduction in cutting force at lower cutting speed in UAT with respect to that in conventional turning (CT). To support this finding, the argument was proposed that when reducing the cutting speed, the tool-material contact time reduces in each ultrasonic oscillation cycle which generates lower stresses during machining and hence the cutting forces are reduced. Unlike UAT, the ultrasonic oscillations are imposed in the axial feed direction in drilling (perpendicular to the cutting speed direction, as explained in Section 4.5). If the argument of the other authors [43, 47] is followed, lower feed rate should result in a higher reduction in thrust force in UAD as compared to CD due to lower tool-material contact time in each ultrasonic oscillation cycle. Although the larger reduction in thrust force in UAD as compared to CD was obtained at 10 m/min in Phase-3. However, due to feed rate being 26.55 and 265.5 mm/min at two cutting speeds, it could be argued that due to the larger separation between tool and material at 26.55 mm/min, the larger reduction in thrust force was obtained in Phase-3.

To verify whether this happened due to larger effective rake angles at low cutting speed or due to larger time interval for tool-material separation at low feed rate, a test was performed in the present research to compare the reduction in thrust force due to ultrasonic assistance at cutting speeds of 10 and 100 m/min at a common feed rate of 26.5 mm/min. The reason for selecting a common feed rate in mm/min unit was to keep the relative separation time between tool and material same at both cutting speeds of 10 and 100 m/min during intermittent cutting action in UAD.

Through the method explained in Section 4.6, the effective normal rake angles at the cutting edges were calculated for 10 and 100 m/min cutting speeds and 26.5 mm/min feed rate using the respective experimental ultrasonic frequencies and amplitudes. The effective normal rake angles are displayed Figure 6-98 and Figure 6-99 for 10 and 100 m/min cutting speeds respectively. Larger maximum effective normal rake angle of 62° is obtained at 10 m/min compared to that of 49° at 100 m/min.

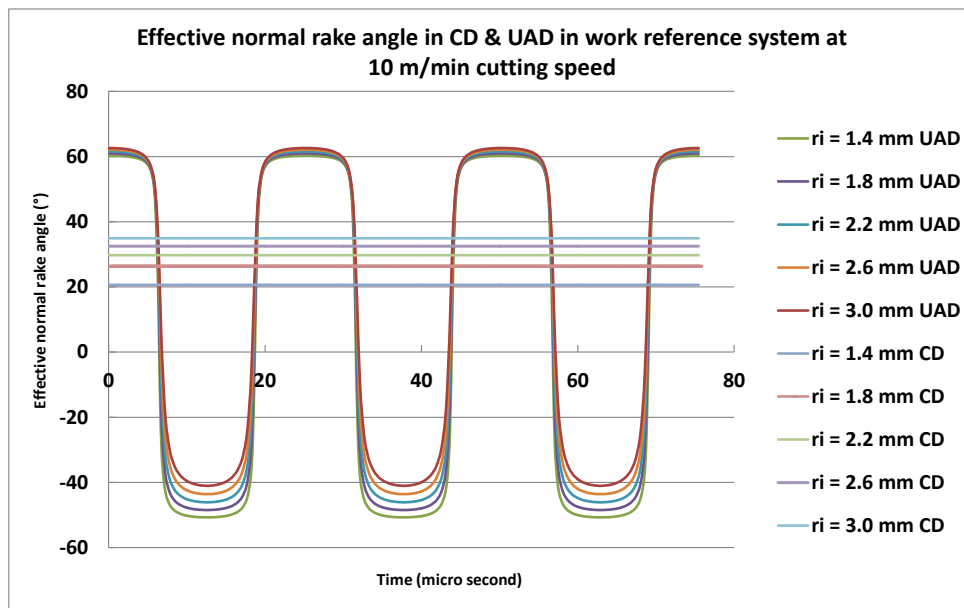


Figure 6-98: Effective normal rake angles at 10 m/min cutting speed and 26.5 mm/min feed rate in CD and UAD

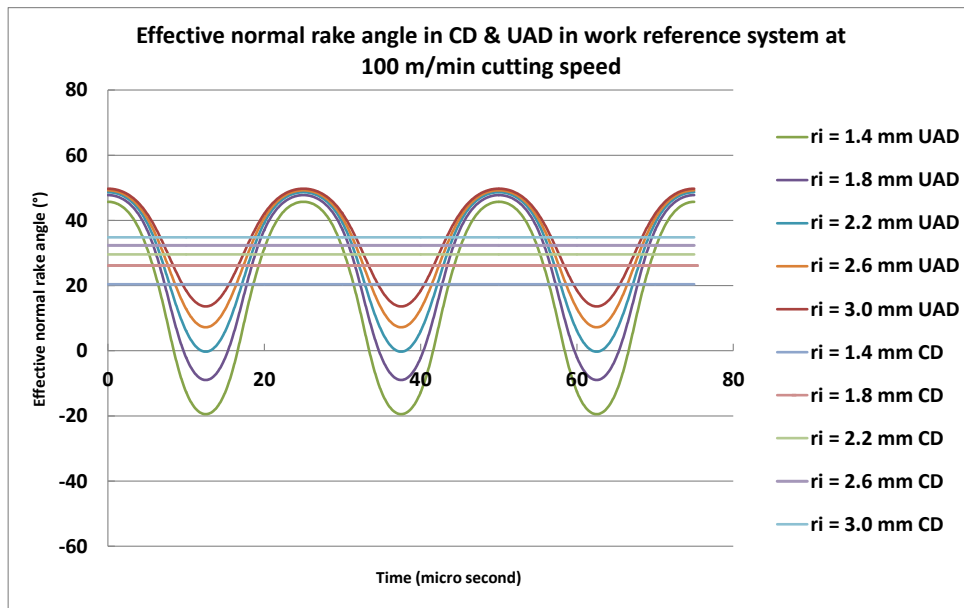


Figure 6-99: Effective normal rake angles at 100 m/min cutting speed and 26.5 mm/min feed rate in CD and UAD

In this test, five holes were drilled consecutively at 100 m/min cutting speed and 26.5 mm/min feed rate in CD and UAD, with and without pilot holes in the same experimental setup described in Section 5.7.3.2 with a new tool. The ultrasonic frequencies at UAD without and with pilot hole drilling were 40320 Hz and 39990 Hz respectively. The ultrasonic oscillation peak-to-peak amplitudes were 6.8 and 6.3 μm respectively. The results obtained with this test were compared with those obtained at 10 m/min cutting speed and 26.5 mm/min feed rate in CD and UAD presented in Table 6-28 for the first five holes. Average thrust forces, percentage reduction due to ultrasonic assistance with respect to CD in both cases of with and without pilot holes obtained at 10 and 100 m/min are presented in Table 6-44 and Table 6-45 respectively.

Table 6-44: Data table for average thrust forces at 10 m/min cutting speed and 26.5 mm/min feed rate in the cases of CD, UAD with and without pilot hole drilling

Hole number	Average thrust force at 10 m/min and percentage reduction of thrust force in UAD with respect to CD					
	CD (N)	UAD (N)	% Reduction	CD with pilot (N)	UAD with pilot (N)	% Reduction
1	37	16	56	18	8	55
2	49	19	61	22	14	37
3	55	22	59	26	16	37
4	60	27	55	34	19	42
5	64	30	54	32	22	31

Table 6-45: Data table for average thrust forces at 100 m/min cutting speed and 26.5 mm/min feed rate in the cases of CD, UAD with and without pilot hole drilling

Hole number	Average thrust force at 100 m/min and percentage reduction of thrust force in UAD with respect to CD					
	CD (N)	UAD (N)	% Reduction	CD with pilot (N)	UAD with pilot (N)	% Reduction
1	32	26	17	22	17	26
2	49	41	16	40	31	22
3	59	51	13	47	38	18
4	65	58	10	50	42	15
5	70	62	12	53	44	16

The comparison of percentage reduction in thrust force due to ultrasonic assistance in comparison to that in CD obtained at 10 and 100 m/min cutting speeds is plotted in Figure 6-100 and Figure 6-101 for the cases of without and with pilot holes.

6: Experimental studies, results and discussions

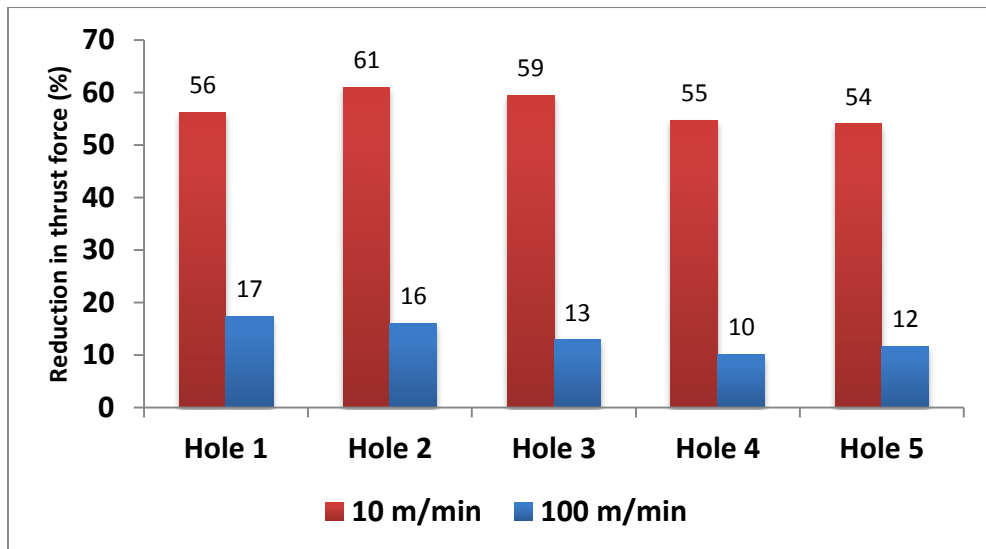


Figure 6-100: Comparison of percentage thrust force reduction due to ultrasonic assistance between 10 and 100 m/min cutting speeds and 26.5 mm/min feed rate in the case of ‘without pilot hole’ drilling

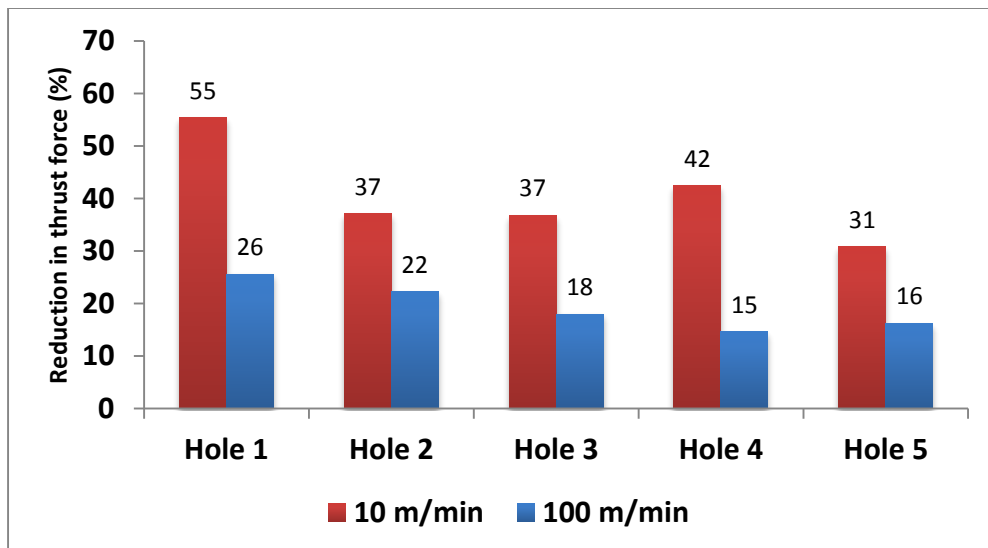


Figure 6-101: Comparison of percentage thrust force reduction due to ultrasonic assistance between 10 and 100 m/min cutting speeds and 26.5 mm/min feed rate in the case of ‘with pilot hole’ drilling

The average tool wear after drilling of five holes at 10 and 100 m/min was found to have a maximum difference of 5 μm . Therefore, it was concluded that tool condition was similar at 10 and 100 m/min after drilling five holes.

When comparing ‘CD with pilot’ and ‘UAD with pilot’, the percentage reduction in thrust force data from Figure 6-101 and similar tool condition at 10 and 100 m/min, clearly indicate that larger reduction in thrust force was obtained at

10 m/min in comparison to 100 m/min with similar tool conditions. Since feed rate was 26.5 m/min at both cutting speeds, therefore, the tool-material separation was same during intermittent cutting action at both cutting speeds. Thus, even if the tool-material separation was the same at 10 and 100 m/min, the reduction in thrust force in ‘UAD with pilot’ as compared to ‘CD with pilot’ is still higher at 10 m/min consistently in five holes. It is to note here that in the cases of ‘CD with pilot’ and ‘UAD with pilot’, there is no chisel edge involvement during drilling. Thus, a larger reduction in thrust force was obtained at lower cutting speed (10 m/min) with the same tool-material separation interval at both cutting speeds during intermittent cutting action when only cutting edges are involved during drilling with similar tool-condition. In the literature, the only reason behind thrust force reduction due to ultrasonic assistance has been reported to be due to an intermittent cutting action of the drill in UAD [25, 40]. However, with the help of machining theory, this test proves that even if the intermittent cutting action is same, a larger reduction in thrust force would be obtained at lower cutting speed due to larger effective rake angles obtained at lower cutting speed in UAD.

It is to note in the present test that while keeping the axial distance moved by the tool per unit time similar at two cutting speeds of 10 and 100 m/min in this test, the uncut chip thickness has been reduced at 100 m/min cutting speed (0.005 mm) as compared to that at 10 m/min (0.05 mm). The reduction of uncut chip thickness at 100 m/min should result in lower machining forces in both CD and UAD as compared to those at 10 m/min cutting speed [168]. Looking at the thrust force data in Table 6-44 and Table 6-45 for the case of CD, it can be seen that reduction of uncut chip thickness from 10 m/min to 100 m/min did not really result in significant reduction of thrust force when increasing the cutting speed from 10 m/min to

100 m/min (5 N maximum reduction). Therefore, it is inferred that the variation in uncut chip thickness did not practically affect the results in this particular test. Nevertheless, the relative reduction of thrust force and torque at constant uncut chip thickness has already been examined in Section 6.3.2.

Thus, minimal effects of similar strain rate variation at two cutting speeds (as discussed in Section 6.3.6.3), minimal damping of amplitude during drilling in Figure 5-5, no practical effect of reduction in uncut chip thickness and constant tool-material separation in this test leave the only possibility that because of larger effective rake angles obtained at lower cutting speed of 10 m/min, larger reduction thrust force has been obtained in UAD with respect to CD when comparing the two cutting speeds of 10 and 100 m/min.

6.4.1 Conclusion

This test proves that due to higher effective normal rake angles at the lower cutting speed of 10 m/min, a larger reduction in thrust force was obtained at lower cutting speed.

7 Conclusions

Referring to the objectives of this research discussed in Chapter 1, the overall objectives were – 1) Determine the mechanism associated with cutting edges in a twist drill causing the reduction in machining forces in UAD of CFRP and its relationship with cutting speed; 2) Determine the underlying relationship in-between machining forces, overall workpiece damage (entrance/exit delamination and internal damage) and cutting speed in CD and UAD of CFRP; and finally, 3) Determine the influence of tool wear on the effectiveness of UAD with respect to cutting speed.

The conclusions from the present research as per these objectives can be stated as follows:

7.1 The mechanism associated with cutting edges in a twist drill causing the reduction in machining forces in UAD of CFRP and its relationship with cutting speed

- With the help of theoretical explanation through machining theory in Section 4.6 and the experimental findings in Sections 6.3.2 and 6.4 in this research, it is concluded that the fundamental reason for the reduction in machining forces associated with cutting edges of twist drill is larger effective rake angles in UAD in comparison to CD. The effective rake angle in UAD increases as the cutting speed is reduced in comparison to that in CD. This causes a greater reduction in machining forces at lower cutting speed in UAD in comparison to those in CD even if the relative separation of tool-material due to intermittent cutting action is same in UAD. In the present case, the percentage reduction in thrust force and torque due to ultrasonic assistance

was 55% and 45% respectively at 10 m/min cutting speed. While those at 100 m/min cutting speed were 20% and 10% respectively, with a new tool.

- With the help of lower wear obtained on the chisel edge of HSS drills in UAD in comparison to CD in Section 6.2.2.4 and lower thrust force from chisel edge obtained in UAD in comparison to CD in Phase-3, Figure 6-74, it is concluded that the fraction of thrust force from chisel edge during drilling is reduced in UAD as compared to CD. However, the specific mechanism which causes this reduction in the forces from chisel edge in UAD has not been investigated and requires further research.

7.2 The underlying relationship in-between machining forces, overall workpiece damage (entrance/exit delamination and internal damage) and cutting speed in CD and UAD of CFRP

7.2.1 Forces and delamination at entrance and exit

- Based on the entrance and exit delamination data discussed in Sections 6.3.3.1 and 6.3.3.2, it is concluded that reduction in thrust force and torque in UAD in comparison to CD results in lower delamination at entrance and exit. In the present case, at the average tool wear length of 52 μm , a reduction of 36% in damage at the entrance and 22% reduction in damage at exit was found corresponding to 40% reduction in thrust force and 46% reduction in torque at 10 m/min cutting speed.
- Based on the results of entrance and exit delamination in Phase-1 and Phase-3 in Chapter-6 (Sections 6.1 and 6.3), it is concluded that the damage at the entrance and exit of the hole is reduced with increasing cutting speed in

both CD and UAD. This takes place because with increasing cutting speed, the cutting temperature increases which softens the matrix, requiring lower cutting force to machine. Thus, lower force at the entrance and exit causes a lower extent of the damage. In the present case in Phase-1 (Section 6.1), the entrance delamination was reduced by 89% in CD and 76% in UAD and the exit delamination was reduced by 40% in CD and 32% in UAD when increasing the cutting speed from 0.942 to 282.6 m/min at a constant feed rate of 0.05 mm/rev with a worn tool.

7.2.2 Internal damage

- Based on the results presented in Phase-1 (Section 6.1), it is concluded that the average internal damage (fibre pull out and fibre disorientation) increases with increasing cutting speed in CD and UAD. In the present case, it increased by 65% in CD and 60% in UAD when increasing the cutting speed from 0.942 to 282.6 m/min at a constant feed rate of 0.05 mm/rev with a worn tool. It took place because of softening of thermally non-conducting matrix to a greater extent due to increase in cutting temperature with increasing cutting speed resulting in a reduction in strength of matrix for supporting the fibres in place.
- Based upon the internal damage results presented in Section 6.3.3.3, it is concluded that greater reduction in internal damage is obtained at higher cutting speed in UAD when compared to CD. In the present case, 100 m/min corresponded 55% and 49% reduction in internal damage in with and without pilot-hole drilling cases while there was no reduction at 10 m/min cutting speed. It took place due to a greater reduction in tool wear causing lower cutting temperature at 100 m/min when comparing CD and UAD.

7.3 Influence of tool wear on the effectiveness of UAD with respect to cutting speed

When comparing CD and UAD, the percentage of reduction in thrust force and torque with increasing tool wear indicated diminishing of the effect of ultrasonic assistance during drilling at all the cutting speeds. In the present case, the percentage reduction of thrust force diminished from 56% at the first hole to 27% at the 60th hole at 10 m/min cutting speed for the case of without pilot. At 100 m/min, the same diminished from 16% to 6% from first to 60th hole. Similarly, the percentage reduction in torque diminished from 49% to 33% at 10 m/min in the case of without pilot. At 100 m/min, the same diminished from 14% to 6%. Similar to thrust force and torque, the reduction in internal damage due to ultrasonic assistance also diminished with increasing tool wear (Figure 6-95). Thus, it can be concluded that the effect of ultrasonic assistance diminished as the tool wear increased from the first hole to 60th hole. It has been found (as discussed in Section 6.3.2.5), this was a result of a reduction in effective normal rake angle with increasing tool wear due to increasing radius of curvature at cutting edge of the drill. This finding has not been reported in the existing literature.

Thus, to achieve the minimum workpiece damage during drilling, variable cutting speed is required. When drilling with CD, at entrance and exit cutting speed should be higher causing a reduction in entrance and exit delamination and it should be lower while CD of the intermediate material of hole causing reduction in internal damage in a hole.

In contrast to CD, when drilling the holes with UAD, due to a large reduction of thrust forces and torque at low cutting speeds in UAD, the cutting speed at the hole-entrance and exit should be low in order to avoid entrance and exit delamination.

7: Conclusions

Since the internal damage is reduced at a high cutting speed in UAD compared to CD, therefore, the cutting speed should be high during UAD of the intermediate material. In addition, the tool should be sharp in order to achieve the maximum effect of ultrasonic assistance in UAD.

8 Suggestions for future work

Although the present research identified the effect of cutting speed in CD and UAD on the workpiece damage, it also points out towards other interesting research areas which could not be investigated in the present research and were suggested to be investigated in the future. The suggested work to be considered for research in future is summarized as follows –

- With the help of pilot-hole drilling with HSS drills in Section 6.2, it was found that the forces from chisel edge are reduced and hence the overall thrust force is reduced causing a reduction in entrance and exit delamination when the chisel edge is involved during drilling in UAD, as discussed in Section 6.2.2.4. In the current research 36% reduction in thrust force after drilling of 10 holes resulted in 32% reduction in tool wear, 27% reduction in maximum delamination damage at the entrance and 23% reduction in maximum delamination damage at the exit. SEM images showed that the reduction in thrust force and tool wear also caused lower thermal damage in UAD than that in CD. Similarly, lower thrust force from chisel edge was obtained in UAD in Phase-3, Figure 6-74. This indicates towards different machining mechanism at chisel edge in UAD compared to CD. It is concluded that the forces from chisel edge also reduce in UAD. In conventional drilling, extrusion at chisel edge has been suggested by Watson [205] at the central portion of chisel edge. At the outer portion of chisel edge, authors argue about orthogonal and oblique machining [174, 205]. Therefore, it is suggested to investigate the mechanism of machining at

chisel edge further which causes a reduction in forces during drilling in UAD.

- In the current research, it was found that the effective clearance angles became negative during UAD. In any machining operation, negative clearance angles are not desired [168, 173]. Therefore, it is suggested to investigate the advanced tool geometries which could achieve positive effective clearance angles in UAD. Further, with those geometries, the effect on forces and damage during drilling of CFRP is suggested to be investigated in future.
- It has been found during the drilling of GFRP [167], that ultrasonic oscillation amplitude is one of the most influencing parameters for a reduction in thrust force and exit delamination. It was found that thrust force was reduced from 30 to 15 N and delamination factor was reduced from 1.4 to 1.25 when oscillation amplitude was increased from 5 to 15 μm . In the present research, the generation of larger amplitudes than 5 μm was difficult with the available equipment. However, According to a private communication with Mr. Markus Baeumler (Product manager and head of technical sales at SAUER GmbH) [210], the ultrasonic actuators which could generate larger amplitudes are in the progress of development. It is suggested to examine the correlation between larger amplitudes, frequencies and the damage (entrance/exit delamination and internal damage) generated at various cutting speeds and feed rates during drilling of CFRP.
- In a recent research [202], it has been found that when a cryogenic coolant is applied during drilling of CFRP, the thrust force is increased while the damage is reduced as compared to that in dry drilling. Since UAD has been

8: Future work

found to cause 55% reduction in thrust force in the present research, it is suggested to implement UAD along with the cryogenic coolant during drilling of CFRP and to examine the thrust force, torque, tool wear and damage generated in all the cases at various cutting speeds and feed rates.

- As found in the present research, the effectiveness of ultrasonic assistance diminishes with increasing tool wear. PCD drills are one of the most wear resistant drills. Therefore, it is suggested to investigate the effect of PCD drills in UAD in comparison to CD for machining forces and workpiece damage.

References

- [1] C. T. Pan and H. Hocheng, "The anisotropic heat-affected zone in the laser grooving of fiber-reinforced composite material," *Journal of Materials Processing Technology*, Nov 1996, Vol. 62, pp. 54-60.
- [2] G. Akoval and ebrary Inc. (2001). *Handbook of composite fabrication*. 1859572634.
- [3] D. F. Liu, Y. J. Tang, and W. L. Cong, "A review of mechanical drilling for composite laminates," *Composite Structures*, Mar 2012, Vol. 94, pp. 1265-1279.
- [4] H. Hocheng, N. H. Tai, and C. S. Liu, "Assessment of ultrasonic drilling of C/SiC composite material," *Composites Part a-Applied Science and Manufacturing*, 2000, Vol. 31, pp. 133-142.
- [5] A. Riveiro, F. Quintero, F. Lusquiños, J. del Val, R. Comesaña, M. Boutinguiza, and J. Pou, "Experimental study on the CO2 laser cutting of carbon fiber reinforced plastic composite," *Composites Part A: Applied Science and Manufacturing*, 2012, Vol. 43, pp. 1400-1409.
- [6] W. Youjun, Z. Dongsheng, and W. Yangyu, *Advanced decisions in engineering practice : selected, peer reviewed papers from the 2014 Global Conference on Digital Design and Manufacturing Technology (DDMTC 2014), November 27-29, 2014, Hanzhong, China*, 9783038354376.
- [7] I. Shyha, S. L. Soo, D. Aspinwall, S. Bradley, R. Perry, P. Harden, and S. Dawson, "Hole quality assessment following drilling of metallic-composite stacks," *International Journal of Machine Tools and Manufacture*, 2011, Vol. 51, pp. 569-578.
- [8] X. Wang, P. Kwon, and R. Pelikhatyy, "Characterization of Fiber Pull-Outs in Drilled CFRP Holes Using Confocal Laser Microscope," in *ASME 2014 International Manufacturing Science and Engineering Conference collocated with the JSME 2014 International Conference on Materials and Processing and the 42nd North American Manufacturing Research Conference*, 2014, p. V002T02A046.
- [9] F. Lachaud, R. Piquet, F. Collombet, and L. Surcin, "Drilling of composite structures," *Composite structures*, 2001, Vol. 52, pp. 511-516.
- [10] W.-C. Chen, "Some experimental investigations in the drilling of carbon fiber-reinforced plastic (CFRP) composite laminates," *International Journal of Machine Tools and Manufacture*, 1997, Vol. 37, pp. 1097-1108.
- [11] S. Arul, L. Vijayaraghavan, S. K. Malhotra, and R. Krishnamurthy, "The effect of vibratory drilling on hole quality in polymeric composites," *International Journal of Machine Tools and Manufacture*, 2006, Vol. 46, pp. 252-259.
- [12] A. M. Abrão, P. E. Faria, J. C. C. Rubio, P. Reis, and J. P. Davim, "Drilling of fiber reinforced plastics: A review," *Journal of Materials Processing Technology*, 2007, Vol. 186, pp. 1-7.
- [13] H. Hocheng and C. Tsao, "Effects of special drill bits on drilling-induced delamination of composite materials," *International Journal of Machine Tools and Manufacture*, 2006, Vol. 46, pp. 1403-1416.
- [14] V. Tagliaferri, G. Caprino, and A. Diterlizzi, "Effect of drilling parameters on the finish and mechanical properties of GFRP composites," *International Journal of Machine Tools and Manufacture*, 1990, Vol. 30, pp. 77-84.
- [15] E. U. Enemuoh, A. S. El-Gizawy, and A. Chukwujekwu Okafor, "An approach for development of damage-free drilling of carbon fiber reinforced thermosets," *International Journal of Machine Tools and Manufacture*, 2001, Vol. 41, pp. 1795-1814.

- [16] S. R. Karnik, V. N. Gaitonde, J. C. Rubio, A. E. Correia, A. M. Abrão, and J. P. Davim, "Delamination analysis in high speed drilling of carbon fiber reinforced plastics (CFRP) using artificial neural network model," *Materials & Design*, 2008, Vol. 29, pp. 1768-1776.
- [17] C. Tsao and H. Hocheng, "Taguchi analysis of delamination associated with various drill bits in drilling of composite material," *International Journal of Machine Tools and Manufacture*, 2004, Vol. 44, pp. 1085-1090.
- [18] C. Tsao, "The effect of pilot hole on delamination when core drill drilling composite materials," *International Journal of Machine Tools and Manufacture*, 2006, Vol. 46, pp. 1653-1661.
- [19] C. Tsao, "Effect of pilot hole on thrust force by saw drill," *International Journal of Machine Tools and Manufacture*, 2007, Vol. 47, pp. 2172-2176.
- [20] M. Won and C. Dharan, "Chisel edge and pilot hole effects in drilling composite laminates," *Journal of manufacturing science and engineering*, 2002, Vol. 124, pp. 242-247.
- [21] C. Tsao and H. Hocheng, "The effect of chisel length and associated pilot hole on delamination when drilling composite materials," *International journal of machine tools and manufacture*, 2003, Vol. 43, pp. 1087-1092.
- [22] C. Tsao and H. Hocheng, "Effects of exit back-up on delamination in drilling composite materials using a saw drill and a core drill," *International Journal of Machine Tools and Manufacture*, 2005, Vol. 45, pp. 1261-1270.
- [23] K. Alam, A. V. Mitrofanov, and V. V. Silberschmidt, "Experimental investigations of forces and torque in conventional and ultrasonically-assisted drilling of cortical bone," *Medical Engineering & Physics*, 2011, Vol. 33, pp. 234-239.
- [24] Y. Wang, M. Cao, Y. Zhao, G. Zhou, W. Liu, and D. Li, "Experimental Investigations on Microcracks in Vibrational and Conventional Drilling of Cortical Bone," *Journal of Nanomaterials*, 2013, Vol. 2013, p. 5.
- [25] B. Azarhoushang and J. Akbari, "Ultrasonic-assisted drilling of Inconel 738-LC," *International Journal of Machine Tools and Manufacture*, 2007, Vol. 47, pp. 1027-1033.
- [26] V. Baghlani, P. Mehbudi, J. Akbari, and M. Sohrabi, "Ultrasonic Assisted Deep Drilling of Inconel 738LC Superalloy," *Procedia CIRP*, 2013, Vol. 6, pp. 571-576.
- [27] Y. S. Liao, Y. C. Chen, and H. M. Lin, "Feasibility study of the ultrasonic vibration assisted drilling of Inconel superalloy," *International Journal of Machine Tools and Manufacture*, Oct 2007, Vol. 47, pp. 1988-1996.
- [28] J. Pujana, A. Rivero, A. Celaya, and L. N. López de Lacalle, "Analysis of ultrasonic-assisted drilling of Ti6Al4V," *International Journal of Machine Tools and Manufacture*, 2009, Vol. 49, pp. 500-508.
- [29] S. S. F. Chang and G. M. Bone, "Burr size reduction in drilling by ultrasonic assistance," *Robotics and Computer-Integrated Manufacturing*, 2005, Vol. 21, pp. 442-450.
- [30] A. Sadek, M. H. Attia, M. Meshreki, and B. Shi, "Characterization and optimization of vibration-assisted drilling of fibre reinforced epoxy laminates," *CIRP Annals - Manufacturing Technology*, 2013, Vol. 62, pp. 91-94.
- [31] H. Hocheng and C. C. Tsao, "The path towards delamination-free drilling of composite materials," *Journal of Materials Processing Technology*, 2005, Vol. 167, pp. 251-264.
- [32] K. A. Fenoughty, A. Jawaid, and I. R. Pashby, "Machining of Advanced Engineering Materials Using Traditional and Laser Techniques," *Journal of Materials Processing Technology*, May 1994, Vol. 42, pp. 391-400.

- [33] I. P. Tuersley, A. Jawaid, and I. R. Pashby, "Various Methods of Machining Advanced Ceramic Materials - Review," *Journal of Materials Processing Technology*, May 1994, Vol. 42, pp. 377-390.
- [34] D. K. Shanmugam, F. L. Chen, E. Siores, and M. Brandt, "Comparative study of jetting machining technologies over laser machining technology for cutting composite materials," *Composite Structures*, 2002, Vol. 57, pp. 289-296.
- [35] C. F. Cheng, Y. C. Tsui, and T. W. Clyne, "Application of a three-dimensional heat flow model to treat laser drilling of carbon fibre composites," *Acta Materialia*, 1998, Vol. 46, pp. 4273-4285.
- [36] W. König, C. Wulf, P. Graß, and H. Willerscheid, "Machining of Fibre Reinforced Plastics," *CIRP Annals - Manufacturing Technology*, 1985, Vol. 34, pp. 537-548.
- [37] M. Ramulu and D. Arola, "The Influence of Abrasive Waterjet Cutting Conditions on the Surface Quality of Graphite-Epoxy Laminates," *International Journal of Machine Tools & Manufacture*, Apr 1994, Vol. 34, pp. 295-313.
- [38] X. Wang, L. J. Wang, and J. P. Tao, "Investigation on thrust in vibration drilling of fiber-reinforced plastics," *Journal of Materials Processing Technology*, 5/15/ 2004, Vol. 148, pp. 239-244.
- [39] Z. Linbo, W. Lijiang, and W. Xin, "Study on vibration drilling of fiber reinforced plastics with hybrid variation parameters method," *Composites Part A: Applied Science and Manufacturing*, 2003, Vol. 34, pp. 237-244.
- [40] F. Makhdum, V. A. Phadnis, A. Roy, and V. V. Silberschmidt, "Effect of ultrasonically-assisted drilling on carbon-fibre-reinforced plastics," *Journal of Sound and Vibration*, 11/24/ 2014, Vol. 333, pp. 5939-5952.
- [41] R. Muhammad, A. Maurotto, M. Demiral, A. Roy, and V. V. Silberschmidt, "Thermally enhanced ultrasonically assisted machining of Ti alloy," *CIRP Journal of Manufacturing Science and Technology*, 2014, Vol. 7, pp. 159-167.
- [42] R. Muhammad, M. S. Hussain, A. Maurotto, C. Siemers, A. Roy, and V. V. Silberschmidt, "Analysis of a free machining $\alpha+\beta$ titanium alloy using conventional and ultrasonically assisted turning," *Journal of Materials Processing Technology*, 2014, Vol. 214, pp. 906-915.
- [43] A. Maurotto, R. Muhammad, A. Roy, and V. V. Silberschmidt, "Enhanced ultrasonically assisted turning of a β -titanium alloy," *Ultrasonics*, 2013, Vol. 53, pp. 1242-1250.
- [44] V. I. Babitsky, A. V. Mitrofanov, and V. V. Silberschmidt, "Ultrasonically assisted turning of aviation materials: simulations and experimental study," *Ultrasonics*, 2004, Vol. 42, pp. 81-86.
- [45] K. Harada and H. Sasahara, "Effect of dynamic response and displacement/stress amplitude on ultrasonic vibration cutting," *Journal of Materials Processing Technology*, 5/1/ 2009, Vol. 209, pp. 4490-4495.
- [46] S. Koshimizu, "Ultrasonic Vibration-Assisted Cutting of Titanium Alloy," *Key Engineering Materials*, September 2008, Vol. 389 - 390, pp. 277-282.
- [47] S. Patil, S. Joshi, A. Tewari, and S. S. Joshi, "Modelling and simulation of effect of ultrasonic vibrations on machining of Ti6Al4V," *Ultrasonics*, 2014, Vol. 54, pp. 694-705.
- [48] F. C. Campbell, *Structural composite materials*. Materials Park, Ohio: ASM International, 2010, 9781615030378.
- [49] J. Y. Sheikh-Ahmad, *Machining of polymer matrix composites*. New York ; London: Springer, 2009, 9780387355399.
- [50] M. M. Schwartz, *Composite materials. Vol.1, Properties, nondestructive testing and repair*. Upper Saddle River, N.J.: Prentice-Hall International, 1997, 0133000478.

- [51] S. Kalpakjian and S. R. Schmid, *Manufacturing engineering and technology*, 4th ed. Upper Saddle River, NJ: Prentice Hall, 2001, 0201361310.
- [52] R. Jamaati, S. Amirkhanlou, M. R. Toroghinejad, and B. Niroumand, "Effect of particle size on microstructure and mechanical properties of composites produced by ARB process," *Materials Science and Engineering: A*, 2011, Vol. 528, pp. 2143-2148.
- [53] D. Gay and S. V. Hoa, *Composite materials : design and applications*, 2nd ed. Boca Raton, Fla.: CRC ; London : Taylor & Francis, 2007, 9781420045192.
- [54] M. M. Schwartz, *Composite materials* Vol. 2. Upper Saddle River, N.J.: Prentice-Hall International, 1997, 0133000397.
- [55] P. K. Mallick, *Fiber-reinforced composites: materials, manufacturing, and design*: CRC press, 2007, 1420005987.
- [56] K. K. Chawla, *Metal matrix composites*: Wiley Online Library, 2006, 3527603972.
- [57] T. Clyne and P. Withers, *An introduction to metal matrix composites*: Cambridge University Press, 1995, 0521483573.
- [58] K. K. Chawla, *Ceramic matrix composites*: Springer, 1998, 1441931244.
- [59] D. Chung, *Carbon fiber composites*: Butterworth-Heinemann, 2012, 0080500730.
- [60] S. P. Rawal, "Metal-matrix composites for space applications," *JOM*, April, 2001 2001, Vol. 53, pp. 14-17.
- [61] E. Savage, *Carbon-carbon composites*: Springer Science & Business Media, 2012, 9401115869.
- [62] J. Sheehan, K. Buesking, and B. Sullivan, "Carbon-carbon composites," *Annual Review of Materials Science*, 1994, Vol. 24, pp. 19-44.
- [63] F. Raether, "CERAMIC MATRIX COMPOSITES- AN ALTERNATIVE FOR CHALLENGING CONSTRUCTION TASKS," *Ceramic Applications*, 2013, Vol. 1, pp. 45-49.
- [64] T. Windhorst and G. Blount, "Carbon-carbon composites: a summary of recent developments and applications," *Materials & Design*, 1997, Vol. 18, pp. 11-15.
- [65] R. Teti, "Machining of composite materials," *CIRP Annals-Manufacturing Technology*, 2002, Vol. 51, pp. 611-634.
- [66] D. R. Mertz, *Application of fiber reinforced polymer composites to the highway infrastructure*: Transportation Research Board, 2003, 0309087694.
- [67] J. Y. Sheikh-Ahmad, *Machining of polymer composites*: Springer, 2009, 0387355391.
- [68] S. Bagherpour, "Fibre reinforced polyester composites," *Edited by Hosam El-Din M. Saleh*, 2012, p. 167.
- [69] D. Hull, *An introduction to composite materials*. Cambridge: Cambridge University Press, 1981, 0521283922
- [70] J. Turner, R. Scaife, and H. El-Dessouky, "Effect of machining coolant on integrity of CFRP composites," *Advanced Manufacturing: Polymer & Composites Science*, 2015,
- [71] R. Selzer and K. Friedrich, "Mechanical properties and failure behaviour of carbon fibre-reinforced polymer composites under the influence of moisture," *Composites Part A: Applied Science and Manufacturing*, 1997, Vol. 28, pp. 595-604.
- [72] R. Teti, "Machining of Composite Materials," *CIRP Annals - Manufacturing Technology*, 2002, Vol. 51, pp. 611-634.
- [73] D. Wang, M. Ramulu, and D. Arola, "Orthogonal cutting mechanisms of graphite/epoxy composite. Part II: multi-directional laminate," *International Journal of Machine Tools and Manufacture*, 1995, Vol. 35, pp. 1639-1648.
- [74] D. H. Wang, M. Ramulu, and D. Arola, "Orthogonal cutting mechanisms of graphite/epoxy composite. Part I: unidirectional laminate," *International Journal of Machine Tools and Manufacture*, 1995, Vol. 35, pp. 1623-1638.

- [75] E. D. Eneyew and M. Ramulu, "Hole Surface Quality and Damage when Drilling Unidirectional CFRP Composites," in *ASME 2012 International Mechanical Engineering Congress and Exposition*, 2012, pp. 2043-2051.
- [76] A. Faraz and D. Biermann, "Experimental Investigations on Drilling of Woven CFRP Epoxy Laminates: The Effect of Pilot-hole or Drill Chisel Edge on Delamination," in *Proceedings of the 36th International MATADOR Conference*, 2010, pp. 223-226.
- [77] S. Rawat and H. Attia, "Characterization of the dry high speed drilling process of woven composites using Machinability Maps approach," *CIRP Annals - Manufacturing Technology*, 2009, Vol. 58, pp. 105-108.
- [78] C. C. Tsao and H. Hocheng, "Effect of tool wear on delamination in drilling composite materials," *International Journal of Mechanical Sciences*, Aug 2007, Vol. 49, pp. 983-988.
- [79] R. Piquet, B. Ferret, F. Lachaud, and P. Swider, "Experimental analysis of drilling damage in thin carbon/epoxy plate using special drills," *Composites Part A: Applied Science and Manufacturing*, 2000, Vol. 31, pp. 1107-1115.
- [80] D. Iliescu, D. Gehin, I. Iordanoff, F. Girot, and M. E. Gutiérrez, "A discrete element method for the simulation of CFRP cutting," *Composites Science and Technology*, 2010, Vol. 70, pp. 73-80.
- [81] A. Koplev, A. Lystrup, and T. Vorm, "The cutting process, chips, and cutting forces in machining CFRP," *Composites*, 1983, Vol. 14, pp. 371-376.
- [82] X. M. Wang and L. C. Zhang, "An experimental investigation into the orthogonal cutting of unidirectional fibre reinforced plastics," *International Journal of Machine Tools and Manufacture*, 2003, Vol. 43, pp. 1015-1022.
- [83] X. Wang and L. Zhang, "An experimental investigation into the orthogonal cutting of unidirectional fibre reinforced plastics," *International journal of machine tools and manufacture*, 2003, Vol. 43, pp. 1015-1022.
- [84] L. M. P. Durão, J. M. R. S. Tavares, V. H. C. de Albuquerque, and D. J. S. Gonçalves, "Damage evaluation of drilled carbon/epoxy laminates based on area assessment methods," *Composite Structures*, 2013, Vol. 96, pp. 576-583.
- [85] L. Durão, A. Magalhães, J. M. R. Tavares, and A. T. Marques, "Delamination analysis after carbon/epoxy plate drilling," *ENVC2005-Encontro Nacional de Visualização Científica 2005*, 2005,
- [86] L. M. P. Durao, J. M. R. Tavares, A. Goncalves de Magalhaes, and A. T. Marques, "Damage analysis of carbon/epoxy plates after drilling," *International Journal of Materials and Product Technology*, 2008, Vol. 32, pp. 226-242.
- [87] H. Ho-Cheng and C. Dharan, "Delamination during drilling in composite laminates," *Journal of Manufacturing Science and Engineering*, 1990, Vol. 112, pp. 236-239.
- [88] S. Jain and D. C. Yang, "Delamination-free drilling of composite laminates," *Journal of Manufacturing Science and Engineering*, 1994, Vol. 116, pp. 475-481.
- [89] J. P. Jung, G. W. Kim, and K. Y. Lee, "Critical thrust force at delamination propagation during drilling of angle-ply laminates," *Composite Structures*, 2005, Vol. 68, pp. 391-397.
- [90] L. M. P. Durao, J. M. R. Tavares, A. Goncalves de Magalhaes, A. T. Marques, and A. P. M. Baptista, "Damage analysis of carbon/epoxy plates after drilling," *International Journal of Materials and Product Technology*, 2008, Vol. 32, pp. 226-242.
- [91] H. Hocheng and C. Tsao, "Comprehensive analysis of delamination in drilling of composite materials with various drill bits," *Journal of Materials Processing Technology*, 2003, Vol. 140, pp. 335-339.

- [92] J. C. Campos Rubio, A. M. Abrão, P. Eustáquio Faria, A. E. Correia, and J. P. Davim, "Delamination in High Speed Drilling of Carbon Fiber Reinforced Plastic (CFRP)," *Journal of Composite Materials*, August 1 2008, Vol. 42, pp. 1523-1532.
- [93] J. P. Davim, J. C. Rubio, and A. M. Abrão, "A novel approach based on digital image analysis to evaluate the delamination factor after drilling composite laminates," *Composites Science and Technology*, Jul 2007, Vol. 67, pp. 1939-1945.
- [94] V. N. Gaitonde, S. R. Karnik, J. C. Rubio, A. E. Correia, A. M. Abrão, and J. P. Davim, "Analysis of parametric influence on delamination in high-speed drilling of carbon fiber reinforced plastic composites," *Journal of Materials Processing Technology*, 7/18/ 2008, Vol. 203, pp. 431-438.
- [95] A. Faraz, D. Biermann, and K. Weinert, "Cutting edge rounding: An innovative tool wear criterion in drilling CFRP composite laminates," *International Journal of Machine Tools and Manufacture*, 2009, Vol. 49, pp. 1185-1196.
- [96] J. P. Davim and P. Reis, "Drilling carbon fiber reinforced plastics manufactured by autoclave—experimental and statistical study," *Materials & Design*, 2003, Vol. 24, pp. 315-324.
- [97] J. Paulo Davim, P. Reis, and C. Conceição António, "Drilling fiber reinforced plastics (FRPs) manufactured by hand lay-up: influence of matrix (Viapal VUP 9731 and ATLAC 382-05)," *Journal of Materials Processing Technology*, 2004, Vol. 155–156, pp. 1828-1833.
- [98] I. Shyha, S. L. Soo, D. Aspinwall, and S. Bradley, "Effect of laminate configuration and feed rate on cutting performance when drilling holes in carbon fibre reinforced plastic composites," *Journal of Materials Processing Technology*, 6/1/ 2010, Vol. 210, pp. 1023-1034.
- [99] A. Faraz and D. Biermann, "Experimental Investigations on Drilling of Woven CFRP Epoxy Laminates: The Effect of Pilot-hole or Drill Chisel Edge on Delamination," in *Proceedings of the 36th International MATADOR Conference*, S. Hinduja and L. Li, Eds., ed: Springer London, 2010, pp. 223-226.
- [100] J. P. Davim and P. Reis, "Study of delamination in drilling carbon fiber reinforced plastics (CFRP) using design experiments," *Composite structures*, 2003, Vol. 59, pp. 481-487.
- [101] N. Kourra, J. Warnett, A. Attridge, E. Kiraci, A. Gupta, S. Barnes, and M. Williams, "Metrological study of CFRP drilled holes with x-ray computed tomography," *The International Journal of Advanced Manufacturing Technology*, 2015/01/22 2015, pp. 1-11.
- [102] A. Gupta, S. Barnes, I. McEwen, N. Kourra, and M. A. Williams, "Study of Cutting Speed Variation in the Ultrasonic Assisted Drilling of Carbon Fibre Composites," in *ASME 2014 International Mechanical Engineering Congress and Exposition*, Montreal, Quebec, Canada, 2014, p. V02BT02A038.
- [103] N. Kourra, M. A. Williams, A. Attridge, J. Warnett, S. Barnes, and A. Gupta, "Analysis of drilled holes on carbon fibre material with X-ray computed tomography," presented at the 2014 IEEE International Workshop on Metrology for Aerospace (MetroAeroSpace), Benevento, Italy, 2014.
- [104] L. M. Durão, A. G. Magalhães, J. M. R. Tavares, and A. T. Marques, "Analyzing objects in images for estimating the delamination influence on load carrying capacity of composite laminates," *ELCVIA: electronic letters on computer vision and image analysis*, 2008, Vol. 7, pp. 11-21.
- [105] A. T. Marques, L. M. Durão, A. G. Magalhães, J. F. Silva, and J. M. R. S. Tavares, "Delamination analysis of carbon fibre reinforced laminates: Evaluation of a special step drill," *Composites Science and Technology*, 2009, Vol. 69, pp. 2376-2382.

- [106] T. Hasiotis, E. Badogiannis, and N. G. Tsouvalis, "Application of Ultrasonic C-Scan Techniques for Tracing Defects in Laminated Composite Materials," *2011*, 2011, Vol. 57,
- [107] A. Kapadia, "Non destructive testing of composite materials," *Best Practice Guide*, 2013, pp. 1-48.
- [108] C. Tsao and Y. Chiu, "Evaluation of drilling parameters on thrust force in drilling carbon fiber reinforced plastic (CFRP) composite laminates using compound core-special drills," *International Journal of Machine Tools and Manufacture*, 2011, Vol. 51, pp. 740-744.
- [109] C. Tsao, "Experimental study of drilling composite materials with step-core drill," *Materials & Design*, 2008, Vol. 29, pp. 1740-1744.
- [110] C. Tsao, "The geometrical effect between stages in step drilling of composite materials," *International Journal of Materials and Product Technology*, 2008, Vol. 32, pp. 202-212.
- [111] C. Tsao, "Thrust force and delamination of core-saw drill during drilling of carbon fiber reinforced plastics (CFRP)," *The International Journal of Advanced Manufacturing Technology*, 2008, Vol. 37, pp. 23-28.
- [112] C. C. Tsao and H. Hocheng, "Computerized tomography and C-Scan for measuring delamination in the drilling of composite materials using various drills," *International Journal of Machine Tools and Manufacture*, 2005, Vol. 45, pp. 1282-1287.
- [113] E. Persson, I. Eriksson, and L. Zackrisson, "Effects of hole machining defects on strength and fatigue life of composite laminates," *Composites Part A: Applied Science and Manufacturing*, 1997, Vol. 28, pp. 141-151.
- [114] E. Persson, I. Eriksson, and P. Hammersberg, "Propagation of hole machining defects in pin-loaded composite laminates," *Journal of Composite Materials*, 1997, Vol. 31, pp. 383-408.
- [115] Z. Hamdoun, L. Guillaumat, and J.-L. Lataillade, "Influence of the drilling quality on the fatigue compression behaviour of carbon epoxy laminates," *International Journal of Fatigue*, 2006, Vol. 28, pp. 1-8.
- [116] H. Hocheng and C. C. Tsao, "Computerized tomography and C-scan for measuring drilling-induced delamination in composite material using twist drill and core drill," *Key engineering materials*, 2007, Vol. 339, pp. 16-20.
- [117] J. P. Davim, P. Reis, and C. C. António, "Experimental study of drilling glass fiber reinforced plastics (GFRP) manufactured by hand lay-up," *Composites Science and Technology*, 2004, Vol. 64, pp. 289-297.
- [118] E. U. Enemuoh, A. S. El-Gizawy, and A. C. Okafor, "An approach for development of damage-free drilling of carbon fiber reinforced thermosets," *International Journal of Machine Tools & Manufacture*, Sep 2001, Vol. 41, pp. 1795-1814.
- [119] A. Faraz, T. Heymann, and D. Biermann, "Experimental investigations on drilling GFRP epoxy composite laminates using specialized and conventional uncoated cemented carbide drills," *Materials and Manufacturing Processes*, 2011, Vol. 26, pp. 609-617.
- [120] C. C. Tsao and H. Hocheng, "Taguchi analysis of delamination associated with various drill bits in drilling of composite material," *International Journal of Machine Tools and Manufacture*, 2004, Vol. 44, pp. 1085-1090.
- [121] E. U. Enemuoh, A. S. El-Gizawy, and A. C. Okafor, "An approach for development of damage-free drilling of carbon fiber reinforced thermosets," *International Journal of Machine Tools and Manufacture*, 2001, Vol. 41, pp. 1795-1814.
- [122] J. P. Davim, P. Reis, and C. C. António, "Drilling fiber reinforced plastics (FRPs) manufactured by hand lay-up: influence of matrix (Viapal VUP 9731 and ATLAC

- 382-05)," *Journal of Materials Processing Technology*, 2004, Vol. 155, pp. 1828-1833.
- [123] C. Tsao and H. Hocheng, "Evaluation of thrust force and surface roughness in drilling composite material using Taguchi analysis and neural network," *Journal of materials processing technology*, 2008, Vol. 203, pp. 342-348.
- [124] D. Kim, M. Ramulu, and X. Doan, "Influence of consolidation process on the drilling performance and machinability of PIXA-M and PEEK thermoplastic composites," *Journal of Thermoplastic Composite Materials*, 2005, Vol. 18, pp. 195-217.
- [125] R. Zitoune, V. Krishnaraj, and F. Collombet, "Study of drilling of composite material and aluminium stack," *Composite Structures*, 2010, Vol. 92, pp. 1246-1255.
- [126] C. Tsao, "Taguchi analysis of drilling quality associated with core drill in drilling of composite material," *The International Journal of Advanced Manufacturing Technology*, 2007, Vol. 32, pp. 877-884.
- [127] K. J. Stout, *The development of methods for the characterisation of roughness in three dimensions*: University of Birmingham, 1993, 0704413132.
- [128] R. Q. Sardinias, P. Reis, and J. P. Davim, "Multi-objective optimization of cutting parameters for drilling laminate composite materials by using genetic algorithms," *Composites Science and Technology*, 2006, Vol. 66, pp. 3083-3088.
- [129] L. M. P. Durão, D. J. Gonçalves, J. M. R. Tavares, V. H. C. de Albuquerque, A. A. Vieira, and A. T. Marques, "Drilling tool geometry evaluation for reinforced composite laminates," *Composite structures*, 2010, Vol. 92, pp. 1545-1550.
- [130] I. S. Shyha, D. K. Aspinwall, S. L. Soo, and S. Bradley, "Drill geometry and operating effects when cutting small diameter holes in CFRP," *International Journal of Machine Tools and Manufacture*, 2009, Vol. 49, pp. 1008-1014.
- [131] S. Jain and D. C. H. Yang, "Effects of Feedrate and Chisel Edge on Delamination in Composites Drilling," *Journal of Manufacturing Science and Engineering*, 1993, Vol. 115, pp. 398-405.
- [132] C. Tsao and H. Hocheng, "Computerized tomography and C-Scan for measuring delamination in the drilling of composite materials using various drills," *International Journal of Machine Tools and Manufacture*, 2005, Vol. 45, pp. 1282-1287.
- [133] C. C. Tsao and H. Hocheng, "Effects of exit back-up on delamination in drilling composite materials using a saw drill and a core drill," *International Journal of Machine Tools & Manufacture*, Sep 2005, Vol. 45, pp. 1261-1270.
- [134] C. Murphy, G. Byrne, and M. Gilchrist, "The performance of coated tungsten carbide drills when machining carbon fibre-reinforced epoxy composite materials," *Proceedings of the Institution of Mechanical Engineers, Part B: Journal of Engineering Manufacture*, 2002, Vol. 216, pp. 143-152.
- [135] S. Lin and I. Chen, "Drilling carbon fiber-reinforced composite material at high speed," *Wear*, 1996, Vol. 194, pp. 156-162.
- [136] K. Weinert and C. Kempmann, "Cutting Temperatures and Their Effects on the Machining Behaviour in Drilling Reinforced Plastic Composites," *Advanced Engineering Materials*, 2004, Vol. 6, pp. 684-689.
- [137] S. Rawat and H. Attia, "Wear mechanisms and tool life management of WC-Co drills during dry high speed drilling of woven carbon fibre composites," *Wear*, 2009, Vol. 267, pp. 1022-1030.
- [138] D. Iliescu, D. Gehin, M. E. Gutierrez, and F. Girot, "Modeling and tool wear in drilling of CFRP," *International Journal of Machine Tools and Manufacture*, 2010, Vol. 50, pp. 204-213.
- [139] S. Malhotra, "Some studies on drilling of fibrous composites," *Journal of Materials Processing Technology*, 1990, Vol. 24, pp. 291-300.

- [140] K.-H. Park, A. Beal, P. Kwon, and J. Lantrip, "Tool wear in drilling of composite/titanium stacks using carbide and polycrystalline diamond tools," *Wear*, 2011, Vol. 271, pp. 2826-2835.
- [141] F. Klocke and C. Würtz, "The use of PCD tools for machining fibre reinforced materials(Polycrystalline Diamond)," *ECCM- 8*, 1998, pp. 509-515.
- [142] C. Murphy, G. Byrne, and M. D. Gilchrist, "The performance of coated tungsten carbide drills when machining carbon fibre-reinforced epoxy composite materials," *Proceedings of the Institution of Mechanical Engineers, Part B: Journal of Engineering Manufacture*, February 1, 2002 2002, Vol. 216, pp. 143-152.
- [143] S. Sakamoto, Y. Kajiwara, and H. Yasui, "Precision drilling of cfrp (carbon fiber reinforced plastics) with coated tools," in *22nd Annual Meeting of the American Society for Precision Engineering, ASPE 2007*, 2007.
- [144] X. Wang, P. Y. Kwon, C. Sturtevant, D. Kim, and J. Lantrip, "Tool wear of coated drills in drilling CFRP," *Journal of Manufacturing Processes*, 2013, Vol. 15, pp. 127-135.
- [145] S. S. C. Tools. *Speed and feed recommendations for high performance double margin twist drill having diamond coating*. Available: <http://www.sgstool.com/PDF-speedfeeds/SGS-Speeds-Feeds-120-120M.pdf>
- [146] R. Weber, M. Hafner, A. Michalowski, and T. Graf, "Minimum Damage in CFRP Laser Processing," *Lasers in Manufacturing 2011: Proceedings of the Sixth International Wlt Conference on Lasers in Manufacturing, Vol 12, Pt B*, 2011, Vol. 12, pp. 302-307.
- [147] A. Klotzbach, M. Hauser, and E. Beyer, "Laser Cutting of Carbon Fiber Reinforced Polymers using Highly Brilliant Laser Beam Sources," *Lasers in Manufacturing 2011: Proceedings of the Sixth International Wlt Conference on Lasers in Manufacturing, Vol 12, Pt A*, 2011, Vol. 12, pp. 572-577.
- [148] F. Muller and J. Monaghan, "Non-conventional machining of particle reinforced metal matrix composite," *International Journal of Machine Tools & Manufacture*, Jul 2000, Vol. 40, pp. 1351-1366.
- [149] H. Ho-Cheng, "A failure analysis of water jet drilling in composite laminates," *International Journal of Machine Tools and Manufacture*, 1990, Vol. 30, pp. 423-429.
- [150] T. C. Lee and C. W. Chan, "Mechanism of the ultrasonic machining of ceramic composites," *Journal of Materials Processing Technology*, Nov 15 1997, Vol. 71, pp. 195-201.
- [151] M. Komaraiah, M. A. Manan, P. Narasimha Reddy, and S. Victor, "Investigation of surface roughness and accuracy in ultrasonic machining," *Precision Engineering*, 1988, Vol. 10, pp. 59-65.
- [152] H. Hocheng and C. C. Hsu, "Preliminary-Study of Ultrasonic Drilling of Fiber-Reinforced Plastics," *Journal of Materials Processing Technology*, Jan 15 1995, Vol. 48, pp. 255-266.
- [153] J. Liu, D. Y. Zhang, L. G. Qin, and L. S. Yan, "Feasibility study of the rotary ultrasonic elliptical machining of carbon fiber reinforced plastics (CFRP)," *International Journal of Machine Tools & Manufacture*, Feb 2012, Vol. 53, pp. 141-150.
- [154] Z. C. Li, L.-W. Cai, Z. J. Pei, and C. Treadwell, "Edge-chipping reduction in rotary ultrasonic machining of ceramics: Finite element analysis and experimental verification," *International Journal of Machine Tools and Manufacture*, 2006, Vol. 46, pp. 1469-1477.
- [155] Z. C. Li, Y. Jiao, T. W. Deines, Z. J. Pei, and C. Treadwell, "Rotary ultrasonic machining of ceramic matrix composites: feasibility study and designed

- experiments," *International Journal of Machine Tools and Manufacture*, 2005, Vol. 45, pp. 1402-1411.
- [156] Q. Feng, W. L. Cong, Z. J. Pei, and C. Z. Ren, "ROTARY ULTRASONIC MACHINING OF CARBON FIBER-REINFORCED POLYMER: FEASIBILITY STUDY," *Machining Science and Technology*, 2012, Vol. 16, pp. 380-398.
- [157] Z. Li, Z. Pei, T. Sisco, A. Micale, and C. Treadwell, "Experimental study on rotary ultrasonic machining of graphite/epoxy panel," in *Proceedings of ASPE Spring Topical Meeting*, 2007.
- [158] V. A. Phadnis, F. Makhdum, A. Roy, and V. V. Silberschmidt, "Drilling in carbon/epoxy composites: Experimental investigations and finite element implementation," *Composites Part A: Applied Science and Manufacturing*, 2013, Vol. 47, pp. 41-51.
- [159] V. Phadnis, F. Makhdum, A. Roy, and V. Silberschmidt, "Drilling-induced damage in CFRP laminates: Experimental and numerical analysis," *Advanced Materials and Structures Iv*, 2012, Vol. 188, pp. 150-157.
- [160] C. Nath and M. Rahman, "Effect of machining parameters in ultrasonic vibration cutting," *International Journal of Machine Tools & Manufacture*, Jul 2008, Vol. 48, pp. 965-974.
- [161] D. E. Brehl and T. A. Dow, "Review of vibration-assisted machining," *Precision Engineering-Journal of the International Societies for Precision Engineering and Nanotechnology*, Jul 2008, Vol. 32, pp. 153-172.
- [162] J. Ramkumar, S. K. Malhotra, and R. Krishnamurthy, "Effect of workpiece vibration on drilling of GFRP laminates," *Journal of Materials Processing Technology*, 2004, Vol. 152, pp. 329-332.
- [163] F. Makhdum, D. N. P. Norddin, A. Roy, and V. V. Silberschmidt, "Ultrasonically assisted drilling of carbon fibre reinforced plastics," *Advanced Materials and Structures Iv*, 2012, Vol. 188, pp. 170-175.
- [164] F. Makhdum, L. T. Jennings, A. Roy, and V. V. Silberschmidt, "Cutting forces in ultrasonically assisted drilling of carbon fibre-reinforced plastics," *Modern Practice in Stress and Vibration Analysis 2012 (Mpsva 2012)*, 2012, Vol. 382,
- [165] V. A. Phadnis, F. Makhdum, A. Roy, and V. V. Silberschmidt, "Experimental and Numerical Investigations in Conventional and Ultrasonically Assisted Drilling of CFRP Laminate," *Procedia CIRP*, 2012, Vol. 1, pp. 455-459.
- [166] C. S. Wu, Y. L. Liu, Y. C. Chiu, and Y. S. Chiu, "Thermal stability of epoxy resins containing flame retardant components: an evaluation with thermogravimetric analysis," *Polymer Degradation and Stability*, 2002, Vol. 78, pp. 41-48.
- [167] P. Mehbudi, V. Baghlani, J. Akbari, A. R. Bushroa, and N. A. Mardi, "Applying Ultrasonic Vibration to Decrease Drilling-Induced Delamination in GFRP Laminates," *Procedia CIRP*, 2013, Vol. 6, pp. 577-582.
- [168] A. B. Chattopadhyay, *MACHINING AND MACHINE TOOLS*: Wiley India Pvt. Limited, 2011, 9788126530984.
- [169] E. M. Trent, *Metal cutting*, 2nd ed. ed. London: Butterworths, 1984, 0408108568 : Unpriced.
- [170] A. Watson and R. Williams, "Specification of the cutting geometry of single point tools and twist drills using the ISO system," *International Journal of Machine Tool Design and Research*, 1977, Vol. 17, pp. 103-116.
- [171] V. P. Astakhov, *Geometry of single-point turning tools and drills : fundamentals and practical applications*. London: Springer, 2010, 9781849960533.
- [172] A. R. Watson, "Geometry of drill elements," *International Journal of Machine Tool Design and Research*, 1985/01/01 1985, Vol. 25, pp. 209-227.

- [173] V. P. Astakhov, *Geometry of single-point turning tools and drills: fundamentals and practical applications*: Springer Science & Business Media, 2010, 1849960534.
- [174] K. SZWAJKA, "Torque and thrust force in drilling," *Annals of Warsaw University of Life Sciences—WULS-SGGW*, 2011, Vol. 76, pp. 108-115.
- [175] P. N. Rao, *Manufacturing Technology: Metal cutting and machine tools. v. 2*, 2013, 9781259029561.
- [176] B. L. Juneja and G. S. Sekhon, *Fundamentals of metal cutting and machine tools*: Wiley, 1987, 0470208600.
- [177] A. Watson, "Geometry of drill elements," *International Journal of Machine Tool Design and Research*, 1985, Vol. 25, pp. 209-227.
- [178] R. Brown and E. Armarego, "Oblique machining with a single cutting edge," *International Journal of Machine Tool Design and Research*, 1964, Vol. 4, pp. 9-25.
- [179] A. Watson, "Drilling model for cutting lip and chisel edge and comparison of experimental and predicted results. III—drilling model for chisel edge," *International Journal of Machine Tool Design and Research*, 1985, Vol. 25, pp. 377-392.
- [180] M. C. Shaw, *Metal cutting principles*. Oxford: Clarendon, 1984, 0198590024.
- [181] D. Arola, M. Ramulu, and D. H. Wang, "Chip formation in orthogonal trimming of graphite/epoxy composite," *Composites Part A: Applied Science and Manufacturing*, 1996, Vol. 27, pp. 121-133.
- [182] L. B. Zhang, L. J. Wang, X. Y. Liu, H. W. Zhao, X. Wang, and H. Y. Luo, "Mechanical model for predicting thrust and torque in vibration drilling fibre-reinforced composite materials," *International Journal of Machine Tools and Manufacture*, 2001, Vol. 41, pp. 641-657.
- [183] E. Armarego and J. Wright, "Predictive models for drilling thrust and torque—a comparison of three flank configurations," *CIRP Annals-Manufacturing Technology*, 1984, Vol. 33, pp. 5-10.
- [184] A. Watson, "Drilling model for cutting lip and chisel edge and comparison of experimental and predicted results. I—initial cutting lip model," *International Journal of Machine Tool Design and Research*, 1985, Vol. 25, pp. 347-365.
- [185] A. Watson, "Drilling model for cutting lip and chisel edge and comparison of experimental and predicted results. II—revised cutting lip model," *International Journal of Machine Tool Design and Research*, 1985, Vol. 25, pp. 367-376.
- [186] R. Neugebauer and A. Stoll, "Ultrasonic application in drilling," *Journal of Materials Processing Technology*, 6/10/ 2004, Vol. 149, pp. 633-639.
- [187] E. Armarego and C. Cheng, "Drilling with flat rake face and conventional twist drills—I. theoretical investigation," *International Journal of Machine Tool Design and Research*, 1972, Vol. 12, pp. 17-35.
- [188] A. R. Watson, "Drilling model for cutting lip and chisel edge and comparison of experimental and predicted results. I — initial cutting lip model," *International Journal of Machine Tool Design and Research*, 1985, Vol. 25, pp. 347-365.
- [189] V. Voort and G. F., *BUEHLER® SUM-MET™ - The Science Behind Materials Preparation*. Lake Bluff: Buehler Ltd., 2011, 0-9752898-0-2.
- [190] S. K. Chapman, *Working with a scanning electron microscope*: Lodgemark, 1986, 0850770939 : No price.
- [191] S. K. Sikdar and M. Chen, "Relationship between tool flank wear area and component forces in single point turning," *Journal of Materials Processing Technology*, 10/6/ 2002, Vol. 128, pp. 210-215.
- [192] (03 SEP). *Web Shop for Associated Production Tools Ltd*. Available: <http://www.shop-apt.co.uk/micro-diameter-carbide-drills-0-2mm-2-9mm/1-5mm->

[micro-diameter-carbide-drill-3-175mm-1-8-shank-12mm-flute-length-altin-coated.html](http://www.cutwel.co.uk/FileDepository//ProductId%20-%203383/YG%20Catalogue%20DJ544.pdf)

- [193] (03 SEP). *Cutwel Limited*. Available: <http://www.cutwel.co.uk/FileDepository//ProductId%20-%203383/YG%20Catalogue%20DJ544.pdf>
- [194] J. P. Davim, *Machining : fundamentals and recent advances*. New York ; London: Springer, 2008, 9781848002128.
- [195] J. W. Nicholson, *The chemistry of polymers*, 4th ed. ed. Cambridge: Royal Society of Chemistry, 2012, 9781849733915.
- [196] Y. Yan, X. Shi, J. Liu, T. Zhao, and Y. Yu, "Thermosetting resin system based on novolak and bismaleimide for resin-transfer molding," *Journal of Applied Polymer Science*, 2002, Vol. 83, pp. 1651-1657.
- [197] H. Stenzenberger. Bismaleimide Resins [Online]. Available: <https://polycomp.mse.iastate.edu/files/2012/01/6-Bismaleimide-Resins.pdf>
- [198] G. DiPaolo, S. G. Kapoor, and R. E. DeVor, "An Experimental Investigation of the Crack Growth Phenomenon for Drilling of Fiber-Reinforced Composite Materials," *Journal of Engineering for Industry*, 1996, Vol. 118, pp. 104-110.
- [199] M. Alauddin, I. A. Choudhury, M. A. El Baradie, and M. S. J. Hashmi, "Plastics and their machining: A review," *Journal of Materials Processing Technology*, 1995, Vol. 54, pp. 40-46.
- [200] K. Morioka, Y. Tomita, and K. Takigawa, "High-temperature fracture properties of CFRP composite for aerospace applications," *Materials Science and Engineering: A*, 2001, Vol. 319–321, pp. 675-678.
- [201] J. B. Schutz, "Properties of composite materials for cryogenic applications," *Cryogenics*, 1998, Vol. 38, pp. 3-12.
- [202] P. Bhudwannachai, "Performance evaluation and analysis of the use of CO2 cooling for conventional drilling of carbon fibre reinforced plastics," PhD, Warwick Manufacturing Group, University of Warwick, 2014.
- [203] A. J. Kinloch, S. J. Shaw, and D. L. Hunston, "Deformation and fracture behaviour of a rubber-toughened epoxy: 2. Failure criteria," *Polymer*, 1983/10/01 1983, Vol. 24, pp. 1355-1363.
- [204] "Private communication with Ms. Nadia Kourra (EngD. Student) and Prof. Mark Williams (Product Evaluation Technologies Group Leader at WMG), 10 Nov, 2015,"
- [205] A. R. Watson, "Drilling model for cutting lip and chisel edge and comparison of experimental and predicted results. III — drilling model for chisel edge," *International Journal of Machine Tool Design and Research*, 1985, Vol. 25, pp. 377-392.
- [206] R. Jasinevicius, A. Porto, J. Duduch, P. Pizani, F. Lanciotti Jr, and F. dos Santos, "Multiple phase silicon in submicrometer chips removed by diamond turning," *Journal of the Brazilian Society of Mechanical Sciences and Engineering*, 2005, Vol. 27, pp. 440-448.
- [207] F. Fang, "Micro/Nano Lithography Advances in micro/nanomachining improve production of thin, brittle wafers," in *Proc. SPIE*, 2006, pp. 366-371.
- [208] Y. Huang and S. Liang, "Modelling of the cutting temperature distribution under the tool flank wear effect," *Proceedings of the Institution of Mechanical Engineers, Part C: Journal of Mechanical Engineering Science*, 2003, Vol. 217, pp. 1195-1208.
- [209] S. Lin, F. Peng, J. Wen, Y. Liu, and R. Yan, "An investigation of workpiece temperature variation in end milling considering flank rubbing effect," *International Journal of Machine Tools and Manufacture*, 2013, Vol. 73, pp. 71-86.
- [210] "Private communication with Mr. Markus Baeumler (Product manager and head of technical sales at SAUER GmbH), 14 May, 2013,"

Appendices

Appendix A

Evidences of zero damage near entrance for Section 6.1.3.2.

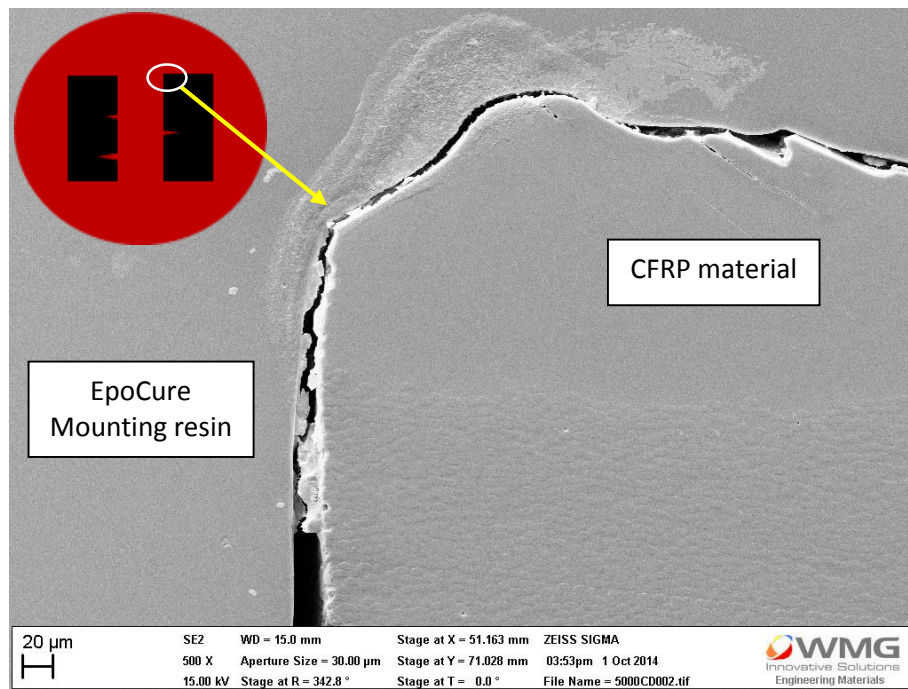


Figure A-1: SEM image near entrance in CD showing zero damage near entrance (94.2 m/min, 0.05 mm/rev). The diagram in the inset shows the location of the specific damage in a mounted sample.

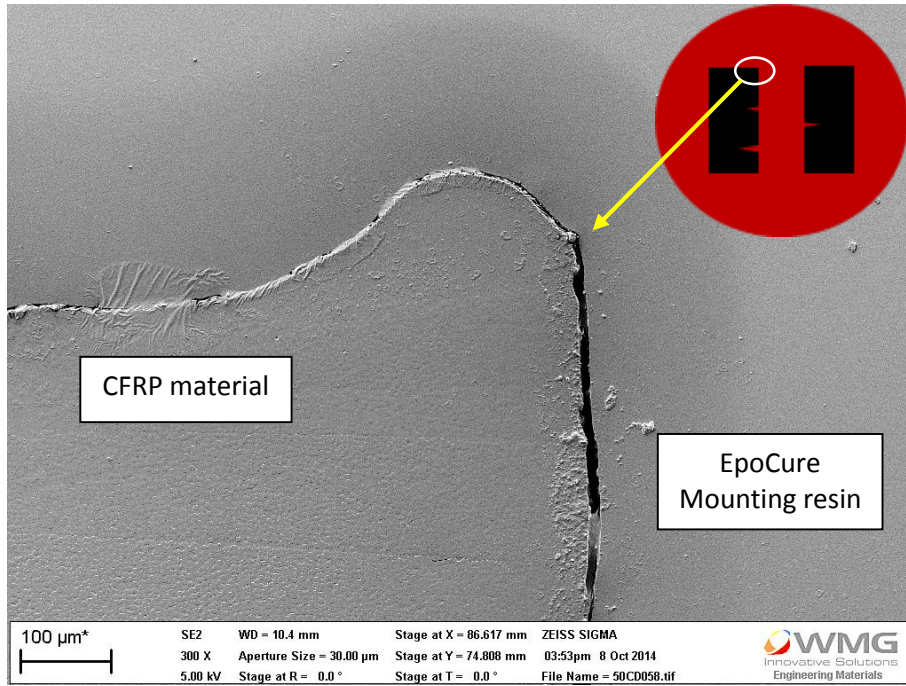


Figure A-2: SEM image near entrance in CD showing zero damage near entrance (0.942 m/min, 0.05 mm/rev). The diagram in the inset shows the location of the specific damage in a mounted sample.

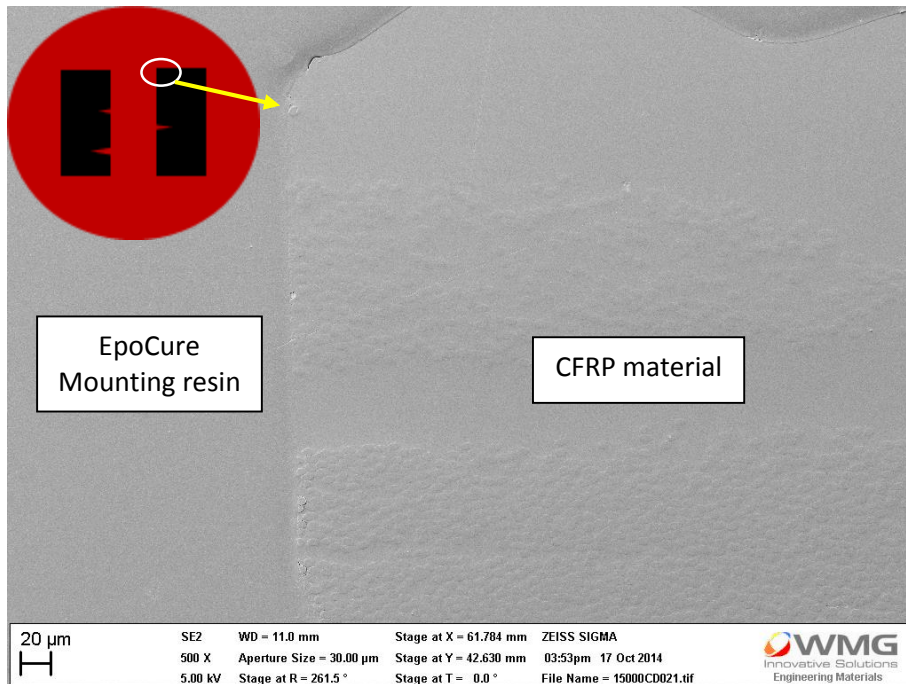


Figure A-3: SEM image near entrance in UAD showing zero damage near entrance (282.6 m/min 0.05 mm/rev). The diagram in the inset shows the location of the specific damage in a mounted sample.

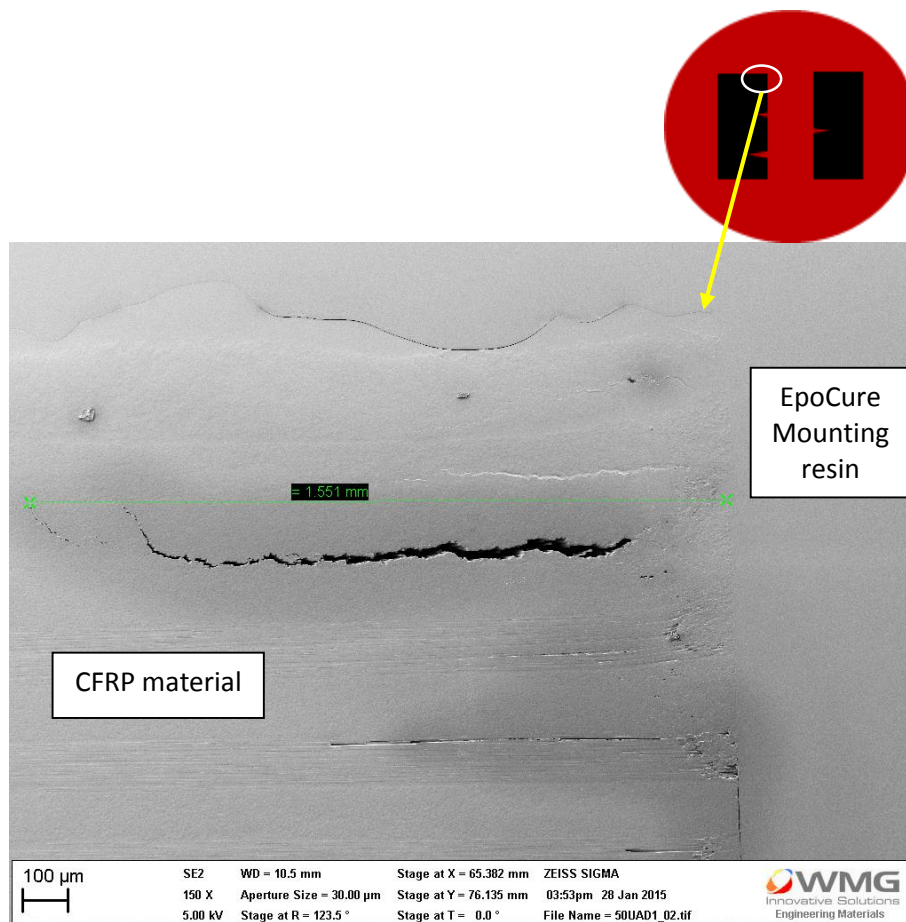


Figure A-5: Measurement of maximum damage depth at the entrance in UAD (0.942 m/min, 0.05 mm/rev). The diagram in the inset shows the location of the specific damage in a mounted sample.

Appendix B

SEM images of chip fragments for Section 6.1.6.



Figure B-1: Chip fragments obtained in CD (282.6 m/min, 0.05 mm/rev)



Figure B-2: Long chip-fragment obtained in UAD (282.6 m/min, 0.05 mm/rev) along with some short and regular chip-fragments



Figure B-3: Chip fragments obtained in UAD (282.6 m/min, 0.05 mm/rev)

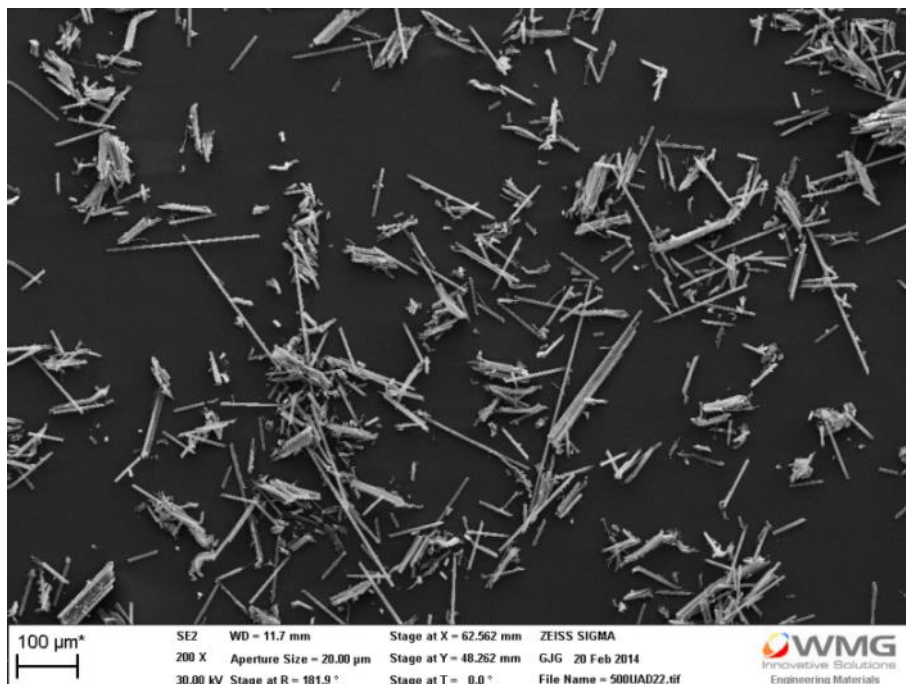


Figure B-4: Loose fibres obtained in the drilling of CFRP in CD as well as UAD (9.42 m/min, 0.05 mm/rev)



Figure B-5: Plastic deformation in the matrix of the chip in UAD (0.942 m/min, 0.05 mm/rev)

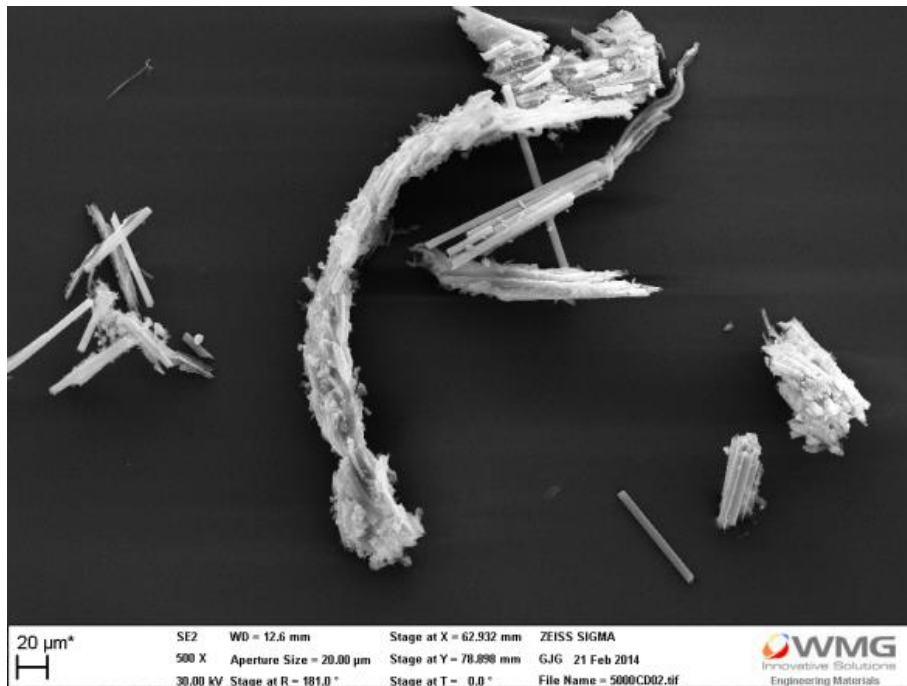


Figure B-6: Chip formation and plastic deformation in the matrix in CD (94.2 m/min, 0.05 mm/rev)

Appendix C

Tool wear images for Section 6.2.2.3.

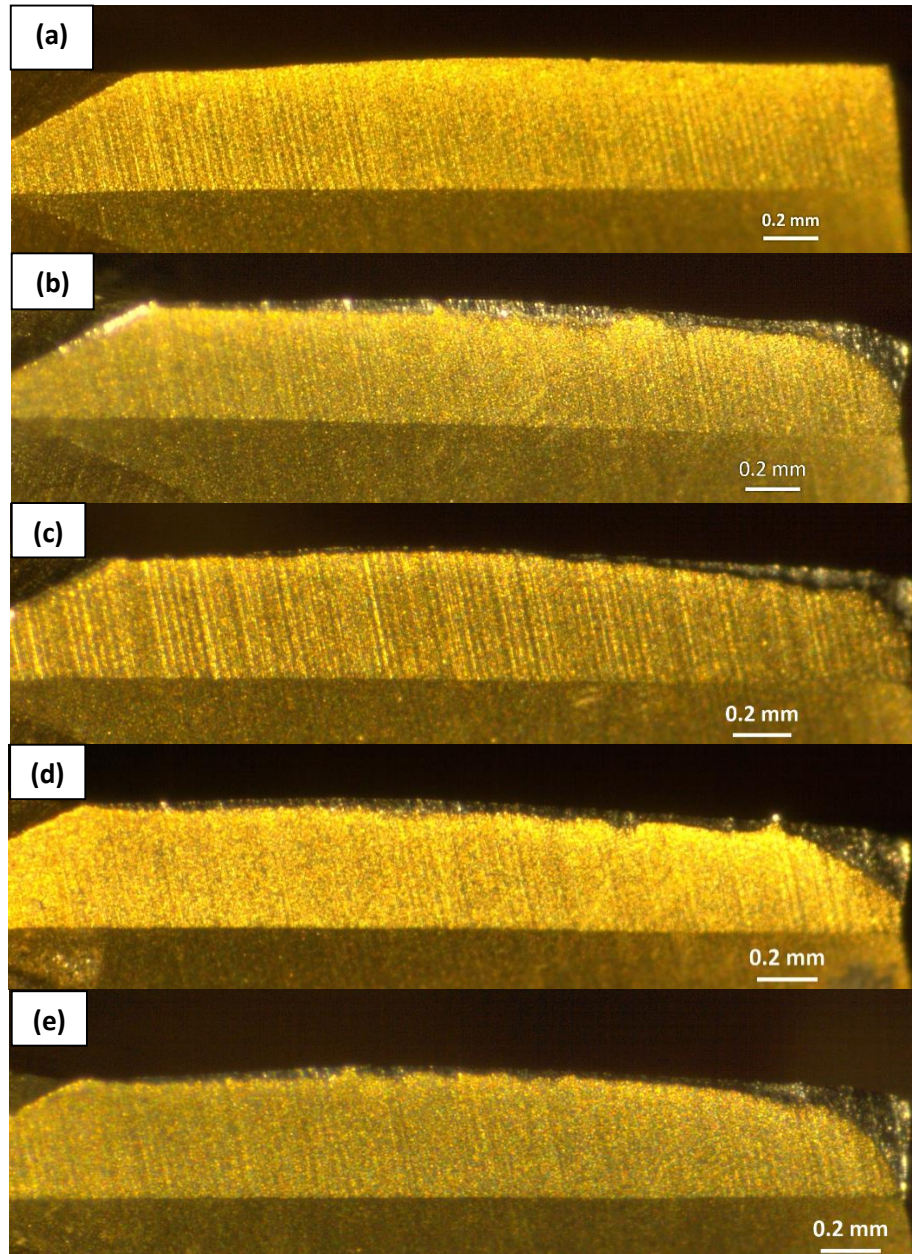


Figure C-1: Condition of tool flank face (a) in the new tool (b) after drilling of first hole in the case of CD without pilot-hole drilling (c) after 1st hole in UAD without pilot (d) after 1st hole in CD with pilot (e) after 1st hole in UAD with pilot-hole drilling

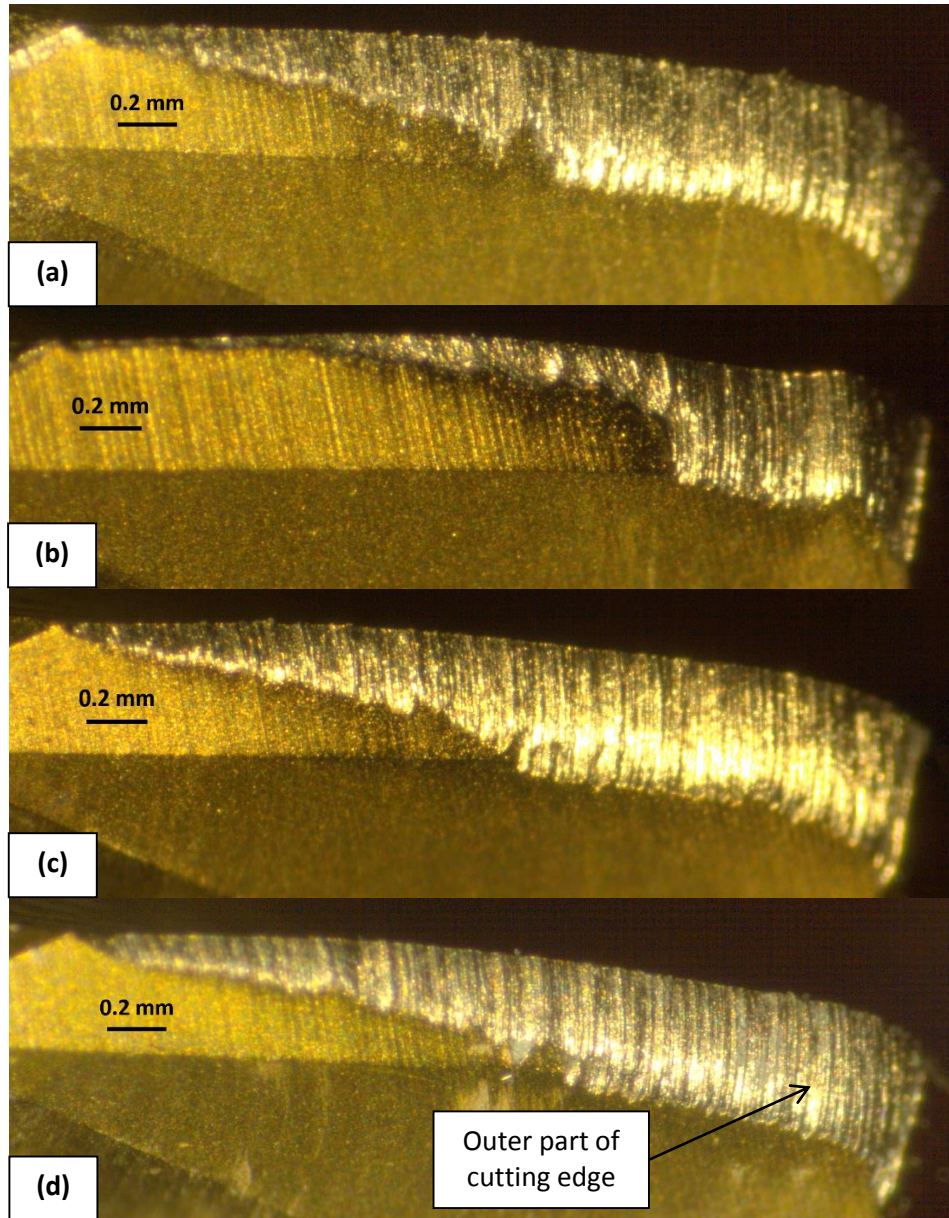


Figure C-2: Tool condition after drilling of 5th hole in (a) CD without pilot (b) UAD without pilot (c) CD with pilot and (d) UAD with pilot-hole drilling

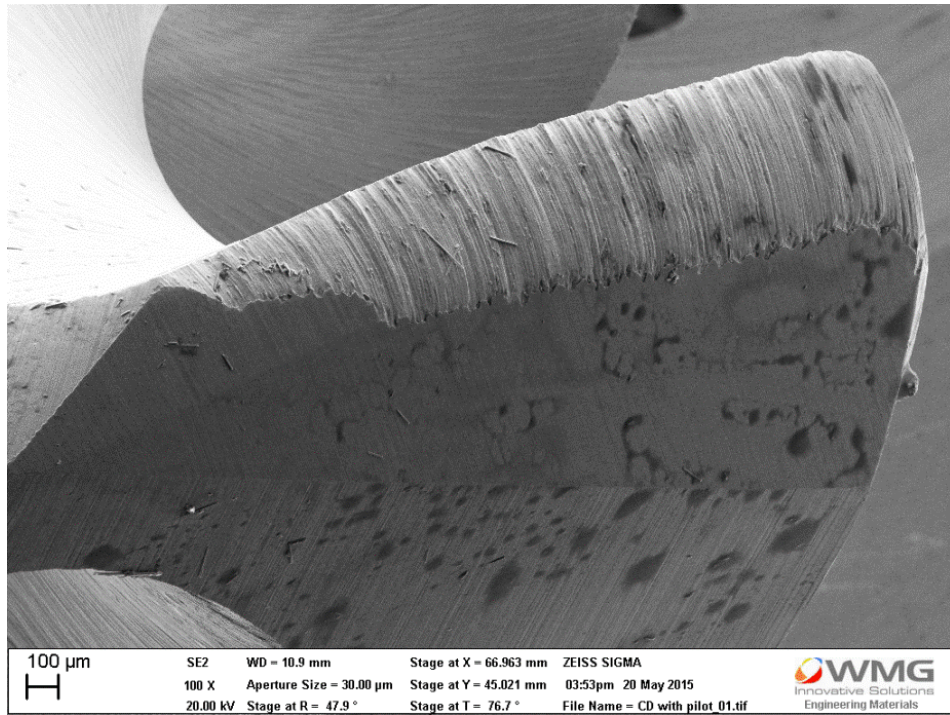


Figure C-3: SEM image of flank surface after 10 holes in the case of CD with pilot holes

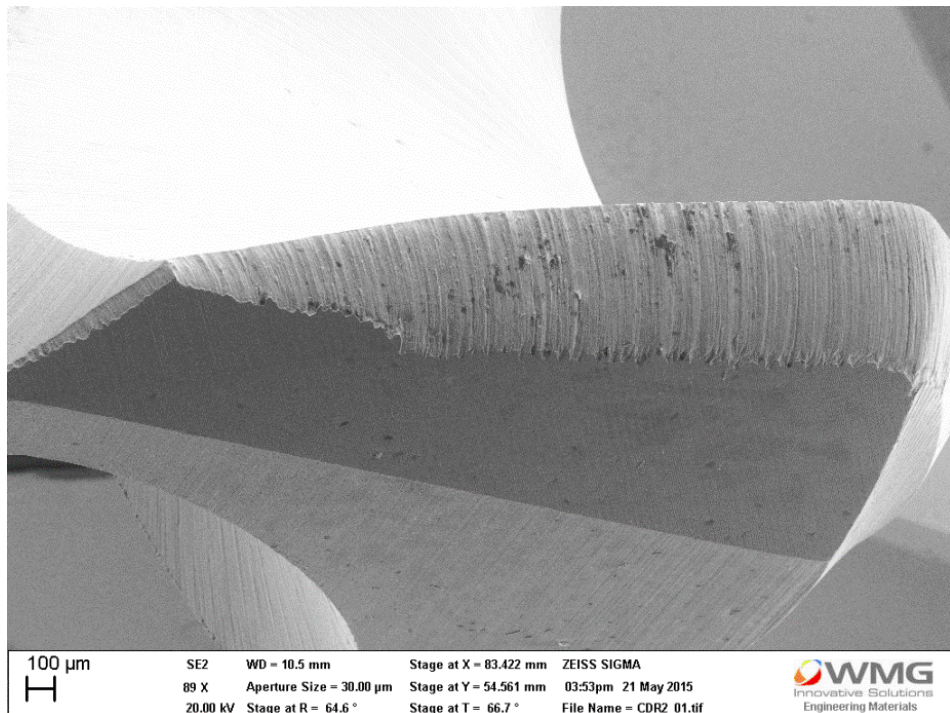


Figure C-4: SEM image of flank surface after 10 holes in the case of CD without pilot holes

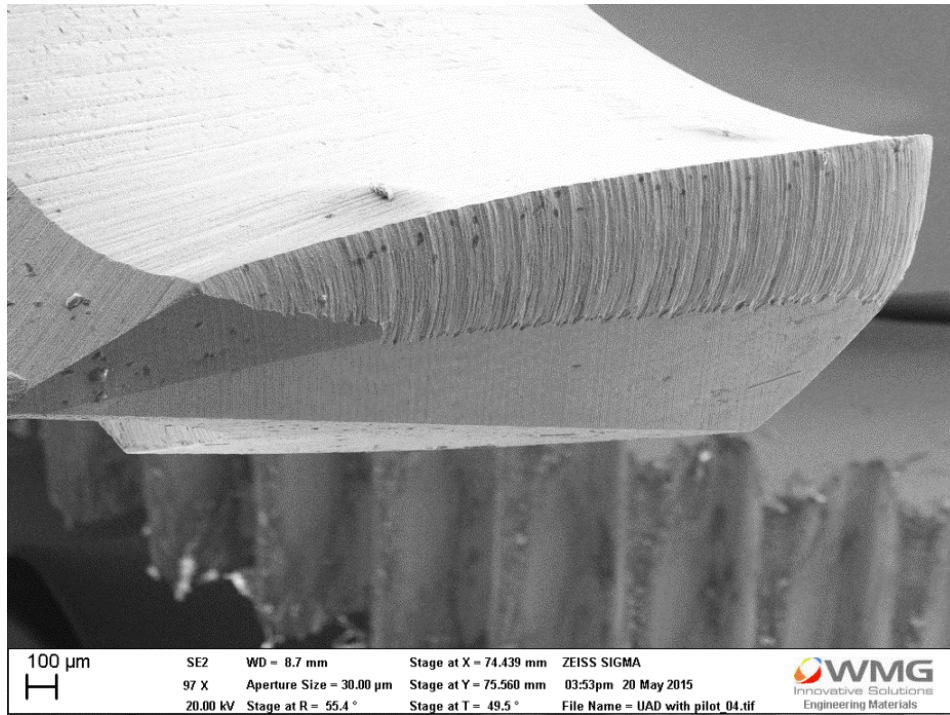


Figure C-5: SEM image of flank surface after 10 holes in the case of UAD with pilot holes

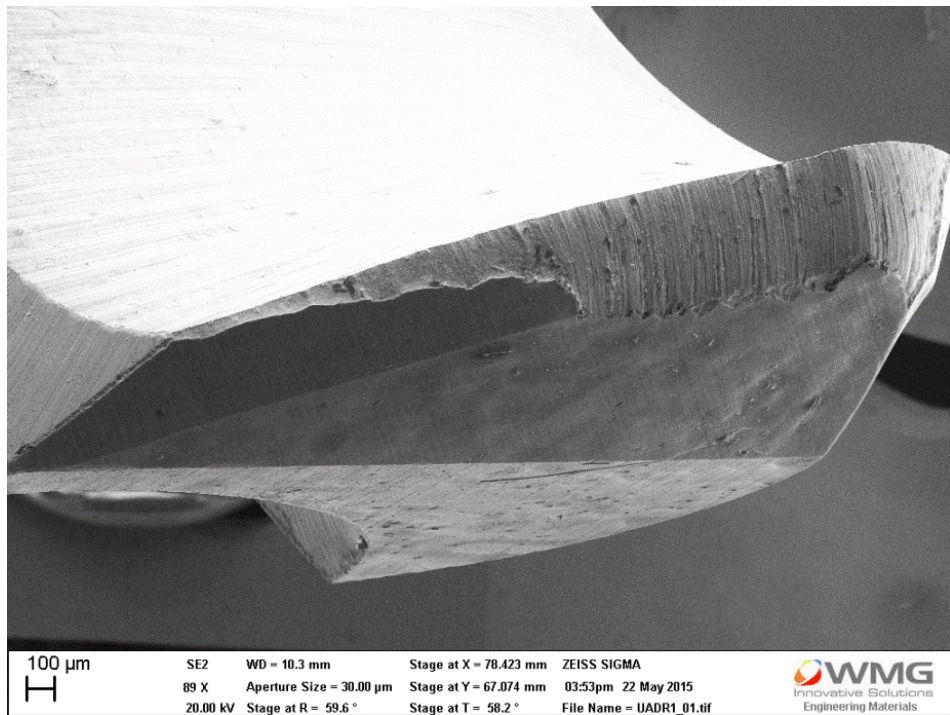


Figure C-6: SEM image of flank surface after 10 holes in the case of UAD without pilot holes

Appendix D

SEM images of the machined surfaces for Section 6.3.4.

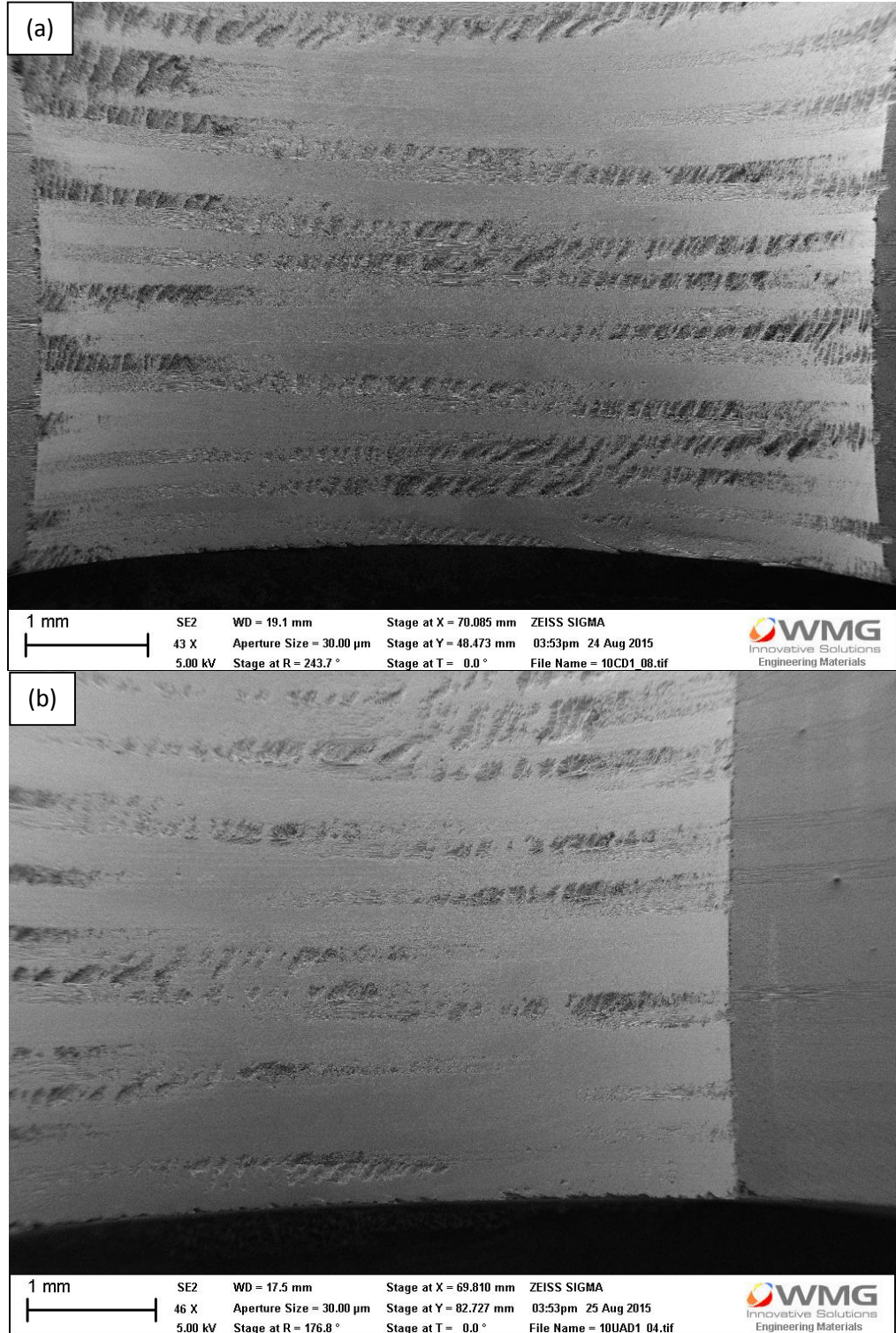


Figure D-1: Machined surface in hole number 1 at 10 m/min cutting speed in (a) CD and (b) UAD

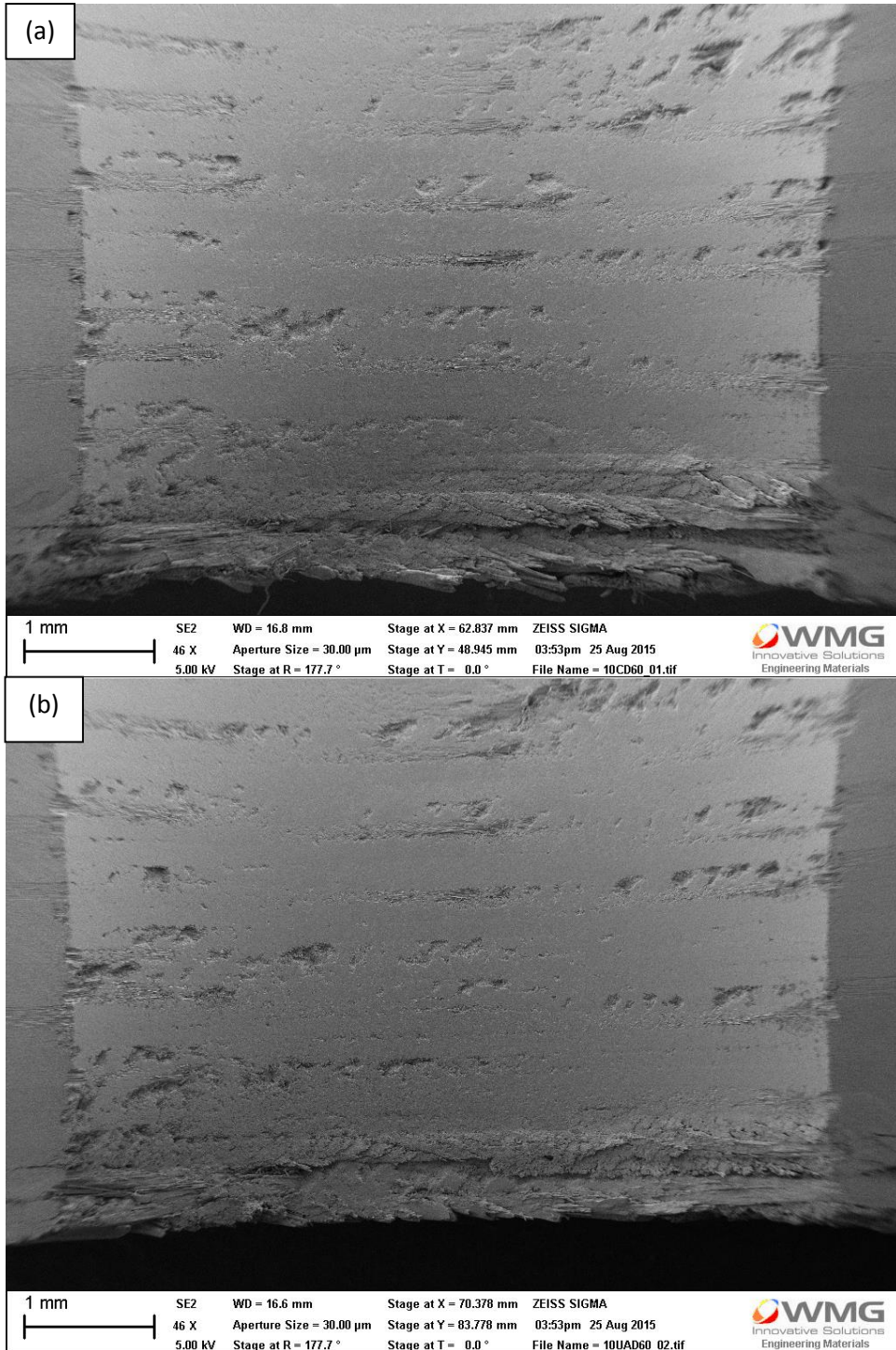


Figure D-2: Machined surface near exit in 60th hole in the case of 10 m/min cutting speed in (a) CD and (b) UAD

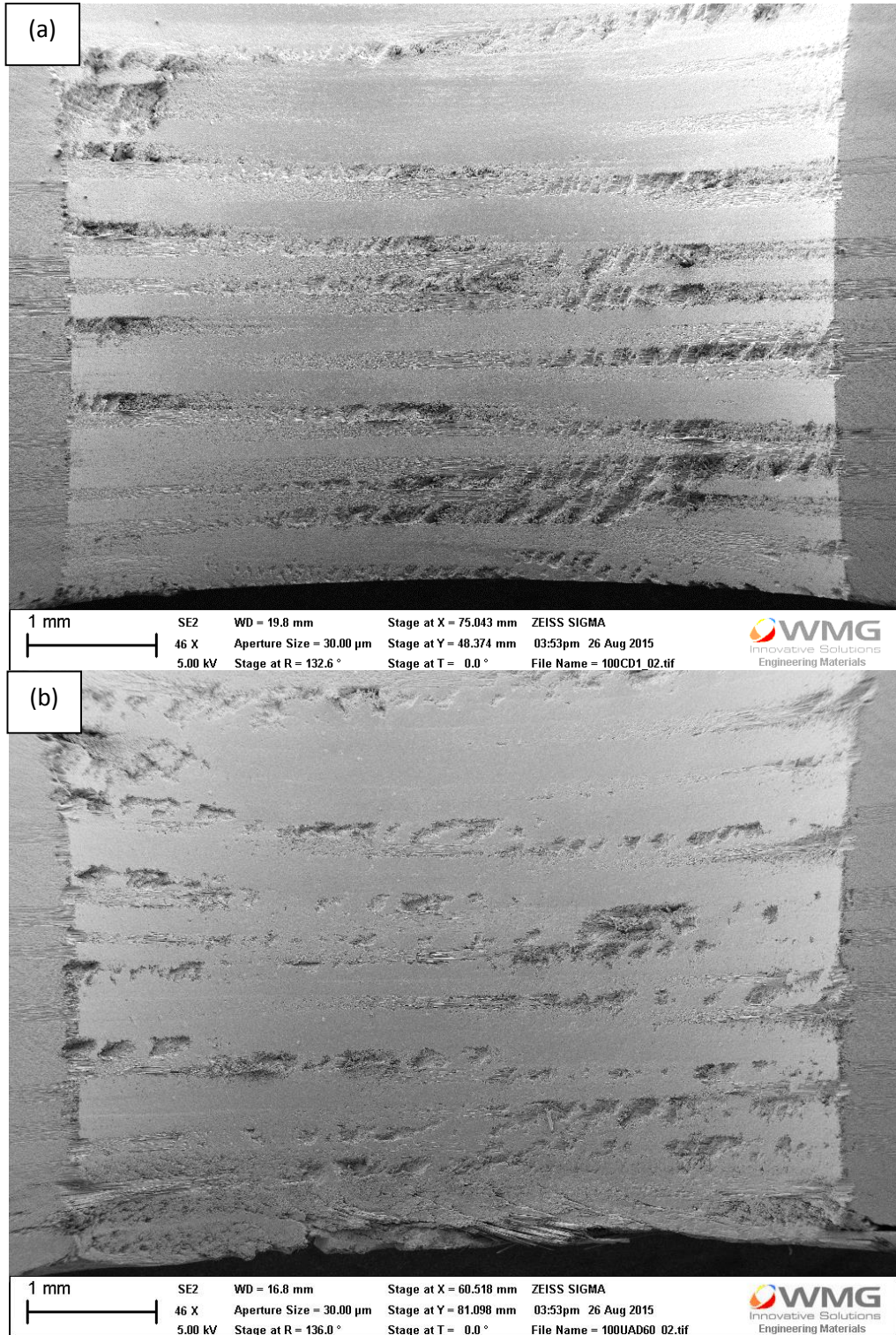


Figure D-3: Machined surface near exit in 60th hole in the case of 100 m/min cutting speed in (a) CD and (b) UAD